Phosphorus pools under pressure: climate change effect in agricultural catchments

Dissertation

der Mathematisch-Naturwissenschaftlichen Fakultät

der Eberhard Karls Universität Tübingen

zur Erlangung des Grades eines

Doktors der Naturwissenschaften

(Dr. rer. nat.)

vorgelegt von

Master of Science physische Geographie Christiane Nagel

geboren in Zittau

Tübingen

2026

Gedruckt mit Genehmigung der Mathematisch-Naturwissenschaftlichen Fakultät der Eberhard Karls Universität Tübingen.

Tag der mündlichen Qualifikation:	03.03.2026
Dekan:	Prof. Dr. Thilo Stehle
1. Berichterstatter/-in:	Prof. Dr. Yvonne Oelmann
2. Berichterstatter/-in:	PD Dr. Steffen Seitz

Selbstständigkeitserklärung

Hiermit erkläre ich, dass ich die vorliegende Arbeit selbstständig und ohne fremde Hilfe verfasst und keine anderen Hilfsmittel als die angegebenen verwendet habe.

Insbesondere versichere ich, dass ich alle wörtlichen und sinngemäßen Übernahmen aus fremden Werken als solche kenntlich gemacht habe.

_____ (Ort, Datum) _____ (Unterschrift)

Table of Contents

List of Figures

List of Tables

Danksagung

An dieser Stelle möchte ich mich sehr herzlich bei meinen Mentoren bedanken. Besonderer Dank gilt Prof. Dr. Yvonne Oelmann und PD Dr. Harald Neidhardt, die mich mit großer Fachkompetenz, wertvollen Anregungen und stetiger Unterstützung durch alle Phasen dieser Arbeit begleitet haben. Ihre kritischen Rückmeldungen und konstruktiven Diskussionen haben entscheidend zur Weiterentwicklung meiner Forschung beigetragen. Beiden Mentoren verdanke ich nicht nur eine ausgezeichnete fachliche Betreuung, sondern auch die Motivation und das Vertrauen, die mich während meiner Promotionszeit getragen haben.

Mein Dank gilt außerdem meinen Kollegen am Geographischen Institut in meiner Arbeitsgruppe Geoökologie Simon Hauenstein, Arnim Kessler, Wen Shao, Yao Li und Camillo Maliqueo-Murga, sowie den Kollegen der anderen Arbeitsgruppen Dr. Peter Kühn, Dr. Steffen Seitz und Dr. Corinna Gall. Durch die angenehme Arbeitsatmosphäre, fachliche Unterstützung und viele bereichernde Diskussionen haben sie wesentlich zum Gelingen dieser Arbeit beigetragen. Besonders hervorheben möchte ich die gute Zusammenarbeit im Labor und bei der Feldarbeit, die ohne eure Hilfe in dieser Form nicht möglich gewesen wäre. Auch der kollegiale Austausch und die gegenseitige Unterstützung im Arbeitsalltag haben diese Zeit für mich sehr wertvoll gemacht.

Des Weiteren möchte ich mich bei unserem Laborteam Sabine Flaiz, Rita Mögenburg und Genoveva Tscholl bedanken, ohne deren Hilfe und Unterstützung die Durchführung meiner Experimente sowie die Erhebung der Daten nicht möglich gewesen wäre.

Zudem möchte ich mich bei unseren studentischen und wissenschaftlichen Hilfskräften bedanken. Durch eure zuverlässige Mitarbeit, euren Einsatz und eure Sorgfalt habt ihr maßgeblich zum reibungslosen Ablauf der Experimente und damit zum Gelingen dieser Arbeit beigetragen. Vor allem durch euren tatkräftigen und selbstständigen Einsatz während meiner Elternzeit konnten meine Experimente beendet werden und die zugehörigen Daten erhoben werden.

Mein Dank gilt der Deutschen Forschungsgemeinschaft DFG, die durch die finanzielle Förderung dieses Projekts (Projektnummer 412678780) die Durchführung der Untersuchungen und damit das Entstehen dieser Arbeit ermöglicht hat. Ebenso bedanke ich mich beim Familienbüro für die finanzielle Unterstützung für studentischen und wissenschaftlichen Hilfskräften während meiner Elternzeit.

Mein herzlichster Dank gilt meiner Familie, die mir nicht nur das Studium ermöglicht, sondern mich auch während meiner gesamten Promotionszeit mit unermüdlicher Unterstützung, Rückhalt und Vertrauen begleitet hat, auch wenn es mal länger dauerte. Ohne ihre beständige Ermutigung wäre diese Arbeit in dieser Form nicht möglich gewesen.

Meinem Mann und unserem Sohn danke ich von Herzen für all die glücklichen Momente, die sie mir während dieser intensiven Zeit geschenkt haben.

Summary

Fertilizer inputs, such as phosphorus (P), to agricultural land are required to ensure adequate levels of crop production to meet the food and fiber demands of a growing population. Natural background P concentrations in soils are generally insufficient to sustain current levels of agricultural production. Consequently, agricultural soils are routinely supplemented with P fertilizers, often at rates exceeding immediate crop demand. (Habibiandehkordi et al., 2019; Roberts et al., 2020). Pronounced amounts of P have accumulated in cultural landscapes, due to prolonged fertilizer application over past decades (Bennett et al., 2001; Lannergård et al., 2020; Sharpley et al., 2013). A pronounced build-up of P stocks has occurred in many agricultural catchments, commonly known as legacy P, rendering agriculture the major source of diffuse P inputs into surface waters (Sandström et al., 2021; Sharpley et al., 1994). From agricultural soils, dissolved P is mobilized through surface runoff and erosion and subsequently transported via the transfer continuum (land-freshwater) through buffer strips until it eventually reaches adjacent drainage ditches (Efobo, 2023; Haygarth et al., 2005).

The loss of P from agricultural catchments increases the risk of eutrophication of water bodies and raise questions regarding the efficiency of current management practices. However, effective management strategies depend on a mechanistic understanding of P dynamics across the transfer continuum. The investigation of P dynamics in vegetated buffer strips (VBS, **Section B**) and drainage ditch sediments (DDS, **Section C**) clarifies how soil properties, hydrological variability, and prior P exposure control P retention, transformation, and mobility. While vegetated buffer strips and drainage ditch sediments are widely used to mitigate P transport from agricultural land to surface waters, their capacity to retain or remobilize P under fluctuating hydrological and redox conditions remains insufficiently understood. In particular, short- to medium-term transformations among labile, mineral-associated, and organic P pools in non-calcareous systems are poorly constrained. This knowledge gap is critical given that climate change is expected to intensify drying–rewetting cycles and extreme rainfall events, potentially enhancing the mobilization and re-release of legacy P from agricultural landscapes.

The aim of this dissertation was to understand the fate of P in VBS (**Section B**) and DDS (**Section C**) under dynamic environmental conditions (i.e., drying-rewetting cycles) by examining P pool transformations through an incubation experiment. Inorganic P (P_i) was added to fresh soil and sediment samples, followed by a 16- to 24-week incubation under different environmental conditions. A five-step sequential extraction scheme was implemented to follow temporal variations in the operationally defined P pools (**Section B** and **Section C**). In addition, for DDS (**Section C**) I applied an innovative isotopic labeling based on the $\delta^{18}O_{Pi}$ analysis of different P_i pools. Moreover, hydrological regimes differing in the duration and frequency of drying and rewetting were applied to investigate their influence on biotic and abiotic processes affecting P retention at different time scales (Bai et al., 2017; Sugiyama et al., 2013).

The results showed that in VBS (**Section B**), additional P_i largely retained in dissolved and labile, surface-adsorbed pools (porewater-P_i and $NaHCO_3$-extractable P_i), with minimal transfer to stable Al- and Fe-bound pools such as NaOH-extractable P_i or CDB-extractable P_i. This pattern suggests sorption

site saturation and highlights a risk of P_i mobilization, particularly under fluctuating moisture conditions that promote redox changes, which can trigger Fe(III)-(oxyhdr)oxide dissolution and alter P_i adsorption. Microbial and enzymatic activity also influenced P transformations, as evidenced by shifts in organic P (P_o) pools and the mineralization of P_o into more bioavailable forms. In contrast, forest soils without prior agricultural P input retained added P_i more effectively in stable NaOH-extractable P_i pools, demonstrating the importance of soil history and saturation in controlling P dynamics.

In DDS (**Section C**), temporally resolved $^{18}O_{Pi}$-labeling revealed rapid transfer of added P_i into labile $NaHCO_3$-extractable P_i and porewater pools immediately after application. During the early incubation phase, P_i was progressively redistributed into more strongly adsorbed NaOH-extractable P_i pools, while microbial activity and enzymatic processes transformed a portion of P_i into P_o, particularly in association with Fe(III)-(oxyhydr)oxide surfaces. This microbial cycling was reflected in the changing isotopic composition of P_i, indicating intracellular and extracellular enzymatic turnover. Over time, the intermediate phase showed a pronounced microbial conversion of strongly bound P_i into P_o, likely facilitated by biofilm formation, whereas the late phase was characterized by microbial dieback and subsequent decay of P_o, resulting in the re-release of P_i and its surface adsorption. These results indicate that long-term P_i retention in non-calcareous drainage ditch sediments is primarily governed by surface adsorption rather than the formation of stable mineral P pools, with the CDB-extractable P_o pool playing an unexpectedly significant role as an intermediate P reservoir.

Collectively, these studies underscore the interplay of biotic and abiotic factors in shaping P transformations and retention in agricultural land. Hydrological variability, microbial activity, and soil properties strongly influence whether P_i remains in labile, surface-adsorbed, or more stable forms. Importantly, the findings highlight the need for temporally resolved monitoring to capture the dynamic behavior of P pools and identify intermediate storage mechanisms such as CDB-extractable P_o. For management strategies aiming to reduce P discharge from agricultural catchments, consideration of soil type, legacy P, hydrological variability, and microbial dynamics is essential, particularly under changing climatic conditions. These insights are crucial for improving the design and effectiveness of buffer zones, drainage ditches, and other landscape-scale measures intended to mitigate P transport to downstream aquatic ecosystems.

Zusammenfassung

Düngemitteleinträge wie Phosphor (P) in landwirtschaftliche Böden sind notwendig, um ausreichende Erträge sicherzustellen und den Bedarf an Nahrungs- und Futtermitteln einer wachsenden Bevölkerung zu decken. Die natürlichen Hintergrundkonzentrationen von P in Böden reichen in der Regel nicht aus, um das heutige Niveau der landwirtschaftlichen Produktion aufrechtzuerhalten. Daher werden landwirtschaftliche Böden routinemäßig mit P-Düngern versorgt, häufig in Mengen, die den unmittelbaren Bedarf der Pflanzen übersteigen (Habibiandehkordi et al., 2019; Roberts et al., 2020). Infolge der langjährigen Düngung haben sich in Kulturlandschaften erhebliche Mengen an P angereichert (Bennett et al., 2001; Lannergård et al., 2020; Sharpley et al., 2013). In vielen landwirtschaftlich genutzten Einzugsgebieten kam es zu einem ausgeprägten Aufbau von P-Vorräten, dem sogenannten Legacy P, wodurch die Landwirtschaft zur wichtigsten diffusen Quelle von P-Einträgen in Oberflächengewässer geworden ist (Sandström et al., 2021; Sharpley et al., 1995). Aus landwirtschaftlichen Böden wird gelöster P durch Oberflächenabfluss und Erosion mobilisiert und entlang des Transferkontinuums (Land–Frischwasser) über Randstreifen transportiert, bis er schließlich angrenzende Entwässerungsgräben erreicht (Efobo, 2023; Haygarth et al., 2005).
Der Verlust von P aus landwirtschaftlichen Einzugsgebieten erhöht das Risiko der Eutrophierung von Gewässern und wirft Fragen zur Wirksamkeit bestehender Managementmaßnahmen auf. Effektive Strategien erfordern jedoch ein mechanistisches Verständnis der P-Dynamik entlang des Transferkontinuums. Die Untersuchung der P-Dynamik in begrünten Randstreifen (VBS, **Abschnitt B)** und in Sedimenten von Entwässerungsgräben (DDS, **Abschnitt C**) verdeutlicht, wie Bodeneigenschaften, hydrologische Variabilität und frühere P-Belastung die Retention, Transformation und Mobilität von P steuern. Obwohl VBS und DDS weit verbreitet eingesetzt werden, um den P-Transport von landwirtschaftlichen Flächen in Oberflächengewässer zu reduzieren, ist ihre Fähigkeit, P unter wechselnden hydrologischen und redox-chemischen Bedingungen zu speichern oder wieder freizusetzen, bislang nur unzureichend verstanden. Insbesondere kurz- bis mittelfristige Umwandlungen zwischen labilen, mineralassoziierten und organischen P-Pools (P_o) in nicht-kalkhaltigen Systemen sind bislang schlecht untersucht. Diese Wissenslücke ist besonders relevant, da der Klimawandel voraussichtlich zu häufigeren Trocken-Wiederbefeuchtungs-Zyklen und Extremniederschlägen führen wird, was die Mobilisierung und erneute Freisetzung von Legacy P aus Agrarlandschaften verstärken kann.

Ziel dieser Dissertation war es, den Verbleib von P in VBS (**Abschnitt B**) und DDS (**Abschnitt C**) unter dynamischen Umweltbedingungen (insbesondere Trocken-Wiederbefeuchtungs-Zyklen) zu untersuchen, indem Umwandlungen zwischen verschiedenen P-Pools in Inkubationsexperimenten analysiert wurden. Dazu wurde an frischen Boden- und Sedimentproben anorganischer P (P_i) zugesetzt, gefolgt von einer 16- bis 24-wöchigen Inkubation unter unterschiedlichen Umweltbedingungen. Ein fünfstufiges sequenzielles Extraktionsverfahren wurde angewendet, um zeitliche Veränderungen der operationell definierten P-Pools zu verfolgen (**Abschnitt B** und **Abschnitt C).** Zusätzlich kam für die DDS (**Abschnitt C**) eine innovative isotopische Markierung mittels $\delta^{18}O_{Pi}$

Analyse verschiedener P_i-Pools zum Einsatz. Darüber hinaus wurden hydrologische Regime mit unterschiedlicher Dauer und Frequenz von Trocken-Wiederbefeuchtungs-Zyklen angewandt, um deren Einfluss auf biotische und abiotische Prozesse der P-Rückhaltung auf unterschiedlichen Zeitskalen zu untersuchen (Bai et al., 2017; Sugiyama et al., 2013).

Die Ergebnisse zeigen, dass in VBS (**Abschnitt B**) zugesetztes P_i überwiegend in gelösten und labilen, oberflächengebundenen Pools (Porenwasser-P_i und $NaHCO_3$-extrahierbares P_i) verbleiben, während nur ein geringer Anteil in stabile Al- und Fe-gebundene Pools wie NaOH- oder CDB-extrahierbares P_i überführt wird. Dieses Muster weist auf eine Sättigung der Sorptionsplätze hin und verdeutlicht ein erhöhtes Risiko der P_i-Mobilisierung, insbesondere unter wechselnden Feuchtebedingungen, die Redoxänderungen fördern und eine Auflösung von Fe(III)-(Oxyhydr)oxiden sowie Veränderungen der P_i-Adsorption auslösen können. Mikrobielle und enzymatische Aktivitäten beeinflussten die P-Transformationen zusätzlich, wie sich in Verschiebungen der P_o-Pools und der Mineralisierung von P_o zu besser verfügbaren Formen zeigte. Im Gegensatz dazu konnten Waldböden ohne vorherige landwirtschaftliche P-Belastung zugesetztes P_i deutlich effektiver in stabilen NaOH-extrahierbaren P_i-Pools binden, was die Bedeutung der Nutzungsgeschichte und der P-Sättigung für die Steuerung der P-Dynamik unterstreicht.

In DDS (**Abschnitt C**) zeigten zeitlich hochaufgelöste $\delta^{18}O_{Pi}$-Markierungsexperimente eine rasche Transformation des zugesetzten P_i in labile $NaHCO_3$-extrahierbare und Porenwasser P_i-Pools unmittelbar nach der Applikation. Während der frühen Inkubationsphase wurde P_i zunehmend in stärker adsorbierte NaOH-extrahierbare P_i-Pools umverteilt, während mikrobielle Aktivität und enzymatische Prozesse einen Teil des P_i in P_o überführten, insbesondere in Assoziation mit Fe(III)-(Oxyhydr)oxid-Oberflächen. Dieser mikrobielle Umsatz spiegelte sich in Veränderungen der isotopischen Zusammensetzung des P_i wider und weist auf intra- und extrazelluläre enzymatische Prozesse hin. In der mittleren Phase kam es zu einer ausgeprägten mikrobiellen Umwandlung stark gebundenen P_i in P_o, vermutlich begünstigt durch Biofilmbildung, während die späte Phase durch mikrobiellen Abbau und anschließenden Zerfall von P_o gekennzeichnet war, was zur erneuten Freisetzung von P_i und dessen Oberflächenadsorption führte. Diese Ergebnisse zeigen, dass die langfristige P_i-Rückhaltung in nicht-kalkhaltigen Sedimenten von Entwässerungsgräben primär durch Oberflächenadsorption und nicht durch die Bildung stabiler mineralischer P-Phasen gesteuert wird, wobei der CDB-extrahierbare P_o-Pool eine unerwartet wichtige Rolle als intermediärer P-Speicher einnimmt.

Insgesamt verdeutlichen diese Studien das enge Zusammenspiel biotischer und abiotischer Faktoren bei der Steuerung von P-Transformationen und -Retention in Agrarlandschaften. Hydrologische Variabilität, mikrobielle Aktivität und Bodeneigenschaften bestimmen maßgeblich, ob P_i in labilen, oberflächengebundenen oder stabileren Formen vorliegt. Besonders hervorgehoben wird die Notwendigkeit zeitlich hochaufgelöster Untersuchungen, um die dynamische Entwicklung der P-Pools und intermediäre Speichermechanismen wie den CDB-extrahierbaren P_o-Pool zu erfassen. Für Managementstrategien zur Reduktion von P-Einträgen aus landwirtschaftlichen Einzugsgebieten ist es entscheidend, Bodentyp, Legacy P, hydrologische Variabilität und mikrobielle Dynamiken zu berücksichtigen, insbesondere vor dem Hintergrund des Klimawandels. Diese Erkenntnisse sind wesentlich für die Verbesserung der Gestaltung und Wirksamkeit von Randstreifen,

Entwässerungsgräben und weiteren landschaftsbezogenen Maßnahmen zur Verringerung des P-Transports in nachgelagerte aquatische Ökosysteme.

Section A

1. General introduction and objectives

Phosphorus (P) is an essential nutrient for agricultural production, yet pronounced amounts have accumulated in our cultural landscapes due to long-term fertilizer application (Bennett et al., 2001; Lannergård et al., 2020; Sharpley et al., 2013). Mineral fertilizers have been used in European agriculture in the beginning of the second half of the 20th century (Spohn et al., 2023). Total P input into Germany sums up to over 200 kilotons per year, mostly in form of P_2O_5 (Mayer et al., 2022). As a result, many agricultural catchments today show elevated soil and sediment P stocks, so-called legacy P. This excess P, accumulated in agricultural catchments over decades, poses a long-term risk that persists long after fertilizer cessation (Habibiandehkordi et al., 2019; Haygarth et al., 2005; He et al., 2023). Dissolved and particulate P can be mobilized via runoff and erosion and subsequently transported into adjacent ditches, streams, and ultimately larger rivers (Efobo, 2023; Haygarth et al., 2005), rendering agriculture the dominant source of diffuse P inputs into surface waters (Sandström et al., 2021; Sharpley et al., 1994). This legacy effect presents a major challenge for the sustainable management of P in agricultural catchments and ultimately poses a threat to both freshwater and marine ecosystems by promoting eutrophication (Bennett et al., 2001; Kleinman et al., 2011; Sharpley et al., 2013).

To reduce the transport of dissolved P from agricultural soils via the transfer continuum (land-freshwater) buffer strips can be established. (Efobo, 2023; Haygarth et al., 2005). According to EU Water Framework Directive, farmers are legally obliged to establish buffer strips along watercourses, but there is no uniform national law prescribing the exact width for all agricultural land (Roberts et al., 2012). However, Vegetated buffer strips (VBS, **Section B**) are widely implemented as mitigation measures to reduce nutrient export. By filtering runoff and stabilizing soils due to a dense root system, VBS contribute to reducing P transfer into drainage networks (Bauke et al., 2022; Roberts et al., 2012). Their efficiency, however, is highly context-dependent, influenced by vegetation type, soil properties, buffer design, and fertilizer input concentrations (Cole et al., 2020; Hille et al., 2019). Importantly, hydrological variability, which is expected to intensify with climate change, strongly modulates their retention capacity. Heavy rainfall and flooding events can reduce P retention or even trigger P mobilization, while drought periods may temporarily enhance sorption but also increase the risk of release upon rewetting (Withers et al., 2009; Young et al., 2021).

Furthermore, mobilized P can be transferred from VBS into sediments of adjacent drainage ditches (DDS, **Section C**), which play an important role in the transfer continuum of P, connecting smaller streams to larger receiving rivers, creeks, and lakes (McDowell and Haygarth, 2024; Pionke et al., 2000; Sharpley et al., 2013). Although the retention of P in streambed sediments of drainage ditches, creeks, and rivers constitutes a vital ecosystem service, this storage is not permanent. Due to the legacy effect, P can be re-released with lag times of years or decades, complicating sustainable nutrient management and posing a persistent risk of eutrophication in freshwater and marine systems (Carpenter, 2005; Haygarth et al., 2014; Kleinman et al., 2011; Lannergård et al., 2020). Therefore, understanding the

dynamics of P storage pools in soils and sediments is critical for mitigating long-term P losses from agricultural landscapes (Neidhardt et al., 2019). To optimize P management in agricultural catchments, it is therefore essential to understand the dynamics of P storage pools in VBS (**Section B**) and DDS (**Section C**), (Neidhardt et al., 2019).

Total P contents in VBS (**Section B**) and DDS (**Section C**) under agricultural influence can be significantly higher than background levels due to excess fertilizer application (Sharpley et al., 2013). Long-term fertilizer use can alter the composition of P fractions in receiving soils and sediments, increasing easily soluble P_i while reducing P_o (Chen et al., 2022). From arable land, P may reach drainage ditches either directly as particulate P via surface runoff and erosion (Reddy et al., 1999) or indirectly as dissolved P_i via subsurface flow through interconnected buffer strips (Shore et al., 2016).

Particulate P typically retains the P pool composition of its source soil, where excess P_i is primarily stored via sorption to positively charged mineral and organic surfaces (labile P_i), Al- and Fe(III)-(oxyhydr)oxide (moderately labile/ stable P_i), and as stable secondary minerals such as octacalcium phosphate (Ca-P_i, stable P) (Cross and Schlesinger, 1995; McDowell and Haygarth, 2024; Reddy et al., 1999; Sharpley et al., 1994).

The storage of P in VBS (**Section B**) and DDS (**Section C**) is controlled by dynamic processes that operate on short to long timescales and directly affect P mobility. Environmental parameters such as hydrological conditions and temperature determine the intensity of the biogeochemical processes involved (Chen et al., 2022; Dupas et al., 2015). Changes in hydrological and redox conditions play a key role in the re-release of P (Reddy et al., 1999), particularly under climate change, which increases the frequency of droughts and heavy rainfall. P transfer from land to streams is generally expected to rise due to higher winter precipitation under temperate climates (Jeppesen et al., 2009). The risk of P mobilization from arable land is particularly high during heavy rainfall events, especially shortly after fertilizer application and tillage (Lucas et al., 2023). The linkage between short- and long-term dynamics of P pools under changing climatic conditions requires further investigation, particularly with regard to the different transformation times of various P pools.

Immediate reactions such as the immobilization of dissolved P_i via surface adsorption occur within seconds to hours (Joshi et al., 2015). Rapid adsorption of P_i results from its interaction with mineral surfaces and organic matter (Mattingly et al., 1975) and is strongly influenced by pH (Barrow, 1984), soil texture, and the initial P pool composition (Liu et al., 2021). Externally applied P disturbs existing equilibria among P pools as it is initially incorporated into the dissolved and labile pools (Chen et al., 2022). This rapid adsorption plays an important role in sediment-water exchange by constraining aqueous P_i concentrations (Lannergård et al., 2020). Continuous inputs subsequently increase the total P content in soils and sediments and shift the pool composition toward moderately labile and stable forms of P_i (Cross and Schlesinger, 1995).

Within days to weeks, adsorbed P_i from the labile pool can be transferred into the moderately labile pool, where Al- and Fe-mineral phases and organic compounds serve as principal sorbents (Joshi et al., 2016). The addition of external P enhances this transfer, with 70-90% of applied P being subsequently fixed as Al- and Fe-P (Chen et al., 2022). Additionally, P may be taken up and retained by microorganisms as P_o within organic molecules (Zhou et al., 2005). Long-term observations over

months capture changes in more stable pools, for example, dissolved P_i may be incorporated into Ca-P_i after several months (Joshi et al., 2016), which considerably reduces its bioavailability and mobility (Shore et al., 2016). Microbial activity and pH values further regulate P retention and mobilization in the mid- to long-term, as well as the redox state, (Joshi et al., 2016; Zhang et al., 2021).

Drying-rewetting cycles strongly influence this P dynamics in VBS (**Section B**) and DDS (**Section C**). Dry periods tend to enhance P retention, whereas rewetting can mobilize P, which is especially relevant for non-calcareous soils where P retention relies on adsorption to Al- and Fe-(oxyhydr)oxides (He et al., 2023; Taalab et al., 2019). For instance, under prolonged water saturation, dissolved P_i concentrations can rise dramatically due to the reductive dissolution of Fe(III)-(oxyhydr)oxide and the mineralization of P_o (Ajmone-Marsan et al., 2006), thereby increasing P losses to adjacent water bodies (Joshi et al., 2016). Moreover, P_i associated with Fe(III)-(oxyhydr)oxide can be utilized and cycled by microorganisms under strongly reducing conditions (Joshi et al., 2015; Wang et al., 2018). Conversely, buffer strips and drainage ditches often fall dry during drought periods, exposing soils and sediments to frequent drying-rewetting cycles that influence the rate and extent of transformations in the moderately labile Fe-P_i pool and P_o pools (Dieter et al., 2015; Sharpley et al., 1994). The return to oxic conditions induces the precipitation of Fe(III)-(oxyhydr)oxide and concomitant fixation of P_i in the moderately labile pool (Barczok et al., 2023). Microbial biomass and activity have been shown to decrease in soils subjected to increasing numbers of drying-rewetting cycles (Yan et al., 2015). Considering these multifaceted processes, the transfer of P between different pools in VBS (**Section B**) and DDS (**Section C**) under fluctuating redox conditions remains complex and insufficiently studied, partly due to methodological limitations (Bauke et al., 2022; Sandström et al., 2021).

In addition, biological processes play an essential role in transforming P pools, yet quantifying their individual contributions remains challenging. Microbially mediated processes further alter pool dynamics on timescales of weeks to months, including intracellular P_i cycling and enzymatic regeneration of P_i from P_o (von Sperber et al., 2014; Liang and Blake, 2006). Advanced approaches, such as the analysis of stable oxygen isotopes in phosphate ($\delta^{18}O_{Pi}$), have recently been applied to disentangle these processes, since isotopic fractionation allows distinguishing biotic from abiotic transformations (Bauke et al., 2022; Blake et al., 2005; Joshi et al., 2016). While abiotic processes such as mineral precipitation do not alter $\delta^{18}O_{Pi}$ values, intra- and extracellular enzymes catalyze the exchange of oxygen isotopes between P_i and ambient water (Blake et al., 2005; Joshi et al., 2016; Melby et al., 2011), thereby modifying $\delta^{18}O_{Pi}$ values (Blake et al., 2001). Two enzymatically controlled fractionation processes are involved: intracellular P_i cycling, representing temperature-dependent equilibrium fractionation, and extracellular regeneration of P_i from P_o by acid phosphatase, which represents kinetic fractionation (Blake et al., 2005; Liang and Blake, 2006; Longinelli and Nuti, 1973; von Sperber et al., 2014). By combining sequential extraction (**Section B** and **Section C**) with isotopic labeling (addition of ^{18}O-enriched P_i, **Section C**), further insights can be gained into biogeochemical P transformations (Joshi et al., 2016). Depending on biological activity, (i) ^{18}O-enriched P_i may be geochemically transformed into stable P compounds such as P-containing minerals, leaving its isotopic signature unaltered and thus elevating $\delta^{18}O_{Pi}$ values in the receiving pools (Jaisi and Blake, 2010). (ii) Alternatively, intense enzymatic cycling of ^{18}O-enriched P_i can shift $\delta^{18}O_{Pi}$ values toward isotopically

lighter compositions, ultimately approaching those of pre-existing labile P_i. The extent of this shift depends on the dominant biological process (greater for intracellular than extracellular cycling) and the overall biological activity in the system (Gross and Angert, 2015; Liang and Blake, 2006; von Sperber et al., 2014).

While VBS (**Section B**) are widely implemented to reduce P transport from arable fields to surface waters, their capacity to retain or remobilize P under dynamic environmental conditions remains insufficiently understood (Chen et al. 2023)**.** Similarly, despite extensive research on P storage and retention in wetlands and river sediments within agricultural catchments, DDS (**Section C**) have received comparatively little attention, despite their widespread occurrence and strategic position at the land-water interface. For both VBS and DDS, considerable knowledge gaps persist regarding how fluctuating hydrological and redox regimes control short- to medium-term P transformations**,** particularly in non-calcareous systems (Baucke et al., 2022; Kleinmann et al., 2011; Sandström et al., 2021). Most existing studies focus on seasonal or long-term P accumulation or mobilization, as well as steady-state conditions, whereas process-based insights into temporal shifts among labile, mineral associated, and P_o pools remain scarce**.** This limitation is critical given that climate change is expected to intensify drying-rewetting cycles and extreme rainfall events, potentially enhancing both the mobilization and re-release of legacy P from agricultural landscapes (Jeppesen et al., 2009; Lucas et al., 2023). Overall, the long-term effectiveness of VBS and DDS as P sinks depends on the transformation and stabilization of inorganic P into more persistent pools (e.g., mineral-associated P_i or P_o). However, the biogeochemical mechanisms governing these transformations, and their sensitivity to changing hydrological and redox conditions, are still poorly constrained**.** Addressing these gaps is essential to improve predictions of P retention and release at agricultural land-water interfaces under future climate scenarios.

Therefore, the overarching objective of this study was to unravel short- and long-term transformations in the P pools of non-calcareous soils of buffer strip (**Section B**) and sediments of drainage ditch (**Section C**) with historical P fertilizer input, mediated by dynamics in the hydrological and redox conditions. In addition, a forest site (FST, **Section B**), unaffected by legacy P, serves as a reference to compare the fate of additional P inputs. By combining sequential extraction (**Section B** and **Section C**) with and $\delta^{18}O_{Pi}$ analysis (**Section C**), this study aims to disentangle the relative contributions of abiotic and biotic processes in controlling P retention and mobility in arable catchments over time. Hydrological conditions differing in the duration and frequency of drying and rewetting were applied to examine their influence affecting P dynamic at multiple timescales (Bai et al., 2017; Sugiyama et al., 2013). In doing so, this work seeks to advance mechanistic understanding of P cycling at critical land-freshwater interfaces that may contribute to the development of management strategies for mitigating P losses from agricultural catchments in a changing climate.

In specific, for VBS (**Section B**) with a history of agricultural P input, I expected that i) additional P_i remains predominantly in the dissolved and labile fractions, while only a smaller proportion is sorbed to Fe associated pools (moderately stable P_i). Furthermore, I assumed that (ii) long drying-rewetting cycles enhance the stabilization of P_i by promoting the repeated formation of amorphous Fe(III)-

(oxyhydr)oxide resulting in a slight but significant increase of Fe-bound P as compared to short drying-rewetting cycles. To further disentangle the role of legacy P in regulating P dynamics under fluctuating hydrological and redox conditions, an additional forest site (FST, **Section B**) unaffected by historical fertilizer inputs was included as a reference system. This site provides an essential contrast to the legacy P-enriched VBS and DDS, allowing a direct comparison of the fate and transformation of newly added P_i in soils with and without a history of P accumulation. I hypothesize that, in the absence of legacy P, (iii) the addition of P_i will promote the formation of more stable P pools due to enhanced surface adsorption to Al- and Fe-(oxihydr)oxides. Furthermore, I expect that (iv) P_i addition will also affect P_o pools, leading to a shift from more strongly bound P_o towards more labile P_o. This transition is interpreted as an indication of increased mineralization and microbial immobilization processes, occurring largely independent of redox conditions.

For DDS (**Section C**) it was hypothesized that excess amounts of P_i are primarily retained in drainage ditch sediments by surface adsorption and the formation of more stable pools (Fe- and Ca-P_i), with retention strongly mediated by redox conditions and microbial activity. Specifically, I expected that (i) directly after labeling, the labile P fraction and its $\delta^{18}O_{Pi}$ signal increase irrespective of hydrological and temperature treatments; (ii) in the first weeks, P_i is transferred from the labile to moderately labile pools while microorganisms simultaneously use the excess P, leading to shifts in $\delta^{18}O_{Pi}$ values through intracellular enzymatic cycling, most pronounced under shorter drying-rewetting intervals; (iii) over weeks to months, microbial phosphatase activity transforms labile and moderately labile P_i into organic P, accompanied by a decrease in $\delta^{18}O_{Pi}$ values, with the strongest effects under favorable microbial conditions; and (iv) long-term exposure to hydrological fluctuations results in microbial death and subsequent release of P_i into the dissolved pool, from where P_i is transferred into more stable pools bound to secondary minerals, again most pronounced under hydrological treatment favorable for microorganisms.

2. Material & Methods

The section bellow is an overview of the methods used for VBS, FST (**Section B**) and DDS (**Section C**) that are essential for understanding the experiment. For a comprehensive description of the method procedure, please refer to the Material and Methods part of the manuscript **Section B** and **Section C**.

2.1. Study sites

Samples for the incubation experiments were collected within the Ammer valley near Tübingen (N 48° 31.050; E 9° 0.790, WGS84), located in the South German Scarplands. The catchment covers an area of 134 km², of which approximately 66% is used for agriculture (Leibundgut and Eisele, 2005; Schwientek et al., 2013). The geological background consists of Lower and Middle Triassic Keuper sequences with sandstones and evaporitic marlstones, as well as aeolian loess, colluvial, and alluvial deposits. Soils are mainly characterized as loamy Fluvisols, Luvisols, and Anthrosols with fine grained

textures dominated by clay (Ad-hoc Boden, 2005). The catchment is characterized as a high-risk area for diffuse nutrient inputs according to the Water Framework Directive (LUBW, 2015). Previous studies reported elevated total P concentrations and an increased proportion of moderately labile and stable P forms in soils and sediments adjacent to arable land (Neidhardt et al., 2019).

For **Section B**, soil samples were collected from a vegetated buffer strip (VBS) adjacent to arable land, from the upper 0-5 cm along a straight south-north transect. Sampling was conducted in real triplicates with 10-15 m spacing between replicates. Additionally, forest soils (FST, unaffected by agricultural legacy P) were collected as a control, 15-20 m further south of the VBS. These samples were also taken from the upper 0-5 cm in real triplicates and processed in the same way as VBS soils. For **Section C**, sediment samples were collected from the streambed of a drainage ditch (DDS) adjacent to the VBS. Samples were taken also from the upper 0-5 cm following a straight orthogonal transect. To account for spatial variability, real triplicate samples were collected with 10-15 m spacing between replicates along the ditch. Sampling positions, land use, and topography of VBS and FST are provided in the supporting information **Table B-S1** and of DDS in the supporting information **Table C-S1.** Overview of the sampling area is presented in **Figure A-1**.

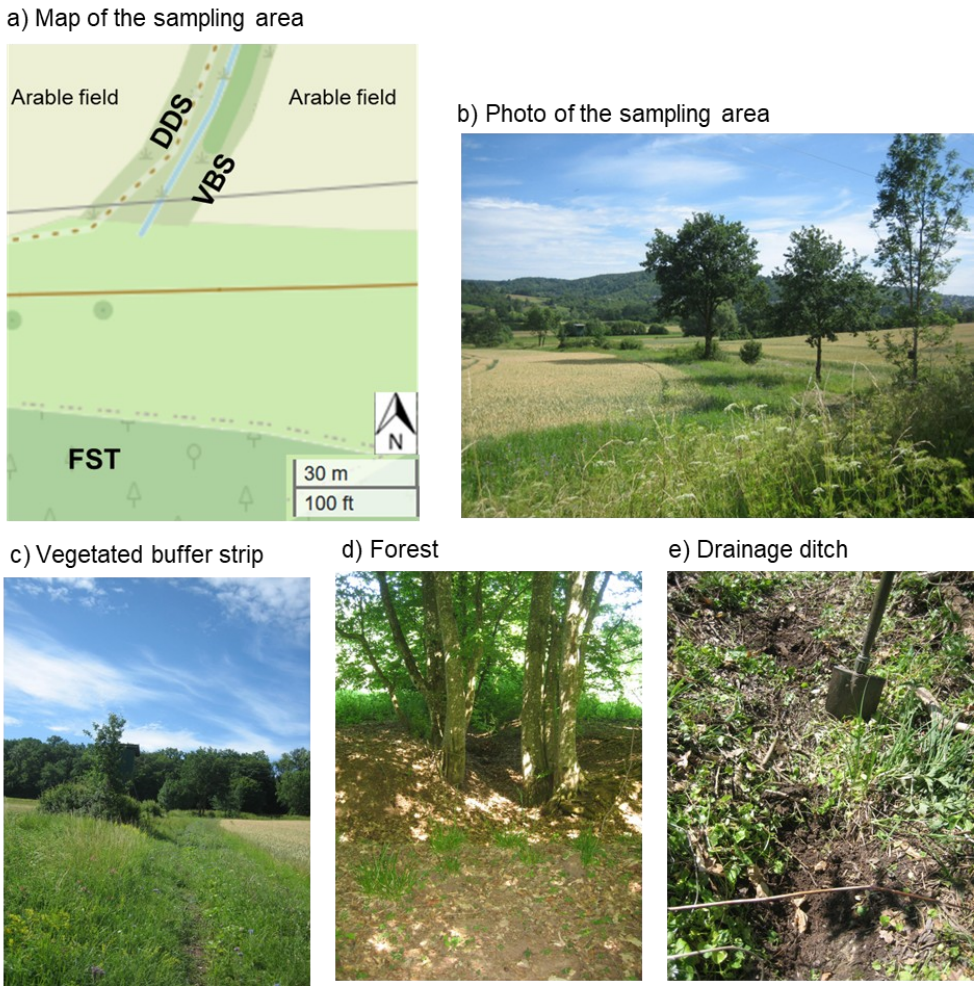

Figure A-1: Sampling sites in the Ammer valley. (a) Map of the sampling area with vegetated buffer strip (VBS), forest (FST) and drainage ditch (DDS) (© *OpenStreetmap contributors*), (b) photo of the sampling area, (c) vegetated buffer strip (d) Forest and (e) drainage ditch.

2.2. Experimental design

Non-calcareous soils from VBS, FST (**Section B**) and the sediments from DDS (**Section C**) were collected, air-dried, sieved to <2 mm, and large roots or organic fragments manually removed. Samples were pre-incubated at room temperature (20°C) with deionized water at a gravimetric water content of approximately 37-38% for two weeks to stabilize microbial activity.

After pre-incubation, 100 g dry weight equivalents of each sample were placed into 200 ml glass jars (height: 8 cm, diameter: 7 cm, WECK), and for VBS and FST (**Section B**) 100 ml of 0.5 g KH_2PO_4 l^{-1} solution was applied. For DDS (**Section C**), 100 ml of ^{18}O-enriched P_i solution (485 mg PO_4-P l^{-1}, +350 ‰ VSMOW) was used. The $^{18}O_{Pi}$ label was synthesized via dissolution of PCl_5 in ^{18}O-enriched water (Melby et al. 2011; Stout et al., 2014). A detailed overview of the synthesis can be found in the supporting information **Section C-S1**).

All samples (VBS, FST, DDS) were conducted in triplicates at two temperatures, 20°C and 5°C, with the latter to suppress microbial activity, and incubated up to 16 weeks (VBS, FST; **Section B**) and 24 weeks (DDS, **Section C**). Two hydrological treatments were applied to all samples:

1. Short-pulsed logged (SPL): Weekly drying and rewetting cycles (8 cycles for VBS and FST (**Section B**); 12 cycles for DDS (**Section C**)).
2. Long-pulsed logging (LPL): Two-week drying and rewetting cycles (4 cycles for VBS and FST (**Section B**); 6 cycles for DDS (**Section C**)).
3. Additionally, DDS (**Section C**) included a permanently waterlogged treatment (L) maintained at 50% gravimetric water content throughout the 24-weeks incubation.

During incubation, at the end of each rewetting interval, porewater was removed using micro suction cups (ecoTech Umwelt-Meßsysteme GmbH, Germany; polyamide membranes, 0.45 µm pore size). For SPL, porewater was extracted weekly, and for LPL biweekly. Water contents were restored by adding deionized water (100 ml per SPL cycle; 50-100 ml biweekly for LPL and L) to maintain target gravimetric water content. Gravimetric water content was periodically measured on 2.5-3.5 g of wet sediment using a halogen dryer (HB43-S, Mettler Toledo) following DIN ISO 11465 (1996) and used to calculate dry-weight concentrations for subsequent chemical analyses.
Temperature was continuously monitored with loggers (WTDL1, ELV Elektronik AG, Germany), and redox potential (E_h) was measured using Pt-electrodes (99.95% Pt, Mansfeld type) coupled with Ag/AgCl reference electrodes (ecoTech Umwelt-Meßsysteme GmbH, Germany). Data were recorded every 3 minutes and retrieved monthly. E_h in VBS and DDS ranged broadly depending on treatment, reflecting the applied hydrological regimes (supporting information **Figure B-S1** and supporting information **Section C-S2, Figure C-S2**).
Sampling for chemical analysis occurred at multiple time points, an overview of the incubation conditions and sampling points is shown in **Table A-1.**

Table A-1: Incubation conditions and sampling points for the samples taken in the Ammer valley.

Samples	Hydrological treatment	Sampling points *	Total incubation time *
Vegetated buffer strip (VBS)	Short-pulsed logged (SPL)	1 d, 8 w, 16 w	16 w
	Long-pulsed logged (LPL)	1 d, 8 w, 16 w	
Drainage ditch sediments (DDS)	Short-pulsed logged (SPL)	1 d, 1 w, 4 w, 16 w, 24 w	24 w
	Long-pulsed logged (LPL)	1 d, 4 w, 8 w, 16 w, 24 w	
	Permanently water-logged (L)	1 d, 4 w, 8 w, 16 w, 24 w	
Forest soil (FST)	Short-pulsed logged (SPL)	1 d, 2 w, 16 w	16 w
	Long-pulsed logged (LPL)	1 d, 4 w, 16 w	

* d = day, w = week(s)

At each time step, porewater was removed, and one set of triplicate samples per treatment was sacrificed for chemical analyses. For pulsed treatments, sampling occurred after wet cycles to avoid

oxic conditions that could interfere with measurements. Setup of the experimental design for VBS, FST and DDS, are shown in **Figure A-2**.

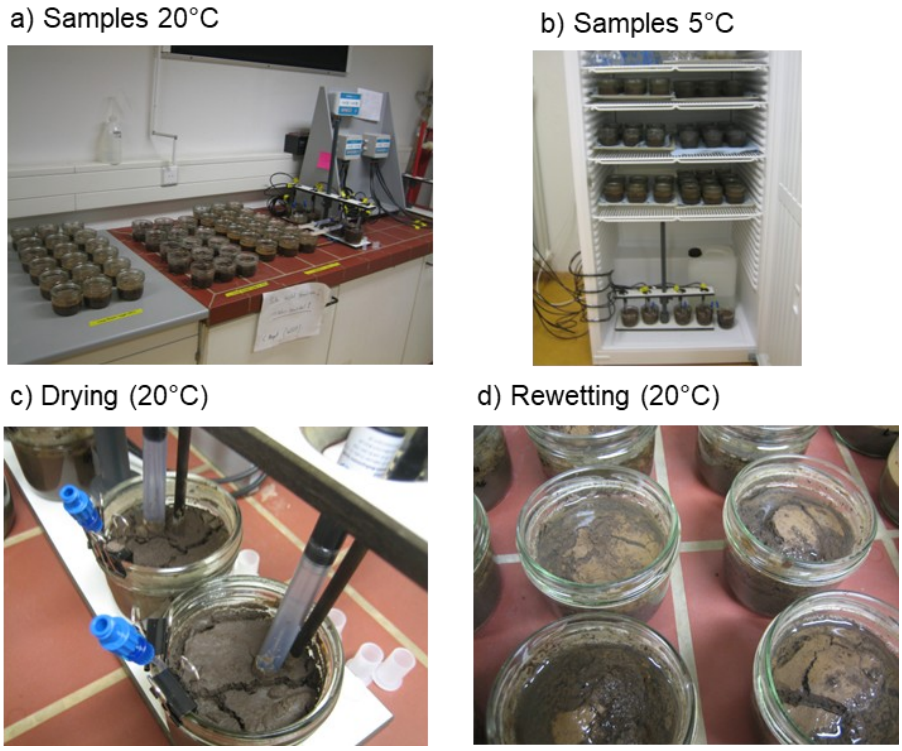

Figure A-2: Setup of the experimental design. (a) Samples incubated at 20°C, (b) samples incubated at 5°C, (c) Samples during drying cycle at 20°C with installed redox electrodes and suction cups, (d) samples during rewetting cycle at 20°C.

2.3. Chemical analyses

Total concentrations of major and trace elements (Al, As, Ca, Cd, Cr, Cu, Fe, K, Mg, Mn, Na, Ni, P, Pb, Zn) in sediment and soil samples were determined after drying at 105°C and homogenization using a planetary ball mill. For acid digestion, 0.5 g of homogenized sample was mixed with 5 ml Milli-Q water, 10 ml 65% HNO_3 (EMSURE, Merck), and 3 ml 37% HCl (ACS reagent, Sigma-Aldrich) in PTFE vessels. Samples were heated to 190 °C for 14 min in a microwave system (START 1500, MLS GmbH) following manufacturer's protocol (method E701). Digests were filtered (Mn 619 G1/4, Macherey-Nagel) and analyzed by ICP-OES (Analytik Jena Specord 200 plus, Germany). Total phosphorus (TP) was measured axial at 213.617 nm (IDL 0.0034–0.0036 mg l^{-1}), and quality controls are provided in supporting information **Table B-S3** and supporting information **Table C-S2.**

Porewater was analyzed for major and trace elements (Al, As, Ca, Cu, K, Mg, Mn, Na, P, Ti, Zn) using ICP-OES. Inorganic phosphate (P_i) was determined photometrically at 880 nm with a Continuous Flow Analyzer (CFA, Analytical AutoAnalyzer 3, SEAL, Germany) using the molybdenum-blue method (Nagul et al., 2015). Acid mono-phosphatase activity (APA) was assessed according to Tabatabai and Bremner (1969), modified by Schinner et al. (2012) and DIN EN ISO 20130; P_i concentrations were measured

by UV-VIS (Analytik Jena Specord 200 plus). Water content (WC) of samples was assessed at each step using a halogen dryer (HB43-S, Mettler Toledo) to calculate dry-weight-based concentrations. Total alkalinity (TA) was determined by titration (MColortest, Merck), and pH was measured in 0.01 M $CaCl_2$ solution following DIN ISO 10390 using a pH meter (WTW pH 3310, glass electrode WTW Plus SenTix 81). For methodological details of the sample analyzing procedure, the reader is referred to the chemical analyses of **Section B and Section C**.

The sequential extraction for assessing different operationally defined P pools in soil and sediment (**Section B** and **Section C**)was carried out following a modified procedure after Hedley (Hedley et al., 1982). In brief, after porewater was removed, 0.5g (equivalent dry weight) of samples were removed from glass jars and subsequently extracted with increasingly potent extraction solutions (0.5 M $NaHCO_3$, followed by 0.1M NaOH, CDB, 1M HCl and finally 0.5M H_2SO_4). The $NaHCO_3$-extractable pool is considered to represent 'labile P_i and P_o' that is loosely adsorbed to mineral surfaces and organic matter (Mattingly et al., 1975). This pool is considered readily bioavailable and is characterized by fast turnover rates (Negassa and Leinweber, 2009; Tiessen, 1993). The second step using NaOH solution is interpreted as moderately labile P, including more stable forms of P_o (e.g., detritus Po) and strongly bound P_i (associated with Al- and FeIII-(oxyhdr)oxides). Next, a citrate-dithionite-bicarbonate (CDB) extraction step followed (Ruttenberg, 1992). Valuable information can be obtained from this step allowing to assess P_i and P_o associated with reducible MnIV- and FeIII-(oxyhydr)oxides (Neidhardt et al., 2021). Under reducing conditions, this pool could rapidly turn from a sink into a source for P_i and P_o (Ajmone-Marsan et al., 2006; Dupas et al., 2015b). If this step is not included, the CDB-extractable P would be extracted by the following HCl-extraction step, a problem already recognized by Joshi et al. (2015). The following HCl-extraction step is commonly interpreted as P_i in primary and secondary minerals (e.g., apatite, octacalcium phosphate) and dominates in Ca-carbonate-rich environments (Eriksson et al., 2016). However, it could also contain P_i and P_o associated with Fe(II)-minerals such as siderite and strengite (Neidhardt et al., 2019). The final H_2SO_4 extraction step is summarized as non-extractable residual-P_i and P_o (Cross and Schlesinger, 1995). Both, HCl- and H_2SO_4-extractable P, are considered as stable and therefore not directly bioavailable P pools. Further details regarding the sequential extraction are provided in supporting information **Section B-S1**. Extraction solutions were analyzed for major and trace elements by ICP-OES, while P_i in the $NaHCO_3$, NaOH, and CDB extracts was also quantified photometrically by CFA. Organic phosphorus (P_o) was calculated as the difference between TP and P_i.

In addition, for DDS (**Section C**) microbial P (P_{mic},) was determined from fresh samples after the method of Kouno et al. (1995), modified by Bünemann et al. (2016) and measured as P_i by UV-VIS, see supporting information **Section C-S1.** For validation of P speciation in different pools, ^{31}P- Nuclear magnetic resonance analyzes (Bruker Avance 600 MHz High Resolution FT-NMR) were carried out for selected sequential extracts of DDS (external analyzes provided by the Central Institute for Engineering, Electronics and Analytics ZEA, Jülich, see supporting information **Section C-S3**). For the isotopic analyses for DDS, P_i in the respective extraction solutions ($NaHCO_3$, NaOH, CDB and HCl) was purified following the protocol of Tamburini et al. (2018) and Joshi et al. (2015). Due to the high methodological

effort, isotopic analyzes of $\delta^{18}O_{Pi}$ values were conducted for 4 time points (initial sample material, after 1 day, after 4 weeks (SPL), respectively 8 weeks (LPL, L) and after 24 weeks). For methodological details of the sample preparation procedure, the reader is referred to supporting information **Section C-S1**. The purified Ag_3PO_4 was finally analyzed in duplicates for $\delta^{18}O_{Pi}$ with a Thermal Conversion Elemental Analyzer (vario PYRO cube, Elementar Analysensysteme GmbH, Langenselbold, Germany) in pyrolysis mode at 1450 °C, coupled to a Continuous Flow Isotope Ratio Mass Spectrometer (IRMS, Isoprime 100, Elementar Analysensysteme GmbH, Langenselbold, Germany). Oxygen isotope ratios are presented in the $\delta^{18}O$ notation as ‰ deviation values related to the VSMOW (Vienna Standard Mean Oceanic Water) international reference standard. International certified reference materials (USGS80, $\delta^{18}O$ = +13.1 ‰; USGS81, $\delta^{18}O$ = +35.4 ‰; Benzoic Acid (IAEA 601), $\delta^{18}O$ = 23.1‰) were used for instrumental calibration and as quality control. Furthermore, an in-house standard (KH_2PO_4, $\delta^{18}O$ = ~13.5 ‰, Fisher Chemical, p.a. ≥99%) was included for checking the reproducibility. The results showed a good accuracy and reproducibility for all reference standard materials, see supporting information **Table C-S3** and **Figure C-S2.** The theoretical oxygen isotopic signature of P_i in equilibrium with pore water ($\delta^{18}O_{Pi\text{-}equ}$) was calculated after Chang and Blake (2015). Differences between calculated $\delta^{18}O_{Pi\text{-}equ}$ and observed $\delta^{18}O_{Pi}$ of a respective P pool are presented as $\Delta^{18}O_{Pi}$ values. Note that negative $\Delta^{18}O_{Pi}$ values indicate higher observed $\delta^{18}O_{Pi}$ than theoretical $\delta^{18}O_{Pi\text{-}equ}$ values (supporting information **Table C-S4**). All data for DDS (**Section C**) are published in the repository (Nagel et al., 2025).

2.4. Statistical analyses and software

Unless otherwise stated, all sample analyses were conducted as true triplicates, and reported values represent mean ± standard deviation. Statistical analyses were performed using Microsoft Excel (versions 1808 and 365, 2019 MSO/2403) and IBM SPSS Statistics (version 29). Data were tested for normality using the Shapiro-Wilk test ($p > 0.05$) and for homogeneity of variances using Levene's test ($p > 0.05$).

To assess statistically significant differences over time within treatments, repeated measures ANOVA was applied ($\alpha = 0.05$), with sampling time as the independent variable (within-subject) and hydrological treatments (SPL, LPL, L) as dependent variables (between-subject). Differences between treatments at each time point were tested using one-way ANOVA. When required, post hoc comparisons were conducted using the least significant difference (LSD) test. Paired t-tests were applied to compare specific time points or treatment pairs.

Figures were generated using Microsoft Excel 365 (version 2403). Literature review was performed via Google Scholar (Alphabet) and Web of Science (Clarivate) and supplemented with Scite (scite.ai). Language editing support was provided by DeepL (DeepL SE) and ChatGPT-4o (OpenAI).

3. General results and discussion

The experimental studies presented in this dissertation investigated P dynamics across contrasting agricultural land-water interface systems, including non-calcareous vegetated buffer strip soils (VBS, **Section B**), undisturbed forest soils (FST, **Section B**), and drainage ditch sediments (DDS, **Section C**). Despite pronounced differences in environmental setting, hydrological regime, and land-use history, all systems exhibited marked temporal shifts in P pool distribution following P_i addition. This underscores the necessity of time-resolved, process-based approaches to adequately capture P cycling at agricultural interfaces. The first experiment (**Section B**) focused on VBS soils and assessed how legacy P saturation, microbial activity, and fluctuating hydrological conditions regulate P retention, transformation, and mobility following additional P_i input. The FST (**Section B**), unaffected by agricultural P loading, served as a reference system to contrast P dynamics under unsaturated sorption conditions. The second experiment investigated short- to long-term transformations of ^{18}O-enriched P_i ($\delta^{18}O_{Pi}$) in DDS (**Section C**) under contrasting hydrological and redox regimes, with particular emphasis on Fe-associated pathways, microbial turnover, and the potential formation of stable P pools.

Across all systems, P dynamics were governed by the interplay of physicochemical and biological processes, notably pH buffering, redox fluctuations, mineral sorption capacity, and microbial activity. Despite clear differences in land-use history, soil properties (e.g., pH values), and hydrological regimes, all systems (VBS, FST and DDS) showed an initial rapid redistribution of added P_i into labile pools, followed by divergent mid- to long-term transformation pathways that reflect their contrasting biogeochemical constraints. Hydrological forcing-controlled oxygen availability and redox conditions, thereby influencing Fe(III)-(oxyhydr)oxide dynamics and associated P binding, while microbial processes mediated both the mineralization of P_o and the redistribution of P_i among labile and mineral-associated pools. The relative importance of these processes differed strongly among systems, reflecting contrasts in legacy P status, mineralogical constraints, and microbial resilience.

In VBS, FST (**Section B**) and DDS (**Section C**), the first 24 hours after P_i addition were characterized by a rapid enrichment of porewater-P_i and $NaHCO_3$-extractable P_i, consistent with fast surface adsorption to mineral and organic surfaces (Barrow, 1984; Helfenstein et al., 2018; Joshi et al., 2016). This initial partitioning reflects the dominance of weak, reversible sorption reactions and confirms that freshly added P_i is highly mobile irrespective of system type. However, the subsequent fate of this P_i diverged markedly between legacy P-affected systems (VBS, DDS) and the non-legacy FST.

Over the 16-week incubation in VBS (**Section B**), water content did not differ significantly between short- (SPL) and long-pulsed (LPL) drying-rewetting regimes during either dry or wet phases. In contrast, redox conditions differed markedly between treatments (**Table B-2 a, b**, **Figure B- S1**). Both regimes showed a rapid drop in redox potential after the first rewetting, followed by alternating weakly to moderately reducing conditions during wet phases and more oxidizing conditions during dry phases, with stronger redox oscillations in the SPL treatment. Soil and porewater pH (**Table B-S4**, **Figure B-S2**) remained stable throughout the incubation, indicating limited pH control on P dynamics. The TA (**Table B-S4**, **Figure B-S3 a, b**) declined significantly in both treatments, while dissolved Fe

concentrations remained unchanged. The APA (**Table B-S4**, **Figure B-S3 c, d**) increased over time in both regimes, reflecting sustained microbial and enzymatic activity. Temperature differences (20 °C vs. 5 °C) had no significant effect on pH, alkalinity, or enzyme activity, but influenced redox dynamics, with SPL showing more pronounced redox fluctuations than LPL.

Throughout the 16-week incubation, a large proportion of added P_i remained in labile pools with only minor transfer (6–8%) into NaOH-extractable P_i (**Figure 2 g, h**). At the end of the incubation, porewater-P_i (**Figure B-2 a, b**) and $NaHCO_3$-extractable P_i (**Figure B-2 c, d**) were still significantly higher as compared to the initial soil (porewater-P_i: +0.1 to 0.3%, $NaHCO_3$-P_i: +9 to +12%). The small transfer into the NaOH-extractable P_i pool reflects limited stabilization due to strong legacy P saturation, where Al- and Fe-(oxyhydr)oxide sorption sites are already largely occupied (Doydora et al., 2020; Neidhardt et al., 2019; Ramler et al., 2024). The high initial abundance of NaOH-extractable P_i further indicates near-saturation of Fe(III)-(hydr)oxide surfaces, constraining additional P_i retention. In addition, contrary to expectations, we did not observe substantial Fe(III) reduction during the wet phases. Generally, dissolved Fe concentrations in porewater and NaOH-extractable P_i (**Figure B-S4 a to d**) remained consistently low, indicating an absence of pronounced reductive dissolution. This observation supports my hypothesis i) for **Section B** that added P_i largely remains mobile (i.e., dissolved and exchangeable surface-bound P fractions) and, to a smaller extent, is retained in stable fractions (e.g., Fe(III)-bound P).

Small pH changes (<0.5 units) further constrained abiotic redistribution, confirming that non-calcareous, P-saturated soils are buffered against pH-driven sorption dynamics (Özkan et al., 2017). Contrary to expectations, drying-rewetting cycles did not induce pronounced Fe(III) reduction or P_i remobilization via reductive dissolution. Instead, increases in CDB-extractable Fe (**Figure B-S4 e, f**), particularly under short pulsed logging (SPL), point to rapid microscale Fe turnover and the accumulation of amorphous Fe(III)-(oxyhydr)oxides without detectable Fe(II) release (Roden et al., 2003).

In addition, microbial processes played a central role in VBS (**Section B**), as indicated by sustained APA and declining NaOH-extractable P_o (**Figure B-2 g, h**). These patterns suggest ongoing enzymatic hydrolysis of moderately labile P_o, releasing P_i that was subsequently reassociated with Fe minerals or incorporated into biofilm-associated pools, reinforced by oxidation and reduction changes (Khorshid et al., 2019). At the end of the 16 weeks, the NaOH-extractable P_o in the SPL treatment (8%) was lower than in the LPL treatment (15%). Here, cell lysis was obviously more pronounced under short fluctuations (SPL) as compared to long fluctuations (LPL). The concurrent increase in CDB-extractable P_o (**Figure B-2 k, l**), indicates that Fe(III)-(oxyhydr)oxide surfaces acted as hotspots for microbial colonization and biofilm formation, hosting a mixture of microbial residues, extracellular polymeric substances, and P_o compounds (Khorshid et al., 2019; Liu et al., 2021; Shi and Xu, 2019). The accumulation of CDB-extractable P_o, accompanied by elevated CDB-extractable Fe concentrations after 16 weeks in both treatments, strongly supports the involvement of Fe(III)-(oxyhydr)oxides as key stabilizing agents for P in this system. However, the CDB-extractable P_o fraction was slightly higher in the SPL treatment (+2%) suggests that short-term waterlogging may promote P stabilization via enhanced microbial activity and dynamic changes in Fe mineral phases, but the difference was not significant. Therefore, my hypothesis ii) for **Section B** was not supported, as short cycles of drying-

rewetting showed a more pronounced transfer of P_i and P_o into the CDB-extractable pools as compared to the long cycles. Nevertheless, this pattern indicates that under short hydrological fluctuations, a greater proportion of P_i may be incorporated into more stable organic forms associated with Fe-OM complexes, whereas under longer fluctuations P tends to remain in more weakly bound NaOH-extractable P_o pools. Thus, P stabilization in VBS occurred mainly via microbially mediated Fe-SOM associations rather than through large-scale redox-driven renewal of sorption sites. There were no significant changes in stable P pools (e.g., HCl- and H_2SO_4-extractable P_t) during the 16 weeks of incubation (**Figure B-S5**), indicating no formation of Ca-P, which may be due to the non-calcareous soil, but also to the duration of the incubation.

In summary for VBS (Section B), most added P remained in labile pools, with only minor transfer into NaOH- and CDB-extractable fractions over time, reflecting limited sorption capacity due to legacy P. Declining NaOH-extractable P_o (SPL) together with increasing CDB-bound P_i and P_o points to microbial hydrolysis and subsequent stabilization on Fe(III)-(hydr)oxide surfaces and biofilm-associated organic matter. This highlights the dominant role of microscale biogeochemical processes in controlling P retention in VBS soils under fluctuating hydrological conditions. Temperature effects (20°C, 5°C) in the P pool composition were observable for porewater P_i as well as $NaHCO_3$-extractable P_i, with consistently higher contributions at 5°C compared to the 20°C treatment in both treatments.

In FST (**Section B**), over 16 weeks, WC (**Table B-2 c, d**) did not differ significantly between the hydrological treatments, indicating comparable moisture conditions during both wet and dry phases. In contrast, pronounced temporal changes in porewater and soil pH (**Figure B-S9 a, b**) were observed in both treatments, with a rapid initial increase to alkaline values (>8) followed by a gradual decline towards near-neutral conditions. The TA (**Table B-S5**, **Figure B-S10 a, b**) increased over time, particularly under LPL, while dissolved Fe concentrations in porewater (**Figure B-S11 a, b**) decreased strongly, especially in SPL, suggesting limited Fe mobilization despite fluctuating redox conditions. The APA (**Table B-S5**, **Figure B-S10 c, d**) declined significantly in both treatments over the incubation period, indicating reduced microbial investment in P_o hydrolysis under sustained incubation. Temperature effects were secondary but evident under LPL, where higher temperature enhanced pH and alkalinity but reduced phosphatase activity. Overall, these results indicate that while hydrological regime had limited influence on bulk moisture status, it strongly modulated redox-sensitive and microbially mediated processes governing P dynamics.

In contrast to VBS, FST (**Section B**) exhibited a substantially higher capacity for P_i stabilization. Following initial adsorption into $NaHCO_3$-extractable P_i (+32%, **Figure B-4 c, d**), added P_i was efficiently redistributed into NaOH- (+42%) and CDB-extractable P_i (+4%) pools (**Figure B-4 e to h**) within weeks, reflecting strong sorption to Al- and Fe(III)-(oxyhydr)oxides (Brödlin et al., 2019; Gustafsson et al., 2012). The increase in CDB-extractable P_i indicates enhanced association of P with amorphous Fe(III)-(oxyhydr)oxides, likely promoted by repeated drying-rewetting cycles and Fe reoxidation. Concurrently, rising NaOH-extractable Pi reflects ongoing secondary P fixation. This redistribution was closely linked to a pronounced increase in pH from acidic towards neutral and slightly alkaline conditions, likely caused by vegetation removal, reduced rhizosphere acidification, and cation release during drying-rewetting

(Lu et al., 2016; Mao et al., 2017). These outcomes confirm my hypothesis iii) for **Section B** that without legacy P, P_i addition increases the relative proportion of more stable pools (NaOH-, CDB-extractable P_i).

In parallel, FST showed a strong buildup of $NaHCO_3$-extractable P_o (+16%, **FigureB-4 i, j**) accompanied by declines in $NaHCO_3$-extractable P_i (**Figure B-4 c, d**).) and NaOH-extractable P_o (**Figure B-4 e, f**). This pattern indicates strong microbially mediated immobilization of added P_i into organic P forms, which is characteristic of P-limited, organic-rich forest soils (Kunito et al., 2021; Liu et al., 2021; Zhou et al., 2017). Forest soils provide abundant substrates for rapid microbial assimilation and microorganisms can immobilize added P by incorporating it into cellular biomass or converting it into $NaHCO_3$-extractable P compounds through metabolic processes (He et al., 2023; Ramler et al., 2022). Elevated pH and abundant organic substrates likely stimulated microbial assimilation, resulting in the accumulation of labile, microbially derived P_o compounds (Kunito et al., 2021; Liu et al., 2020).

The Declines in $NaHCO_3$-extractable P_i and NaOH-extractable P_o indicate that P_i was mobilized both directly from porewater and via microbial mineralization of moderately labile P_o. Microbial phosphatases hydrolyze P_o, releasing P_i that is subsequently assimilated into biomass or transformed into labile organic P forms (Liu et al., 2021). Drying-rewetting cycles further enhance these processes by stimulating microbial turnover and P_o release during cell lysis, highlighting the key role of biotic activity over purely abiotic sorption (Chen et al., 2023; Zhang et al., 2023). Abiotic processes may also contribute to the rise in $NaHCO_3$-extractable P_o through transient organo-mineral complexes formed between organic P and SOM, alongside microbial assimilation (Dodd et al., 2015). Biotic and abiotic processes drive the observed decline in $NaHCO_3$-extractable P_i and NaOH-extractable P_o, alongside an increase in $NaHCO_3$-extractable P_o, as P_i is rapidly incorporated into microbial biomass and labile organic forms, with moisture fluctuations and redox changes modulating these transformations. Short drying-rewetting cycles (SPL) accelerate microbial turnover and P_o accumulation, while long cycles (LPL) slow P_o buildup and stabilization (Brödlin et al., 2019; van Dinh et al., 2018). The absence of significant differences between SPL and LPL suggests that the forest soil's high SOM content and well-established organo-mineral associations buffered microbial and abiotic P transformation processes against hydrological disturbance. Consequently, my hypothesis iv) for **Section B**, which proposed that long drying-rewetting cycles promote microbial adaptation and thus a more pronounced buildup of P_o compared to short cycles, cannot be confirmed.

In summary for FST (**Section B**), added P_i was first adsorbed onto mineral and organic surfaces, creating a dominant $NaHCO_3$-extractable P_i pool, before gradually transferring into more stable NaOH- and CDB-extractable P_i fractions. This process was driven by pH increases, Fe(III) reoxidation, and mineral precipitation, indicating that P_i addition stimulates secondary P fixation in forest soils. Concurrently, microbial uptake and abiotic adsorption increased $NaHCO_3$-extractable P_o, showing that in organic-rich, non-legacy forest soils, drying-rewetting cycles primarily enhance microbial assimilation and secondary P stabilization, irrespective of fluctuation duration. Temperature effects (20°C, 5°C) were clearly pronounced In the LPL treatment, with significantly higher contribution of NaOH-extractable P_i

at 20°C and significantly lower amounts of $NaHCO_3$- and NaOH-extractable P_o at 20°C compared to 5°C.

For DDS (**Section C**), the three treatments resulted in significant changes in several variables during 24 weeks of incubation. The variation in the WC, due to the the drying-rewetting cycles, in the pulsed logged treatments (SPL, LPL) influenced the E_h values. Here, the SPL and the LPL treatments showed pronounced changes between oxic and strongly reducing during the dry and wet cycles (**Table C-2, Figure C-S1**). However, in both treatments fluctuations in E_h values showing decreasing amplitudes and stabilized between 4 to 16 weeks in the range of slightly and moderately reducing conditions towards the end of each wet cycle and to oxic conditions during dry cycles. In contrast in the permanently waterlogged treatment (L) the E_h was constantly in a strongly reducing condition (**Figure C-S1**). Porewater pH (**Figure C-2 a to c)** increased in all treatments (> 8), while sediment pH (**Figure C-2 d to f**) remained slightly lower (around 7). I attribute this increase in pH to the growth and metabolic activity of microorganisms, which consumed dissolved CO_2 under saturated conditions, causing a decrease in $H_2CO_{3\,(aq)}$ and therefore H^+ concentrations (Lu et al., 2016). The TA (**Figure C-1**) decreased in SPL and LPL but initially increased in L, and dissolved Mn and Fe (**Figure C-S3**) peaked early in L before declining in all treatments. The impact of metabolic activity was further reflected by a decrease in TA and E_h and is linked of pH, TA and E_h to the microbial mineralization of organic matter (Bünemann et al., 2015; Husson et al., 2013). Microbial P (P_{mic}) initially rose during the first 4 weeks, then declined to near zero. The APA (**Figure C-3 d to f**) dropped in SPL and LPL during the first 4 weeks, stabilizing thereafter, whereas APA increased in L. Isotopic labeling ($\delta^{18}O_{H_2O}$, **Figure C-4 a to c**) showed rapid incorporation into porewater within 4 weeks, with higher values in L, driving corresponding $\delta^{18}O_{Pi}$ changes. ^{31}P NMR confirmed P_i presence in $NaHCO_3$- and NaOH-extractable pools (supporting information **Section C-S3**), while CDB and HCl pools were below detection. Lower incubation temperature (5°C) reduced sediment pH and $\delta^{18}O_{H_2O}$ values.

For P pools, DDS (**Section C**) displayed the most dynamic P cycling, driven by strong redox gradients and microbial stress under fluctuating or permanently waterlogged conditions. Similar to soils of VBS and FST, added P_i (here: $^{18}O_{Pi}$) was initially transferred into porewater- (**Figure C-5**) and $NaHCO_3$-extractable P_i (**Figure C-6 a to c**), thereby tripling its relative proportion (**Figure C-S4**). At near-neutral pH, P_i was initially present mainly as $H_2PO_4^-$ and HPO_4^{2-}, promoting adsorption onto mineral surfaces and soil organic matter, while porewater showed a rapid enrichment of dissolved P_i within 24 hours, highlighting its role as a transient P pool. This observation is in line with my hypothesis i) for **Section C** that applied P_i readily partitioned into porewater and the labile $NaHCO_3$-extractable P_i pool. Following the P concentration increase, $\delta^{18}O_{Pi}$ values (‰ VSMOW) of the $NaHCO_3$-extractable P_i pool increased by +117 ‰ (**Table 4**).

Subsequently, P_i was redistributed into NaOH-extractable P_i (**Figure C-6 d to f**) during the early phase (first 4 weeks), primarily driven by rising pH rather than by reductive dissolution of Fe(III)-(oxyhydr)oxides (Zhou et al., 2005). Reductive dissolution of Fe(III)-(oxyhydr)oxides was neither reflected in the NaOH-P_i pool, nor in the concentrations of dissolved Fe and Mn in porewater (**Figure C-S6**). Stable oxygen isotope data ($\delta^{18}O_{Pi}$, **Figure C-8**) revealed intensive microbial overprinting during

this phase, indicating intracellular P_i cycling and exchange of oxygen isotopes with ambient water prior to reassociation with mineral surfaces (Joshi et al., 2016; von Sperber et al., 2014). The isotopically heavier ^{18}O was released from the applied $^{18}O_{Pi}$ into porewater as $H_2{}^{18}O$ through intracellular enzymatic cycling, followed by the (re)release of P_i from microbial biomass and its transfer into the NaOH-extractable P_i pool. In the pulsed-logged treatments, the concurrently lower P_{mic} concentrations (**Figure C-3 d, e**) indicate that drying-induced microbial stress reduced biomass, thereby promoting P_i remobilization (Luo et al., 2022), most pronounced in the SPL treatment. Compared to the drying-rewetting treatments, the permanently waterlogged treatment (L) showed a lower proportion of $NaHCO_3$-extractable P_i (**Figure C-6 c**), indicating enhanced remobilization of labile P_i under sustained anoxic conditions (Zhang et al., 2021). At the same time, all treatments exhibited a slight but significant increase in CDB-extractable P_o (**Figure C-7 d to f**), suggesting ongoing microbially mediated transformation of P_i into Fe-associated organic P that intensified in the following weeks. My hypothesis ii) for **Section C** was partially confirmed, as labile P_i was transferred into the moderately labile NaOH-extractable P_i pool. Furthermore, microbial overprinting was visible in the $\delta^{18}O_{Pi}$ values prior to the transfer of P_i into the NaOH-extractable P_i pool. The higher P_{mic} concentrations in the LPL and L treatments suggest more favorable living conditions for microorganism, whereas other microbially induced effects were similar among all three treatments.

During the intermediate phase (4 to 8/16 weeks), a pronounced accumulation of CDB-extractable P_o (**Figure C-7 d to f**) occurred across all treatments, accompanied by an increase in NaOH-extractable P_o (**Figure C-7 a to c**) and H_2SO_4-extractable TP (**Figure C-6 m to o**), highlighting an underestimated but important pathway of temporary P immobilization. The CDB-extractable P_o pool likely represents biofilm-associated P_o bound to reducible Fe phases, formed through microbial assimilation, turnover, and the incorporation of organic residues on Fe(III)-(oxyhydr)oxide surfaces (Bi et al., 2024; Roden, 2003). I therefore assume that Fe(III)-oxides served as a primary host for the biofilms produced by the microorganisms (Bi et al., 2014; Jarvie et al., 2002; Wu et al., 2018), considering the pronounced proportion of CDB-extractable P_o and concentrations of CDB-extractable Fe (**Figure C-S6**). Regarding the relative proportions of the P pools, the CDB-P_o pool was significantly lower in the SPL and L treatments as in the LPL treatment, which we attribute to a slower microbially mediated conversion of P_i into P_o, resulting from highly unfavorable living conditions for microorganisms (Luo et al., 2022). In the L treatment, microorganisms initially adapted to anoxic conditions by shifting to Mn(IV)- and Fe(III)-reducing metabolisms, as indicated by rising dissolved Mn, Fe, (**Figure C-S3 c, f**) and TA, but after four weeks microbial activity declined markedly, reflected by decreasing Mn and Fe concentrations and a strong reduction in P_{mic} (**Figure C-3 c**). This microbial inhibition and partial dieback under prolonged anoxic conditions likely resulted from limited oxygen diffusion and toxic effects, with increased APA indicating cell lysis and release of extracellular enzymes, although effects on P pools became evident only later. In the drying-rewetting treatments (SPL, LPL), microbial conditions were also stressful, as shown by declining P_{mic} (**Figure C-3 a, b**), while temperature exerted a clear control on labile P_i dynamics, with higher $NaHCO_3$- and NaOH-extractable P_i at 20 °C, especially in LPL, indicating enhanced transformation of weakly bound P_i into Al- and Fe-associated pools at warmer temperatures. In the same period, in the L and LPL treatments, the $\delta^{18}O$ values in the NaOH-extractable P_i pool (**Figure**

C-8 d to f) increased despite concentration losses, indicating labeling without de-labeling, likely due to reduced microbial activity. In contrast, $\delta^{18}O$ in the $NaHCO_3$-extractable P_i pool (**Figure C-8 a to c)** decreased in LPL after 8 weeks, reflecting faster P_i exchange and ongoing microbial turnover, while the NaOH-extractable P_i pool remained more stable. In agreement with my hypothesis iii) for **Section C**, I observed a gradual build-up and subsequent decline of P_o, which is, however, particularly susceptible to drying and rewetting, as well as to lower temperatures, which both inhibit biologically mediated P transformation processes. However, this storage was transient. Continued hydrological stress led to microbial dieback, reflected by declining P_{mic}, while extracellular enzyme activity persisted (Schimel et al., 2018; Zhang et al., 2021).

In the late phase (8/16 to 24 weeks), the breakdown and mineralization of P_o resulted in declining CDB-extractable P_o and a renewed increase in $NaHCO_3$- and NaOH-extractable P_i (**Figure C-6**), indicating a shift back towards surface-adsorbed, potentially mobile P forms. This increase in surface-adsorbed P_i also corresponded to the observed increase in pH and concomitant decline in dissolved P_i concentrations in porewater (Barrow et al., 2020). In the L treatment, the CDB-extractable P_o pool (**Figure C-7 f**) was lowest, indicating that prolonged anoxic conditions suppressed microbial conversion of P_i into P_o. Strongly reducing redox conditions likely promoted transfer of Fe(III)-bound P_i into the labile $NaHCO_3$-extractable P_i pool, increasing P_i mobility and potential downstream eutrophication (Ajmone-Marsan et al., 2006). In the SPL treatment, microbial communities were more resilient to short drying-rewetting cycles, reflected in both P pool composition and minimal $\delta^{18}O_{Pi}$ label loss in the $NaHCO_3$-extractable P_i pool (**Figure C-8 a**) after 4 weeks. Over time, repeated cycles led to increased microbial adaptation, allowing continued activity and P turnover even under frequently fluctuating moisture conditions (De Nijs et al., 2019). In agreement with my hypothesis iv) for **Section C**, I observed microbial dieback, but, however, no concomitant release of P_i into the dissolved P pool. We also observed no concentration increase in the stable P pools (Ca-P_i). This lack of long-term P_i incorporation into the Ca-P_i pool could be linked to the general absence of $CaCO_3$ in the drainage ditch sediments, consequently rendering non-calcareous sediments especially unsuitable for the long-term fixation of P_i.

In summary, DDS (**Section C**) showed highly dynamic P cycling, with P_i initially accumulating in porewater and $NaHCO_3$-extractable P_i pools before partial transfer into NaOH-extractable P_i, largely driven by pH changes and microbial activity. Microbial processes also temporarily immobilized P in CDB-extractable P_o, particularly via biofilm formation on Fe(III)-(oxyhydr)oxides, but this pool was transient and declined under prolonged anoxia or drying-rewetting stress. Overall, labile P_i remained mobile, microbial communities adapted to frequent fluctuations, and long-term stabilization into Ca-P pools was limited due to the non-calcareous sediment composition. A temperature effect (20°C, 5°C) was evident in the removal of the $^{18}O_{Pi}$ label at 5 °C, which was less pronounced, as well as other properties such as P_{mic} and APA, suggesting that the microorganisms suffered greatly under the treatments applied and that microbial turnover was reduced at lower temperatures (von Sperber et al., 2015; Wallenstein et al., 2009).

Synthesizing across all systems (VBS, FST, DDS), clear contrasts in stabilization potential emerge. The FST (**Section B**) without legacy P showed the strongest and most persistent transfer of P_i into

moderately stable mineral-associated and organic pools. The VBS (**Section B**), despite their role as landscape filters, exhibited limited additional sorption capacity and relied mainly on microbial and Fe-associated microscale processes for short-term P retention. The DDS (**Section C**) functioned as highly dynamic, temporary P sinks, where microbial turnover and redox fluctuations continuously redistributed P between labile and moderately labile pools but prevented long-term immobilization, particularly in non-calcareous sediments lacking Ca-P stabilization pathways.

Overall, the results demonstrate that the duration and frequency of drying-rewetting cycles critically control whether VBS and DDS act as temporary sinks or sources of phosphorus along the transfer continuum. It appears that long-pulsed drying-rewetting (LPL) favored repeated redistribution of P between labile and Fe-associated pools, promoting the mobilization of legacy P from VBS (**Section B**) and its subsequent transfer into drainage ditches (**Section C**). Under continued hydrological variability, especially under prolonged waterlogging (L), DDS functioned as transient P buffers rather than long-term sinks, facilitating the onward transport of remobilized P to surface waters and thereby increasing the risk of downstream eutrophication under climate change.

The findings suggest that P retention at agricultural land-water interfaces is governed by firmly coupled microscale interactions between hydrological variability, microbial activity, Fe mineral dynamics, and legacy P saturation, rather than by bulk redox conditions or mineralogy alone. Both VBS (**Section B**) and DDS (**Section C**) acted as short-term sinks for added P_i, primarily through rapid surface adsorption and transient microbial immobilization. However, their long-term effectiveness was strongly constrained once sorption sites were saturated or microbial stress and redox fluctuations destabilized previously immobilized P pools, leading to renewed accumulation of labile P_i fractions. In contrast, the FST (**Section B**), unaffected by historical P inputs, exhibited a high intrinsic capacity for sustained P sequestration through efficient transfer into Al- and Fe-associated pools and microbial incorporation into P_o, highlighting the critical role of land-use history and sorption site availability.

4. Conclusion

This dissertation addressed critical knowledge gaps regarding P retention and remobilization via the transfer continuum, based on the examples of VBS (**Section B**) and DDS (**Section C**), two widespread but mechanistically understudied interface systems in agricultural landscapes. While VBS are widely implemented to reduce P transfer from arable land to surface waters, and wetlands and river sediments have been extensively studied as P sinks, considerably less is known about how VBS and DDS respond to fluctuating hydrological and redox conditions, particularly in non-calcareous systems. Most previous studies have focused on long-term P accumulation or steady-state conditions, leaving short- to medium-term transformations among labile, mineral-associated, and organic P pools largely unresolved. This gap is especially critical in the context of climate change, which is expected to intensify drying-rewetting cycles and extreme rainfall events, thereby increasing the mobilization and re-release of legacy P from agricultural catchments.

The experimental results demonstrate that P dynamics at the agricultural land-water interfaces are strongly constrained by legacy P status, mineralogical properties, specifically the absence of Ca carbonates and the dominance of Fe(III)-(oxyhydr)oxides, and hydrological variability. In VBS (**Section B**) with a long history of agricultural P inputs, the capacity to retain additional P_i in stable pools was markedly limited. A large proportion of added P persisted in mobile and exchangeable fractions, while only minor amounts were incorporated into more stable Fe-associated P_i and P_o pools. This pattern indicates strong sorption site saturation and a high susceptibility of VBS soils to P_i remobilization under fluctuating drying-rewetting conditions. Consequently, continued P_i inputs from adjacent arable fields may undermine the nutrient retention function of buffer strips in non-calcareous systems, increasing the risk of P leaching and downstream eutrophication under climate-driven hydrological variability.

In contrast, the non-legacy FST (**Section B**) exhibited a substantially higher capacity for long-term P_i stabilization. Efficient transfer of P_i into Al- and Fe-associated pools, together with increasing surface-bound organic P fractions, indicated that P_i inputs stimulated microbial assimilation and enzymatic cycling, promoting temporary immobilization in organic pools. These coupled abiotic and biotic processes highlight the strong buffering capacity of soils without prior P saturation, even under altered hydrological regimes, and underscore the fundamental importance of land-use history for evaluating P retention potential.

The DDS (**Section C**) functioned as highly dynamic, short- to mid-term P storage systems. Although net changes in total P pools over the 24-week incubation were small, temporally resolved measurements and $^{18}O_{Pi}$ labeling revealed pronounced internal transformations driven by pH-dependent adsorption, microbial uptake, and biofilm formation on Fe(III)-(oxyhydr)oxide surfaces. Under prolonged hydrological stress, microbial biomass declined, yet extracellular enzyme activity persisted, sustaining organic P mineralization and continued P cycling. Microbial decay and P_o mineralization ultimately led to renewed enrichment of surface-bound labile P_i, demonstrating that long-term P retention in DDS is dominated by reversible sorption processes rather than the formation of stable mineral P phases.

Taken together, these findings show that VBS (**Section B**) and DDS (**Section C**) can act as effective short-term sinks for agricultural P inputs, but their long-term effectiveness is inherently limited once sorption capacities are saturated or when hydrological and redox conditions fluctuate. The FST (**Section B**) provide a contrasting reference system, illustrating the stabilization potential of non-legacy soils with unsaturated mineral surfaces and active microbial immobilization. Overall, this dissertation underscores the necessity of explicitly considering temporal dynamics, microbial processes, and legacy P saturation when assessing P retention at land-water interfaces. Small but highly dynamic landscape elements such as buffer strips and drainage ditches represent critical control points for P transfer from agricultural land to surface waters. When their storage capacities are exceeded or destabilized, they may rapidly shift from sinks to sources of P. These insights emphasize the need for site-specific nutrient management strategies that limit further P accumulation, account for hydrological variability, and acknowledge the central role of microscale biogeochemical processes in regulating P mobility under climate-driven changes in redox and moisture regimes.

5. Outlook

For VBS and FST (**Section B**) future research should place stronger emphasis on the dynamics of specific P_o pools across systems with contrasting P legacies. In particular, mechanistic insights into microbial transformation pathways, enzymatic regulation, and the formation and breakdown of organo-mineral complexes are needed to better disentangle the interplay between biotic and abiotic processes controlling P retention and release. Comparative studies across legacy and non-legacy systems would help to clarify how prior P saturation constrains stabilization pathways and alters microbial P cycling. In addition, future work should explicitly address the effects of fertilizer type, application frequency, and long-term input regimes on soil P dynamics. Repeated P additions may fundamentally alter nutrient cycling, microbial community structure, and the balance between P_i and P_o pools, particularly in soils with contrasting P histories. Integrating experimental approaches with long-term field observations will be crucial to evaluate how management practices interact with hydrological variability and climate-induced changes in drying-rewetting frequency. Such knowledge is essential for developing and optimizing buffer strip and land-use management strategies aimed at minimizing P losses from agricultural catchments under future climate conditions.

Future studies on DDS (**Section C**) should explicitly acknowledge that key P transformation processes can only be resolved through temporally high-resolution monitoring. The present study revealed that the CDB-extractable P_o pool represents an important, yet often overlooked, mid-term P storage compartment. This finding highlights that P_o dynamics should not be underestimated, particularly in biologically active environments characterized by strong hydrological variability, such as small, nutrient-rich streams and drainage ditches in agricultural landscapes. The results of this dissertation further indicate that long-term P_i retention in non-calcareous DDS is primarily governed by reversible surface adsorption processes rather than by the formation of stable mineral P phases. This implies a high sensitivity of sediment-bound P to changing redox and moisture conditions, with potential consequences for P remobilization during hydrological extremes. Future research should therefore combine sequential extraction, isotopic tracing, and microbial analyses to better quantify the stability, turnover, and reactivation potential of sedimentary P pools. Overall, these findings emphasize the role of small streams and drainage ditches as critical interim P storage zones situated between arable land and downstream water bodies. This connectivity should be more explicitly considered in catchment-scale management strategies aimed at reducing P export, particularly under climate scenarios that promote more frequent drying-rewetting cycles and extreme flow events.

6. References

Ad-hoc-AG Boden (2005): Bodenkundliche Kartieranleitung, 5. Auflage, Hannover.

Ajmone-Marsan, F., Côté, D., & Simard, R. R. (2006). Phosphorus transformations under reduction in long-term manured soils. Plant and soil, 282, 239-250. https://doi.org/10.1007/s11104-005-5929-6.

Bai, J., Ye, X., Jia, J., Zhang, G., Zhao, Q., Cui, B., & Liu, X. (2017). Phosphorus sorption-desorption and effects of temperature, pH and salinity on phosphorus sorption in marsh soils from coastal wetlands with different flooding conditions. Chemosphere, 188, 677-688. https://doi.org/10.1016/j.chemosphere.2017.08.117.

Barrow, N. J. (1984). Modelling the effects of pH on phosphate sorption by soils. Journal of Soil Science, 35(2), 283-297. https://doi.org/10.1111/j.1365-2389.1984.tb00283.x.

Barczok, M., Smith, C., Di Domenico, N., Kinsman-Costello, L., Singer, D., & Herndon, E. (2023). Influence of contrasting redox conditions on iron (oxyhydr) oxide transformation and associated phosphate sorption. Biogeochemistry, 166(2), 87-107. https://doi.org/10.1007/s10533-023-01094-z.

Bauke, S. L., Wang, Y., Saia, S. M., Popp, C., Tamburini, F., Paetzold, S., ... & von Sperber, C. (2022). Phosphate oxygen isotope ratios in vegetated riparian buffer strip soils. Vadose Zone Journal, 21(3), e20193. https://doi.org/10.1002/vzj2.20193.

Bennett, E. M., Carpenter, S. R., & Caraco, N. F. (2001). Human impact on erodable phosphorus and eutrophication: a global perspective: increasing accumulation of phosphorus in soil threatens rivers, lakes, and coastal oceans with eutrophication. BioScience, 51(3), 227-234. https://doi.org/10.1641/0006-3568(2001)051.

Bi, Z., Liu, Y., Rutoh, W. C., & Huang, Y. (2024). Influence of operation sequences on phosphorus recovery by polyphosphate-accumulating organisms biofilm: Performance, kinetics and metabolic response. Journal of Water Process Engineering, 61, 105356. https://doi.org/10.1016/j.jwpe.2024.105356.

Blake, R. E., O'Neil, J. R., & Surkov, A. V. (2005). Biogeochemical cycling of phosphorus: insights from oxygen isotope effects of phosphoenzymes. American Journal of Science, 305(6-8), 596-620. https://doi.org/10.2475/ajs.305.6-8.596.

Brödlin, D., Kaiser, K., Kessler, A., & Hagedorn, F. (2019). Drying and rewetting foster phosphorus depletion of forest soils. *Soil Biology and Biochemistry*, *128*, 22-34. https://doi.org/10.1016/j.soilbio.2018.10.001.

Bünemann, E. K. (2015). Assessment of gross and net mineralization rates of soil organic phosphorus–A review. Soil Biology and Biochemistry, 89, 82-98. https://doi.org/10.1016/j.soilbio.2015.06.026.

Carpenter, S. R. (2005). Eutrophication of aquatic ecosystems: bistability and soil phosphorus. Proceedings of the National Academy of Sciences, 102(29), 10002-10005. https://doi.org/10.1073/pnas.0503959102.

Chen, J., Xu, H., Seven, J., Zilla, T., Dippold, M. A., & Kuzyakov, Y. (2023). Microbial phosphorus recycling in soil by intra-and extracellular mechanisms. ISME Communications, 3(1), 135. https://doi.org/10.1038/s43705-023-00340-7.

Chen, X., Yan, X., Wang, M., Cai, Y., Weng, X., Su, D., ... & Zhang, F. (2022). Long-term excessive phosphorus fertilization alters soil phosphorus fractions in the acidic soil of pomelo orchards. Soil and Tillage Research, 215, 105214. https://doi.org/10.1016/j.still.2021.105214.

Cole, L. J., Stockan, J., & Helliwell, R. (2020). Managing riparian buffer strips to optimise ecosystem services: A review. *Agriculture, ecosystems & environment*, *296*, 106891. https://doi.org/10.1016/j.agee.2020.106891.

Cross, A. F., & Schlesinger, W. H. (1995). A literature review and evaluation of the. Hedley fractionation: Applications to the biogeochemical cycle of soil phosphorus in natural ecosystems. Geoderma, 64(3-4), 197-214. https://doi.org/10.1016/0016-7061(94)00023-4.

De Nijs, E. A., Hicks, L. C., Leizeaga, A., Tietema, A., & Rousk, J. (2019). Soil microbial moisture dependences and responses to drying–rewetting: the legacy of 18 years drought. Global Change Biology, 25(3), 1005-1015. https://doi.org/10.1111/gcb.14508.

Dieter, D., Herzog, C., & Hupfer, M. (2015). Effects of drying on phosphorus uptake in re-flooded lake sediments. Environmental Science and Pollution Research, 22, 17065-17081. https://doi.org/10.1007/s11356-015-4904-x.

DIN EN ISO 20130:2021-02: Bodenbeschaffenheit - Messung von Enzymaktivitätsmustern in Bodenproben mit kolorimetrischen Substraten in Mikrotiterplatten (ISO 20130:2018); Deutsche Fassung EN ISO 20130:2020.

DIN ISO 10390 (2005): Bodenbeschaffenheit—Bestimmung des pH Wertes. ISO 10390.

DIN ISO 11465 (1996-12). Bodenbeschaffenheit-Bestimmung der Trockensubstanz und des Wassergehalts auf Grundlage der Masse-Gravimetrisches Verfahren (ISO 11465: 1993).

Doydora, S., Gatiboni, L., Grieger, K., Hesterberg, D., Jones, J. L., McLamore, E. S., ... & Duckworth, O. W. (2020). Accessing legacy phosphorus in soils. *Soil systems*, *4*(4), 74. https:// doi:10.3390/soilsystems4040074.

Dupas, R., Delmas, M., Dorioz, J. M., Garnier, J., Moatar, F., & Gascuel-Odoux, C. (2015). Assessing the impact of agricultural pressures on N and P loads and eutrophication risk. Ecological Indicators, 48, 396-407. https://doi.org/10.1016/j.ecolind.2014.08.007.

Efobo O. (2023). Transport of Suspended Sediments and Phosphorus in an Agricultural Watershed: A Case Study of the Money Creek Watershed, Central Illinois (Master's thesis, Illinois State University). https://doi.org/10.30707/ETD2023.20231004061828269197.999980.

Eriksson, A. K., Hesterberg, D., Klysubun, W., & Gustafsson, J. P. (2016). Phosphorus dynamics in Swedish agricultural soils as influenced by fertilization and mineralogical properties: Insights gained from batch experiments and XANES spectroscopy. Science of the Total Environment, 566, 1410-1419. https://doi.org/10.1016/j.scitotenv.2016.05.225.

Gross, A., & Angert, A. (2015). What processes control the oxygen isotopes of soil bio-available phosphate. Geochimica et Cosmochimica Acta, 159, 100-111. https://doi.org/10.1016/j.gca.2015.03.023.

Gustafsson, J. P., Mwamila, L. B., & Kergoat, K. (2012). The pH dependence of phosphate sorption and desorption in Swedish agricultural soils. Geoderma, 189, 304-311. https://doi.org/10.1016/j.geoderma.2012.05.014.

Habibiandehkordi, R., Lobb, D. A., Owens, P. N., & Flaten, D. N. (2019). Effectiveness of vegetated buffer strips in controlling legacy phosphorus exports from agricultural land. Journal of environmental quality, 48(2), 314-321. https://doi:10.2134/jeq2018.04.0129.

Haygarth, P. M., Condron, L. M., Heathwaite, A. L., Turner, B. L., & Harris, G. P. (2005). The phosphorus transfer continuum: linking source to impact with an interdisciplinary and multi-scaled approach. Science of the total environment, 344(1-3), 5-14. https://doi.org/10.1016/j.scitotenv.2005.02.001.

Haygarth, P. M., Jarvie, H. P., Powers, S. M., Sharpley, A. N., Elser, J. J., Shen, J., ... & Liu, X. (2014). Sustainable phosphorus management and the need for a long-term perspective: The legacy hypothesis. https://doi: 10.1021/es502852s.

He, L. P., Jia, K. T., Liu, D., Wang, K. H., Duan, L. Y., & Lin, J. J. (2023). Effects of phosphorus fertilizer application rate on transformation processes of phosphorus fractions in the purple alluvial soil of a riparian zone. Journal of Mountain Science, 20(6), 1561-1574. https://doi.org/10.1007/s11629-022-7707-9.

Hedley, M. J., Stewart, J. W. B., & Chauhan, B. (1982). Changes in inorganic and organic soil phosphorus fractions induced by cultivation practices and by laboratory incubations. Soil Science Society of America Journal, 46(5), 970-976. https://doi.org/10.2136/sssaj1982.03615995004600050017x.

Helfenstein, J., Tamburini, F., von Sperber, C., Massey, M. S., Pistocchi, C., Chadwick, O. A., ... & Frossard, E. (2018). Combining spectroscopic and isotopic techniques gives a dynamic view of phosphorus cycling in soil. Nature communications, 9(1), 3226. https://doi.org/10.1038/s41467-018-05731-2.

Hille, S., Graeber, D., Kronvang, B., Rubæk, G. H., Onnen, N., Molina-Navarro, E., ... & Stutter, M. I. (2019). Management options to reduce phosphorus leaching from vegetated buffer strips. *Journal of environmental quality*, *48*(2), 322-329. https:// doi:10.2134/jeq2018.01.0042.

Hoffmann, C. C., Kjaergaard, C., Uusi-Kämppä, J., Hansen, H. C. B., & Kronvang, B. (2009). Phosphorus retention in riparian buffers: review of their efficiency. *Journal of environmental quality*, *38*(5), 1942-1955. https://doi.org/10.2134/jeq2008.0087.

Jaisi, D. P., & Blake, R. E. (2010). Tracing sources and cycling of phosphorus in Peru Margin sediments using oxygen isotopes in authigenic and detrital phosphates. Geochimica et Cosmochimica Acta, 74(11), 3199-3212. https://doi.org/10.1016/j.gca.2010.02.030.

Jeppesen, E., Kronvang, B., Meerhoff, M., Søndergaard, M., Hansen, K. M., Andersen, H. E., ... & Olesen, J. E. (2009). Climate change effects on runoff, catchment phosphorus loading and lake ecological state, and potential adaptations. Journal of environmental quality, 38(5), 1930-1941. https://doi.org/10.2134/jeq2008.0113.

Joshi, S. R., Kukkadapu, R. K., Burdige, D. J., Bowden, M. E., Sparks, D. L., & Jaisi, D. P. (2015). Organic matter remineralization predominates phosphorus cycling in the mid-bay sediments in the Chesapeake Bay. Environmental science & technology, 49(10), 5887-5896. https://doi.org/10.1021/es5059617.

Joshi, S. R., Li, X., & Jaisi, D. P. (2016). Transformation of phosphorus pools in an agricultural soil: An application of oxygen-18 labeling in phosphate. Soil Science Society of America Journal, 80(1), 69-78. https://doi.org/10.2136/sssaj2015.06.0219.

Khorshid, M. S. H., Kruse, J., Semella, S., Vohland, M., Wagner, J. F., & Thiele-Bruhn, S. (2019). Phosphorus fractions and speciation in rural and urban calcareous soils in the semiarid region of Sulaimani city, Kurdistan, Iraq. *Environmental Earth Sciences*, *78*(16), 531. https://doi.org/10.1007/s12665-019-8543-2.

Kleinman, P., Sharpley, A., Buda, A., McDowell, R., & Allen, A. (2011). Soil controls of phosphorus in runoff: Management barriers and opportunities. Canadian Journal of Soil Science, 91(3), 329-338. https://doi.org/10.4141/cjss09106.

Kouno, K., Tuchiya, Y., & Ando, T. (1995). Measurement of soil microbial biomass phosphorus by an anion exchange membrane method. Soil Biology and Biochemistry, 27(10), 1353-1357. https://doi.org/10.1016/0038-0717(95)00057-L.

Kunito, T., Haraguchi, S., Hanada, K., Fujita, K., Moro, H., Nagaoka, K., & Otsuka, S. (2021). pH is the dominant factor controlling the levels of phytate-like and DNA-like phosphorus in 0.5 M NaHCO3-extracts of soils: Evaluation with phosphatase-addition approach. *Geoderma*, *398*, 115113. https://doi.org/10.1016/j.geoderma.2021.115113.

Lannergård EE, Agstam-Norlin O, Huser BJ, Sandström S, Rakovic J, Futter MN. (2020). New insights into legacy phosphorus from fractionation of stream bed sediment. Journal of Geophysical Research: Biogeosciences 125(9). https://doi.org/10.1029/2020JG005763.

Leibundgut, C., & Eisele, M. (2005). Weiterentwicklung des Bewertungsverfahrens „Hydrologische Güte "als Expertensystem zum operationellen Einsatz im Flussgebietsmanagement. Abschlußbericht–Programm Lebensgrundlage Umwelt und ihre Sicherung, FKZ BWC.

Liang, Y., & Blake, R. E. (2006). Oxygen isotope signature of Pi regeneration from organic compounds by phosphomonoesterases and photooxidation. Geochimica et Cosmochimica Acta, 70(15), 3957-3969. https://doi.org/10.1016/j.gca.2006.04.036.

Liu, J., Lu, H., Wu, L., Kerr, P. G., & Wu, Y. (2021). Interactions between periphytic biofilms and dissolved organic matter at soil-water interface and the consequent effects on soil phosphorus fraction changes. Science of the Total Environment, 801, 149708. https://doi.org/10.1016/j.scitotenv.2021.149708.

Longinelli, A., & Nuti, S. (1973). Revised phosphate-water isotopic temperature scale. Earth and Planetary Science Letters, 19(3), 373-376. https://doi.org/10.1016/0012-821X(73)90088-5.

Lu, H., Wan, J., Li, J., Shao, H., & Wu, Y. (2016). Periphytic biofilm: A buffer for phosphorus precipitation and release between sediments and water. Chemosphere, 144, 2058-2064. https://doi.org/10.1016/j.chemosphere.2015.10.129.

LUBW. (2015). Abschätzung der erforderlichen Reduzierung von Nährstoffeinträgen in die Fließgewässer Baden-Württembergs. Place published: LUBW Landesanstalt für Umwelt, Messungen und Naturschutz Baden-Württemberg, Karlsruhe.

Lucas, E., Kennedy, B., Roswall, T., Burgis, C., & Toor, G. S. (2023). Climate change effects on phosphorus loss from agricultural land to water: a review. Current Pollution Reports, 9(4), 623-645. https://doi.org/10.1007/s40726-023-00282-7.

Mao, Q., Lu, X., Zhou, K., Chen, H., Zhu, X., Mori, T., & Mo, J. (2017). Effects of long-term nitrogen and phosphorus additions on soil acidification in an N-rich tropical forest. *Geoderma*, *285*, 57-63. https://doi.org/10.1016/j.geoderma.2016.09.017.

Mayer, N., & Kaltschmitt, M. (2022). Closing the phosphorus cycle: Current P balance and future prospects in Germany. Journal of cleaner production, 347, 131272. https://doi.org/10.1016/j.jclepro.2022.131272.

Mattingly, G. E. G., Chater, M., & Johnston, A. E. (1975). Experiments made on Stackyard Field, Woburn, 1876-1974. III. Effects of NPK Fertilisers and Farmyard Manure on Soil Carbon, Nitrogen and Organic Phosphorus. Rothamsted Experimental Station Report, 1974(2), 61-77. https://doi.org/10.23637/ERADOC-1-33160.

McDowell, R. W., & Haygarth, P. M. (2024). Reducing phosphorus losses from agricultural land to surface water. Current Opinion in Biotechnology, 89, 103181. https://doi.org/10.1016/j.copbio.2024.103181.

Melby, E. S., Soldat, D. J., & Barak, P. (2011). Synthesis and detection of oxygen-18 labeled phosphate. Plos one, 6(4), e18420. https://doi.org/10.1371/journal.pone.0018420.

Nagel, C., Neidhardt, H., Oelmann, Y. (2025). Data from: Dynamics of phosphorus pools in drainage ditch sediments within an agricultural catchment [Dataset]. Dryad. https://doi.org/10.5061/dryad.2z34tmpxm.

Nagul, E. A., McKelvie, I. D., Worsfold, P., & Kolev, S. D. (2015). The molybdenum blue reaction for the determination of orthophosphate revisited: Opening the black box. Analytica chimica acta, 890, 60-82. https://doi.org/10.1016/j.aca.2015.07.030.

Neidhardt, H., Achten, F., Kern, S., Schwientek, M., & Oelmann, Y. (2019). Phosphorus pool composition in soils and sediments of transitional ecotones under the influence of agriculture. Journal of environmental quality, 48(5), 1325-1335. https://doi.org/10.2134/jeq2019.01.0012.

Neidhardt, H., Rudischer, S., Eiche, E., Schneider, M., Stopelli, E., Duyen, V. T., ... & Berg, M. (2021). Phosphate immobilisation dynamics and interaction with arsenic sorption at redox transition zones in floodplain aquifers: Insights from the Red River Delta, Vietnam. Journal of Hazardous Materials, 411, 125128. https://doi.org/10.1016/j.jhazmat.2021.125128.

Özkan, U., & Gökbulak, F. (2017). Effect of vegetation change from forest to herbaceous vegetation cover on soil moisture and temperature regimes and soil water chemistry. *Catena*, *149*, 158-166. http://dx.doi.org/10.1016/j.catena.2016.09.017.

Pionke, H. B., Gburek, W. J., & Sharpley, A. N. (2000). Critical source area controls on water quality in an agricultural watershed located in the Chesapeake Basin. Ecological engineering, 14(4), 325-335. https://doi.org/10.1016/S0925-8574(99)00059-2.

Ramler, D., & Strauss, P. (2024). Site matters: site-specific factors control phosphorus retention in buffer strip soils under concentrated field runoff. *Environmental Science and Pollution Research*, *31*(35), 48154-48163. https://doi.org/10.1007/s11356-024-34383-7.

Reddy, K. R., Kadlec, R. H., Flaig, E., & Gale, P. M. (1999). Phosphorus retention in streams and wetlands: a review. Critical reviews in environmental science and technology, 29(1), 83-146. https://doi.org/10.1080/10643389991259182.

Roberts, W. M., Stutter, M. I., & Haygarth, P. M. (2012). Phosphorus retention and remobilization in vegetated buffer strips: a review. *Journal of environmental quality*, *41*(2), 389-399. https://doi:10.2134/jeq2010.0543.

Ruttenberg, K. C. (1992). Development of a sequential extraction method for different forms of phosphorus in marine sediments. Limnology and oceanography, 37(7), 1460-1482. https://doi.org/10.4319/lo.1992.37.7.1460.

Sandström, S., Futter, M. N., O'Connell, D. W., Lannergård, E. E., Rakovic, J., Kyllmar, K., ... & Djodjic, F. (2021). Variability in fluvial suspended and streambed sediment phosphorus fractions among small agricultural streams (Vol. 50, No. 3, pp. 612-626). https://doi.org/10.1002/jeq2.20210.

Schimel, J. P. (2018). Life in dry soils: effects of drought on soil microbial communities and processes. Annual review of ecology, evolution, and systematics, 49(1), 409-432.) https://doi.org/10.1146/annurev-ecolsys-110617-062614.

Schinner, F., Öhlinger, R., Kandeler, E., & Margesin, R. (Eds.). (2012). Methods in soil biology. Springer Science & business media.

Schwientek, M., Osenbrück, K., & Fleischer, M. (2013). Investigating hydrological drivers of nitrate export dynamics in two agricultural catchments in Germany using high-frequency data series. Environmental earth sciences, 69, 381-393. https://doi.org/10.1007/s12665-013-2322-2.

Sharpley, A. N., Chapra, S. C., Wedepohl, R., Sims, J. T., Daniel, T. C., & Reddy, K. R. (1994). Managing agricultural phosphorus for protection of surface waters: Issues and options. Journal of environmental quality, 23(3), 437-451. https://doi.org/10.2134/jeq1994.00472425002300030006x.

Sharpley, A., Jarvie, H. P., Buda, A., May, L., Spears, B., & Kleinman, P. (2013). Phosphorus legacy: overcoming the effects of past management practices to mitigate future water quality impairment. Journal of environmental quality, 42(5), 1308-1326. https://doi.org/10.2134/jeq2013.03.0098.

Shi, S., & Xu, G. (2019). Identification of phosphorus fractions of biofilm sludge and phosphorus release, transformation and modeling in biofilm sludge treatment related to pH. Chemical Engineering Journal, 369, 694-704.

Shore, M., Jordan, P., Mellander, P. E., Kelly-Quinn, M., Daly, K., Sims, J. T., ... & Melland, A. R. (2016). Characterisation of agricultural drainage ditch sediments along the phosphorus transfer continuum in two contrasting headwater catchments. Journal of Soils and Sediments, 16(5), 1643-1654. https://doi.org/10.1007/s11368-015-1330-0.

Spohn, M., Braun, S., & Sierra, C. A. (2023). Continuous decrease in soil organic matter despite increased plant productivity in an 80-years-old phosphorus-addition experiment. *Communications earth & environment*, *4*(1), 251. https://doi.org/10.1038/s43247-023-00915-1.

Stout, L. M., Joshi, S. R., Kana, T. M., & Jaisi, D. P. (2014). Microbial activities and phosphorus cycling: An application of oxygen isotope ratios in phosphate. Geochimica et Cosmochimica Acta, 138, 101-116. https://doi.org/10.1016/j.gca.2014.04.020.

Sugiyama, S., & Hama, T. (2013). Effects of water temperature on phosphate adsorption onto sediments in an agricultural drainage canal in a paddy-field district. Ecological engineering, 61, 94-99. https://doi.org/10.1016/j.ecoleng.2013.09.053.

Taalab, A. S., Ageeb, G. W., Siam, H. S., & Mahmoud, S. A. (2019). Some characteristics of calcareous soils. A review as Taalab1, GW Ageeb2, Hanan S. Siam1 and Safaa A. Mahmoud1. *Middle East J*, *8*(1), 96-105.

Tabatabai, M. A., & Bremner, J. M. (1969). Use of p-nitrophenyl phosphate for assay of soil phosphatase activity. *Soil biology and biochemistry*, *1*(4), 301-307.

Tamburini, F., Pistocchi, C., Helfenstein, J., & Frossard, E. (2018). A method to analyse the isotopic composition of oxygen associated with organic phosphorus in soil and plant material. European Journal of Soil Science, 69(5), 816-826. https://doi.org/10.1111/ejss.12693.

von Sperber, C., Kries, H., Tamburini, F., Bernasconi, S. M., & Frossard, E. (2014). The effect of phosphomonoesterases on the oxygen isotope composition of phosphate. Geochimica et Cosmochimica Acta, 125, 519-527. https://doi.org/10.1016/j.gca.2013.10.010.

Wallenstein, M. D., McMahon, S. K., & Schimel, J. P. (2009). Seasonal variation in enzyme activities and temperature sensitivities in Arctic tundra soils. Global Change Biology, 15(7), 1631-1639. https://doi.org/10.1111/j.1365-2486.2008.01819.x.

Wang, H., Liu, S., Zhang, X., Mao, Q., Li, X., You, Y., ... & Mo, J. (2018). Nitrogen addition reduces soil bacterial richness, while phosphorus addition alters community composition in an old-growth N-rich tropical forest in southern China. *Soil Biology and Biochemistry*, *127*, 22-30. https://doi.org/10.1016/j.soilbio.2018.08.022.

Withers, P. J. A., Hartikainen, H., Barberis, E., Flynn, N. J., & Warren, G. P. (2009). The effect of soil phosphorus on particulate phosphorus in land runoff. *European Journal of Soil Science*, *60*(6), 994-1004. https://doi:10.1111/j.1365-2389.2009.01161.x.

Wu, Y., Liu, J., & Rene, E. R. (2018). Periphytic biofilms: a promising nutrient utilization regulator in wetlands. Bioresource technology, 248, 44-48. https://doi.org/10.1016/j.biortech.2017.07.081.

Yan, N., Marschner, P., Cao, W., Zuo, C., & Qin, W. (2015). Influence of salinity and water content on soil microorganisms. International soil and water conservation Research, 3(4), 316-323. https://doi.org/10.1016/j.iswcr.2015.11.003.

Young, E. O., Ross, D. S., Jaisi, D. P., & Vidon, P. G. (2021). Phosphorus transport along the cropland–riparian–stream continuum in cold climate agroecosystems: A review. *Soil systems*, *5*(1), 15. https://doi.org/10.3390/soilsystems5010015.

Zhang, S., Yang, X., Hsu, L. C., Liu, Y. T., Wang, S. L., White, J. R., ... & Rinklebe, J. (2021). Soil acidification enhances the mobilization of phosphorus under anoxic conditions in an agricultural soil: Investigating the potential for loss of phosphorus to water and the associated environmental risk. Science of the Total Environment, 793, 148531). https://doi.org/10.1016/j.scitotenv.2021.148531.

Zhou, A., Tang, H., & Wang, D. (2005). Phosphorus adsorption on natural sediments: Modeling and effects of pH and sediment composition. Water research, 39(7), 1245-1254. https://doi.org/10.1016/j.watres.2005.01.026.

Zhou, Z., Wang, C., & Jin, Y. (2017). Stoichiometric responses of soil microflora to nutrient additions for two temperate forest soils. *Biology and Fertility of Soils*, *53*(4), 397-406. https://doi: 10.1007/s00374-017-1188-y.

Section B

Vegetated buffer strips under pressure: Phosphorus dynamics in soils with and without fertilizer history

Christiane Nagel[1]*, Yvonne Oelmann[1], Harald Neidhardt[1]

[1]Geoecology, Eberhard Karls University Tübingen, 72070 Tübingen, Germany

*harald.neidhardt@uni-tuebingen.de

Author	**Author position**	**Scientific ideas %**	**Data generation %**	**Analysis & interpretation %**	**Paper writing %**
Christiane Nagel	1	15	100	60	80
Prof. Dr. Yvonne Oelmann	2	45	0	20	10
PD Dr. Harald Neidhardt	3	40	0	20	10
Titel of paper:		Vegetated Buffer Strips Under Pressure: Phosphorus Dynamic in Soils with and without Fertilizer History			
Status in publication process:		Submission in progress, *Journal of Soil Science and Plant Nutrients*			

Abstract

Vegetated buffer strips (VBS) act as critical retention zones for phosphorus (P), preventing transfer from agricultural fields to adjacent aquatic systems. Although P retention and remobilization in VBS have been examined over long timescales, short- to medium-term transformations among specific P pools during extreme weather events causing drying-rewetting events remain insufficiently understood. Specifically, the question remains open if VBS function as temporary sinks or sources for P, especially when fertilizer-derived P inputs from agricultural fields persist. We therefore investigated P dynamics in VBS soils with historical P accumulation in comparison to undisturbed forest soils (FST) under contrasting hydrological treatments. After adding dissolved inorganic P (P_i), soils were incubated for 16 weeks under short-pulsed (SPL, weekly) and long-pulsed (LPL, biweekly) drying-rewetting cycles at both, 20 °C and 5 °C. Sequential P extractions were used to track P_i and organic P (P_o) across pools ranging from labile ($NaHCO_3$- and NaOH-extractable) to more stable fractions (CDB-, HCl-, H_2SO_4-extractable). Over 16 weeks, surface-bound P_i ($NaHCO_3$-extractable) dominated in the VBS soil, with a limited transfer into more stable pools (NaOH-extractable). Stable P_i and P_o (CDB-extractable) increased under the SPL treatment, whereas P_o mineralization and P_i stabilization were reduced under the LPL treatment. In contrast, the FST soil showed greater increases in stable P pools (NaOH- and CDB-extractable P_i), indicating a higher P retention capacity. These findings highlight the vulnerability of VBS functioning under short- to mid-term changing hydrological conditions and underscore the need for adaptive management in agricultural landscapes.

1. Introduction

To reduce phosphorus (P) exports form agricultural lands, vegetated buffer strips (VBS) have been widely established, especially in Europe (Habibiandehkordi et al., 2019). The primary function of VBS is to separate arable land from adjacent surface waters and therefore to act as important retention zones for P and other nutrients (Roberts et al. 2012). They form unique ecosystems in agricultural landscapes which are rich in biodiversity, inheriting the once complex riparian ecosystems. Here, VBS modify the delivery tier of the P transfer continuum in agricultural landscapes by deflecting runoff through denser vegetation (Roberts et al. 2012). Dense root systems and stems further stabilize VBS soils and sediments, reducing bank erosion and improving soil permeability (Cole et al. 2020). In addition, VBS physically filter soil particles from water in overland flow, and thereby, reduce nutrient loads and their transport rates (Bauke et al., 2022; Roberts et al., 2012). Therefore, their effectiveness in retaining P depends strongly on factors such as vegetation type, buffer design, and adjacent fertilizer inputs (Cole et al., 2020; Hille et al., 2019). However, the capability in mitigating P loss is influenced by pronounced hydrological dynamics typical in agricultural landscapes, which can lead to rapid nutrient transport. Thus, VBS must be adaptable to fluctuating hydrological conditions, as they experience rapid runoff during wet periods and slower flows during dry periods (Cole et al., 2020).

The regular application of mineral fertilizers (P_2O_5) has led to the long-term accumulation of P in many agricultural catchments (Chen et al., 2022). When inorganic P (P_i) is applied, it undergoes sorption, precipitation, and complexation with organic matter, processes that limit its immediate availability to plants and also contribute to long-term accumulation and eventual saturation of sorption sites (Chen et al., 2022; Doydora et al., 2020). Legacy P, namely P that accumulated in agricultural catchments over decades, poses a long-term risk pertaining long after the cease of fertilizer application (Haygarth et al., 2005; He et al., 2023; Habibiandehkordi et al., 2019). Legacy P-affected soils of arable fields and adjacent VBS typically contain high concentrations of total P, with the largest proportion commonly represented by P_i bound to Al- and Fe-oxyhydroxides and, after long-term fertilizer inputs, increasingly to the stable Ca-P_i pool (Chen et al., 2022, He et al., 2023). In contrast, natural non-legacy soils exhibit markedly lower total P concentrations and respective surface-bound P_i pools are substantially smaller, whereas the proportion of organically bound P is considerably higher (De Schrijver et al., 2012; Niederberger et al., 2019).
Once accumulated, P can be re-released through various physical, chemical, or biological mechanisms, contributing to eutrophication and the resulting degradation of water quality in adjacent surface waters. A high hydrological variability can reinforce the mobility and transfer of P, especially during heavy rainfall events (Withers et al., 2009; Young et al., 2021). Climate change further exacerbates the mobility of P within agricultural catchments by altering precipitation patterns, leading for example to more frequent and intense rainfall events that increase surface runoff (Haygarth et al. 2005, Reddy et al. 1999).

In non-calcareous soils (as in the present study), minerals like iron (Fe) and aluminum (Al) play a crucial role in the retention and mobilization of P (Hoffmann et al. 2009). In particular, amorphous Fe-oxyhydroxides exhibit a high specific surface area and therefore a strong capacity to bind P_i, whereas more crystalline Fe forms provide lower but more persistent sorption capacities. Dry periods have the

potential to further enhance P retention by Fe(III)-oxides. Under oxic conditions, Fe(II) is oxidized, leading to the precipitation of Fe(III)-oxides and concomitant fixation of P_i (Roden et al., 2003). Under anoxic conditions, following long flooding phases, P_i can be (re-)mobilized due to a decline in the redox potential and the subsequent reductive dissolution of Fe(III)-oxides (Ajmone-Marsan et al., 2006; Barczok et al., 2023; Dupas et al., 2015). The release of Fe(III)-bound P_i and microbial P_o can briefly increase dissolved P_i concentrations in solution, thereby contributing to P loss (Ajmone-Marsan et al. 2006; He et al., 2023; Joshi et al. 2016). These stabilization and mobilization processes are influenced by the duration of oxic and anoxic phases. Short-pulsed drying-rewetting cycles foster Fe(III)-oxide dissolution as they create rapid and repetitive redox fluctuations that continually destabilize Fe minerals, generating fresh amorphous Fe(III)-oxides, and preventing the system from entering stable oxic or anoxic phases (Roberts et al. 2012). Long-pulsed cycles allow Fe(III)-oxides to age and stabilize, reducing their dissolution potential (Roberts et al. 2012).

Microorganisms are capable of both, uptake and release of P, thereby converting P_i into P_o and vice versa (Cole et al., 2020; Roberts et al., 2012). For example, the microbial transformation of P_o into bio-available P_i is dependent on temperature, moisture, and oxygen availability (Roberts et al., 2012; Doydora et al., 2020). Here, P_i can be released from P_o substrates due to phosphatase-mediated mineralization of organic matter (OM), while at the same time, P_i is also incorporated into new intracellular P_o compounds (Khorshid et al., 2019). In this context the amount of bio-available P plays a crucial role. In natural soils without historical fertilizer input (non-legacy P sites), P represents a limiting nutrient, resulting in the tight biological recycling of P_i from P_o (Siegenthaler et al., 2022). If additional P_i is introduced externally, microbial growth increases along with build-up of biomass where P_i is transferred and stored in P_o compounds (He et al., 2023; Ramler et al., 2022). In legacy P-enriched soils, P is often no longer the limiting nutrient, and microbial activity is saturated, meaning additional bio-available P_i does not stimulate further activity (Taalab et al., 2019).

Hydrological changes affect P cycling in soils especially through drying-rewetting events. Under drying conditions, P is assimilated and temporarily retained by microorganisms through conversion into P_o molecules (He et a., 2023). When conditions are too dry, microorganism suffer and reach a dormant state where metabolic processes stop and P_i is no longer incorporated into P_o (Lu et al., 2016; Luo et al., 2022). After rewetting, the spontaneous increase in the moisture gradient leads to osmotic stress, causing dieback and lysis of microbial cells (Ajmone-Marsan et al., 2006; Chen et al., 2023; Zhang et al., 2023). Following longer periods of water saturation, microbial communities adapt to hydrological conditions resulting in an enhanced metabolic activity along with the buildup of P_o compounds (Chen e al., 2023).

Soil pH is another key factor governing P dynamics, as it influences both sorption processes and microbially mediated transformations by altering chemical equilibria and microbial functioning. An increasing pH modulates the surface charge of Al- and Fe-oxyhydroxides, increasing the proportion of negatively charged surface sites and thereby altering their affinity for P, with particularly strong effects on weakly bound P_i fractions. In addition, pH increases often reflect elevated microbial activity and P_o mineralization (Young et al., 2021).

Biological processes, combined with abiotic factors, ultimately determine how effectively VBS can retain P from agricultural runoff through adsorption and transformation (Habibiandehkordi et al., 2019; Ramler et al., 2024). Although legacy P accumulation in VBS is well documented (Cole et al., 2020; Doydora et al., 2020; He et al., 2023), several critical knowledge gaps remain regarding P dynamics under fluctuating hydrological conditions (Baucke et al., 2022; Kleinmann et al., 2011). Previous research has largely focused on steady-state moisture conditions or broad-scale seasonal variability, while hydrologic variability and short- to mid-term redox fluctuations relevant for VBS have received far less attention. In particular, the timing and frequency of drying-rewetting events, which strongly modify Fe mineral transformations and consequently P mobility, remain poorly constrained (Chen et al., 2022). Additionally, while effects of long-term excessive P fertilization on total soil P stocks are well documented, its imprint on individual P pools, particularly P_o pools, under dynamic redox conditions remains poorly understood (Chen et al., 2022).

Our experimental design specifically addresses the aforementioned unresolved aspects by investigating short- and mid-term transformations of P in non-calcareous VBS soils under varying hydrological and redox conditions. We focused on drying-rewetting dynamics and assessed abiotic and biotic factors influencing P retention over time. We included an adjacent forest site (FST) as a control, which has been covered with trees for at least 60 (Neidhardt et al., 2019) years and is unaffected by anthropogenic P inputs.

We hypothesized that:
Following a history of agricultural P input,
(H1) further P_i addition to VBS soils remains mobile (i.e., dissolved and exchangeable surface-bound P) and, to a smaller extent, is retained in stable fractions (e.g., Fe(III)-bound P); and

(H2) long drying-rewetting cycles enhance the stabilization of P_i by promoting the repeated formation of amorphous Fe(III)-oxides resulting in a slight but significant increase of Fe-bound P as compared to short drying-rewetting cycles.

In the absence of legacy P,
(H3) P_i addition increases the proportion of strongly bound P_i (i.e., Al- and Fe-oxyhydroxide bound P_i) due to the availability of free sorption sites, and enhances the buildup of P_o by subsequent microbial incorporation; and

(H4) long drying-rewetting cycles promotes adaption of microbial communities, and thus a more pronounces buildup of P_o as compared to short drying-rewetting cycles.

2. Methods

2.1. Origin of samples

Samples for the incubation experiment were collected from a vegetated buffer strip adjacent to agricultural land within the Ammer valley near Tübingen, located in the South German Scarplands

region (N 48° 31.050, E 9° 0790; WGS84) In the 134 km^2 large catchment, about 66% of the land is used for agriculture (Leibundgut and Eisele, 2005; Schwientek et al., 2013). The geological background is represented by Lower and Middle Triassic Keuper sequences, thin sequences of sandstones and evaporitic marlstones, as well as aeolian, colluvial, and alluvial deposits. Soils in the Ammer valley floodplain are mainly composed of loamy Fluvisols, Luvisols, and Anthrosols with a fine grain size composition dominated by clay (Ad-hoc Boden, 2005).

Soil samples from a VBS were collected at 0 - 5 cm depth following a straight orthogonal transect from south to north. To account for potentially site-specific spatial variability, samples were collected in triplicates with a distance of 10 - 15 m between each replicate.

Control soil samples of FST were taken in a forested area 15 to 20 meters further south adjacent to the arable land. Here, the top 0-5 cm were collected in triplicates, too, and processed as the VBS samples. The two sites generally share the same geological background (Neidhardt et al., 2019). Further details, such as the position of the sampling sites, local land use and topography are provided in **Table B-S1.** An image of the sampling area is shown in **Figure B-1**.

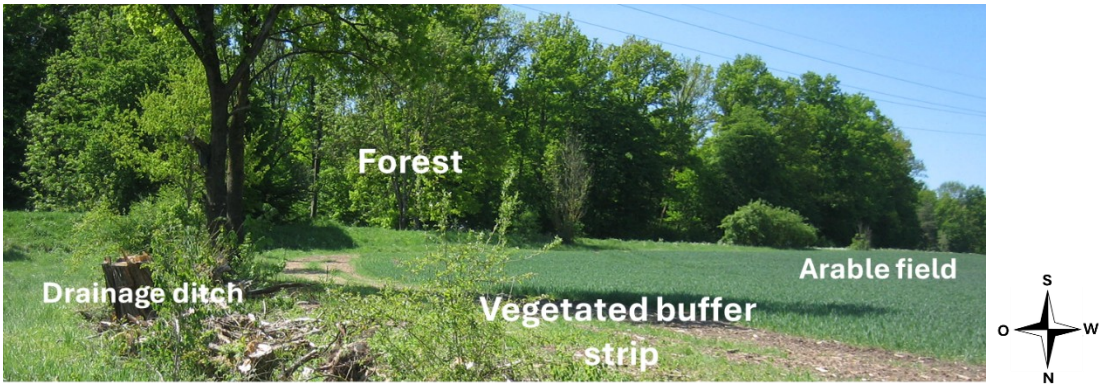

Figure B-1: Sampling site in the Ammer valley, west of Tübingen, Germany. Picture illustrating the sampling sites of vegetated buffer strip (VBS), between drainage ditch and arable field, and forest soil (FST) adjacent to the arable land.

Concentrations of the P pools of the initial soil samples of VBS and FST soils are shown in **Table B-1**. The arable soil included in **Table B-1** serves as a representative legacy P soil, as it has been continuously used as agricultural land since 1829 (Tübinger Blätter, 1974). The VBS soil represents the legacy P influenced site and FST the non-legacy P site.

Table B-1: P pool concentrations of the initial soils of arable soil (AS), vegetated buffer strip (VBS) and forest (FST). Values represent means and standard deviations of the triplicates.

P pool	Initial soil AS	Initial soil VBS	Initial soil FST
$NaHCO_3$ - P_i (mg kg^{-1})	76.1 ± 4.12	111 ± 18	50.9 ± 26.7
NaOH - P_i (mg kg^{-1})	230 ± 58.4	194 ± 87	80.0 ± 9.5
CDB - P_i (mg kg^{-1})	93.7 ± 22.1	60.8 ± 29.7	63.3 ± 11.6
$NaHCO_3$ - P_o (mg kg^{-1})	0.0 ± 0.0	46.4 ± 5.5	11.2 ± 16.1
NaOH - P_o (mg kg^{-1})	112 ± 22.0	174 ± 70	237 ± 23
CDB - P_o (mg kg^{-1})	153 ± 12.5	169 ± 44	0.0 ± 0.0
HCl - P_t (mg kg^{-1})	569 ± 63.0	273 ± 141	30.6 ± 17.5
H_2SO_4 - P_t (mg kg^{-1})	90.9 ± 11.5	-	94.2 ± 10.1
Sum extractable P_t (mg kg^{-1})*	979 ± 27	1169 ± 43	540 ± 29
Aqua regia P_t (mg kg^{-1})	947 ± 61.6	1099 ± 40.9	-

* Sum of P_t from Hedley extraction measured at ICP-OES

- No data

2.2. Experimental design

The non-calcareous soils of the VBS and the FST plots were air-dried, sieved (<2 mm), and larger organic fragments manually removed. Samples were then pre-incubated with deionized water at 38% water content (according to the previously determined water holding capacity) for two weeks at 20°C. After pre-incubation, 100 g dry-weight equivalents of soil were placed into 200 ml jars, and 100 ml of P_i solution (0.5 g KH_2PO_4 l^{-1}) was added to each jar, respectively. Soil properties of VBS and FST before (initial soil) and 24 hours after P_i addition are presented in **Table B-S2**.

Unless otherwise stated, all analyses were conducted for the triplicate samples. Two hydrological regimes were applied: i) short-pulsed logged (SPL) with weekly drying-rewetting cycles (8 cycles in total) and ii) long-pulsed logged (LPL) with two-week cycles (4 cycles in total). Two temperatures were applied: 20°C and 5°C, the latter to suppress microbial activity (**Table B-2**). During the 16-week long incubation, soil samples were taken destructively at three time points for VBS (after 1 day, 8 weeks, 16 weeks) and at three points for FST (after 1 day, 2/4 weeks, 16 weeks). At the end of each cycle, porewater was removed by embedded micro-suction cups (90mm long, ecoTech Umwelt-Meßsysteme GmbH, Germany, equipped with polyamide membranes and a 0.45 µm pore size), and soil samples were prepared for chemical analysis. Every other week (or weekly for SPL), 100 ml of deionized water was added to maintain a constant water content (WC) over 50%. Temperature was monitored at 5 - 6 cm depth using a temperature logger (WTDL1, ELV Elektronik AG, Germany), and the oxidation reduction potential (ORP) was measured in VBS with Pt-electrodes (ecoTech Umwelt-Meßsysteme GmbH, Germany) after Mansfeld. Data were recorded every 3 minutes and retrieved monthly. Respective E_h values were recalculated to the standard hydrogen electrode (SHE) according to the Nernst equation (**Table B-2**). E_h values ranged from -425 to +383 mV in VBS.

Table B-2: Water content (WC %) and redox potential E_h (mV) at 20°C and 5°C in soils of vegetated buffer strip (VBS) and forest (FST) plots. (a, c) short-pulsed logged (SPL) and (b, d) long-pulsed logged (LPL) treatments. Values represent means ± standard deviations of WC and minimum and maximum ± standard deviations of E_h for all dry and all wet cycles.

Treatment	n (number of cycles) during 16 weeks of incubation	WC (%)		Redox potential E_h (mV)	
VBS		**20°C**	**5°C**	**20°C**	**5°C**
a) SPL	Wet cycles (n = 8)	50.4 ± 4.7	52.3 ± 7.5	-424 ± 196	+69.0 ± 51.2
	Dry cycles (n = 8)	37.9 ± 2.6	36.1 ± 2.2	+225 ± 56	+383 ± 83
b) LPL	Wet cycles (n = 4)	59.6 ± 17.4	51.1 ± 8.1	-392 ± 146	-124 ± 39
	Dry cycles (n = 4)	30.0 ± 5.4	23.1 ± 11.4	+313 ± 23	+297 ± 38
FST					
c) SPL	Wet cycles (n = 8)	51.4 ± 3.8	55.1 ± 6.9	No data of redox potential available	
	Dry cycles (n = 8)	35.4 ± 1.7	39.8 ± 3.4		
d) LPL	Wet cycles (n = 4)	60.5 ± 8.3	53.8 ± 8.1		
	Dry cycles (n = 4)	29.9 ± 6.1	1.1 ± 9.3		

2.3. Chemical analyses

To trace transformations of different soil P pools over time after of the addition of P_i, a sequential extraction scheme was carried out following a modified procedure after Hedley at al. (1982). For detailed information, the reader is referred to supporting information **Section B-S1**. In brief, increasingly strong chemical solutions were used to extract 0.5 g dry-weight equivalent of fresh soil samples (0.5 M $NaHCO_3$ -> 0.1 M NaOH -> citrate dithionite bicarbonate (CDB) -> 1 M HCl -> 0.5 M H_2SO_4). Here, loosely adsorbed P and organic matter is considered to be extractable with the $NaHCO_3$ solution, representing 'labile P_i and P_o' (Mattingly et al., 1975). This pool is readily bioavailable and therefore characterized by fast turnover rates (Negassa and Leinweber, 2009; Tiessen, 1993). More stable forms of P_o (e.g., detritus P_o) and strongly bound P_i associated with Al- and Fe-oxyhydroxides were extracted with the NaOH solution, referred to 'moderately labile P_i and P_o' in the following. Next, a citrate dithionite bicarbonate (CDB) step was applied to extract 'moderately stable P', representing P_i and P_o associated with reducible Mn(IV)- and Fe(III)-oxyhydroxides (Neidhardt et al., 2021). This pool can rapidly turn from a sink into a source for P under anoxic and reducing conditions (Ajmone-Marsan et al., 2006; Dupas et al., 2015). The CDB-step was applied directly before the extraction with HCl solution, to distinguish redox sensitive Pi and Po from P_i in primary and secondary Ca-minerals (e.g., apatite, octacalcium phosphate), which has been previously argued by Joshi et al. (2015). The latter is referred to as 'stable P pool' (non-bioavailable) and dominates in Ca-carbonate-rich environments (Eriksson et al., 2016). However, this extraction could also contain P_i and P_o associated with Fe(II)-minerals such as siderite and strengite (Neidhardt et al., 2019). Furthermore, the strongly acidic solution is known to hydrolyze P_o compounds, (Pierzynski, 2000) which is why no P_o was detectable in our measurements. Non-

extractable residual P (Cross and Schlesinger, 1995) was extracted using H_2SO_4 solution and is considered also as part of the 'stable P' fraction.

Concentrations of dissolved major and trace elements (Al, Ca, Fe, Mg, Mn, P) in the extraction solutions and porewater were analyzed by Optical emission spectrometry with inductively coupled plasma (ICP-OES, Optima 5300 DV, PerkinElmer). Total P (TP) concentrations were measured axial at a wavelength of 213.617 nm, achieving an instrumental detection limit (IDL) of 0.004 ± 0.001 µg l^{-1}. Quality controls and respective recovery rates are represented in **Table B-S3**. Concentrations of P_i in porewater and the $NaHCO_3$, NaOH and CBD extraction solutions were measured additionally photometrically by CFA (Continuous flow analyzer, Analytical AutoAnalyzer 3, SEAL, Germany) by the Mo-blue method (wavelength: 880 nm, idl: 0.004 ± 0.001 mg l^{-1} PO_4-P), (Nagul et al., 2015). Concentrations of P_o were calculated as the difference between TP and P_i. Total concentrations of major and trace elements (Al, As, Ca, Cd, Cr, Cu, Fe, K, Mg, Mn, Na, Ni, P, Pb, Zn) were determined from *aqua regia* digestions (method E701 protocol provided by the manufacturer, similar to DIN EN 16174).
Acid phosphatase activity (APA) as enzyme activity (EA) was determined following the method developed by Tabatabai and Bremner (1969), modified by Schinner et al. (1991), and released P_i was measured by UV-VIS (Analytik Jena Specord 200 plus, Germany). The EA was calculated following DIN EN ISO 20130, further details are provided in the supporting information **Section B-S1**.
At each time step, immediately after sampling, the WC was assessed using a halogen dryer (HB43-S, Metler Toledo) to calculate the dry-weight concentrations of samples that were extracted freshly (sequential extraction, APA). For the determination of porewater and soil pH (0.01 M $CaCl_2$), a pH-meter (WTW pH 3310 with glass electrode WTW Plus SenTix 81) was used. Total alkalinity (TA) of porewater was measured with an alkalinity test KIT (MColortest, Merck).

2.4. Statistical analysis and software use

Statistical analyses were performed using Microsoft Excel (Version 1808, 2019 MSO) and IBM SPSS Statistics (Version 29). Data were tested for normality (Shapiro-Wilk test, $p > 0.05$) and homogeneity of variance (Levene's test, $p > 0.05$). Repeated measures ANOVA was used to assess statistically significant differences over time ($\alpha = 0.05$), with sampling time as the independent variable (within-subject) and hydrological treatment (SPL, LPL) as dependent variables (between-subject). When significant effects were detected, *post hoc* comparisons were conducted using the least significant difference (LSD) test. Paired *t*-tests were applied to assess differences between specific time points or treatments.
Figures were generated using Microsoft Excel 365 (Version 2403). Literature review was conducted via Google Scholar (Alphabet) and Web of Science (Clarivate) and supplemented with Scite (scite.ai). Language editing support was provided by DeepL (DeepL SE) and ChatGPT-4o (OpenAI).

3. Results

3.1. Vegetated buffer strip (VBS)

3.1.2. Temporal changes in soil properties over 16 weeks

Over 16 weeks of incubation at 20°C, no significant difference in WC (%) was observed between the two treatments during both dry (SPL: 37.9 ± 2.6%, LPL: 30.0 ± 5.4%) and wet cycles (SPL: 50.4 ± 4.7%, LPL: 59.6 ± 17.4%). However, significant differences were found in the redox potential (E_h) between the applied drying-rewetting regimes (**Table B-2 a, b**, **Figure B-S1**). In the SPL treatment, the E_h decreased significantly ($p < 0.01$) after the first rewetting to -424 mV, then remained moderately reducing during the wet cycles (-50 to +50 mV) and weakly reducing during the dry cycles (+200 to +225 mV). In the LPL treatment, the E_h dropped to -391 mV after the first rewetting, followed by moderately reducing conditions (-170 to -40 mV) and weakly reducing conditions during the dry cycles (+200 to +313 mV) (**Figure B-S1**).

The pH values generally remained stable throughout the incubation, ranging from 7.3 to 7.6 for $pH_{porewater}$ and 6.6 to 6.8 for pH_{soil} (**Table B-S4**, **Figure B-S2**). The TA significantly decreased in both treatments after 16 weeks. In SPL ($p < 0.01$), the TA dropped from 491 ± 166 (day 1) to 185 ± 107 mg l^{-1}, while in LPL ($p < 0.05$), it decreased to 294 ± 177 mg l^{-1} (**Table B-S4, Figure B-S3 a, b**). Notably, dissolved Fe concentrations in porewater remained stable (**Figure B-S4 a, b**).

The APA increased significantly in both treatments after 16 weeks ($p < 0.05$), from 16.6 ± 5.7 (day 1) to 28.2 ± 16.7 µg PNP g^{-1} h^{-1} in SPL, and 25.2 ± 9.4 µg PNP g^{-1} h^{-1} in LPL, respectively (**Table B-S4**, **Figure B-S3 c, d**).

During the 16 weeks of incubation, the temperatures were constant around 20°C at room temperature (22.5°C ± 0.8) and at 5°C in the fridge (5.6°C ± 0.2). Despite the temperature differences, there were no significant differences in pH values (**Figure B-S2**), TA and APA (**Figure B-S3**). The E_h differed significantly in the SPL treatment, with less reducing conditions during the rewetting cycles (-50 to +100 mV) and more strongly oxidizing conditions during the drying cycles (+340 to 380 mV, **Figure B-S1 a**) compared to the LPL treatment (+250 to +300; -50 to -150 mV, **Figure B-S1 b**).

3.1.2. Phosphorus pool changes in vegetated buffer strip soil

One day after the addition of P_i solution, the relative proportions of the P pools showed partially pronounced changes compared to the initial soil, especially porewater- and $NaHCO_3$-extractable P_t (**Figure B-S5**). Here, the relative proportion of porewater P_t increased significantly from 0.12 ± 0.1 to 2.36 ± 0.7% (thereof 0.9 ± 0.7% P_i and 1.2 ± 0.3 P_o), whereas $NaHCO_3$-extractable P_t increased significantly from 14 ± 1 to 37 ± 6% (with 37 ± 8% P_i and 0.1 ± 0.0% P_o).

Over the 16 weeks of incubation, the relative contribution of P_i and P_o in the different P pools changed significantly in both treatments (SPL, LPL). In SPL, 8 weeks after P_i addition, the contribution of porewater-P_i (**Figure B-2 a**) and $NaHCO_3$-extractable P_i (**Figure B-2 c**) to TP decreased significantly to 0.16 ± 0.0 and 21 ± 6%, respectively. These contributions remained constant until the end (porewater-P_i: 0.19 ± 0.0%, $NaHCO_3$-P_i: 25 ± 2%). After 16 weeks, porewater-P_i and $NaHCO_3$-extractable P_i were

still significantly higher as compared to the initial soil (porewater-P_i: +0.1%, $NaHCO_3$-P_i: +12%). The CDB-extractable P_i (**Figure B-2 i**) showed a small but significant increase from 4 ± 1 to 5 ± 1%, while the NaOH-extractable P_o (**Figure B-2 g**) decreased significantly from 12 ± 3 to 8 ± 3% after 16 weeks. At the same time, CDB-extractable P_o increased significantly from 9 ± 4 to 12 ± 3% (**Figure B-2 k**).

In LPL, the porewater-P_i (**Figure B-2 b**) decreased significantly to 0.14 ± 0.0% after 8 weeks and remained constant thereafter (0.23 ± 0.0%). Moreover, $NaHCO_3$-extractable P_i (**Figure B-2 d**) decreased considerably from 37 ± 2 to 19 ± 9%. Proportions of porewater-P_i and $NaHCO_3$-extractable P_i were generally higher than the initial soil (porewater-P_i: +0.3%, $NaHCO_3$-extractable P_i: +9%). Regarding P_o, NaOH-extractable P_o (**Figure B-2 h**) decreased significantly from 12 ± 3 to 8 ± 2% and then increased slightly after 16 weeks to 15 ± 9%. Also, CDB-extractable P_o (**Figure B-2 l**) increased significantly ($p < 0.05$) from 9 ± 4 to 12 ± 4% and remained constant till the end (11 ± 4%).

Moreover, Fe concentrations in the NaOH extraction step remained stable throughout both treatments (2031 ± 37 versus 1459 ± 48 and1640 ± 53 mg kg^{-1}, respectively, **Figure B-S4 c, d**). In the CDB extraction step, however, Fe concentrations increased significantly ($p < 0.05$) in both treatments (5690 ± 1390 to 10980 ± 1940 and 11150 ± 446 mg kg^{-1}, respectively, **Figure B-S4 e, f**).

Stable P pools (e.g., HCl- and H_2SO_4-extractable P_t) showed no significant changes during the 16 weeks of incubation (**Figure B-3, Figure B-S5**). The detailed results for all P pool concentrations over the 16 weeks are provided in **Figures B-S6 to B-S8.**

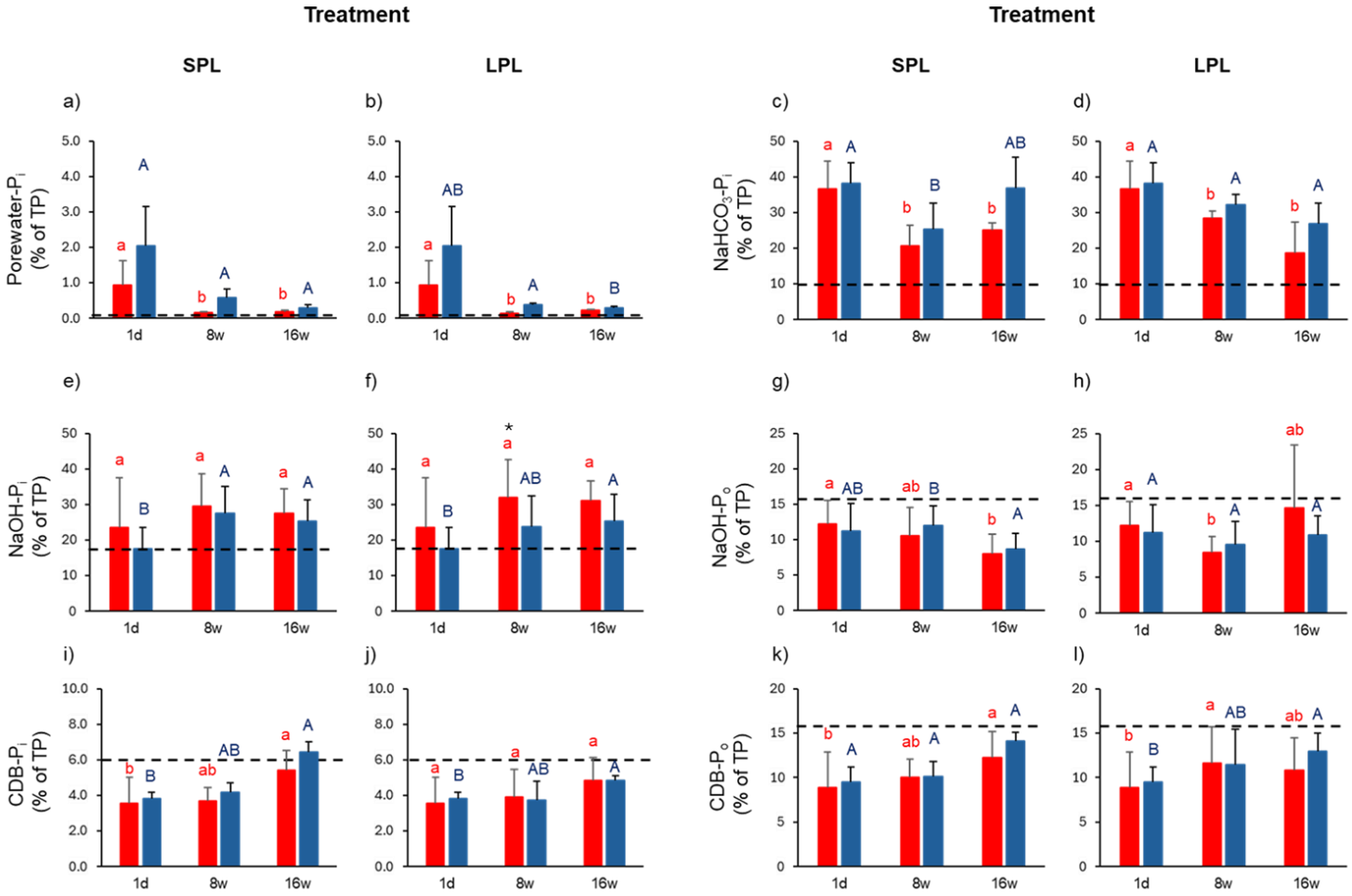

Figure B-2: Temporal variation in P pool composition in the short-pulsed logged (SPL) and long-pulsed logged (LPL) treatments of the vegetated buffer strip soil (VBS). (a, b) Percental proportions of porewater-P_i (% of TP), (c, d) $NaHCO_3$-P_i (% of TP), (e, f) NaOH-P_i (% of TP), (g, h) NaOH-P_o (% of TP), (I, j) CDB-P_i (% of TP) and (k, l) CDB-P_o (% of TP) from beginning (1 day after P_i addition) until the end of the incubation (after 16 weeks). Red bars represent 20°C conditions, blue bars represent 5°C conditions. Small letters show significant differences between samples of 20°C, capital letters show differences between samples of 5°C at the respective point in time. Asterisks illustrate significant differences between 20°C and 5°C at the respective point in time (* $p < 0.05$, ** $p < 0.01$, *** $p < 0.001$). Black dashed lines display respective mean values of the initial soil.

Regarding the two hydrological treatments SPL and LPL, no significant differences in the relative P pool proportions occurred after the 16 weeks of incubation (**Figure B-3**).

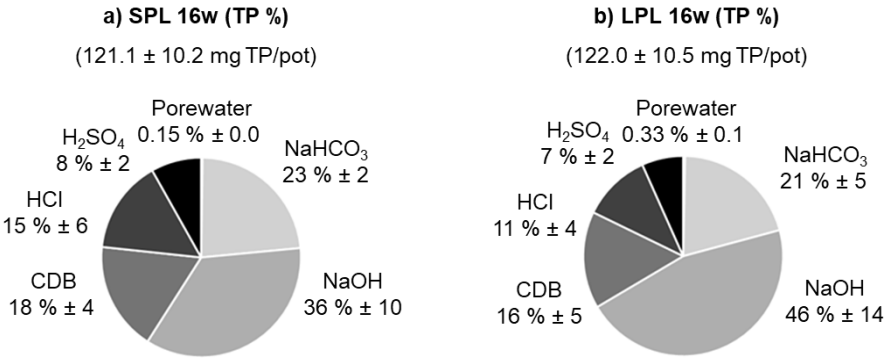

Figure B-3: Relative contribution of the sum of P_i and P_o (P_t) to total P (TP) in the different P pools of the vegetated buffer strip soil (VBS) at 20°C. Absolute amount of TP calculated based on the respective concentration for each pool and the volume of porewater and dry-weight of soil, respectively, within the experimental pots. TP (%) after 16 weeks (16w) of incubation for (a) short-pulsed logged (SPL) and (b) long-pulsed logged (LPL) treatments. Numbers in brackets representing mean contents of total P (mg TP) per pot (triplicates).

Temperature effects in the relative in the relative P pool proportions occurred only after 8 weeks in the LPL treatment for NaOH-extractable P_i, with significantly higher values in the 20°C treatment as compared to the 5°C treatment (31.9 ± 10.7 versus 23.8 ± 8.7%, **Figure B-2 f**). Over the full 16-week incubation period, a pronounced difference was observable for porewater P_i (**Figure B-2 a, b**) as well as $NaHCO_3$-extractable P_i (**Figure B-2 c, d**), with consistently higher contributions to TP at 5°C compared to the 20°C treatment in both treatments.

3.2. Forest soil

3.2.1. Temporal changes in soil properties over 16 weeks

During 16 weeks of incubation at 20°C, no significant difference was observed between the WC of the two treatments. During the wet cycles, values ranged from 54.0 to 64.5% in the SPL treatment, and 60.2 to 60.8% in the LPL treatment. During the dry cycles, both treatments showed a range in WC spanning from 29.9 to 35.4% (**Table B-2 c, d**).

The $pH_{porewater}$ values (**Figure B-S9 a, b**) showed no significant differences between the two hydrological treatments. However, the $pH_{porewater}$ values increased significantly in both treatments from 5.7 ± 0.4 to over 8 (SPL: 8.4, LPL: 8.5) in the first two weeks (SPL) and four weeks (LPL), respectively, before declining to 7.5 ± 0.2 after 16 weeks. At the same time, pH_{soil} values (**Figure B-S9 c, d**) increased from 5.6 ± 0.4 to 6.1 ± 0.1, with significant changes over time in the SPL treatment ($p < 0.05$) (**Table B-S5, Figure B-S9**).

The TA values in porewater increased slightly in the SPL treatment from initially 65.5 ± 34.7 to 86.7 ± 35.2 mg l^{-1}, and significantly in the LPL treatment up to 140.1 ± 17.3 mg l^{-1} (**Table B-S5**, **Figure B-S10 a, b**). Dissolved Fe in porewater decreased significantly by 93% in SPL (0.005 ± 0.0 mg l^{-1}) and was over ten times lower than in the LPL treatment (0.065 ± 0.1 mg l^{-1}) (**Figure B-S11 a, b**).
In both treatments, APA decreased significantly (**Table B-S5**, **Figure B-S10 c, d**) after 16 weeks. In SPL, APA dropped from 133 ± 47.1 to 46.0 ± 12.9 µg PNP g^{-1} h^{-1} ($p < 0.01$), and in LPL, it decreased to 50.4 ± 19.2 µg PNP g^{-1} h^{-1} ($p < 0.05$), respectively.
During the 16 weeks of incubation, the temperatures were constant around 20°C at room temperature (19.1°C ± 0.1) and at 5°C in the fridge (5.2°C ± 0.2). The two temperatures resulted in significant differences of several soil variables, but only in the LPL treatment. Here, the pH_{H2O} and TA values after 16 weeks were significantly higher at 20°C as compared to 5°C (**Figure B-S9 a, b**, **Figure B-S10 a, b**). However, the APA values were significantly lower at 20°C as compared to the 5°C treatment (**Figure B-S10 c, d**).

3.2.2. Phosphorus pool changes in the forest soil

One day after P_i addition, the relative contribution of TP changed significantly for all P pools compared to the initial soil, except for HCl-extractable P_t (**Figure B-S12**). Porewater-P_t increased significantly from 0.08 ± 0.0 to 22.7 ± 1.0 % (thereof 21.3 ± 0.7% P_i and 1.4 ± 0.3% P_o) and $NaHCO_3$-extractable P_t from 11 ± 2 to 43 ± 2% (42 ± 5% P_i, 1 ± 0 P_o).

Over 16 weeks of incubation, significant changes in the relative contribution of the P pools occurred when compared to one day after P_i addition, which were generally independent of the hydrological treatment. The relative proportion of P_i in porewater decreased significantly ($p < 0.01$) back to 0 ± 0% in both treatments (**Figure B-4 a, b**). In addition, the $NaHCO_3$-extractable P_i decreased significantly to 6 ± 3% (SPL, $p < 0.05$) and to 10 ± 2% (LPL, $p < 0.01$, **Figure B-4 c, d**). In the same period, the NaOH-extractable P_i increased significantly from 15 ± 1 to 56 ± 6% (SPL, $p < 0.01$) and to 57 ± 2% (LPL, $p < 0.01$, **Figure B-4 e, f**). Also, CDB-extractable P_i rose from 4 ± 2 to 8 ± 1% (SPL, $p < 0.05$) and to 7 ± 1% (LPL, $p < 0.05$, **Figure B-4 g, h**).
Over 16 weeks of incubation, the concentration of Fe in the NaOH extraction step (**Figure B-S11 c, d**). decreased in both treatments from 3190 ± 560 to 1200 ± 530 (SPL, $p < 0.05$) and to 1750 ± 90 mg kg^{-1} (LPL). The Fe concentrations in the CDB step (**Figure B-S11 e, f**) remained almost constant from beginning (5330 ± 340 mg kg^{-1}) until the end (5550 ± 460 and 4860 ± 230 mg kg^{-1}, respectively).
More stable pools, such as HCl- and H_2SO_4-extractable P_t, did not change significantly over time and were close to one day after the addition of P_i. Details regarding the P pools are presented in **Figures B-S12 and in Figure B-5**.
The relative contribution of P_o to TP changed significantly in both treatments after 16 weeks of incubation. Here, the proportion of $NaHCO_3$-extractable P_o increased significantly from 3 ± 2 to 21 ± 8% (SPL) and to 17.6 ± 3.3% (LPL; **Figure B-4 i, j**). At the same time, the proportion of NaOH-extractable

P_o decreased significantly in both treatments ($p < 0.01$) from 14 ± 4 to 4 ± 2% (SPL and LPL) (**Figure B-4 k, l**). Measured concentrations of the P pools are shown in **Figures B-S13 to B-S15**.

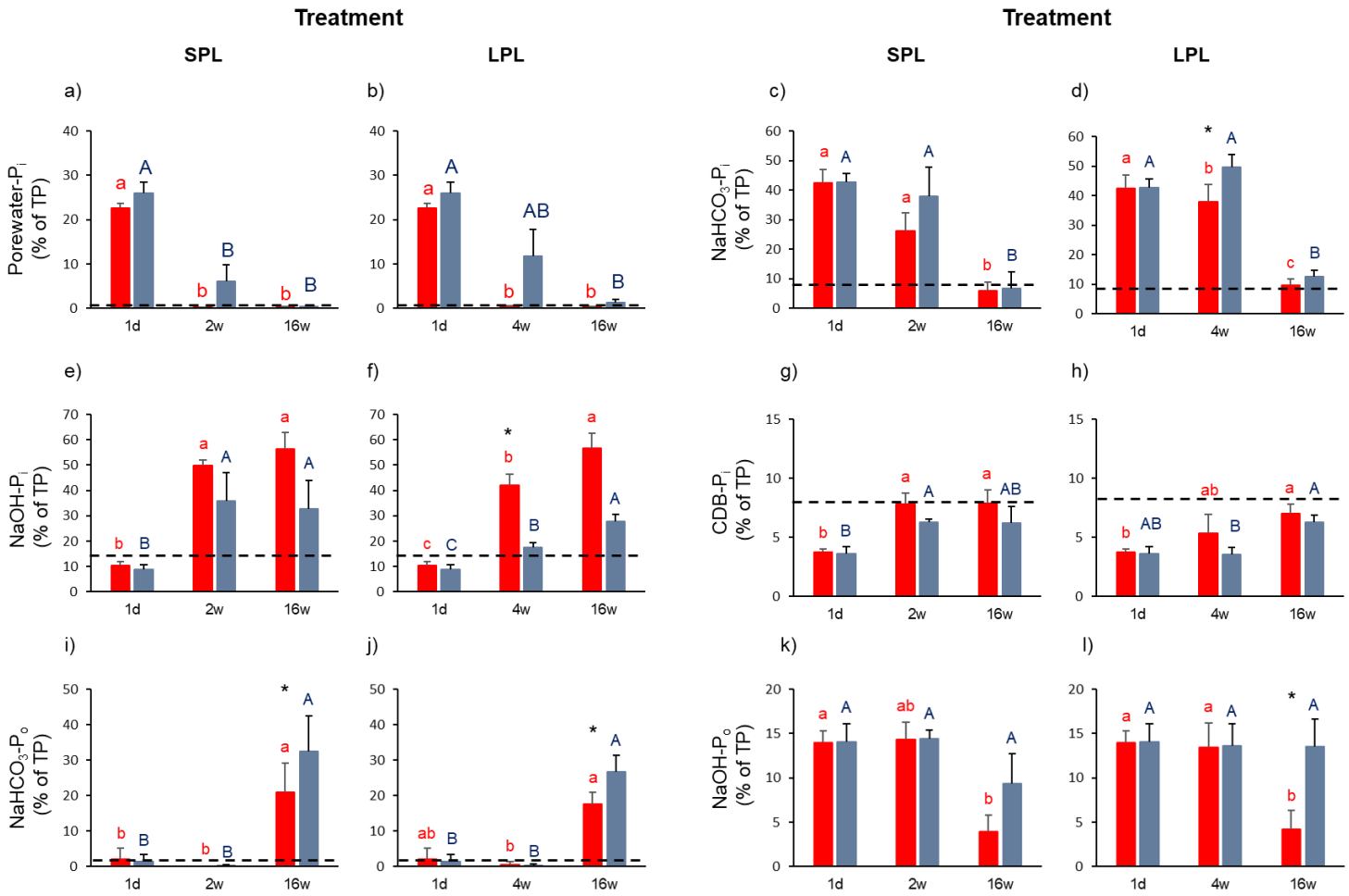

Figure B-4: Temporal variation in P pool composition in the short-pulsed logged (SPL) and long-pulsed logged (LPL) treatments of the forest soil (FST). (a, b) Percental proportions of porewater-P_i (% of TP), (c, d) $NaHCO_3$-P_i (% of TP), (e, f) NaOH-P_i (% of TP), (g, h) CDB-P_i (% of TP), (I, j) $NaHCO_3$-P_o (% of TP) and (k, l) NaOH-P_o (% of TP, initial soil 44%) from beginning (1 day after P_i addition) until the end of the incubation (after 16 weeks). Red bars represent 20°C conditions, blue bars represent 5°C conditions. Small letters show significant differences between samples of 20°C, capital letters show differences between samples of 5°C at the respective point in time. Asterisks illustrate significant differences between 20°C and 5°C at the respective point in time (* $p < 0.05$, ** $p < 0.01$, *** $p < 0.001$). Black dashed lines display mean values of initial soil (% of TP).

Throughout the 16-week incubation, significant differences concerning the two hydrological treatments SPL and LPL were only visible for CDB-extractable P_i (**Figure B-4 g, h**) after the first drying-rewetting cycle (two weeks for SPL, four weeks for LPL). Here, a stronger increase occurred in the SPL treatment (+5.0 %) than in the LPL treatment (+2.0%). At the end of the incubation, there were no statistically significant differences in the relative contribution of the P pools between the two hydrological treatments (**Figure B-5**).

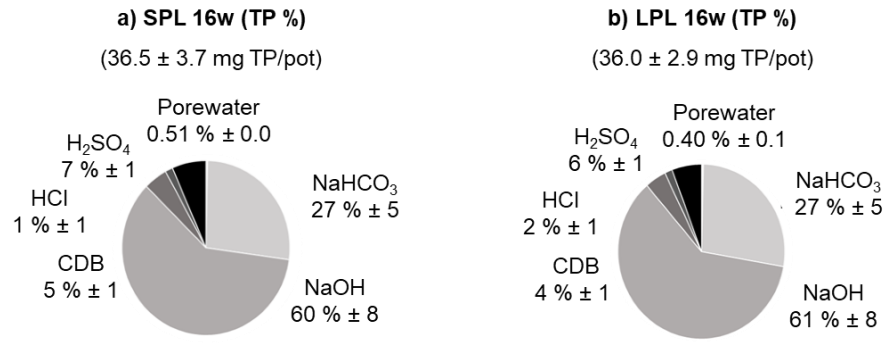

Figure B-5: Relative contribution of the sum of P_i and P_o (Pt) to total P (TP) in the different P pools of the forest soil (FST) at 20°C. Absolute amount of TP calculated based on the respective concentration for each pool and the volume of porewater and dry-weight of soil, respectively, within the experimental pots. TP (%) after 16 weeks (16w) of incubation for (a) short-pulsed logged (SPL) and (b) long-pulsed logged (LPL) treatments. Numbers in brackets representing mean contents of total phosphorus (mg TP) per pot (triplicates).

Temperature effects in the SPL treatment were only observable for the $NaHCO_3$-extractable P_o after 16 weeks with significantly higher values for the 5°C treatment as compared to 20°C (33 ± 9.9 versus 22.5 ± 8.2%; **Figure B-4 i**). In the LPL treatment, the temperature effects were more pronounced. After 16 weeks of incubation, the proportion of NaOH-extractable P_i was significantly higher at 20°C than at 5°C (48.9 ± 5.8 versus 28.1 ± 2.9%; **Figure B-4 f**), whereas the relative contribution of $NaHCO_3$-extractable P_o was significantly lower at 20°C compared to 5°C (18.3 ± 3.3 versus 26.8 ± 4.7%; **Figure B-4 j**). Similarly, the amount of NaOH-extractable P_o was significantly lower at 20 C as compared to 5 °C (4.3 ± 2.1 versus 13.5 ± 3.1%; **Figure B-4 l**)

3.3. Comparison VBS and FST

The comparison between VBS and FST at 20°C showed significant differences in the relative composition of the P pools. In the initial soils, NaOH-P_o was significantly lower (16 ± 5%, **Figure B-6 a**), whereas CDB-P_o was significantly higher (16 ± 3%, **Figure B-6 b**) in VBS compared to FST (NaOH-P_o: 44 ± 4%; CDB-P_o 0 ± 0%, **Figure B-6 b**).

At the end of the incubation, 16 weeks after P_i addition, clear contrasts in P pool composition were evident between VBS and FST for the different hydrological treatments. Under short cycles of drying-rewetting (16w, SPL), the proportions of $NaHCO_3$-P_i (28 ± 2%) and CDB-P_o (12 ± 2%) were significantly higher in VBS than in FST (16w, SPL: $NaHCO_3$-P_i: 6 ± 3%; CDB-P_o: 0 ± 0%). Under long cycles of

drying-rewetting (16w, LPL), the proportions of $NaHCO_3$-P_o (1 ± 0%), NaOH-P_i (31 ± 5%) and CDB-P_i (5 ± 1%) in VBS were significantly lower compared to FST (16w, LPL: $NaHCO_3$-P_o: 18 ± 3%; NaOH-P_i: 57 ± 6%; CDB-P_i: 7 ± 1%). Furthermore, the proportion CBD-P_o was significantly higher in VBS (6 ± 3%) than in FST (0 ± 0%).

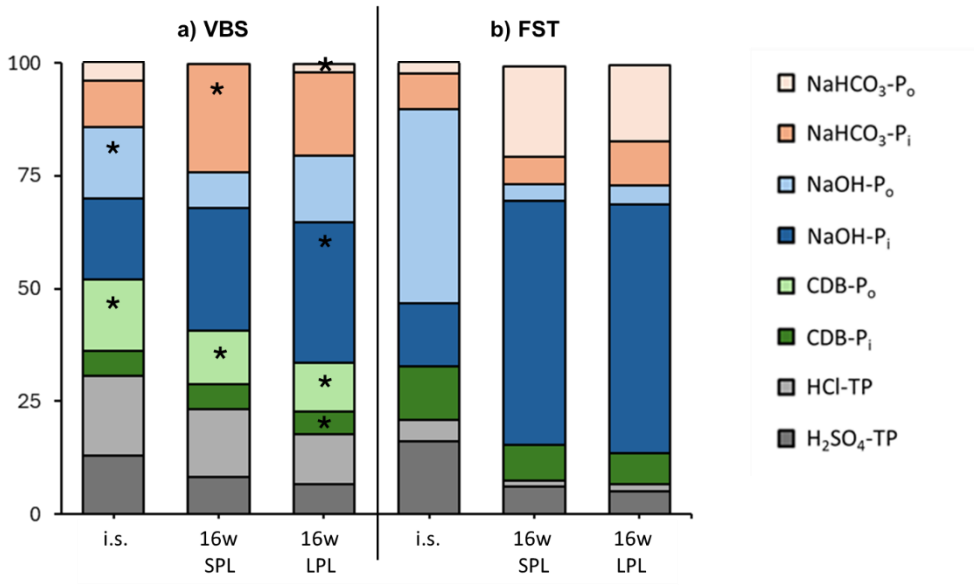

Figure B-6: Comparison of P pool proportions in soils of (a) vegetated buffer strip (VBS) and (b) forest (FST) at 20°C. Different colors represent the respective P pools of the initial soils (i.s.) and 16 weeks (16w) after P_i addition for the short-pulsed logged (SPL) and long-pulsed logged (LPL) treatments. Asterisks in (a) illustrate significant differences between VBS and FST of the initial soils, 16 w (SPL) and 16w (LPL) (* $p < 0.05$, ** $p < 0.01$, *** $p < 0.001$).

4. Discussion

4.1. Phosphorus pool dynamics in vegetated buffer strip soil

In the first 24 hours after P_i addition, significant increases in porewater-P_i (+2%) and $NaHCO_3$-extractable P_i (+20%) were observed (**Figure B-S5**). This observation is consistent with previous studies (Barrow, 1984; Helfenstein et al., 2018), suggesting a rapid transfer of dissolved P_i into the labile (i.e. exchangeable) pool via surface adsorption.

After 8 weeks following P_i addition, porewater-P_i (**Figure B-2 a, b**) and $NaHCO_3$-extractable P_i (**Figure B-2 c, d**) decreased and a minor part (6 - 8%) was transferred into the NaOH-extractable P_i pool in both treatments (**Figure B-2 e, f**), likely due to sorption on Fe(III)-(hydr)oxide surfaces as well as microbial uptake. A major proportion of the added P_i remained in the porewater and $NaHCO_3$-extractable P_i pool, with $NaHCO_3$-extractable P_i being the second largest pool after 16 weeks (21%). Such rapid exchange is consistent with the dominance of weak sorption reactions typically observed in soils with a high initial P availability (Eriksson et al., 2016). The modest transfer into NaOH-P_i after 16 weeks is consistent with strong legacy P saturation in these buffer strip soils, where Fe- and Al-associated sorption sites are already largely occupied (Doydora et al., 2020; Neidhardt et al., 2019; Ramler et al., 2024). The high initial abundance of NaOH-extractable P_i further indicates near-saturation of Fe(III)-(hydr)oxide surfaces, constraining additional P_i retention. This supports our hypothesis (H1) that added P_i largely remains mobile (i.e., dissolved and exchangeable surface-bound P fractions) and, to a smaller extent, is retained in stable fractions (e.g., Fe(III)-bound P).

However, we assumed that drying-rewetting cycles would enhance P_i stabilization through frequent redox oscillations and repeated formation of fresh amorphous Fe(III)-(hydr)oxides, thereby increasing Fe-bound P over time, especially in the LPL treatment. Our results partially support this mechanism but also reveal a more complex pathway. Contrary to expectations, we did not observe substantial Fe(III) reduction during the wet phases. Generally, dissolved Fe concentrations in porewater and NaOH-extractable P_i (**Figure B-S4 a to d**) remained consistently low, indicating an absence of pronounced reductive dissolution. Normally, reducing conditions would be expected to liberate Fe(II) and mobilize Fe-bound P_i, yet this did not occur.

Instead, both treatments, particularly SPL, showed increases in CDB-extractable Fe (**Figure B-S4 e, f**), implying the accumulation of amorphous Fe(III)-(hydr)oxides that are dissolved in the CDB step (Roden et al., 2003). Importantly, such increases can occur without detectable Fe(II) release to the porewater, because rapid oxidation-reduction cycles at the microscale may not produce a measurable Fe reduction signal (Roden et al., 2003). Short drying-rewetting cycles likely accelerated this fine-scale Fe(III)-(hydr)oxide turnover, generating repeated pulses of fresh sorption surfaces.

In addition, the SPL treatment also exhibited a slightly higher increase in CDB-extractable P_o. This indicates that microbial residues and biofilm associated P_o accumulated on Fe(III)-(hydr)oxide surfaces during repeated drying-rewetting pulses (Khorshid et al., 2019). Drying-rewetting cycles are known to induce cell turnover and release of organic compounds, which can subsequently associate with Fe minerals and other soil constituents (Liu et al., 2021). Given the pronounced proportion of CDB-P_o and the elevated concentrations of CDB-extractable Fe after 16 weeks in both treatments (**Figure B-2 k, l**), it is highly likely that Fe(III)-(hydr)oxides played an active role in P stabilization in our experiment. We

propose that Fe(III)-(hydr)oxides served as preferential colonization sites for microbial biofilms (Zhang et al., 2018). Generally, Fe(III)-reducing bacteria are known to colonize Fe(III) mineral surfaces, where P_i is often adsorbed, and to develop biofilms in association with other microorganisms (Roden, 2003; Lu et al., 2016). Such biofilms consist of microbial cells, residues of lysed organisms, and extracellular polymeric substances that host a range of P_o compounds, including phospholipids, nucleic acids, phosphoproteins, and phosphate esters (Liu et al., 2021; Shi and Xu, 2019). These observations suggest that enhanced P stabilization occurs mainly through the associated accumulation of Fe-bound P_i and P_o, rather than through extensive Fe reduction-oxidation cycling. The CDB-extractable P_o pool was marginally higher in the SPL treatment (+2%), suggesting that short waterlogging periods may enhance P sorption through microbial activity and dynamics in the Fe-mineralogy. This may further indicate that more P_i is incorporated into stable organic compounds (Fe-OM complexes) under short fluctuations, while it remains in more loosely bound NaOH-extractable P_o under longer fluctuations.

However, a significant decrease in the NaOH-P_o pool observed in the SPL treatment after 16 weeks and in the LPL treatment after 8 weeks (**Figure B-2 g**) indicates ongoing microbial activity, recognizable by the relatively high APA values (**Figure B-S3 c, d**). Staddon et al. (2001) demonstrated that increased enzymatic activity in VBS soils matched larger microbial populations. The APA values during the 16 weeks indicate that microorganism still released phosphatase enzymes, which are capable of hydrolyzing P_o compounds and releasing P_i (Bauke et al. 2022, Helfenstein et al., 2018). Once P_o is hydrolyzed, the released P_i can be sorbed to soil minerals (Fe, Al, Ca compounds) or immobilized (retained) in the microbial biomass (Roberts et al. 2012). Thus, the subsequent hydrolysis of associated P_o compounds by the activity of extracellular acid phosphatases provides a source for P_i, which is subsequently transferred to the various P_i pools in the soil (Gharu et al., 2016).
Considering the increase in CDB-extractable P_i during 16 weeks of incubation (**Figure B-2 l, j**), which was accompanied by a decline in NaOH-extractable P_o (**Figure B-2 g, h**), we suggest that a part of NaOH-extractable P_o was hydrolyzed and become more strongly associated with crystalline Fe(III)-(hydr)oxides. The formation of Fe-OM complexes via the reaction of OM with Fe(III)-(hydr)oxides like ferrihydrite and the coprecipitation of ternary compounds was suggested for example by Luo et al. 2022, which could further contribute to the build-up of the CDB-P_o pool (Khorshid et al., 2019). Subsequently, P_i and P_o were shifted into the CDB pool, reinforced by oxidation and reduction changes (Khorshid et al., 2019). Additionally, microbial cell lysis during rewetting may also release P_o into the soil solution, that can make up to 41 - 44% of the respective pool (Gu et al., 2018). At the end of the 16 weeks, the NaOH-extractable P_o continuously declined in the SPL treatment reaching a proportion of 8%, and increased slightly again in the LPL treatment, reaching 15%. Here, cell lysis was obviously more pronounced under short fluctuations (SPL) as compared to long fluctuations (LPL). Thus, our second hypothesis (H2) was not supported, as short cycles of drying-rewetting showed a more pronounced transfer of P_i and P_o into the CDB-extractable pools as compared to the long cycles. However, the magnitude of this effect was modest and the mechanistic driver was the accumulation of biofilm-associated P on Fe(III)-(hydr)oxide surfaces rather than redox-driven sorption site renewal.

In summary, most P was rapidly incorporated into labile pools (porewater- and $NaHCO_3$-extractable P_i) following P_i addition, while only minor proportions were gradually transferred into the NaOH- and CDB-extractable pools over 16 weeks. This pattern indicates a limited sorption capacity due to legacy P and

the dominance of microbial and Fe(III)-(hydr)oxide-associated stabilization processes. The concurrent decline of NaOH-extractable P_o and increase of CDB-extractable P_i and P_o suggest microbial hydrolysis and subsequent association of released P with Fe(III)-(hydr)oxides and biofilm-derived organic complexes under fluctuating redox conditions. This highlights the importance of biogeochemical microsite processes, rather than classical redox-driven Fe cycling, in governing P retention under fluctuating hydrological regimes in VBS soils.

4.2. Behavior of phosphorus pools in forest soil (FST)

One day after P_i addition, most of the added P was found in form of dissolved P_i in porewater (+21%) as well as $NaHCO_3$-extractable P_i (+31%) (**Figure B-S12**). The principal P_i pool with a relative proportion of >40% was represented by $NaHCO_3$-extractable P_i., which agrees with previous studies (Barrow et al., 2020). Here, P adsorption onto mineral surfaces and organic matter represents the most important initial P_i binding mechanism (Joshi et al., 2015; Zhijing et al., 2011).

Over the 16 weeks of incubation with cyclic drying-rewetting, several biotic and abiotic processes resulted in the redistribution of P_i into the NaOH- and CDB-extractable P_i pools (**Figure B-4 e to h**). The transfer of P_i into the NaOH-extractable P_i pool was closely linked to a significant increase in pH accompanied by the decline of APA, which could be due to the exclusion of vegetation and removal of roots that are largely responsible for proton and APA exudation (Lu et al., 2016). Weakly bound $NaHCO_3$-extractable P_i, (e.g., by changes of mineral surface charges and sorption competition with OH^-) is mobilized, while enhancing strong adsorption to metal oxides and hydroxides (Barrow et al., 2020; Zhou et al., 2005). The increase in CDB-extractable P_i therefore suggests that loosely bound P became associated with more crystalline Fe(III)-(hydr)oxides, a dynamic likely fostered by the frequent drying-rewetting cycles. This process is driven by Fe(III) reoxidation and mineral precipitation (Zhang et al., 2021). In addition, the pronounced increase in NaOH-extractable P_i indicates active secondary P fixation (Condron et al., 2005). These outcomes confirm our third hypothesis (H3): without legacy P, P_i addition increases the relative proportion of more stable pools (NaOH-, CDB-extractable P_i).

After 16 weeks, the proportion of $NaHCO_3$-extractable P_o increased significantly in both treatments by 18 to 21% (**Figure B-4 i, j**), which was accompanied by decreases in $NaHCO_3$- extractable P_i and NaOH- extractable P_o (**Figure B-4 k, l**). These trends reflect a strong biological and organo-mineral coupling that is characteristic for forest soils, which are typically P-limited, causing microbial communities to respond strongly to additional P_i inputs through increased assimilation and biomass production (Zhou et al., 2017). In addition, forest soils are rich in organic matter and provide abundant substrates for rapid microbial assimilation (Chacón et al., 2005; Liu et al., 2019). Following P_i addition, microorganisms can immobilize P_i by incorporating it into cellular biomass or transforming it into $NaHCO_3$-extractable P_o compounds through metabolic processes (He et al., 2023; Ramler et al., 2022). The elevated pH may have further stimulated microbial activity, enhancing the conversion of P_i into P_o (Kunito et al., 2021; Liu et al., 2020). This biotic immobilization results in a net increase in the $NaHCO_3$-extractable P_o pool, which commonly contains microbial-derived and easily mineralizable P_o forms such as phosphate monoesters, diesters, phospholipids, and nucleic acids (Liu et al., 2021; Shi and Xu, 2019).

At the same time, the observed declines in $NaHCO_3$-extractable P_i and NaOH-extractable P_o suggest that P_i was taken up not only directly from porewater, but also indirectly through the mineralization of moderately labile P_o. Microbial phosphatases can hydrolyze NaOH-extractable P_o, releasing P_i that subsequently becomes incorporated into microbial biomass or converted into easily extractable P_o forms including phosphate monoesters, diesters, phospholipids, and nucleic acids (Liu et al., 2021; Shi and Xu, 2019). Drying-rewetting cycles enhance these processes by stimulating microbial turnover and releasing P_o during cell lysis (Chen et al., 2023; Zhang et al., 2023). The reduction in NaOH-extractable P_o reflects an active microbial turnover rather than purely abiotic sorption processes.

However, abiotic stabilization processes may further contribute to the increase in $NaHCO_3$-extractable P_o. Organic P compounds can associate with SOM through adsorption or molecular incorporation, forming transient organo-mineral complexes that are captured in the $NaHCO_3$-extractable P_o fraction (Dodd et al., 2015). Such associations can occur simultaneously with microbial assimilation, especially in SOM-rich forest soils where dissolved organic ligands enhance P complexation pathways (Dodd et al., 2015).

Together, these biotic and abiotic mechanisms explain the pattern of declining $NaHCO_3$-extractable P_i and NaOH-extractable P_o alongside increasing $NaHCO_3$-extractable P_o, as added P_i is rapidly mobilized into microbial biomass and labile organic forms, supported by ongoing mineralization of moderately labile P_o and stabilization within SOM-rich compounds. Moisture fluctuations, redox changes, and microbial nutrient demand modulate these transformations, highlighting that P_i addition indirectly affects P_o pool composition. Incubation studies have shown that short drying-rewetting cycles favor microbial turnover and rapid P_o formation, leading to higher accumulation of P_o ($NaHCO_3$-extractable P_o), whereas long cycles allow microbial communities to adapt, but slowing down P_o buildup (NaOH-extractable P_o) and stabilization of P_o molecules (Brödlin et al., 2019; van Dinh et al., 2018).

Despite these expectations, our experiment did not reveal any significant differences between short and long drying-rewetting cycles in the forest soil. This suggests that the forest soil system is inherently more resilient to variations in hydrological fluctuation length, likely due to its high SOM content, stable microbial community structure, and well-established organo-mineral associations that buffer microbial and abiotic P transformation processes against short-term disturbance. Consequently, our fourth hypothesis (H4), which proposed that long drying-rewetting cycles promote microbial adaptation and thus a more pronounced buildup of P_o compared to short cycles, cannot be confirmed.

In summary, added P_i was initially adsorbed to mineral and organic surfaces, forming a dominant $NaHCO_3$-extractable P_i pool, before transfer into more stable NaOH- and CDB-extractable P_i pools. These transformations were driven by pH increases, Fe(III) reoxidation, and mineral precipitation, confirming that P_i addition promotes secondary fixation in forest soils. Simultaneously, microbial immobilization and abiotic adsorption promoted a rise in $NaHCO_3$-extractable P_o. These findings highlight that in organic-rich forest soils without legacy P, drying-rewetting dynamics mainly enhance microbial assimilation and secondary P fixation, leading to a gradual stabilization of added P, regardless of the duration of the fluctuations.

5. Conclusion

Due to legacy P, VBS soils are hardly capable of retaining additional P_i in the long term under climate change induced dynamics in hydrological regimes. On the contrary, fluctuating redox conditions may even lead to P remobilization. The small proportion of NaOH-extractable P_i in both hydrological treatments highlights this limited sorption potential and implies a risk of P_i leaching, particularly under conditions promoting runoff. The low incorporation in the CDB-extractable P_i and P_o pool also indicates limited storage capacity into more stable pools. In addition, the persistence of a large proportion of the added P in the $NaHCO_3$-extractable P_i fraction further supports the assumption that, in the presence of legacy P, leaching losses from Ca-carbonate-free buffer strips are likely to occur especially under fluctuating drying-rewetting conditions irrespective of the duration. Here, continued P_i input from adjacent arable fields may undermine the ability of buffer zones to retain nutrients and protect surface waters from eutrophication.

In contrast, non-legacy soils can store substantial amounts of P_i in specific pools over the long term, visible in the NaOH- and CBD-P_i pools of the investigated forest soil. Here, our results suggest an effective adsorption of P_i onto Al- and Fe-(hydr)oxides as well as onto more crystalline Fe(III)-(hydr)oxides. In addition, the transformation into $NaHCO_3$-extractable P_o suggests that P_i input stimulates microbial or enzymatic activity, potentially decreasing the risk of P (re)mobilization by hydrolysis of P_o compounds. Even under the pressure of climate change and the resulting alterations in the hydrological regime, forest soils show a stronger buffering capacity to retain P in specific pools over extended periods - a capacity that VBS soils seem to no longer possess.

Our experiment demonstrated that in soils with legacy P, abiotic processes such as adsorption, precipitation, and mineral fixation dominate P transformations, while in non-legacy P soils, biotic processes such as microbial assimilation, turnover, and P_o formation govern the redistribution and stabilization of added P_i. Future research should address the critical dynamics of specific P_o pools across different systems (legacy P, non-legacy P) including microbial transformation mechanisms, to better understand the interplay of biotic and abiotic processes. Moreover, it should be concerned with the effects of different kinds and application frequencies of P fertilizer to evaluate how repeated P inputs influence nutrient cycling, microbial community structure, and P availability in soils with contrasting P legacies, helping to develop and optimize management strategies aimed at reducing P losses from agricultural catchments under changing climate conditions.

Acknowledgements

The authors would like to thank the German Research Foundation (DFG) for funding (NE-1852/4-1, Project number: 412678780). We are further grateful for further financial support through the Equal Opportunities Commission of the University of Tübingen. We also thank our laboratory staff (Sabine Flaiz, Rita Mögenburg) and students and student helpers (Diana Fiedler, Carolin Rieber, Louis Hausner, Pauline Stiller, Silvana Oldenburg, Niklas Wendenburg, Hannah Lemke, Lukas Schwella, Aline Ott-Fuchs, Pauline Röhner), as well as our colleagues from the AG Geoecology (Simon Hauenstein, Arnim Kessler, Wen Shao, Camilo Maliqueo-Murga) for support of our project.

6. References

Ad-hoc-AG Boden (2005): Bodenkundliche Kartieranleitung, 5. Auflage, Hannover.

Ajmone-Marsan, F., Côté, D., & Simard, R. R. (2006). Phosphorus transformations under reduction in long-term manured soils. Plant and soil, 282, 239-250. https://doi.org/10.1007/s11104-005-5929-6.

Barczok, M., Smith, C., Di Domenico, N., Kinsman-Costello, L., Singer, D., & Herndon, E. (2023). Influence of contrasting redox conditions on iron (oxyhydr) oxide transformation and associated phosphate sorption. Biogeochemistry, 166(2), 87-107. https://doi.org/10.1007/s10533-023-01094-z.

Barrow, N. J. (1984). Modelling the effects of pH on phosphate sorption by soils. Journal of Soil Science, 35(2), 283-297. https://doi.org/10.1111/j.1365-2389.1984.tb00283.x.

Barrow, N. J., Debnath, A., & Sen, A. (2020). Measurement of the effects of pH on phosphate availability. Plant and Soil, 454, 217-224. https://doi.org/10.1007/s11104-020-04647-5.

Bauke SL, Wang Y, Saia SM, Popp C, Tamburini F, Paetzold S, et al. (2022). Phosphate oxygen isotope ratios in vegetated riparian buffer strip soils. Vadose Zone Journal, 21(3), e20193.

Brödlin, D., Kaiser, K., Kessler, A., & Hagedorn, F. (2019). Drying and rewetting foster phosphorus depletion of forest soils. Soil Biology and Biochemistry, 128, 22-34. https://doi.org/10.1016/j.soilbio.2018.10.001.

Bünemann, E. K. (2015). Assessment of gross and net mineralization rates of soil organic phosphorus-A review. Soil Biology and Biochemistry, 89, 82-98. https://doi.org/10.1016/j.soilbio.2015.06.026.29

Chacón, N., Dezzeo, N., Munoz, B., & Rodríguez, J. M. (2005). Implications of soil organic carbon and the biogeochemistry of iron and aluminum on soil phosphorus distribution in flooded forests of the lower Orinoco River, Venezuela. Biogeochemistry, 73(3), 555-566. https://doi.org/10.1007/s10533-004-1773-7.

Chen, J., Xu, H., Seven, J., Zilla, T., Dippold, M. A., & Kuzyakov, Y. (2023). Microbial phosphorus recycling in soil by intra-and extracellular mechanisms. ISME Communications, 3(1), 135. https://doi.org/10.1038/s43705-023-00340-7.

Cole, L. J., Stockan, J., & Helliwell, R. (2020). Managing riparian buffer strips to optimise ecosystem services: A review. Agriculture, ecosystems & environment, 296, 106891. https://doi.org/10.1016/j.agee.2020.106891.

Condron, L. M., & Tiessen, H. (2005). Interactions of organic phosphorus in terrestrial ecosystems. In Organic phosphorus in the environment (pp. 295-307). Wallingford UK: CABI publishing. https://doi.org/10.1079/9780851998220.0295.

Cross, A. F., & Schlesinger, W. H. (1995). A literature review and evaluation of the. Hedley fractionation: Applications to the biogeochemical cycle of soil phosphorus in natural ecosystems. Geoderma, 64(3-4), 197-214. https://doi.org/10.1016/0016-7061(94)00023-4.

De Schrijver, A., Vesterdal, L., Hansen, K., De Frenne, P., Augusto, L., Achat, D. L., ... & Verheyen, K. (2012). Four decades of post-agricultural forest development have caused major redistributions of soil phosphorus fractions. Oecologia, 169(1), 221-234. https://doi.org/10.1007/s00442-011-2185-8.

DIN ISO 10390 (2005): Bodenbeschaffenheit—Bestimmung des pH Wertes. ISO 10390.

DIN ISO 11465 (1996-12). Bodenbeschaffenheit-Bestimmung der Trockensubstanz und des Wassergehalts auf Grundlage der Masse-Gravimetrisches Verfahren (ISO 11465: 1993).

DIN EN ISO 20130:2021-02: Bodenbeschaffenheit - Messung von Enzymaktivitätsmustern in Bodenproben mit kolorimetrischen Substraten in Mikrotiterplatten (ISO 20130:2018); Deutsche Fassung EN ISO 20130:2020.

Dinh, M. V., Guhr, A., Weig, A. R., & Matzner, E. (2018). Drying and rewetting of forest floors: dynamics of soluble phosphorus, microbial biomass-phosphorus, and the composition of microbial communities. Biology and Fertility of Soils, 54(6), 761-768. https://doi.org/10.1007/s00374-018-1300-y.

Dodd, R. J., & Sharpley, A. N. (2015). Recognizing the role of soil organic phosphorus in soil fertility and water quality. Resources, Conservation and Recycling, 105, 282-293. http://dx.doi.org/10.1016/j.resconrec.2015.10.001.

Doydora, S., Gatiboni, L., Grieger, K., Hesterberg, D., Jones, J. L., McLamore, E. S., ... & Duckworth, O. W. (2020). Accessing legacy phosphorus in soils. Soil systems, 4(4), 74. https:// doi:10.3390/soilsystems4040074.

Dupas, R., Delmas, M., Dorioz, J. M., Garnier, J., Moatar, F., & Gascuel-Odoux, C. (2015). Assessing the impact of agricultural pressures on N and P loads and eutrophication risk. Ecological Indicators, 48, 396-407. https://doi.org/10.1016/j.ecolind.2014.08.007.

Eriksson, A. K., Hesterberg, D., Klysubun, W., & Gustafsson, J. P. (2016). Phosphorus dynamics in Swedish agricultural soils as influenced by fertilization and mineralogical properties: Insights gained from batch experiments and XANES spectroscopy. Science of the Total Environment, 566, 1410-1419. https://doi.org/10.1016/j.scitotenv.2016.05.225.

Gharu, A. D., & Tarafdar, J. C. (2016). Efficiency of phosphatases in mobilization of native phosphorus fractions under different vegetation. Agricultural Research, 5(4), 335-345. https://doi.org/10.1007/s40003-016-0235-5.

Gu, S., Gruau, G., Malique, F., Dupas, R., Petitjean, P., & Gascuel-Odoux, C. (2018). Drying/rewetting cycles stimulate release of colloidal-bound phosphorus in riparian soils. Geoderma, 321, 32-41. https://doi.org/10.1016/j.geoderma.2018.01.015.

Habibiandehkordi, R., Lobb, D. A., Owens, P. N., & Flaten, D. N. (2019). Effectiveness of vegetated buffer strips in controlling legacy phosphorus exports from agricultural land. Journal of environmental quality, 48(2), 314-321. https://doi:10.2134/jeq2018.04.0129

Haygarth, P. M., Jarvie, H. P., Powers, S. M., Sharpley, A. N., Elser, J. J., Shen, J., ... & Liu, X. (2014). Sustainable phosphorus management and the need for a long-term perspective: The legacy hypothesis. https://doi: 10.1021/es502852s.

He, L. P., Jia, K. T., Liu, D., Wang, K. H., Duan, L. Y., & Lin, J. J. (2023). Effects of phosphorus fertilizer application rate on transformation processes of phosphorus fractions in the purple alluvial soil of a riparian zone. Journal of Mountain Science, 20(6), 1561-1574. https://doi.org/10.1007/s11629-022-7707-9.

Hedley, M. J., Stewart, J. W. B., & Chauhan, B. (1982). Changes in inorganic and organic soil phosphorus fractions induced by cultivation practices and by laboratory incubations. Soil Science Society of America Journal, 46(5), 970-976. https://doi.org/10.2136/sssaj1982.03615995004600050017x.

Helfenstein, J., Tamburini, F., von Sperber, C., Massey, M. S., Pistocchi, C., Chadwick, O. A., ... & Frossard, E. (2018). Combining spectroscopic and isotopic techniques gives a dynamic view of phosphorus cycling in soil. Nature communications, 9(1), 3226. https://doi.org/10.1038/s41467-018-05731-2.

Hille, S., Graeber, D., Kronvang, B., Rubæk, G. H., Onnen, N., Molina-Navarro, E., ... & Stutter, M. I. (2019). Management options to reduce phosphorus leaching from vegetated buffer strips. Journal of environmental quality, 48(2), 322-329. https:// doi:10.2134/jeq2018.01.0042.

Hoffmann, C. C., Kjaergaard, C., Uusi-Kämppä, J., Hansen, H. C. B., & Kronvang, B. (2009). Phosphorus retention in riparian buffers: review of their efficiency. Journal of environmental quality, 38(5), 1942-1955. https://doi.org/10.2134/jeq2008.0087.

Joshi, S. R., Kukkadapu, R. K., Burdige, D. J., Bowden, M. E., Sparks, D. L., & Jaisi, D. P. (2015). Organic matter remineralization predominates phosphorus cycling in the mid-bay sediments in the Chesapeake Bay. Environmental science & technology, 49(10), 5887-5896. https://doi.org/10.1021/es5059617.

Joshi, S. R., Li, X., & Jaisi, D. P. (2016). Transformation of phosphorus pools in an agricultural soil: An application of oxygen-18 labeling in phosphate. Soil Science Society of America Journal, 80(1), 69-78. https://doi.org/10.2136/sssaj2015.06.0219.

Khorshid, M. S. H., Kruse, J., Semella, S., Vohland, M., Wagner, J. F., & Thiele-Bruhn, S. (2019). Phosphorus fractions and speciation in rural and urban calcareous soils in the semiarid region of Sulaimani city, Kurdistan, Iraq. Environmental Earth Sciences, 78(16), 531. https://doi.org/10.1007/s12665-019-8543-2.

Kleinman, P., Sharpley, A., Buda, A., McDowell, R., & Allen, A. (2011). Soil controls of phosphorus in runoff: Management barriers and opportunities. Canadian Journal of Soil Science, 91(3), 329-338. https://doi.org/10.4141/cjss09106.

Kunito, T., Haraguchi, S., Hanada, K., Fujita, K., Moro, H., Nagaoka, K., & Otsuka, S. (2021). pH is the dominant factor controlling the levels of phytate-like and DNA-like phosphorus in 0.5 M NaHCO3-extracts of soils: Evaluation with phosphatase-addition approach. Geoderma, 398, 115113. https://doi.org/10.1016/j.geoderma.2021.115113.

Leibundgut, C., & Eisele, M. (2005). Weiterentwicklung des Bewertungsverfahrens „Hydrologische Güte “als Expertensystem zum operationellen Einsatz im Flussgebietsmanagement. Abschlußbericht-Programm Lebensgrundlage Umwelt und ihre Sicherung, FKZ BWC.

Liu, J., Lu, H., Wu, L., Kerr, P. G., & Wu, Y. (2021). Interactions between periphytic biofilms and dissolved organic matter at soil-water interface and the consequent effects on soil phosphorus fraction changes. Science of the Total Environment, 801, 149708. https://doi.org/10.1016/j.scitotenv.2021.149708.

Lu, H., Wan, J., Li, J., Shao, H., & Wu, Y. (2016). Periphytic biofilm: A buffer for phosphorus precipitation and release between sediments and water. Chemosphere, 144, 2058-2064. https://doi.org/10.1016/j.chemosphere.2015.10.129.

Luo, X., Yang, Y., Xie, S., Wang, W., Li, N., Wen, C., ... & Chen, L. (2022). Drying and rewetting induce changes in biofilm characteristics and the subsequent release of metal ions. Journal of Hazardous Materials, 433, 128832. https://doi.org/10.1016/j.jhazmat.2022.128832.

Mattingly, G. E. G., Chater, M., & Johnston, A. E. (1975). Experiments made on Stackyard Field, Woburn, 1876-1974. III. Effects of NPK Fertilisers and Farmyard Manure on Soil Carbon, Nitrogen and Organic Phosphorus. Rothamsted Experimental Station Report, 1974(2), 61-77. https://doi.org/10.23637/ERADOC-1-33160.

Nagul, E. A., McKelvie, I. D., Worsfold, P., & Kolev, S. D. (2015). The molybdenum blue reaction for the determination of orthophosphate revisited: Opening the black box. Analytica chimica acta, 890, 60-82. https://doi.org/10.1016/j.aca.2015.07.030.

Negassa, W., & Leinweber, P. (2009). How does the Hedley sequential phosphorus fractionation reflect impacts of land use and management on soil phosphorus: A review. Journal of Plant Nutrition and Soil Science, 172(3), 305-325. https://doi.org/10.1002/jpln.200800223.

Neidhardt, H., Achten, F., Kern, S., Schwientek, M., & Oelmann, Y. (2019). Phosphorus pool composition in soils and sediments of transitional ecotones under the influence of agriculture. Journal of environmental quality, 48(5), 1325-1335. https://doi.org/10.2134/jeq2019.01.0012.

Neidhardt, H., Rudischer, S., Eiche, E., Schneider, M., Stopelli, E., Duyen, V. T., ... & Berg, M. (2021). Phosphate immobilisation dynamics and interaction with arsenic sorption at redox transition zones in floodplain aquifers: Insights from the Red River Delta, Vietnam. Journal of Hazardous Materials, 411, 125128. https://doi.org/10.1016/j.jhazmat.2021.125128.

Niederberger, J., Kohler, M., & Bauhus, J. (2019). Distribution of phosphorus fractions with different plant availability in German forest soils and their relationship with common soil properties and foliar P contents. Soil, 5(2), 189-204. https://doi.org/10.5194/soil-5-189-2019).

Pierzynski, G. M. (2000, June). Methods of phosphorus analysis for soils, sediments, residuals, and waters.

Reddy, K. R., Kadlec, R. H., Flaig, E., & Gale, P. M. (1999). Phosphorus retention in streams and wetlands: a review. Critical reviews in environmental science and technology, 29(1), 83-146. https://doi.org/10.1080/10643389991259182.

Ramler, D., Stutter, M., Weigelhofer, G., Quinton, J. N., Hood-Nowotny, R., & Strauss, P. (2022). Keeping up with phosphorus dynamics: overdue conceptual changes in vegetative filter strip research and management. Frontiers in Environmental Science, 10, 764333. https://doi.org/10.3389/fenvs.2022.764333.

Ramler, D., & Strauss, P. (2024). Site matters: site-specific factors control phosphorus retention in buffer strip soils under concentrated field runoff. Environmental Science and Pollution Research, 31(35), 48154-48163. https://doi.org/10.1007/s11356-024-34383-7.

Roberts, W. M., Stutter, M. I., & Haygarth, P. M. (2012). Phosphorus retention and remobilization in vegetated buffer strips: a review. Journal of environmental quality, 41(2), 389-399. https:// doi:10.2134/jeq2010.0543.

Roden, E. E. (2003). Fe (III) oxide reactivity toward biological versus chemical reduction. Environmental Science & Technology, 37(7), 1319-1324.

Schinner, F., Öhlinger, R., Kandeler, E., & Margesin, R. (Eds.). (2012). Methods in soil biology. Springer Science & business media.

Schwientek, M., Osenbrück, K., & Fleischer, M. (2013). Investigating hydrological drivers of nitrate export dynamics in two agricultural catchments in Germany using high-frequency data series. Environmental earth sciences, 69, 381-393. https://doi.org/10.1007/s12665-013-2322-2.

Shi, S., & Xu, G. (2019). Identification of phosphorus fractions of biofilm sludge and phosphorus release, transformation and modeling in biofilm sludge treatment related to pH. Chemical Engineering Journal, 369, 694-704.

Siegenthaler, M. B., Ramoneda, J., Frossard, E., & Meszaros, E. (2022). Microbial community responses to phosphorus and nitrogen inputs in the organic soil horizons of two contrasting temperate beech forests. Applied Soil Ecology, 172, 104357. https://doi.org/10.1016/j.apsoil.2021.104357.

Staddon, W. J., Locke, M. A., & Zablotowicz, R. M. (2001). Microbiological characteristics of a vegetative buffer strip soil and degradation and sorption of metolachlor. Soil Science Society of America Journal, 65(4), 1136-1142.

Taalab, A. S., Ageeb, G. W., Siam, H. S., & Mahmoud, S. A. (2019). Some characteristics of calcareous soils. A review as Taalab1, GW Ageeb2, Hanan S. Siam1 and Safaa A. Mahmoud1. Middle East J, 8(1), 96-105.

Tabatabai, M. A., & Bremner, J. M. (1969). Use of p-nitrophenyl phosphate for assay of soil phosphatase activity. Soil biology and biochemistry, 1(4), 301-307.

Tiessen, H. (1993). Characterization of Available P by Sequential Fractionation. CRC Press, Soil Sampling and Method of Analysis, pp. 75-87.

Tübinger Blätter, Jahrgang 61. (1974): Tübinger Verkehrsverein e.V. (Hrsg.). Tübingen. http://doi.org/10.20345/digitue.21077.

Withers, P. J. A., Hartikainen, H., Barberis, E., Flynn, N. J., & Warren, G. P. (2009). The effect of soil phosphorus on particulate phosphorus in land runoff. European Journal of Soil Science, 60(6), 994-1004. https://doi:10.1111/j.1365-2389.2009.01161.x.

Young, E. O., Ross, D. S., Jaisi, D. P., & Vidon, P. G. (2021). Phosphorus transport along the cropland-riparian-stream continuum in cold climate agroecosystems: A review. Soil systems, 5(1), 15. https://doi.org/10.3390/soilsystems5010015.

Zhang, Y., Xu, B., Han, J., & Shi, L. (2021). Effects of drying-rewetting cycles on ferrous iron-involved denitrification in paddy soils. Water, 13(22), 3212. https://doi.org/10.3390/w13223212.

Zhou, Z., Wang, C., & Jin, Y. (2017). Stoichiometric responses of soil microflora to nutrient additions for two temperate forest soils. Biology and Fertility of Soils, 53(4), 397-406. https://doi: 10.1007/s00374-017-1188-y.

Zhijing, C. A. O., Zhang, X., & Nanshan, A. I. (2011). Effect of sediment on concentration of dissolved phosphorus in the Three Gorges Reservoir. International Journal of Sediment Research, 26(1), 87-95). https://doi.org/10.1016/S1001-6279(11)60078-4.

Supporting information Section B

Supporting information Section B-S1: Chemical analyses

Sequential phosphorus extraction scheme

The sequential extraction for assessing different operationally defined P pools was carried out following a modified procedure after Hedley (Hedley et al., 1982). In brief, samples were subsequently extracted with increasingly potent extraction solutions (0.5M $NaHCO_3$, followed by 0.1M NaOH, CDB solution, 1M HCl and finally 0.5M H_2SO_4). For the extraction of the operationally defined P pools, 0.5 g (dry weight equivalent) of fresh sample material was weighted into 50 ml centrifuge tubes. All extraction steps were performed subsequently within 72 hours, extraction solutions were stored in a fridge at 4°C until analysis.

First labile P_i and P_o adsorbed on surfaces were removed by 0.5M $NaHCO_3$ (Roth GmbH, p.a. ≥ 98 %) (Bowman and Cole, 1978). Therefore, 20 ml of 0.5M $NaHCO_3$ were added to every sample and shaken for 30 minutes on a horizontal shaker, then centrifuged (2500 RPM, 10 minutes) and filtered through a wrinkle filter (MN 619, Machery-Nagel). This procedure was repeated 2 times with 20 ml $NaHCO_3$, shaken for 30 minutes. The extracts of all repetitions were collected and unified. More repetitions were not required according to a pre-experiment, in which $NaHCO_3$-extractable PO_4-P concentrations dropped to below 0.01 mg l^{-1} (third repetition) and 0.001 mg l^{-1} (fourth repetition). Finally, one wash step with ultrapure water (Milli-Q) for neutralizing the sample materials was added, shaken for 30 minutes.

Next, 0.1M NaOH (Sigma-Aldrich, p.a. ≥ 98 %) solution was used to remove moderately labile P_i and P_o compounds held more strongly to mineral surfaces (McLaughlin et al., 1977). Here, 30 ml of 0.1M NaOH were added, shaken for 16 hours on a horizontal shaker and centrifuged (2500 RPM, 10 minutes). There was one repetition with 30 ml NaOH shaken for 30 minutes, which was unified with the previously extracted NaOH solution. Results of a pre-experiment showed that PO_4-P concentrations rapidly dropped with following repetitions (< 0.02 mg l^{-1} after second repetition). After that, one wash step with ultrapure water was applied.

Next, a citrate-dithionite-bicarbonate (CDB) extraction step was applied to remove P_i associated with Fe(III)- and Mn(IV)-oxides and -hydroxides. The CDB extraction solution comprised a mixture of Na-citrate (p.a., Merck), $NaHCO_3$ (p.a., Roth GmbH) and sodium dithionite (p.a., Merck). For this, 1.5 l of 0.3M Na-citrate and 1.5 l 1M $NaHCO_3$ were mixed and a total of 45 ml were added to each sample, followed by an addition of 1.125 g Na-dithionite (p.a., Merck) and shaking for 8 hours on a horizontal shaker and centrifuging (2500 RPM, 10 minutes). Afterwards, three repetitions of extraction with 20 ml 0.5M $NaHCO_3$, each shaken for 30 minutes, were added in order to avoid carry-over effects through re-adsorption of P. More repetitions were not required according to a pre-experiment.

The next step used a 1M HCl (p.a. ≥ 37 %, Sigma-Aldrich) extraction solution, where mainly apatite is targeted (Williams et al., 1971). Therefore, 25 ml of 1M HCl were added to each sample and samples were placed over night into a water bath at 25°C. Afterwards samples were shaken for 30 minutes on a horizontal shaker and centrifuged (2500 RPM, 10 minutes). One repetition with 25 ml HCl for 30 minutes in the water bath at 25°C followed. Both solutions were unified for the analysis. Also, three wash steps (each 30 minutes) with ultrapure water followed for neutralizing the pH-value.

Finally, stable forms of P_o and relatively insoluble P_i were dissolved by 20 ml of 0.5M H_2SO_4 (≥ 98 %, Merck) after heating samples to 550°C in ceramic crucibles in a muffle oven (Nabertherm, Naber Industrieofenbau, Germany). After the addition of 0.5M H_2SO_4 , sample remains were shaken for 16 hours on a horizontal shaker and centrifuged (2500 RPM, 10 minutes). Note that these sample were not used for stable oxygen isotope analysis due to alteration of the isotopic oxygen ratios resulting from through the treatment.

Acid phosphatase activity (APA)

The acid mono-phosphatase activity (APA) was determined following the method developed by Tabatabai and Bremner (1969), modified by Schinner et al. (1991) and DIN EN ISO 20130. The following solutions were prepared to determine APA:

1. modified universal buffer (12.1 g Tris-(hydroxymethyl) aminomethane (AppliChem GmbH, p.a.), 11.6 g Maleic acid (Roth, p.a. ≥ 99%), 12 g citric acid (Sigma-Aldrich, p.a.) and 6.3 g boracic (Merck, p.a.), diluted in 500 ml 1M NaOH (Sigma-Aldrich, p.a. ≥ 98 %), filled up to 1000 ml with Milli-Q water, pH set to 6.5 with 0.1M HCl (p.a. ≥ 37 %, Sigma-Aldrich)
2. 0.1M substrate solution (4.27 g of p-Nitrophenylphosphate-disodium-tetrahydrate (PNP, Roth, p.a. ≥99%) diluted in 100 ml of the modified universal buffer)
3. 0.5M $CaCl_2$ solution
4. 0.5M NaOH

To determine the APA, 1.0 g of fresh sediment was weighted into a 50 ml tube and filled with 1 ml of the substrate solution and 4 ml of the modified universal buffer. Next, samples were shaken and incubated at 37°C for one hour. After the incubation, 1 ml of the $CaCl_2$ and 4 ml of the NaOH solution were added to each tube. The tubes were filled up with Milli-Q water, shaken and filtered with a wrinkle filter (MN 619, Machery-Nagel). Concentrations of P_i were finally measured immediately by UV-VIS (Analytik Jena Specord 200 plus, Germany).

Table B-S1: Overview of the sampling site in the Ammer catchment where soil samples of the vegetated buffer strip (VBS) and forest (FST) were collected from three adjacent spots.

Study site	**Samples**	**Coordinates (WGS84)**	**Topography**	**Geology**	**Soil type in the area***	**Land use (vegetation)**
Vegetated buffer strip	Soil	N 48° 31.050 E 9° 0.790	Elevation: 345 m N.N. Slope: 6.5 %	Keuper (kmGr: Gipskeuper)	Vertisols	Vegetated (mostly grasses, few shrubs)
Forest	Soil	N 48° 31.032 E 9° 0.791	Elevation: 345 m N.N. Slope: 0 %	Keuper (kmGr: Gipskeuper)	Luvisol Vertisols	Forestry (Hornbeams, Oaks)

* LGRB (2017)

Table B-S2: Properties of initial soil and 24 hours after adding P_i solution to the vegetated buffer strip soil (a, VBS) and forest soil (b, FST). Values represent means and standard deviations of the triplicates. WC = water content, APA = acid phosphatase activity.

Property a) VBS	Initial soil	24 hours after P_i addition	Parameter	Initial soil	24 hours after P_i addition
WC (%)	38.7 ± 1.0	51.8 ± 4.8	**$NaHCO_3$ - P_o (mg kg^{-1})**	46.4 ± 5.5	0.00 ± 0.00
pH porewater	7.52 ± 0.23	7.28 ± 0.21	**NaOH - P_o (mg kg^{-1})**	174 ± 70	403 ± 49
pH soil	6.91 ± 0.12	6.55 ± 0.11	**CDB - P_o (mg kg^{-1})**	169 ± 44	109 ± 49
APA (µg PNP g h^{-1})	16.2 ± 8.9	16.2 ± 7.3	**HCl – TP (mg/kg)**	273 ± 141	144 ± 56
Porewater - P_i (mg l^{-1})	0.41 ± 0.10	12.5 ± 1.2	**H_2SO_4 – TP (mg/kg)**	- ± -	913 ± 723
$NaHCO_3$ - P_i (mg kg^{-1})	111 ± 18	471 ± 77.1	**Aqua regia TP (mg kg^{-1})**	1099 ± 40.9	1400 ± 64
NaOH - P_i (mg kg^{-1})	194 ± 87	337 ± 30	**$CaCO_3$ (wt%)***	<0.78	
CDB - P_i (mg kg^{-1})	60.8 ± 29.7	44.0 ± 17.0			
Property b) FST	**Initial soil**	**24 hours after P_i addition**	**Parameter**	**Initial soil**	**24 hours after P_i addition**
WC (%)	38.3 ± 4.1	49.9 ± 9.1	**$NaHCO_3$ - P_o (mg kg^{-1})**	11.2 ± 16.1	16.1 ± 76.1
pH porewater	-	5.66 ± 0.43	**NaOH - P_o (mg kg^{-1})**	237 ± 23	219 ± 5
pH soil	5.94 ± 0.42	5.60 ± 0.41	**CDB - P_o (mg kg^{-1})**	0.00 ± 0.00	0.00 ± 0.00
APA (µg PNP g h^{-1})	158 ± 38	133 ± 47	**HCl – TP (mg/kg)**	30.6 ± 17.5	32.8 ± 32.0
Porewater - P_i (mg l^{-1})	0.08 ± 0.11	357 ± 16	**H_2SO_4 – TP (mg/kg)**	94.2 ± 10.1	131 ± 15
$NaHCO_3$ - P_i (mg kg^{-1})	50.9 ± 26.7	673 ± 148	**Aqua regia TP (mg kg^{-1})**	- ± -	1314 ± 279
NaOH - P_i (mg kg^{-1})	80.0 ± 9.5	162 ± 13	**$CaCO_3$ (wt%)***	<0.78	
CDB - P_i (mg kg^{-1})	63.3 ± 11.6	104 ± 9.60			

- No data
* Neidhardt et al., 2019

Table B-S3: Quality controls (QC, p.a, Roth GmbH) and their respective recovery rates (% of certified value including ± as standard deviation) of the major and trace elements determined in the ICP-OES runs. Quality controls covering different concentrations (0.1 to 10 mg l^{-1}) were prepared in 0.2M HNO3 (65 %). Instrumental detection limit (IDL): 0.004 to 0.001 mg l^{-1}. All concentration values reported in mg l^{-1}.

Al 396.153 axial		**Ca 317.933 radial**		**Fe 238.204 axial**	
QC target concentration	**Measured concentration**	**QC target concentration**	**Measured concentration**	**QC target concentration**	**Measured concentration**
0.20	0.20	0.20	0.20	0.20	0.20
2.00	2.04	0.01	1.00	1.00	0.99
2.00	1.99	0.02	2.00	2.00	1.99
10.0	9.99	10.0	10.0	10.0	9.93
Recovery Rate [%] ± Std. dev.	**90.1 ± 3.51%**		**97.7 ± 0.06%**		**105 ± 0.02%**
Mg 285.213 radial		**Mn 257.610 radial**		**P 213.617 axial**	
QC target concentration	**Measured concentration**	**QC target concentration**	**Measured concentration**	**QC target concentration**	**Measured concentration**
0.20	0.20	0.10	0.10	0.20	0.20
1.00	0.99	0.50	0.50	1.00	1.00
2.00	1.99	1.00	1.00	2.00	2.01
10.0	9.93	5.00	5.01	10.0	9.94
Recovery Rate [%] ± Std. dev.	**101 ± 0.03%**		**103 ± 0.01%**		**101 ± 0.01%**

Table B-S4: Changes in soil properties during 16 weeks of incubation under 20°C conditions in vegetated buffer strip soil (VBS). (a) short-pulsed logged (SPL (b) long-pulsed logged (LPL) treatments. Arrows representing directions of changes, asterisks significant differences between 1 day and 16 weeks after P_i addition calculated by repeated measurement ANOVA (* $p < 0.05$, ** $p < 0.01$, *** $p < 0.001$).

Soil properties	Treatment	
	a) SPL	b) LPL
Water content (WC)	↑↓ *	↑↓ *
Redox potential (E_h)	↑↓ ***	↑↓ ***
pH porewater	→	→
pH soil	↓ *	→
APA (µg PNP g^{-1} h^{-1})	↑	↑ *
Total alkalinity (mg HCO_3^- l^{-1})	↓ **	↓ *
→ stable ↑ increase ↓ decrease	For WC and E_h ↑ increase (drying) ↓ decrease (rewetting)	
* Significant differences between 1 day and 16 weeks (* $p < 0.05$, ** $p < 0.01$, *** $p < 0.001$)		

Table B-S5: Changes in soil properties during 16 weeks of incubation under 20°C conditions in forest soil (FST). (a) short-pulsed logged (SPL (b) long-pulsed logged (LPL) treatment. Arrows representing directions of changes, asterisks significant differences between 1 day and 16 weeks after P_i addition calculated by repeated measurement ANOVA (* $p < 0.05$, ** $p < 0.01$, *** $p < 0.001$).

Soil properties	**Treatment**	
	a) SPL	**b) LPL**
Water content (WC)	↑↓ *	↑↓ *
pH porewater	↑ *	↑ *
pH soil	↑ *	↑
APA (µg PNP g^{-1} h^{-1})	↓ **	↓ *
Total alkalinity (mg HCO_3^- l^{-1})	↑	↑ *
→ stable ↑ increase ↓ decrease	For WC and E_h ↑ increase (drying) ↓ decrease (rewetting)	

* Significant differences between 1 day and 16 weeks
(* $p < 0.05$, ** $p < 0.01$, *** $p < 0.001$)

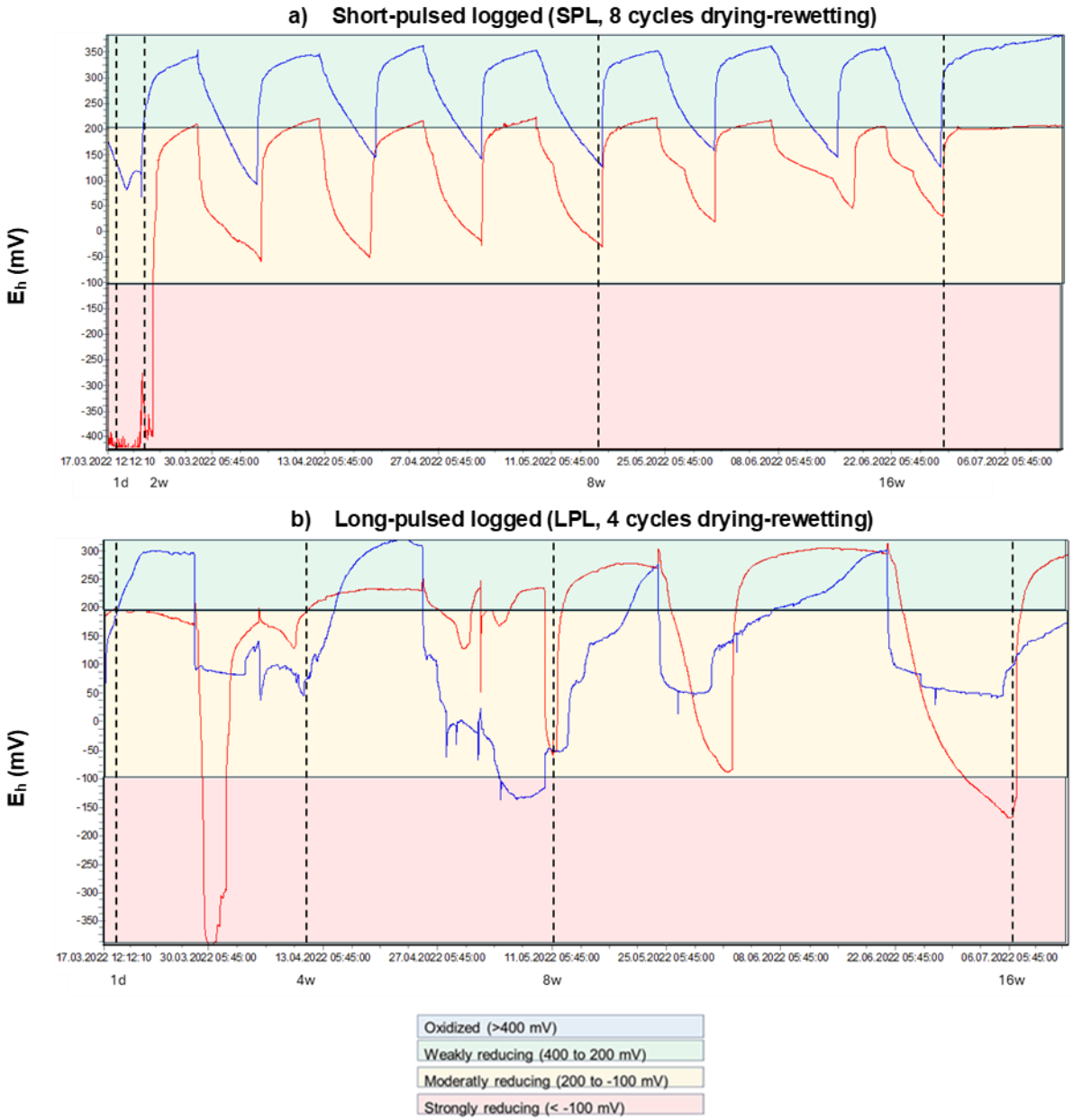

Figure B-S1: Temporal variation in redox potential (E_h) in vegetated buffer strip soil (VBS) during the experiment. E_h (mV) of (a) the short-pulsed logged (SPL) and (b) long-pulsed logged (LPL) over 16 weeks of incubation. Red line representing 20°C temperature treatments, blue line indicating 5°C treatments. Black dashed lines show time steps of sampling.

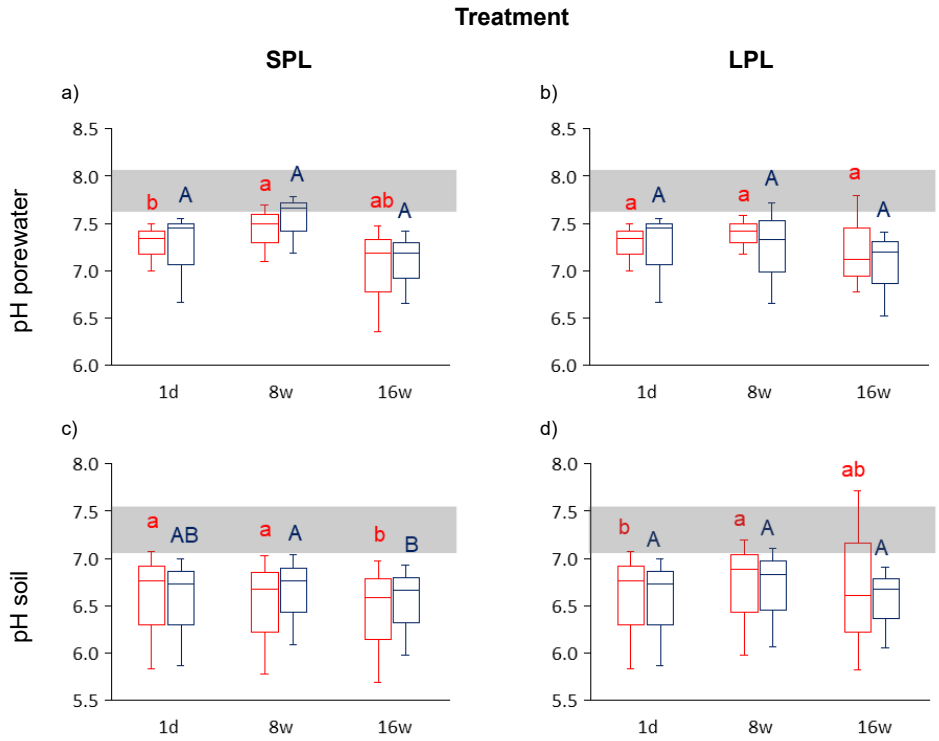

Figure B-S2: Temporal variation in pH concentrations in porewater and soil in the short-pulsed logged (SPL) and long-pulsed logged (LPL) treatments in vegetated buffer strip soil (VBS). (a, b) pH porewater, (c, d) pH soil from beginning (1 day after P_i addition) until the end of the incubation (after 16 weeks). Red boxplots represent 20°C conditions, blue boxplots represent 5°C conditions. Small letters show significant differences between groups of 20°C, capital letters show differences between groups of 5°C. Asterisks illustrate significant differences between 20°C and 5°C at the respective point in time (* $p < 0.05$, ** $p < 0.01$, *** $p < 0.001$). Shaded grey area symbolizes pH values of the initial soil.

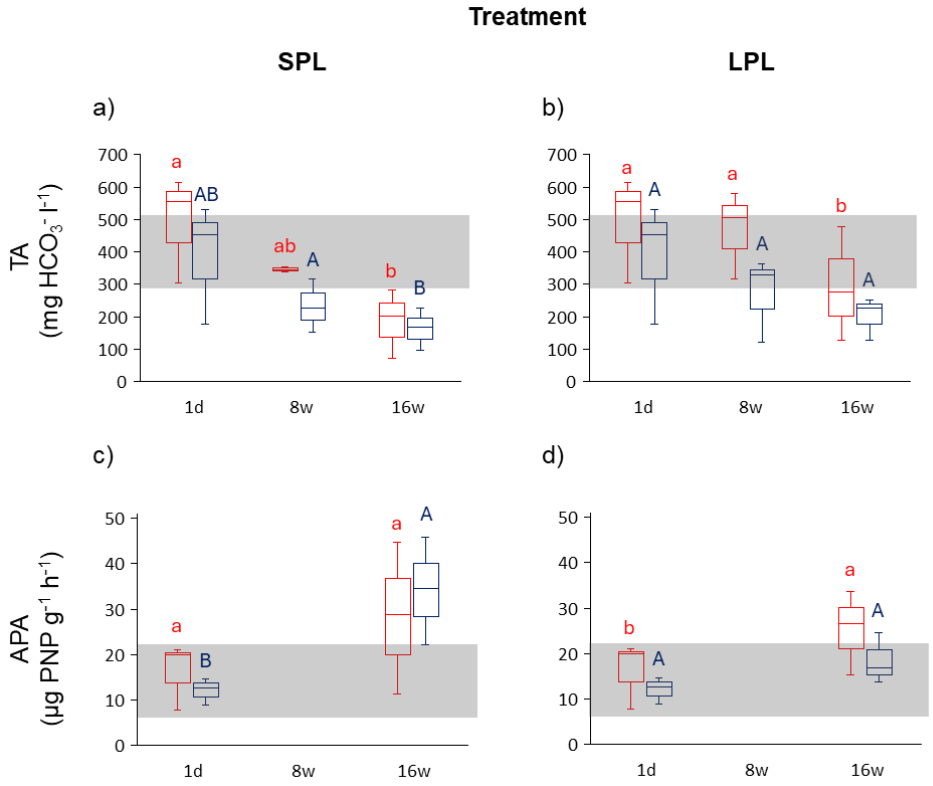

Figure B-S3: Temporal variation in total alkalinity (TA) and acid mono-phosphatase activity (APA) in vegetated buffer strip soil (VBS). TA and APA concentrations of (a, c) short-pulsed logged and (b, d) long-pulsed logged (LPL) treatments from beginning (1 day after P_i addition) until the end of the incubation (after 16 weeks). Red boxplots represent 20°C conditions, blue boxplots represent 5°C conditions. Small letters show significant differences between samples of 20°C, capital letters show differences between samples of 5°C at the respective point in time. Asterisks illustrate significant differences between 20°C and 5°C at the respective point in time (* $p < 0.05$, ** $p < 0.01$, *** $p < 0.001$). Shaded grey area symbolizes concentration of the initial soil.

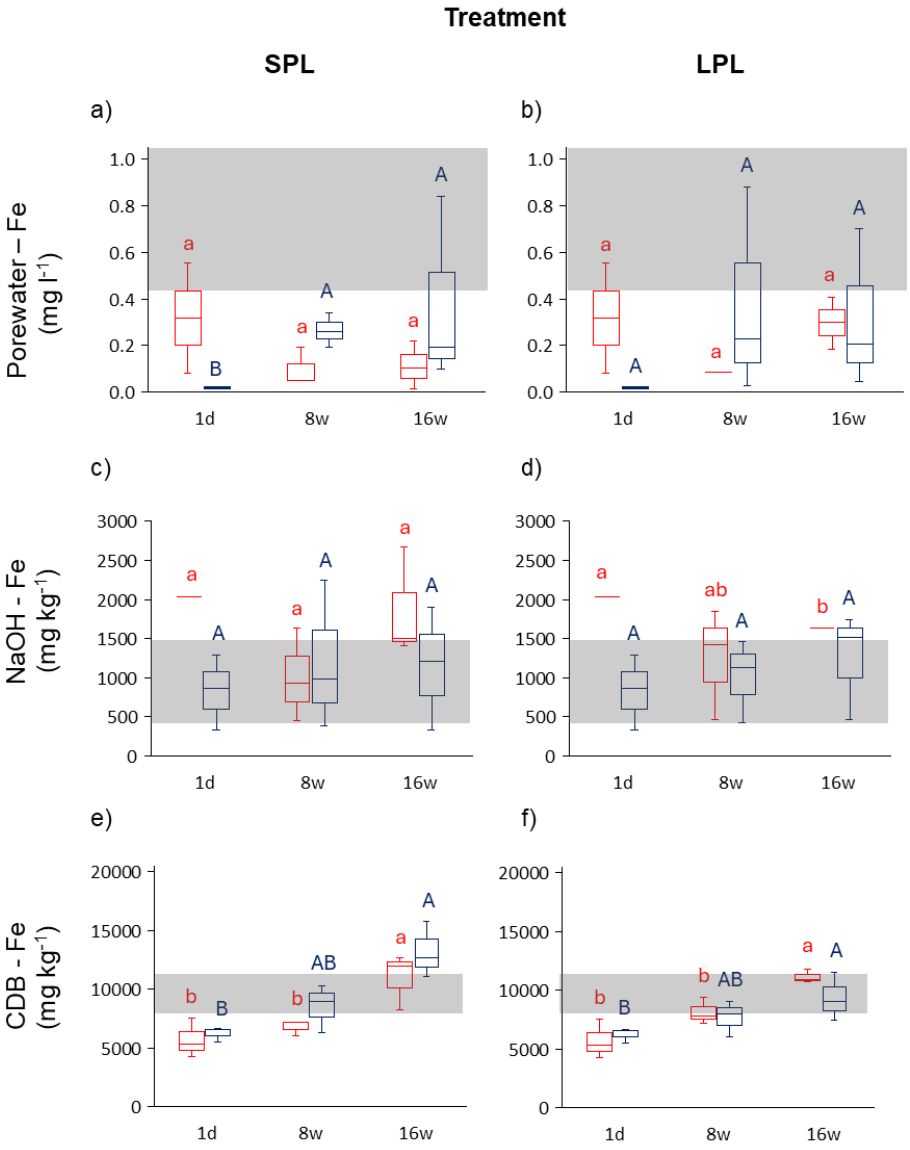

Figure B-S4: Temporal variation in iron (Fe) concentrations in porewater and extraction solutions of the short-pulsed logged (SPL) and long-pulsed logged (LPL) treatments of the vegetated buffer strip soil (VBS). (a, b) Porewater-Fe (mg l^{-1}) concentrations, (c, d) NaOH-extractable Fe (mg l^{-1}) concentrations and (e, f) CDB-extractable Fe (mg l^{-1}) concentrations from beginning (1 day after P_i addition) until the end of the incubation (after 16 weeks). Red boxplots represent 20°C conditions, blue boxplots represent 5°C conditions. Small letters show significant differences between samples of 20°C, capital letters show differences between samples of 5°C at the respective point in time. Asterisks illustrate significant differences between 20°C and 5°C at the respective point in time (* $p < 0.05$, ** $p < 0.01$, *** $p < 0.001$).

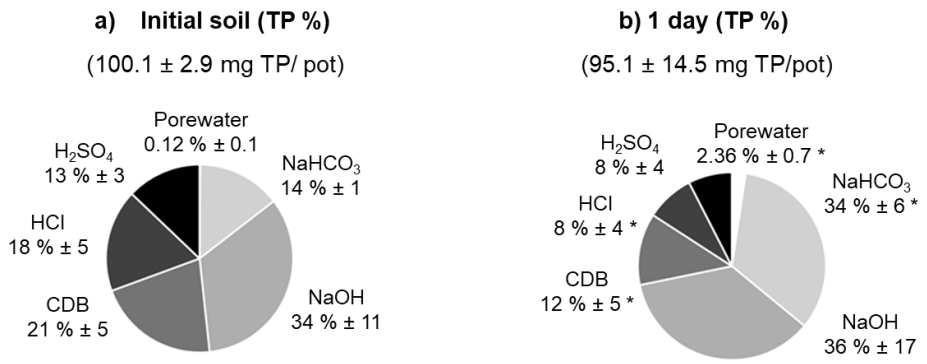

Figure B-S5: Relative contribution of the sum of inorganic (P_i) and organic (P_o) phosphorus proportions to total phosphorus (TP) in the different P pools of the vegetated buffer strip soil (VBS) at 20°C. Relative contribution of porewater P_i + P_o, $NaHCO_3$-extractable P_i + P_o, NaOH-extractable P_i + P_o, CDB-extractable P_i + P_o, HCl-extractable TP and H_2SO_4-extractable TP to TP, calculated based on the respective concentration for each pool and the volume of porewater and dry-weight of soil, respectively, within the experimental pots. (a) at the beginning (initial sample prior P_i addition), (b) after one day (24 hours after P_i addition). Numbers in brackets representing mean contents of TP (mg per pot, n=3 per time step). Asterisks indicating significant differences (* $p < 0.05$, ** $p < 0.01$, *** $p < 0.001$) between the relative proportions of TP of the respective P pools one day after P_i addition as compared to the initial soil.

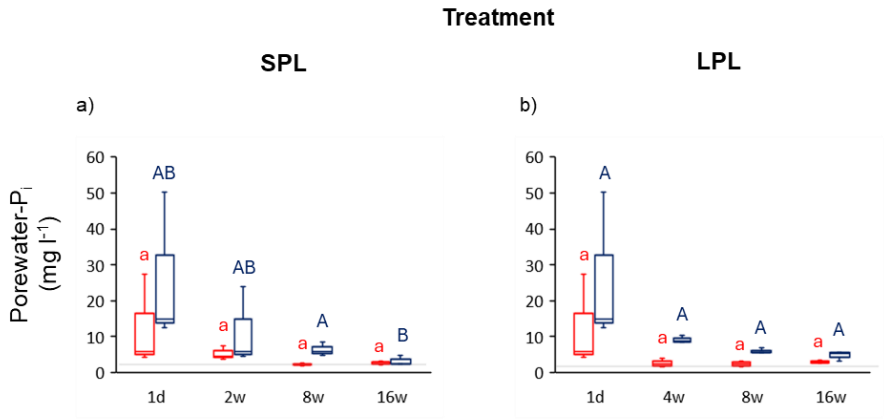

Figure B-S6: Temporal variation in dissolved inorganic P (P_i) in porewater of the vegetated buffer strip soil (VBS). Porewater-P_i (mg l^{-1}) concentrations in the (a) short-pulsed logged (SPL) and (b) long-pulsed logged (LPL) treatments from beginning (1 day after P_i addition) until the end of the incubation (after 16 weeks). Red boxplots represent 20°C conditions, blue boxplots represent 5°C conditions. Small letters show significant differences between samples of 20°C, capital letters show differences between samples of 5°C at the respective point in time. Asterisks illustrate significant differences between 20°C and 5°C at the respective point in time (* $p < 0.05$, ** $p < 0.01$, *** $p < 0.001$). Shaded grey area symbolizes concentration of the initial soil.

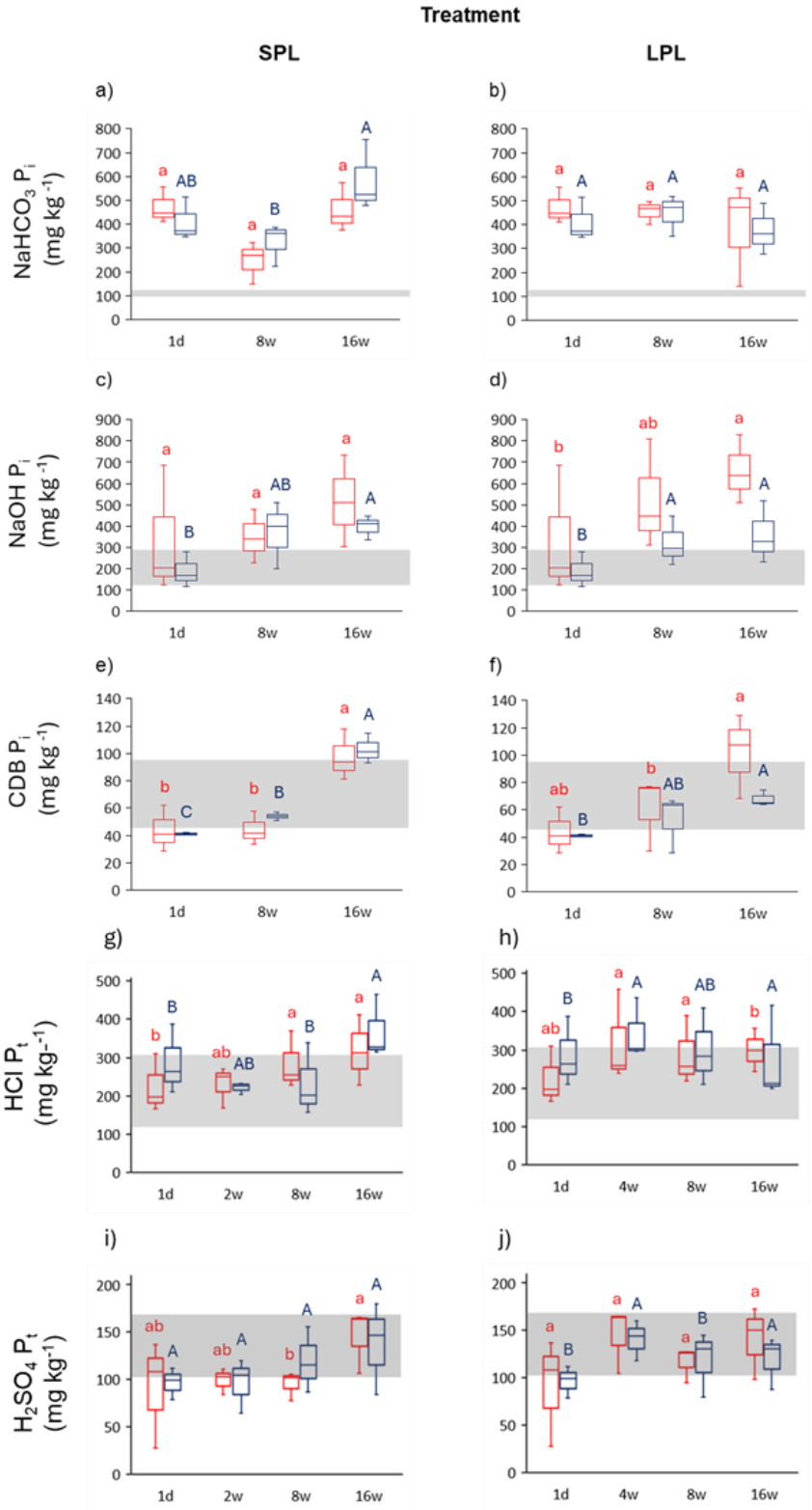

Figure B-S7: Temporal variation in inorganic (P_i) and total (P_t) phosphorus and concentrations in soil P pools of the short-pulsed logged (SPL) and long-pulsed logged (LPL) treatments in the vegetated buffer strip soil (VBS). (a, b) $NaHCO_3$-extractable P_i (mg kg^{-1}) concentrations, (c, d) NaOH-extractable P_i (mg kg^{-1}) concentrations and (e, f) CDB-extractable P_i (mg kg^{-1}), (g, h) HCl P_t (mg kg^{-1}) and H_2SO_4 P_t (mg kg^{-1}) concentrations from beginning (1 day after P_i addition) until the end of the incubation (after 16 weeks). Red boxplots represent 20°C conditions, blue boxplots represent 5°C conditions. Small letters show significant differences between samples of 20°C, capital letters show differences between samples of 5°C at the respective point in time. Asterisks illustrate significant differences between 20°C and 5°C at the respective point in time (* $p < 0.05$, ** $p < 0.01$, *** $p < 0.001$). Shaded grey area symbolizes concentration of the initial soil.

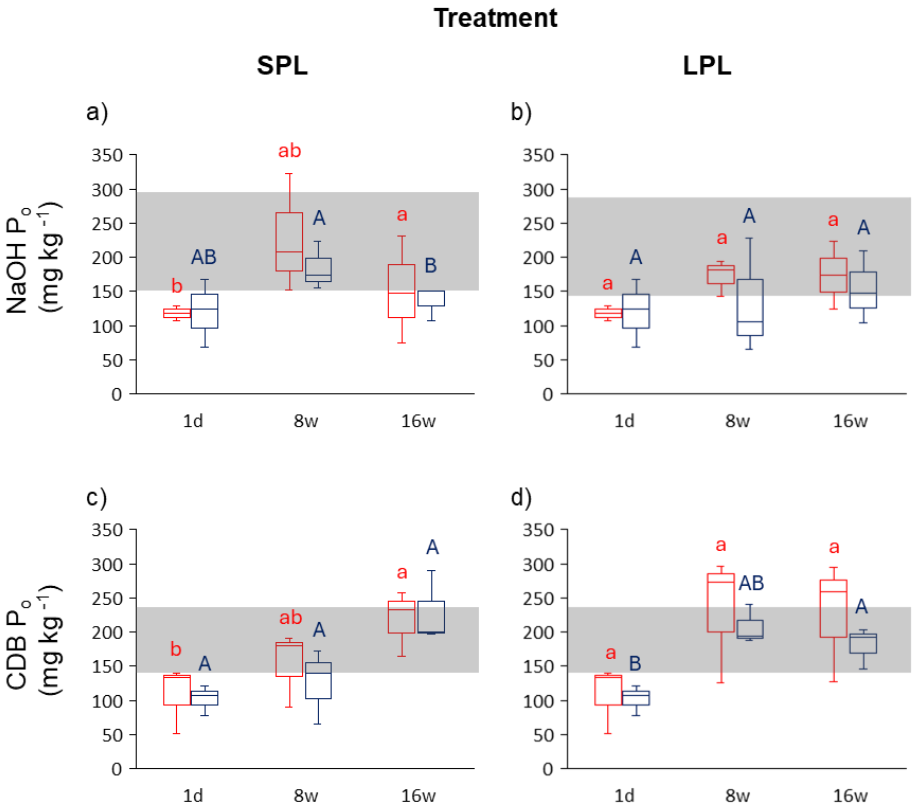

Figure B-S8: Temporal variation in organic phosphorus (P_o) concentrations in the NaOH- and CDB-P pools in the short-pulsed logged (SPL) and long-pulsed logged (LPL) treatments in the vegetated buffer strip soil (VBS). (a, b) NaOH-extractable P_o (mg kg^{-1}) concentrations, (c, d) CDB-extractable P_o (mg kg^{-1}) concentrations from beginning (1 day after P_i addition) until the end of the incubation (after 16 weeks). Red boxplots represent 20°C conditions, blue boxplots represent 5°C conditions. Small letters show significant differences between samples of 20°C, capital letters show differences between samples of 5°C at the respective point in time. Asterisks illustrate significant differences between 20°C and 5°C at the respective point in time (* $p < 0.05$, ** $p < 0.01$, *** $p < 0.001$). Shaded grey area symbolizes concentration of the initial soil.

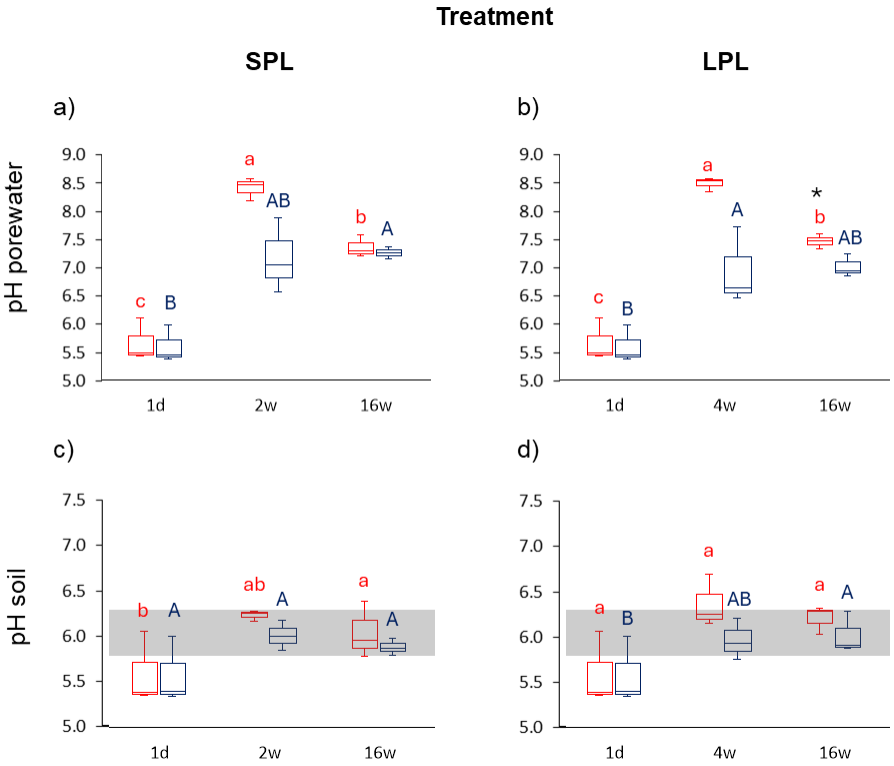

Figure B-S9: Temporal variation in pH concentrations in porewater and soil in the short-pulsed logged (SPL) and long-pulsed logged (LPL) treatments of the forest soil (FST). (a, b) pH porewater, (c, d) pH soil from beginning (1 day after P_i addition) until the end of the incubation (after 16 weeks). Red boxplots representing 20°C conditions, blue boxplots represent 5°C conditions. Small letters show significant differences between samples of 20°C, capital letters show differences between samples of 5°C at the respective point in time. Asterisks illustrate significant differences between 20°C and 5°C at the respective point in time (* $p < 0.05$, ** $p < 0.01$, *** $p < 0.001$). Shaded grey area symbolizes pH values of the initial soil.

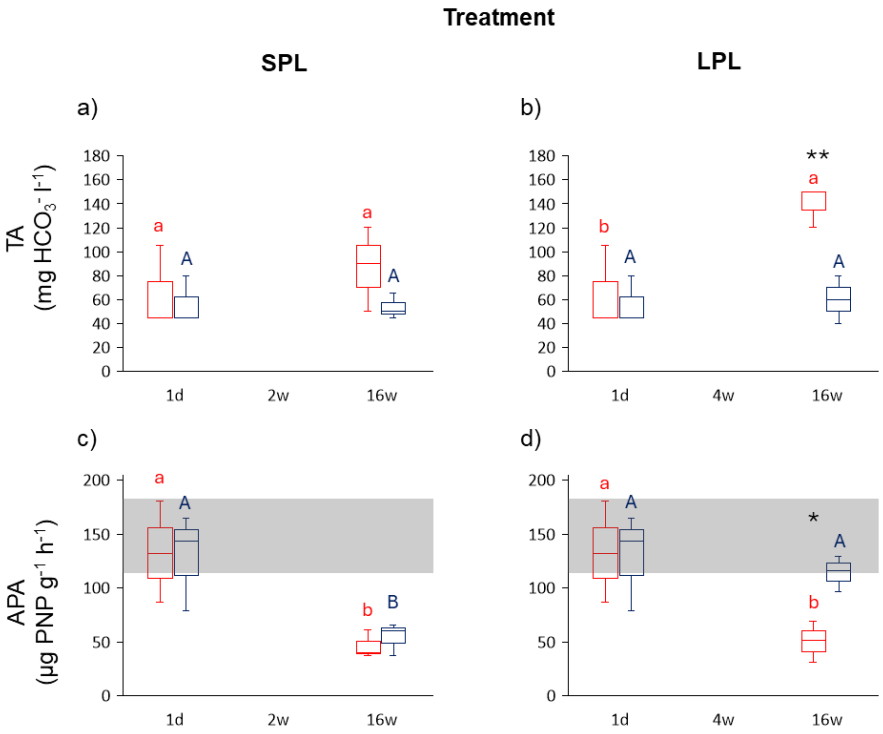

Figure B-S10: Temporal variation in total alkalinity (TA) and acid mono-phosphatase activity (APA) in the short-pulsed logged (SPL) and long-pulsed logged (LPL) treatments of the forest soil (FST). (a, b) TA concentrations (mg HCO_3^- l^{-1}) and (c, d) APA concentrations (µg PNP g^{-1} h^{-1}) from beginning (1 day after P_i addition) until the end of the incubation (after 16 weeks). Red boxplots represent 20°C conditions, blue boxplots represent 5°C conditions. Small letters show significant differences between samples of 20°C, capital letters show differences between samples of 5°C at the respective point in time. Asterisks illustrate significant differences between 20°C and 5°C at the respective point in time (* $p < 0.05$, ** $p < 0.01$, *** $p < 0.001$). Shaded grey area symbolizes concentration of the initial soil.

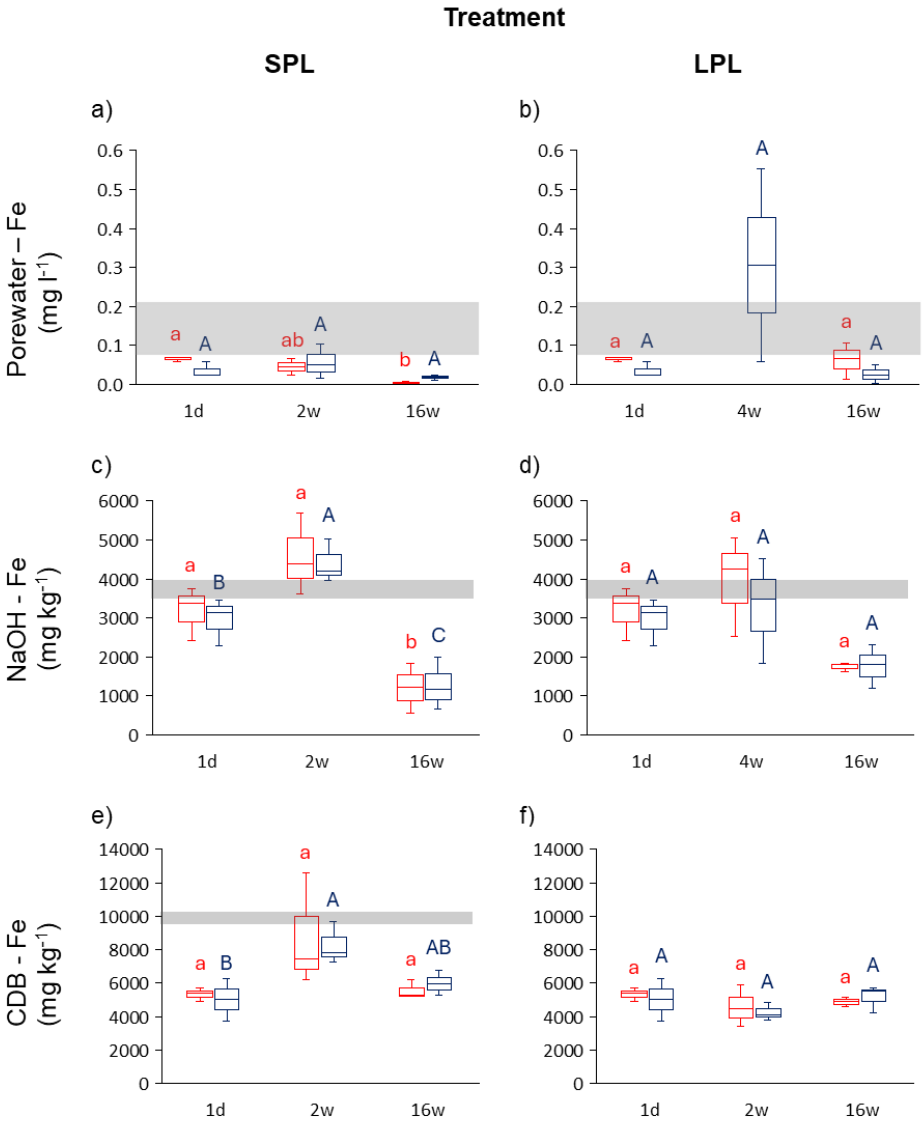

Figure B-S11: Temporal variation in iron (Fe) concentrations in porewater and extraction solutions in the short-pulsed logged (SPL) and long-pulsed logged (LPL) treatments of the forest soil (FST). (a, b) Porewater-Fe (mg l^{-1}) concentrations, (c, d) NaOH-extractable Fe (mg l^{-1}) concentrations and (e, f) CDB-extractable Fe (mg l^{-1}) concentrations from beginning (1 day after P_i addition) until the end of the incubation (after 16 weeks). Red boxplots represent 20°C conditions, blue boxplots represent 5°C conditions. Small letters show significant differences between samples of 20°C, capital letters show differences between samples of 5°C at the respective point in time. Asterisks illustrate significant differences between 20°C and 5°C at the respective point in time (* $p < 0.05$, ** $p < 0.01$, *** $p < 0.001$).

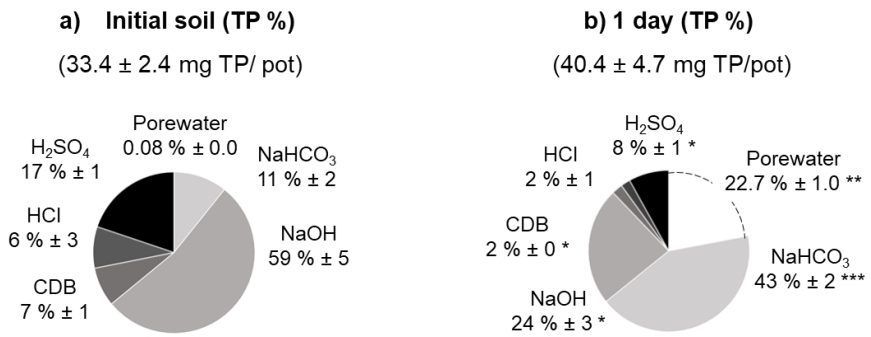

Figure B-S12: Relative contribution of the sum of inorganic (P_i) and organic (P_o) phosphorus to total P (TP) in the different P pools of the forest soil (FST) at 20°C. Contribution of porewater P_i + P_o, $NaHCO_3$-extractable P_i + P_o, NaOH-extractable P_i + P_o, CDB-extractable P_i + P_o, HCl-extractable TP and H_2SO_4-extractable TP to TP, calculated based on the respective concentration for each pool and the volume of porewater and dry-weight of soil, respectively, within the experimental pots. (a) at the beginning (initial sample), (b) after one day (24 hours after P_i addition). Numbers in brackets representing mean contents of total phosphorus (mg TP) per pot (triplicates). Asterisks indicating significant differences between (b) initial sample and one day after P_i addition (* $p < 0.05$, ** $p < 0.01$, *** $p < 0.001$).

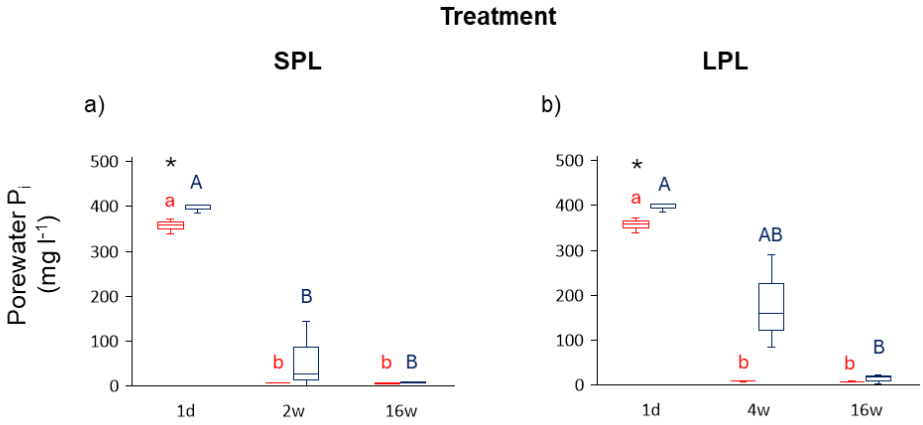

Figure B-S13: Temporal variation in dissolved inorganic P (P_i) in porewater of the forest soil (FST). Porewater-P_i (mg l^{-1}) concentrations in the (a) short-pulsed logged (SPL) and (b) long-pulsed logged (LPL) treatments from beginning (1 day after P_i addition) until the end of the incubation (after 16 weeks). Red boxplots represent 20°C conditions, blue boxplots represent 5°C conditions. Small letters show significant differences between samples of 20°C, capital letters show differences between samples of 5°C at the respective point in time. Asterisks illustrate significant differences between 20°C and 5°C at the respective point in time (* $p < 0.05$, ** $p < 0.01$, *** $p < 0.001$). Shaded grey area symbolizes concentration of the initial soil.

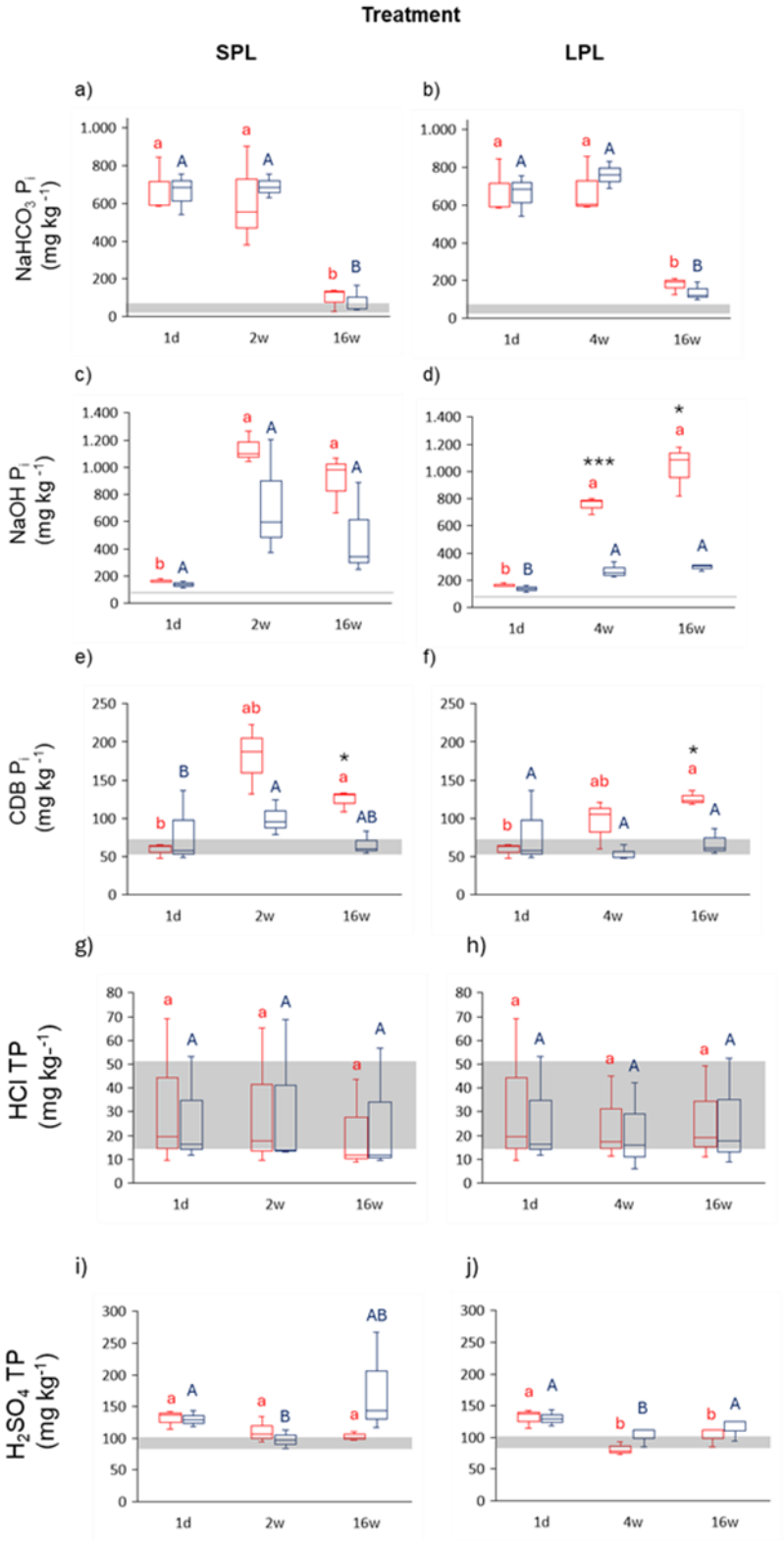

Figure B-S14: Temporal variation in inorganic (P_i) and total (P_t) phosphorus and concentrations in soil P pools of the short-pulsed logged (SPL) and long-pulsed logged (LPL) treatments in the forest soil (FST). (a, b) $NaHCO_3$-extractable P_i (mg kg^{-1}) concentrations, (c, d) NaOH-extractable P_i (mg kg^{-1}) concentrations and (e, f) CDB-extractable P_i (mg kg^{-1}), (g, h) HCl P_t (mg kg^{-1}) and H_2SO_4 P_t (mg kg^{-1}) concentrations from beginning (1 day after P_i addition) until the end of the incubation (after 16 weeks). Red boxplots represent 20°C conditions, blue boxplots represent 5°C conditions. Small letters show significant differences between samples of 20°C, capital letters show differences between samples of 5°C at the respective point in time. Asterisks illustrate significant differences between 20°C and 5°C at the respective point in time (* $p < 0.05$, ** $p < 0.01$, *** $p < 0.001$). Shaded grey area symbolizes concentration of the initial soil.

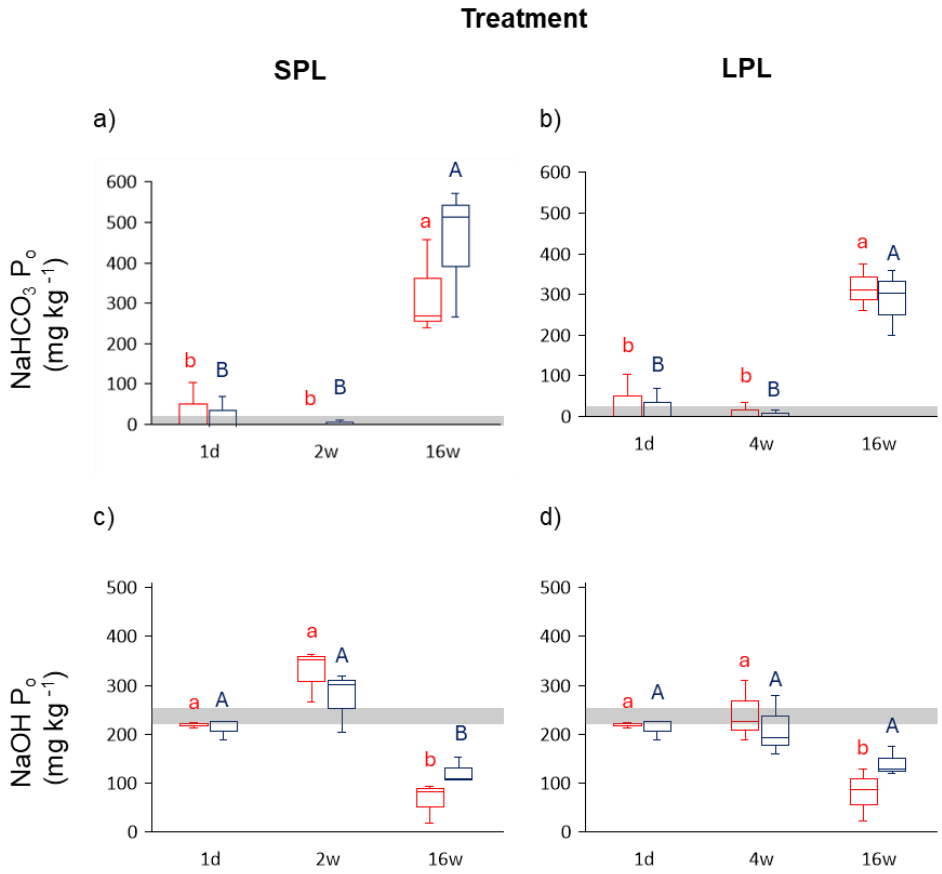

Figure B-S15: Temporal variation in organic phosphorus (P_o) concentrations in the $NaHCO_3$- and NaOH-P pools of the short-pulsed logged (SPL) and long-pulsed logged (LPL) treatments of the forest soil (FST). (a, b) NaOH-extractable P_o (mg kg^{-1}) concentrations, (c, d) CDB-extractable P_o (mg kg^{-1}) concentrations from beginning (1 day after P_i addition) until the end of the incubation (after 16 weeks). Red boxplots represent 20°C conditions, blue boxplots represent 5°C conditions. Small letters show significant differences between samples of 20°C, capital letters show differences between samples of 5°C at the respective point in time. Asterisks illustrate significant differences between 20°C and 5°C at the respective point in time (* $p < 0.05$, ** $p < 0.01$, *** $p < 0.001$). Shaded grey area symbolizes concentration of the initial soil.

References

DIN EN ISO 20130:2021-02: Bodenbeschaffenheit - Messung von Enzymaktivitätsmustern in Bodenproben mit kolorimetrischen Substraten in Mikrotiterplatten (ISO 20130:2018); Deutsche Fassung EN ISO 20130:2020.

Hedley, M. J., Stewart, J. W. B., & Chauhan, B. (1982). Changes in inorganic and organic soil phosphorus fractions induced by cultivation practices and by laboratory incubations. Soil Science Society of America Journal, 46(5), 970-976. https://doi.org/10.2136/sssaj1982.03615995004600050017x.

LGRB. 2017. Kartendienst des Landesamt für Geologie, Rohstoffe und Bergbau.

McLaughlin, J. R., Ryden, J. C., & Syers, J. K. (1977). Development and evaluation of a kinetic model to describe phosphate sorption by hydrous ferric oxide gel. Geoderma, 18(4), 295-307. https://doi.org/10.1016/0016-7061(77)90038-6.

Neidhardt, H., Achten, F., Kern, S., Schwientek, M., & Oelmann, Y. (2019). Phosphorus pool composition in soils and sediments of transitional ecotones under the influence of agriculture. Journal of environmental quality, 48(5), 1325-1335. https://doi.org/10.2134/jeq2019.01.0012.

Schinner, F., Öhlinger, R., Kandeler, E., Schinner, F., Öhlinger, R., & Kandeler, E. (1991). Bestimmung der Phosphomonoesterase-Aktivität (saure und alkalische Phosphatase) nach Tabatabai und Bremner (1969), Eivazi und Tabatabai (1977), mod. *Bodenbiologische Arbeitsmethoden*, 154-157. https://doi.org/10.1007/978-3-642-97284-3_35.

Tabatabai, M. A., & Bremner, J. M. (1969). Use of p-nitrophenyl phosphate for assay of soil phosphatase activity. Soil biology and biochemistry, 1(4), 301-307. https://doi.org/10.1016/0038-0717(69)90012-1.

Williams, J. D. H., Syers, J. K., Harris, R. F., & Armstrong, D. E. (1971). Fractionation of inorganic phosphate in calcareous lake sediments. *Soil Science Society of America Journal*, *35*(2), 250-255. https://doi.org/10.2136/sssaj1971.03615995003500020023x.

Section C

Dynamic in phosphorus pools in drainage ditch sediments within an agricultural catchment

Christiane Nagel, Harald Neidhardt*, Yvonne Oelmann

Geoecology, Eberhard Karls University Tübingen, 72070 Tübingen, Germany

*Corresponding author: Harald Neidhardt

Geoecology, University of Tuebingen

Ruemelinstr. 19-23, 72070 Tübingen, Germany

Author	Author position	Scientific ideas %	Data generation %	Analysis & interpretation %	Paper writing %
Christiane Nagel	1	15	100	60	60
PD Dr. Harald Neidhardt	2	45	0	20	30
Prof. Dr. Yvonne Oelmann	3	40	0	20	10
Titel of paper:		Dynamics of phosphorus pools in drainage ditch sediments within an agricultural catchment			
Status in publication process:		Published in *Applied Geochemistry* https://doi.org/10.1016/j.apgeochem.2025.106633			

Abstract

Hydrological dynamics in drainage ditch sediments (DDS) may impact phosphorus (P) retention and its potential (re-)release to connected waters. We aimed at understanding the fate of P in DDS under dynamic environmental conditions (i.e., drying-rewetting cycles) by examining P pool transformations through an isotopic labelling and incubation experiment. Fresh sediment samples were labeled with ^{18}O-enriched inorganic P (P_i), followed by a 24-week incubation under different environmental conditions. A five-step sequential extraction scheme was combined with $\delta^{18}O$ analysis of P_i ($\delta^{18}OP_i$) to follow changes in the operationally defined P pools. First, few P pools showed significant changes, but time-resolved results revealed a dynamic interplay between redox conditions, microbial activity and P dynamics. A subsequent decline in microbial P concentrations suggested cell death and reduced microbial activity, likely caused by hydrological stress. However, extracellular acid phosphatase activity remained stable. This suggests that while microbial populations were affected, their enzymatic functions persisted, revealing microbial dynamics and stress responses under changing environmental conditions. The $\delta^{18}O_{Pi}$ values in surface-adsorbed pools retained traces of the original P_i label after 24 weeks, allowing tracking of long-term P transformations and distinguishing biological and geochemical reactions. Our results further reflected dynamic transformations of P_i into organic P and vice-versa, which was largely influenced by the hydrological regime and raised the re-mobilization potential of P_i in the long term. Future studies should consider pronounced dynamics within P pools that can only be observed through close temporal monitoring, which may not be evident in simple before-and-after comparisons.

Key words: phosphorus**,** phosphate oxygen isotopes**,** drainage-ditch sediments, microbial cycling**,** acid phosphatase activity, climate change

1. Introduction

Pronounced amounts of phosphorus (P) have accumulated in our cultural landscapes (Bennett et al., 2001; Lannergård et al., 2020; Sharpley et al., 2013). Due to prolonged fertilizer application over the past decades, a pronounced build-up of P stocks occurred in many agricultural catchments, rendering agriculture as the major source of diffuse P inputs into surface waters (Sandström et al., 2021; Sharpley et al., 1995). From agricultural soils, P is mobilized through surface runoff and erosion and is then transported laterally until it eventually reaches adjacent drainage ditches (Efobo, 2023; Haygarth et al., 2005). Drainage ditches play an important role in the transfer continuum of P as they connect smaller streams to larger receiving rivers, creeks and streams (McDowell and Haygarth, 2024; Pionke et al., 2000; Sharpley et al., 2013). Although the retention of P in stream-bed sediments of drainage ditches, creeks and rivers is a vital ecosystem service, P can be gradually re-released over time with a lag time of years or decades (Carpenter, 2005; Haygarth et al., 2014; Lannergård et al., 2020; McDowell and Sharpley, 2002; Van Ee, 2021). This so-called 'legacy effect' presents a significant challenge for the sustainable management of P in agricultural catchments and ultimately, poses a threat to both freshwater ecosystems and oceans alike by enforcing eutrophication (Bennett et al., 2001; Hamilton, 2012; Kleinman et al., 2011; Sharpley et al., 2013). Thus, to optimize the management of P in agricultural catchments, it is essential to understand the dynamics of P-storage pools in stream-bed and drainage ditch sediments (Neidhardt et al., 2019). Most previous studies investigated P-storage dynamics in stream-bed sediments of wetlands or rivers within agricultural catchments, whereas drainage ditches received little attention so far.

Total P contents in drainage ditch sediments (DDS) under agricultural influence can be significantly higher than background levels due to large amounts of P fertilizer applications, known as excess P (Sharpley et al., 2013). The long-term application of fertilizer P may exert a pronounced influence on the P fractions of receiving soils and sediments, e.g., an increase of easily soluble P and reduced proportions of organic P (P_o) (Chen et al., 2022). From arable land, P may reach drainage ditches either directly in in form of particulate P via surface-runoff and erosion (Reddy et al., 1999), or indirectly as dissolved inorganic P (P_i) over interconnected vegetated buffer strips via subsurface flow (Shore et al., 2016). Particulate P has an initial P pool composition that resembles its source (arable soil), in which excess P_i is primarily stored by sorption to positively charged surfaces of minerals and organic matter (labile P_i), Al- and Fe(III)-oxides (moderately labile P_i) and the formation of secondary minerals such as octacalcium phosphate (stable Ca-P_i) (Cross and Schlesinger, 1995; McDowell and Sharpley, 2002; Reddy et al., 1999; Rubæk et al., 2013; Sharpley et al., 1994).

The storage of P in drainage ditch sediments is controlled by dynamic processes, with transformations of P pools occurring over a short to long time that affect its mobility. Prevailing environmental conditions, such as hydrological regime and temperature, determine the intensity of the biogeochemical processes involved (Dupas et al., 2015a; Frossard et al., 2000; Schoumans, 2014). Changes in the hydrological regime and associated redox conditions play a key role in the subsequent re-release of P_i (Reddy et al., 1999), particularly under the impact of climate change that raises the risk of prolonged droughts and heavy rainfall events. Transfer of P from land to streams is generally expected to increase due to higher winter rainfall under temperate climate (Jeppesen et al., 2009). Furthermore, the risk of P mobilization from arable land is highest when heavy rainfall occurs, especially shortly after fertilizer application and

plowing (Lucas et al., 2023). Thus, the linkage between short- and long-term dynamics of P pools under a changing climate requires further attention.

Immediate reactions, such as immobilization of dissolved P_i from solution by surface adsorption, occur within seconds to hours (Zhijing et al., 2011). The rapid adsorption of P_i presumably results from the reaction of P_i with mineral surfaces and organic matter (Mattingly et al., 1975) and is strongly affected by pH (Barrow, 1984), soil texture and the initial P pool composition (Li et al., 2021). Externally applied P disturbs the equilibria of existing P pools as it is initially transferred into the dissolved and labile P pools (Chen et al. 2022). The rapid adsorption of P_i plays an important role in controlling sediment-water exchange as it constrains P_i concentrations in the aqueous phase (Slomp et al., 1998). Furthermore, due to continuous inputs, the P content in sediments subsequently increases and the pool composition shifts towards moderately labile and stable forms of P_i (Cross and Schlesinger, 1995). Within days to weeks, adsorbed P_i from the labile P pool can be transferred into the moderately labile P pool, with aluminum (Al) and iron (Fe) mineral phases and organic compounds acting as principal sorbents (Joshi et al., 2016). The addition of external P enhances this transfer, a large part (70–90%) of applied P can be subsequently fixed as Fe-P and Al–P (Chen et al., 2022). In addition, P might also be taken up and retained by microorganisms, which is then retained as P_o within organic molecules (Zhu et al., 2018). Redox state, pH and microbial activity further control the retention of P in the mid- to long-term (Frossard et al. 2000; Schlesinger et al., 1998). For example, after a few weeks of water saturated conditions, dissolved P_i in the solution can increase dramatically due to the reductive dissolution of Fe(III)-oxides and the mineralization of P_o-containing organic molecules (Ajmone-Marsan et al., 2006). To observe changes in the more stable P pools, long-term observations are required. For example, dissolved P_i can be transferred into the Ca-P_i pool after several months (Joshi et al., 2016), which does not only largely reduce its bioavailability, but also its mobility (Edwards and Withers, 2007; Shore et al., 2017).

Changes in the hydrological regime may further impact P storage dynamics in the long-term. During periods of prolonged water saturation, P_i can be mobilized from the labile and moderately labile P_i pools due to a decline in the redox potential and the subsequent reductive dissolution of Fe(III)-oxides (Ajmone-Marsan et al., 2006; Barczok et al., 2023; Dupas et al., 2015b). Moreover, P_i associated with Fe(III)-oxides can be utilized and intensively cycled by microorganisms under strongly reducing redox conditions (Joshi et al., 2015, Yuan et al., 2022). Otherwise, drainage ditches and small streams often fall dry during periods of drought, so that sediments are affected by frequent drying and rewetting cycles, which influence the rate and extent of transformations in the moderate labile Fe-P_i pool as well as organic P pools (Dieter et al., 2015; Sharpley et al., 1994; Turner and Haygarth, 2001). A return to oxic conditions results in the precipitation of Fe(III)-oxides and a concomitant fixation of P_i in the moderately labile pool (Barczok et al., 2023). Furthermore, microbial biomass and activity have been shown to decrease in soils with an increasing number of drying and rewetting cycles (Yan et al., 2015). Considering these manifold processes involved, the transfer of P between different pools in drainage ditch sediments under the influence of changing redox conditions is complex and also remains generally understudied due to methodological limitations (Bauke et al., 2022; Sandström et al., 2021).

Biological processes play an important role in the transformation of the various P pools, but quantifying their individual role is difficult. In this context, stable oxygen isotope ratios in phosphate ($\delta^{18}O_{Pi}$) have been successfully applied to study P cycling in soils as well as freshwater and marine sediments

(Ajmone-Marsan et al., 2006; Joshi et al., 2016; Bauke et al., 2022). While abiotic processes such as mineral precipitation do not cause a change in $\delta^{18}O_{Pi}$ values, intra- and extracellular enzymes of microorganisms catalyze an exchange of O isotopes between P_i and ambient water (Blake et al. 2005; Joshi et al., 2016; Melby et al. 2011), thereby altering the $\delta^{18}O_{Pi}$ values (Blake et al., 2001). There are two enzymatically controlled fractionation processes at work; the intracellular cycling of P_i which represents a temperature-dependent isotopic equilibrium fractionation and the extracellular regeneration of P_i from P_o by acid phosphatase, which presents a kinetic fractionation (Blake et al., 2005; Liang and Blake, 2006; Longinelli and Nuti, 1973; von Sperber et al., 2014).

By combining isotopic labeling (addition of ^{18}O-enriched P_i) with a sequential extraction procedure, further insight can be gained regarding the biogeochemical transformation of P pools (Joshi et al., 2016). Depending on the intensity of biological activity (i) ^{18}O-enriched P_i can be geochemically transformed into stable P compounds such as P-containing minerals rendering the initial $\delta^{18}O_{Pi}$ value of the P_i label unaltered, thereby raising the $\delta^{18}O_{Pi}$ value of the receiving pool(s) (Jaisi and Blake, 2010). ii) ^{18}O-enriched P_i can be intensely cycled by enzymes, which shifts $\delta^{18}O_{Pi}$ values of the label towards isotopically lighter $\delta^{18}O_{Pi}$ values and ultimately, toward those of labile P_i already present. The extent of this shift depends on the biological process at work (being larger for intracellular than for extracellular enzymes) and on the overall biological activity in the system observed (Gross and Angert, 2015; Liang and Blake, 2006; von Sperber et al., 2014).

In sum, the long-term storage of P in drainage ditch sediments largely depends on the transfer and fixation of P_i into more stable pools (e.g. P_o, Ca-P_i). As previously outlined, little is known regarding the underlying biogeochemical transformation processes that ultimately control the storage and the potential re-release of P_i to surface waters in agricultural catchments. Therefore, our overarching objective was to unravel short- and long-term transformations in the P_i pools of non-calcareous drainage ditch sediments that are mediated by dynamics in the hydrological regime and redox conditions. We applied an innovative isotopic labeling and incubation approach based on the $\delta^{18}O_{Pi}$ analysis of different P_i pools over time, allowing us to observe temporal variations in the P pools. Moreover, hydrological regimes differing in the duration and frequency of drying and rewetting were applied to investigate their influence on biotic and abiotic processes affecting P retention at different time scales (Bai et al., 2017; Sugiyama et al., 2013). The underlying working hypothesis of our study was that excess amounts of P_i are retained by drainage ditch sediments by surface adsorption and the formation of stable P_i pools (Fe- and Ca-P_i), which is controlled by prevailing redox conditions and microbial activities. The following specific hypotheses were addressed:

H1: Directly after labeling (initial phase), concentrations of the labile P fraction ($NaHCO_3$-P_i) and corresponding $\delta^{18}O_{Pi}$ values increase irrespective of the hydrological regime and temperature treatment.

H2: In the first weeks (early phase), labile P_i is transferred to the moderately labile pool (NaOH-P_i). In addition, microorganisms make use of the excess P resulting in an increase of labile and moderately labile P_i and in a shift of the corresponding $\delta^{18}O_{Pi}$ values through intracellular enzymatic cycling. The microbially induced effects are most pronounced for the treatments with shorter drying and rewetting

intervals, which represent more favorable living conditions as compared to longer waterlogged intervals.

H3: Over weeks to months (intermediate phase), ongoing acid phosphatase activity leads to the microbial turnover and transformation of labile and moderately labile P_i into P_o. This is accompanied by a further decrease in the $\delta^{18}O_{Pi}$ values of labile and moderately labile P_i. Microbially induced effects further increase and become more pronounced in the treatments providing favorable living conditions for microorganisms.

H4: Long-term exposure to different hydrological regimes over months (late phase) leads to microbial death and a concomitant release of P_i into the dissolved P pool. From the dissolved pool, P_i is subsequently transferred into the stable P pools. Again, induced changes are most pronounced in the treatments in which living conditions are favorable for microorganisms.

2. Methods

2.1. Origin of samples

Sediment samples for the isotopic labeling and incubation experiment were collected from the stream bed of a drainage ditch adjacent to agricultural land within the Ammer valley near Tübingen (E 500969.172; N 5373752.969, UTM-WGS84). The 134 km^2 large catchment is located in the South German Scarplands with 66% being represented by arable land (Leibundgut and Eisele, 2005; Schwientek et al., 2013). Small straightened streams framed by buffer srips and dense networks of drainage ditches dominate in this cultural landscape, while natural riparian vegetation is absent. The entire catchment has been characterized as a high-risk area for diffuse inputs of priority compounds (including P) according to the Water Framework Directive (LUBW, 2015). Soils and sediments adjacent to arable land contain high total P concentrations as well as an increased proportion of moderately labile and stable forms of P (Neidhardt et al., 2019).

Drainage ditch sediment samples were collected at 0 - 5 cm depth following a straight orthogonal transect in a local drainage ditch. To account for potentially site-specific spatial variability, samples were collected in triplicates with a distance of 10 - 15 m downstream between each replicate. Properties of the initial samples are shown in **Table C-1,** the position of the samples, land use and topography are provided in **Table C-S1.**

Table C-1: Properties of initial drainage ditch sediment and 24 hours after adding of the isotopic label (roots removed, sieved to <2 mm). Values shown represent means and respective standard deviations for the triplicate samples.

Properties	Initial samples	24 hours after labeling	Properties	Initial samples	24 hours after labeling
WC (%)	25.5 ± 9.7	52.3 ± 3.9	**HCl – TP (mg/kg)**	123 ± 2	114 ± 8
$pH_{porewater}$	7.67 ± 0.13	7.25 ± 0.01	**H_2SO_4 – TP (mg/kg)**	237 ± 20	181 ± 11
$pH_{sediment}$	6.86 ± 0.03	6.76 ± 0.10	**TP (mg kg^{-1})**	861 ± 68	1270 ± 139
APA (µg PNP g^{-1} h^{-1})	74.2 ± 13.0	65.1 ± 7.6	**$\delta^{18}O_{H2O}$ porewater (‰ VSMOW)**	-9.6 ± 0.3	-6.73 ± 0.43
P_{mic} - P_i (mg kg^{-1})	39.7 ± 9.9	41.9 ± 19.5	**$\delta^{18}O_{Pi}$ $NaHCO_3$ (‰ VSMOW)**	18.8 ± 1.9	143 ± 62
porewater - P_i (mg l^{-1})	0.21 ± 0.12	22.6 ± 0.9	**$\delta^{18}O_{Pi}$ NaOH (‰ VSMOW)**	22.4 ± 0.4	26.0 ± 9.1
$NaHCO_3$ - P_i (mg kg^{-1})	68.5 ± 29.4	541 ± 69	**$\delta^{18}O_{Pi}$ CDB (‰ VSMOW)**	18.4 ± 0.5	28.2 ± 4.8
NaOH - P_i (mg kg^{-1})	225 ± 16	240 ± 27	**$\delta^{18}O_{Pi}$ HCl (‰ VSMOW)**	20*	31.8 ± 0.1
CDB - P_i (mg kg^{-1})	108 ± 9	121 ± 25	**C_{org} (%)**	0.00 ± 0.04	-
$NaHCO_3$ - P_o (mg kg^{-1})	48.7 ± 47.0	0.00 ± 0.00	**C_{inorg} (%)**	3.60 ± 1.05	-
NaOH - P_o (mg kg^{-1})	218 ± 10	141 ± 18	**$CaCO_3$ (%)**	LDL	-
CDB - P_o (mg kg^{-1})	20.0 ± 30.3	19.9 ± 7.5			

* Data from H. Neidhardt, 2019
- no data
LDL: lower detection limit

2.2. Experimental design

The non-calcareous drainage ditch sediments were dried at room temperature and then sieved to the fine fraction (<2 mm, Retsch) with roots and larger fragments of organic matter being removed manually by tweezers. The sediments were pre-incubated with deionized water at a constant water content of 37.5 weight% for two weeks at 20°C. After pre-incubation, 100 g (dry-weight equivalent) of sediment were distributed into 200 ml glass jars (height: 8 cm, diameter: 7 cm, WECK) and 100 ml of ^{18}O-enriched PO_4 solution (485 mg PO_4-P l^{-1}, +350 ‰ VSMOW) was added to each jar with a volumetric cylinder. The liquid ^{18}O-P_i label was synthesized from the dissolution of PCl_5 in ^{18}O-enriched water (Melby et al., 2011; Stout et al., 2014). For further details, the reader is referred to supporting information **Section C-S1**.

Following pre-incubation and isotopic labelling, the following three treatments with different hydrological regimes were applied over a period of 24 weeks: i) Short-pulsed logged (SPL) with one-week cycles of drying and rewetting (i.e. one week waterlogged followed by one-week dry conditions, 12 cycles in total). ii) Long-pulsed logged (LPL) with two-weeks cycles of drying and rewetting (i.e. two-week waterlogged followed by two-week dry conditions, 6 cycles in total). iii) Permanently waterlogged (L) with constant water saturation, resulting in a gravimetric water content (WC) of 50%. All treatments were conducted in triplicates and at two different temperatures (20°C and 5°C).

At the end of each waterlogged interval, porewater was removed on a weekly (SPL), respectively biweekly (LPL) basis using embedded micro suction cups (90mm long, ecoTech Umwelt-Meßsysteme GmbH, Germany, equipped with polyamide membranes and a 0.45 µm pore size). Each time, 50 ml (20°C treatments) to 80 ml (5°C treatments, less evaporation) of porewater were recovered, thereby adjusting the WC to 20% to 25% for the following dry cycles.

The gravimetric water content (WC) was assessed for each sample from 2.5 to 3.5 g of wet sediment with a halogen dryer (HB43-S, Mettler Toledo) and was calculated as mass% after DIN ISO (11465, 1996). Water contents were used to calculate the respective dry-weight concentrations of samples that were extracted moist (sequential extraction, P_{mic}, phosphatase activity).

During the 24 weeks of incubation, rewetting in the SPL and LPL treatments was achieved by adding 100 ml of deionized water per jar at the end of each dry cycle. To compensate for evaporation losses in the L treatment at 20°C, 50 ml of deionized water was applied biweekly right before the sediment surface was no longer covered by water and/ or the WC dropped below 50%, (in total 12 times, biweekly). At 5°C there was almost no weight loss, so respective samples were rewetted with 50 ml deionized water only twice (after 2 and 4 months).

The temperature (°C) was continuously monitored at 5 to 6 cm depth (Temperature Data Logger WTDL1, ELV Elektronik AG, Germany). Temperature data was recorded in 3-minute intervals (tolerance range ± 0.0625°C/ ± 0.5°C) and read out once a month via a USB connection and processed by a PC software (LogView V2.7.6, LogView Studio, Germany, supporting information **Section C-S2**). Moreover, the redox potential (E_h) was measured with redox electrodes after Mansfeld (99.95% Pt, resolution 1 mV) coupled with Ag/AgCl reference electrodes (filling 3 M KCl+AgCl, both electrodes from ecoTech Umwelt-Meßsysteme GmbH, Germany). The E_h was recorded in 3-minute intervals (measuring range ± 1250 mV) with a connection module (enviLog Midi SDI-12, ecoTech Umwelt-Meßsysteme GmbH, Germany) and read out once a month via a USB connection and processed by a PC software (CSView 2 – csv V 1.00, GeoPrecison GmbH, Germany). The treatments with various hydrological regimes and

different temperatures achieved the desired effects related to the E_h, see **Table C-2**, **Table C-S2 and Figure C-S1**.

Table C-2: Water content (WC %) and redox potential E_h (mV). (a) short-pulsed logged (SPL), (b) long-pulsed logged (LPL) and (c) waterlogged (L) treatments, at different hydrological regimes. The water content of the logged treatment was held constant over the time of incubation.

Treatment	n (number of cycles)	WC (%)		Redox potential E_h (mV)	
		20°C	5°C	20°C	5°C
a) SPL	Wet cycles (n = 12)	49.7 ± 3.5	47.2 ± 1.6	-471 ± 93	-391 ± 6
	Dry cycles (n = 12)	37.9 ± 2.6	36.1 ± 2.2	+325 ± 88	+355 ± 4
b) LPL	Wet cycles (n = 6)	51.4 ± 2.1	44.9 ± 3.2	-557 ± 14	-348 ± 8
	Dry cycles (n = 6)	30.0 ± 5.4	23.1 ± 11.4	+466 ± 28	+358 ± 14
c) L	Beginning (after 24 hours)	52.3 ± 3.9	46.8 ± 1.2	-411 ± 27 ^{L}	-367 ± 5
	End (after 24 weeks)	61.1 ± 3.4	56.0 ± 2.1	-470 ± 137 ^{L}	-475 ± 145

Superscript capital letters: sig. difference between 20°C and 5°C treatments (L: sig lower, H: sig higher)

Sediment samples were harvested at specified intervals, starting 24 hours after label application and at 1 (only SPL), 4, 8 (only LPL, L), 16 and 24 weeks. At each time step, one set of the treatments was sacrificed and used for the chemical analyzes (n = 3). The sampling was conducted for the pulsed logged treatments after the end of the respective wet cycles, as most analyses would not be possible under oxic conditions.

2.3. Chemical analyses

Total concentrations of major and trace elements (including total P, TP) in the sediment samples were obtained after drying (105°C) and homogenization (planetary ball mill) by an acid pressure digestion. Here, 0.5 g of homogenized sample material was mixed with 5 ml Milli-Q water, 10 ml 65% HNO_3 (EMSURE, Merck) and 3 ml 37% HCl (ACS reagent, Sigma-Aldrich) in polytetrafluoroethylene beakers. Then, the samples were heated to 190 °C for 14 minutes in a laboratory microwave system (START 1500 Microwave Extractor, MLS GmbH) following the manufacturer's method E701 (MLS GmbH). The digestion solutions were filtered (Mn 619 G1/4, Macherey-Nagel) and finally analyzed by Optical Emission Spectrometry with inductively coupled plasma (ICP-OES, Analytik Jena Specord 200 plus, Germany). Total phosphorous (TP) was measured axial at a wavelength of 213.617 nm, achieving an instrumental detection limit (IDL) of 0.0034 ± 0.001 mg l^{-1}. Quality controls and respective recovery rates are presented in **Table C-S2**.

Porewater was analyzed for major and trace elements by ICP-OES. Additionally, P_i was determined photometrically at a wavelength of 880 nm using a Continuous Flow Analyzer (CFA, Analytical AutoAnalyzer 3, SEAL, Germany, idl: 0.004 ± 0.001 mg l^{-1}) and the Mo-blue method (Nagul et al., 2015). For $\delta^{18}O_{Pi\text{-}H2O}$ values, porewater was measured by a Laser Water Isotope Analyzer (LWIA, Los Gatos,

Model IWA-45-E, externally at AgroIsolab, Jüllich, Germany). The total alkalinity (TA) was measured by titration with an alkalinity-test-KIT (MColortest, Merck), pH values were measured after DIN ISO 10390 from 0.01 M $CaCl_2$ solution using a pH-meter (WTW pH 3310 with glass electrode WTW Plus SenTix 81). No analysis of porewater-P_i and TA could be made in the SPL treatment after 4 weeks of incubation due to a too small sample volume.

The sequential extraction for assessing different operationally defined P pools was carried out following a modified procedure after Hedley (Hedley et al., 1982). In brief, samples were subsequently extracted with increasingly potent extraction solutions (0.5 M $NaHCO_3$, followed by 0.1M NaOH, CDB, 1M HCl and finally 0.5M H_2SO_4). The $NaHCO_3$-extractable pool is considered to represent 'labile P_i and P_o' that is loosely adsorbed to mineral surfaces and organic matter (Mattingly et al., 1975). This pool is considered readily bioavailable and is characterized by fast turnover rates (Negassa and Leinweber, 2009; Tiessen, 1993). The second step using NaOH solution is interpreted as moderately labile P, including more stable forms of P_o (e.g., detritus Po) and strongly bound P_i (associated with Al- and FeIII-oxides and hydroxides). Next, a citrate-dithionite-bicarbonate (CDB) extraction step followed (Ruttenberg, 1992). Valuable information can be obtained from this step allowing to assess P_i and P_o associated with reducible MnIV- and FeIII-oxides and hydroxides (Neidhardt et al., 2021). Under reducing conditions, this pool could rapidly turn from a sink into a source for P_i and P_o (Ajmone-Marsan et al., 2006; Dupas et al., 2015b). If this step is not included, the CDB-extractable P would be extracted by the following HCl step, a problem already recognized by Joshi et al. (2015). The following HCl-step is commonly interpreted as P_i in primary and secondary minerals (e.g., apatite, octacalcium phosphate) and dominates in Ca-carbonate-rich environments (Eriksson et al., 2016). However, it could also contain P_i and P_o associated with Fe(II)-minerals such as siderite and strengite (Neidhardt et al., 2019). The final H_2SO_4 extraction step is summarized as non-extractable residual-P_i and P_o (Cross and Schlesinger, 1995). Both, HCl- and H_2SO_4-extractable P, are considered as stable and therefore not directly bioavailable P pools. Further details regarding the sequential extraction are provided in supporting information **Section B-S1**.

All extraction solutions were analyzed regarding major and trace elements by ICP-OES including total dissolved P. Additionally, dissolved P_i in the extraction solutions of the $NaHCO_3$, NaOH and CBD step was measured by CFA. Microbial P (P_{mic},) was determined from fresh samples after the method of Kouno et al. (1995), modified by Bünemann et al. (2016), see supporting information **Section C-S1**. Acid mono-phosphatase activity (APA) was determined following the method developed by Tabatabai and Bremner (1969), modified by Schinner et al. (1991) and DIN EN ISO 20130 (further details provided in supporting information **Section C-S1**). Concentrations of P_i for calculating P_{mic} and APA were measured immediately by UV-VIS (Analytik Jena Specord 200 plus, Germany), while larger sample sets ($NaHCO_3$, NaOH and CBD extraction solutions) were analyzed by CFA. The concentration of P_o was calculated as the difference in P_t and P_i.

For validation of P speciation in different pools, ^{31}P- Nuclear magnetic resonance analyzes (supporting information **Section C-S3**) were carried out (Bruker Avance 600 MHz High Resolution FT-NMR) for selected sequential extracts (external analyzes provided by the Central Institute for Engineering, Electronics and Analytics ZEA, Jülich).

For the isotopic analyses, P_i in the respective extraction solutions ($NaHCO_3$, NaOH, CDB and HCl) was purified following the protocol of Tamburini et al. (2018) and Joshi et al. (2015). Due to the high

methodological effort, isotopic analyzes of $\delta^{18}O_{Pi}$ values were conducted for 4 time points (initial sample material, after 1 day, after 4 weeks (SPL), respectively 8 weeks (LPL, L) and after 24 weeks). For methodological details of the sample preparation procedure, the reader is referred to supporting information **Section C-S1**. The purified Ag_3PO_4 was finally analyzed in duplicates for $\delta^{18}O_{Pi}$ with a Thermal Conversion Elemental Analyzer (vario PYRO cube, Elementar Analysensysteme GmbH, Langenselbold, Germany) in pyrolysis mode at 1450 °C, coupled to a Continuous Flow Isotope Ratio Mass Spectrometer (IRMS, Isoprime 100, Elementar Analysensysteme GmbH, Langenselbold, Germany). Oxygen isotope ratios are presented in the $\delta^{18}O$ notation as ‰ deviation values related to the VSMOW (Vienna Standard Mean Oceanic Water) international reference standard. International certified reference materials (USGS81, $\delta^{18}O_{Pi}$ = +13.1 ‰; USGS81, $\delta^{18}O_{Pi}$ = +35.4 ‰; IAEA 601, $\delta^{18}O_{Pi}$ = 23.1‰) were used for instrumental calibration and as quality control. Furthermore, an in-house standard (KH_2PO_4, $\delta^{18}O_{Pi}$ = ~13.5 ‰, Fisher Chemical, p.a. ≥99%) was included for checking the reproducibility. The results showed a good accuracy and reproducibility for all reference standard materials, see **Table C-S3 and Figure C-S2**.

The theoretical oxygen isotopic signature of P_i in equilibrium with pore water ($\delta^{18}O_{Pi\text{-}equ}$) was calculated after Chang and Blake (2015). Differences between calculated $\delta^{18}O_{Pi\text{-}equ}$ and observed $\delta^{18}O_{Pi}$ of a respective P pool are presented as $\Delta^{18}O_{Pi}$ values. Note that negative $\Delta^{18}O_{Pi}$ values indicate higher observed $\delta^{18}O_{Pi}$ than theoretical $\delta^{18}O_{Pi\text{-}equ}$ values.

Expected $\delta^{18}O_{Pi}$ values for the NaOH-P_i pool at a respective time step ($\delta^{18}O$ NaOH-$P_{i\ (expected\ ti)}$) were calculated with a simple mass balance considering the $\delta^{18}O$ values of the receiving P_i pool (here: NaOH) at time point t_i prior and after label transfer, the label value of the source P_i pool (here: $NaHCO_3$-P_i pool) as well as the P_i concentration change in the receiving P_i pool at the time point t_i (see equation I). Assuming that there was no value change due to microbial activity, we chose the $\delta^{18}O_{Pi}$ values of the $NaHCO_3$-P_i pool 1 day after labeling as the original source value. Our expected values consider no fractionation, which we regard as negligible in the case of sorption to Fe(III)-oxides based on Jaisi et al. (2011). As t_i, we selected the first time point after label application (i.e. 4 weeks in case of the SPL treatment, 8 weeks for the LPL and L treatments), because only in this situation it was possible to identify the receiving and source pool unambiguously.

$$\delta^{18}O\ NaOH\text{-}P_{i\ (expected\ ti)}) = ((NaOH\text{-}P_{i\ (1d)} * \delta^{18}O\ NaOH\text{-}P_{i\ (1d)}) + (NaOH\text{-}P_{i\ (ti\text{-}1)} * \delta^{18}O\ NaHCO_3\text{-}P_{i\ (1d)})) / (NaOH\text{-}P_{i\ (1d)} + NaOH\text{-}P_{i\ (ti\text{-}1)}) \quad (I)$$

With:

$\delta^{18}O$ NaOH-$P_{i\ (expected\ ti)}$: expected $\delta^{18}O$ values at time point t_i (4 / 8 weeks) assuming no value overprint occurred by enzymatic cycling

NaOH-$P_{i\ (1d)}$: P_i concentration in the NaOH pool 1 day after labeling (mg kg^{-1})

$\delta^{18}O$ NaOH-$P_{i\ (1d)}$: $\delta^{18}O_{Pi}$ value in the NaOH pool 1 after labeling (‰ VSMOW)

NaOH-$P_{i\ (ti\text{-}1)}$: P_i concentration change at time point t_i of incubation and prior time point (mg kg^{-1}, 4 weeks – 1 day (SPL); 8 weeks – 1 day (LPL, L))

$\delta^{18}O$ $NaHCO_3$-$P_{i\ (1d)}$: $\delta^{18}O_{Pi}$ value in the $NaHCO_3$ pool 1 after labeling (‰ VSMOW)

2.4. Statistical analyses and software

Sample analyzes were, if not stated otherwise, carried out as real triplicates and values reported represent mean values including standard deviation (indicated as ±). Statistical analyses were conducted in Excel (version 1808, 2019 MSO) and SPSS (IBM SPSS Statistics, Version 29). The data was checked for normal distribution (Shapiro-Wilk test, $p > 0.05$) and homogeneity of variances (Levene´s test; $p > 0.05$). Repeated Measures ANOVA was used to test differences within a treatment across the different time points (significance level: 0.05). One-way ANOVA was used to test differences between the treatments for each of the dependent variables (P pools, P_{mic}, APA, $\Delta^{18}O_{Pi}$). A non-parametric LSD post-hoc test (Least Significant Difference) was applied if required. To determine mean differences between two pairs or time points, a paired t-test was used.

Literature research was conducted by Google Scholar (Alphabet) and Web of Science (Clarivate) and was complemented by Scite_ (scite.ai). Language editing was supported by DeepL (DeepL SE) and ChatGPT 4o (OpenAI).

3. Results

3.1. General overview - Temporal changes and treatment effects

Hydrological regime and E_h: In 24 weeks of incubation at 20°C, the three treatments resulted in significant changes in several variables (see **Table C-3** for a summarizing overview), especially in WC and E_h values. The WC in the two pulsed logged treatments (SPL and LPL) ranged between 49 and 62% during the wet cycles, and from 23 to 38% for the dry cycles. This variation in the WC further influenced the E_h values. Here, the SPL and the LPL treatments showed pronounced changes between oxic (+378 to +464 mV) and strongly reducing (-556 to -392 mV) during the dry and wet cycles (**Table C-2, Figure C-S1**). However, fluctuations in E_h values changed over time for both treatments, showing decreasing amplitudes. In the SPL treatment, the fluctuation in E_h values stabilized between 4 to 16 weeks in the range of slightly and moderately reducing conditions towards the end of each wet cycle. The fluctuations were similar for the LPL treatment, although redox conditions were more reducing at the end of each wet cycle. During the dry cycles, the E_h rose in both treatments to oxic conditions (> + 400 mV). In contrast to the two dynamic treatments, the WC in the permanently waterlogged treatment (L) constantly remained around 52% (± 9%), while the E_h was constantly in a strongly reducing condition (-501 ± 36 mV). More detailed information about the progression of the respective E_h values is provided in **Figure C-S1.**

Table C-3: Changes in several properties during 24 weeks of incubation at 20°C. (a) short-pulsed logged (SPL) (b) long-pulsed logged (LPL) and (c) permanently waterlogged (L) treatments. Arrows represent the direction of changes, asterisks illustrate significant differences (24 weeks vs. initial values directly after label application; rmANOVA: * $p < 0.05$, ** $p < 0.01$, *** $p < 0.001$).

Sediment properties	**Treatment (20°C)**		
	a) SPL	**b) LPL**	**c) L**
Water content	↑↓ *	↑↓ *	→
Redox potential (Eh)	↑↓ *	↑↓ *	→
$pH_{porewater}$	↑ **	↑ ***	↑ **
$pH_{sediment}$	↑	↑	↑ **
Porewater – Fe (mg l^{-1})	↓	↓	↓
Porewater – Mn (mg l^{-1})	↓ *	↓ **	↓ *
$\delta^{18}O_{H2O}$ porewater (‰ VSMOW)	↑ ***	↑ ***	↑ ***
Microbial P (mg kg^{-1})	↓	↓	↓
Acid phosphatase activity (µg PNP g^{-1} h^{-1})	↓	↓	↓ *
Total alkalinity (mg HCO_3^- l^{-1})	↓ **	↓ **	→

→ stable ↑ increase ↓ decrease WC: ↓ (drying) ↑ (rewetting) E_h: ↑ (drying) ↓ (rewetting)

Porewater and pH: Regarding the porewater, TA values showed a similar behavior for the SPL and LPL treatments. In both treatments, TA decreased significantly ($p < 0.05$) from 389 ± 27 to 198 ± 23 mg l^{-1} after 16 weeks, representing an average decrease of 51% (**Figure C-1**). In the L treatment, TA first increased significantly ($p < 0.05$) after 4 weeks peaking around 850 mg l^{-1} and stabilized thereafter at slightly higher values as compared to the beginning of the experiment (average increase of 12%).

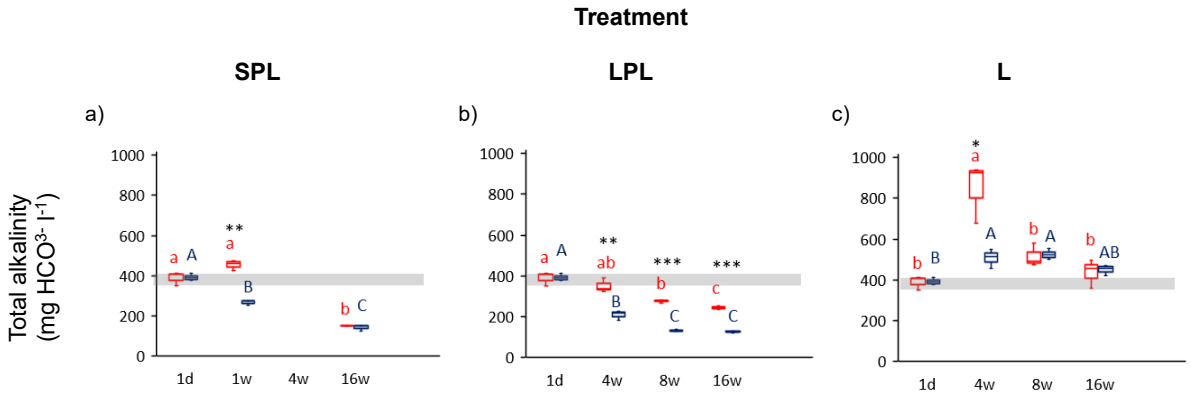

Figure C-1: Temporal variation of total alkalinity in the short-pulsed logged (SPL), long-pulsed logged (LPL) and permanently waterlogged (L) treatments. Total alkalinity (mg HCO_3^- l^{-1}) from beginning (1 day after labeling) till the end of the incubation (after 24 weeks). Red boxplots represent 20°C temperature treatments, blue boxplots represent 5°C treatments. Small letters show significant differences between groups of 20°C, capital letters show differences between groups of 5°C. Asterisks illustrate significant differences between 20°C and 5°C at the respective point in time (* $p < 0.05$, ** $p < 0.01$, *** $p < 0.001$). Shaded grey area symbolizes respective concentrations of the initial sediment.

The pH_{H2O} values increased significantly ($p < 0.001$) in all three treatments after 24 weeks of incubation from 7.7 ± 0.1 (initial sample material) to 8.5 ± 0.2 (**Figure C-2 a to c**). The $pH_{sediment}$ values varied as well during the 24 weeks, but the range was generally lower (6.8 to 7.1, **Figure C-2 d to f**) as compared to the pH_{H2O}.

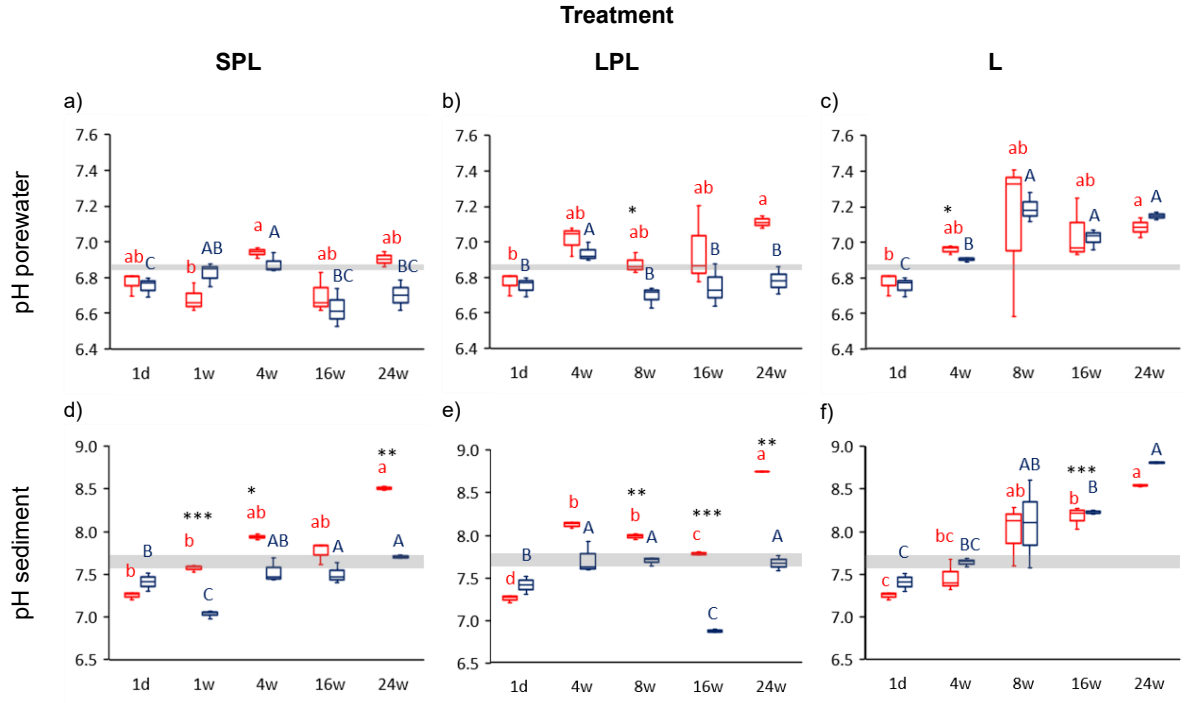

Figure C-2: Temporal variation in pH in porewater and sediment in the short-pulsed logged (SPL), long-pulsed logged (LPL) and permanently waterlogged (L) treatments. (a, b, c) $pH_{porewater}$, (d, e, f) $pH_{sediment}$ from beginning (1 day after labeling) until the end of the incubation (after 24 weeks). Red boxplots represent 20°C temperature treatments, blue boxplots represent 5°C treatments. Small letters indicating significant differences between groups of 20°C, capital letters differences between groups of 5°C. Asterisks illustrate significant differences between 20°C and 5°C at the respective point in time (* $p < 0.05$, ** $p < 0.01$, *** $p < 0.001$). Shaded grey area symbolizes respective values of the initial sediment.

Furthermore, dissolved Mn and Fe peaked at 4 weeks in the L treatment (Mn: 4.3 ± 0.8 mg l^{-1}, Fe: 2.6 ± 1.0 mg l^{-1}) and reached higher total concentrations as compared to the other two treatments (**Figure C-S3**). However, both Mn and Fe concentrations dropped after 24 weeks to similarly low concentrations (Mn: < 0.7 mg l^{-1}, Fe: < 0.1 mg l^{-1}) in all three treatments.

Biological variables: The P_{mic} concentrations increased slightly in the first 4 weeks from 33.9 ± 14.2 mg kg^{-1} to concentrations between 61.6 to 89.5 mg kg^{-1} (+88 to +170 %). After 8 weeks, P_{mic} decreased towards zero (between 9.1 and 26.5 mg kg^{-1}) in the L treatment and after 16 weeks in the SPL and LPL treatments (**Figure C-3 a to c**).

The enzyme activity was another variable that showed pronounced changes over time (**Figure C-3 d to f**). In the SPL and LPL treatments, APA decreased significantly in the first 4 weeks from 65.1 ± 7.5 to 26.5 and 40.1 µg PNP g^{-1} h^{-1}, respectively (- 38 to –60 %). Afterwards, APA values remained at a stable level until the end of the experiment. In the L treatment, APA values significantly increased up to 106 ±18 µg PNP g^{-1} h^{-1}.

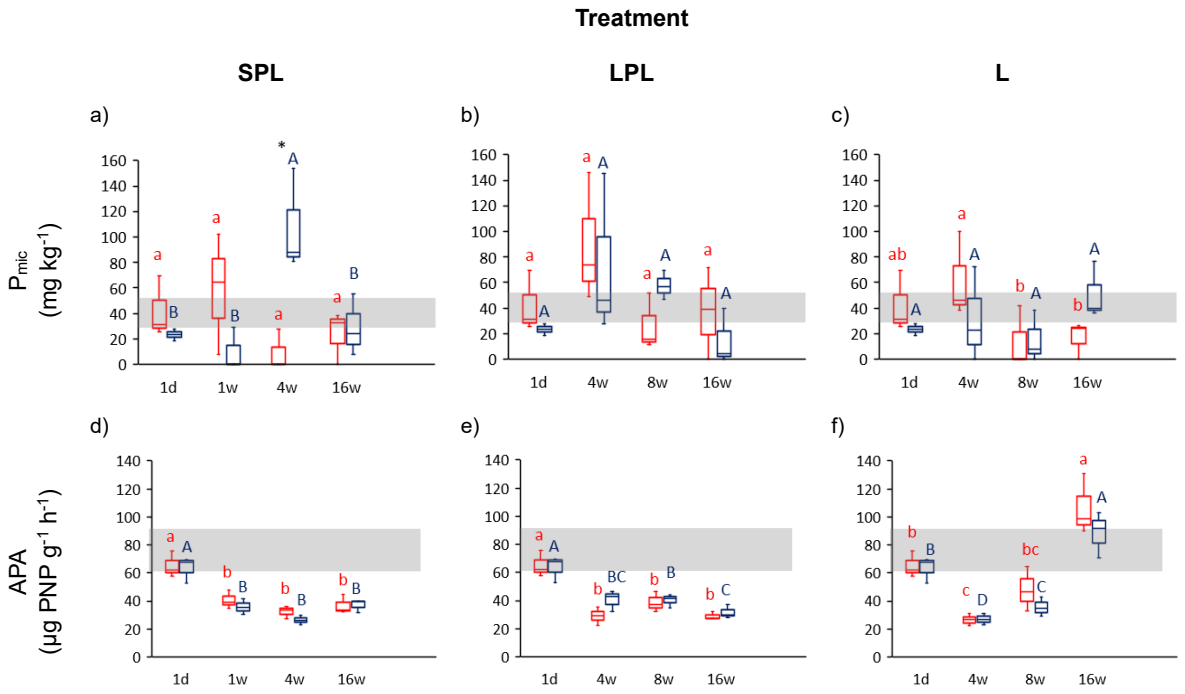

Figure C-3: Temporal variation in inorganic microbial phosphorus concentrations (P_{mic}) and acid phosphatase activity (APA) in the short-pulsed logged (SPL), long-pulsed logged (LPL) and permanently waterlogged (L) treatments. (a, b, c) P_{mic} concentrations (mg kg^{-1}), (d, e, f) enzyme activity (µg PNP g^{-1} h^{-1}) from beginning (1 day after labeling) until the end of the incubation (after 24 weeks). Red boxplots represent 20°C temperature treatments, blue boxplots represent 5°C treatments. Small letters show significant differences between groups of 20°C, capital letters show differences between groups of 5°C. Asterisks illustrate significant differences between 20°C and 5°C at the respective point in time (* $p < 0.05$, ** $p < 0.01$, *** $p < 0.001$). Shaded grey area symbolizes respective values of the initial sediment.

Isotope and ^{31}P NMR analyses: A significant increase ($p < 0.001$) was visible in the measured $\delta^{18}O_{H2O}$ (‰ VSMOW) values in porewater 4 weeks after adding the label. The $\delta^{18}O_{H2O}$ values rose from -9.6 ± 0.3 ‰ and ranged between -0.5 ‰ (SPL) and +5.8 ‰ (L), before values slightly decreased until the end

of the incubation (**Figure C-4 a to c**). Also, the $\delta^{18}O_{H2O}$ values in the L treatment were consistently higher as compared to the SPL and LPL treatments. Because of the changing $\delta^{18}O_{H2O}$ values in porewater, $\delta^{18}O_{Pi\text{-}equ}$ values changed consequently (**Figure C-4 d to f**).

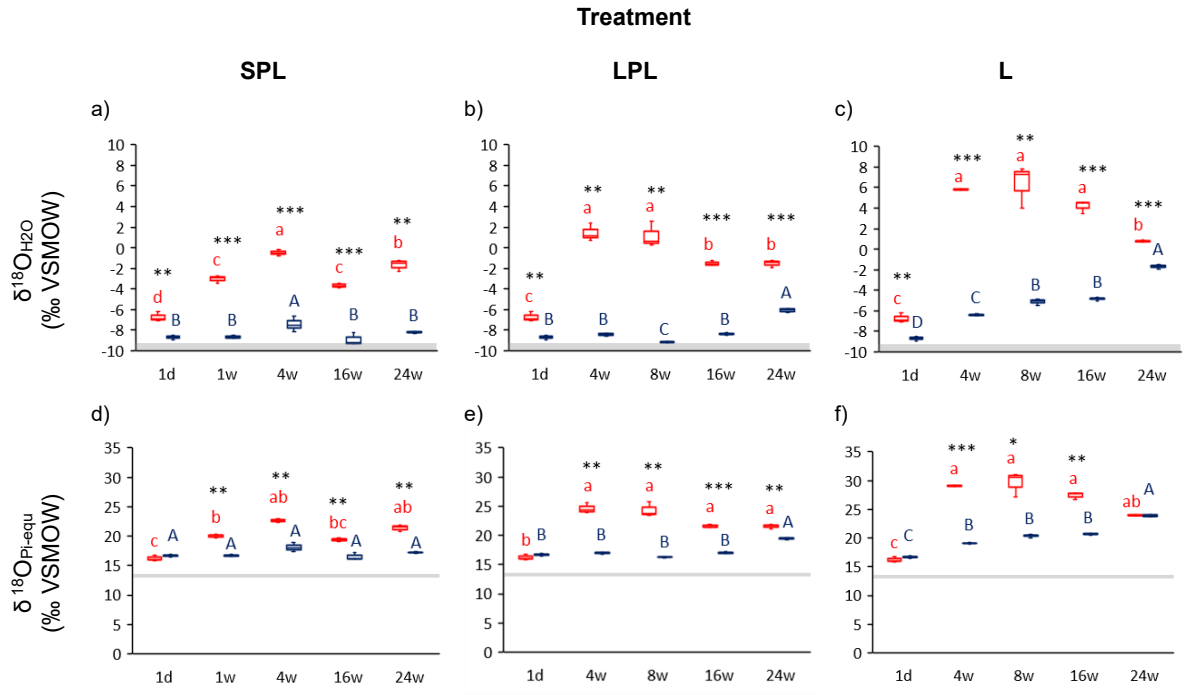

Figure C-4: Temporal variation in $\delta^{18}O_{H2O}$ values in porewater during the incubation in the short-pulsed logged (SPL), long-pulsed logged (LPL) and permanently waterlogged (L) treatments. (a, b, c) Observed $\delta^{18}O$ values in porewater ($\delta^{18}O_{H2O}$, ‰ VSMOW), (d, e, f) calculated theoretical equilibrium ($\delta^{18}O_{Pi\text{-}equ}$, ‰ VSMOW) after Chang and Blake (2015) from beginning (1 day after labeling) until the end of the incubation (after 24 weeks). Red boxplots represent 20°C temperature treatments, blue boxplots represent 5°C treatments. Small letters show significant differences between groups of 20°C, capital letters show differences between groups of 5°C. Asterisk illustrate significant differences between 20°C and 5°C at the respective point in time (* $p < 0.05$, ** $p < 0.01$, *** $p < 0.001$). Shaded grey area symbolizes respective values of the initial sediment.

The results of the ^{31}P NMR analysis showed only peaks for P_i in the $NaHCO_3$- and NaOH-extraction solutions (see Supporting information **Section C-S3**), which agreed with respective P_i and P_o concentrations obtained from UV-Vis and ICP-OES. For the CDB- and HCl-extraction solutions, no reliable signals could be obtained from ^{31}P NMR due to low P concentrations, which was additionally complicated by matrix effects.

Temperature effects: During the 24 weeks of incubation the temperatures were constant at around 20°C at room temperature (19.7°C ± 0.1) and 5°C (5.5°C ± 2.2). Furthermore, $pH_{sediment}$ and $\delta^{18}O_{H2O}$ values were significantly lower at 5°C as compared to the 20°C treatment (**Figure C-2 d to f; Figure C-4 a to c**).

3.2. Changes in P pools

3.2.1. Initial labelling

Directly (1 day) after addition of the $^{18}O_{Pi}$ label, P_i concentrations in porewater and the $NaHCO_3$-P_i pool were significantly increased (**Table C-1**). Porewater-P_i increased from 0.21 ± 0.1 to 23.2 ± 0.9 mg l^{-1} ($p < 0.001$, **Table C-4, Figure C-5**) and $NaHCO_3$-P_i from 68.5 ± 29.5 to 541 ± 69 mg kg^{-1} ($p < 0.01$, **Table C-4, Figure C-6 a to c**). The P_i concentrations of other P pools were not affected by the label (i.e., P_{mic}, NaOH-P_i) at this point, or showed only slight changes due to a large variability among replicates (i.e., CDB-P_i, HCl-TP, H_2SO_4-TP).

Total P concentrations in the experimental pots rose, on average, from 79.1 ± 4.4 mg TP (before) to 88.0 ± 4.1 mg TP after label application. This changed the relative proportion of TP in the various P pools (**Figure C-S4**), with a significant increase of porewater-P (from 0 to 2% of TP) and $NaHCO_3$-P (from 11 to 32% of TP).

Following the concentration increase, $\delta^{18}O_{Pi}$ values (‰ VSMOW) of the $NaHCO_3$-P_i pool increased from 25 ± 2 to 143 ± 62 ‰ (**Table C-4**). The $\delta^{18}O_{Pi}$ values of the other P_i Pools were not or only slightly affected (NaOH-P_i decreased by 2 ‰, CDB-P_i increased by 6 ‰).

In the following 24 weeks, P pools and other variables showed distinct trends, based on which we decided to divide the experiment into the following three phases (early, intermediate and late).

Table C-4: Changes in P concentrations and O isotope composition in various P pools (Porewater -P_i, $NaHCO_3$ -P_i, NaOH - P_i, CDB - P_i, HCl- TP, H_2SO_4 -TP). (a) 20°C conditions and (b) 5°C conditions. Arrows represent changes between initial sediment and 24 hours after labeling. Asterisks illustrate significant differences between initial sediment and 24 hours after labeling (* $p < 0.05$, ** $p < 0.01$, *** $p < 0.001$).

Phosphorus fraction	Temperature a) 20°C	Temperature b) 5°C
Porewater - P_i (mg l^{-1})	↑ ***	↑ **
$NaHCO_3$ - P_i (mg kg^{-1})	↑ **	↑ *
NaOH - P_i (mg kg^{-1})	↑	↓
CDB - P_i (mg kg^{-1})	↑	↓ *
HCl - TP (mg kg^{-1})	↓	↓ *
H_2SO_4 - TP (mg kg^{-1})	↓ *	↓ *
$\delta^{18}O_{H2O}$ Porewater (mg kg^{-1})	↑	↑
$\delta^{18}O_{Pi}$ $NaHCO_3$ (‰ VSMOW)	↑	↑

→ stable ↑ increase ↓ decrease

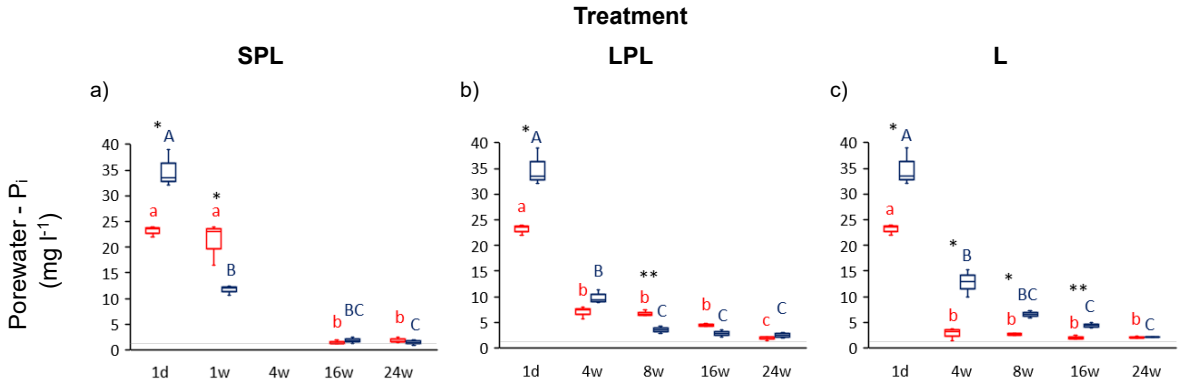

Figure C-5: Temporal variation in inorganic phosphorus (P_i) concentrations in porewater in the short-pulsed logged (SPL), long-pulsed logged (LPL) and permanently waterlogged (L) treatments. Porewater-P_i (mg l^{-1}) concentrations from beginning (1 day after labeling) until the end of the incubation (after 24 weeks). Red boxplots represent 20°C temperature treatments, blue boxplots represent 5°C treatments. Small letters show significant differences between groups of 20°C, capital letters show differences between groups of 5°C. Asterisks illustrate significant differences between 20°C and 5°C at the respective point in time (* $p < 0.05$, ** $p < 0.01$, *** $p < 0.001$). Shaded grey area symbolizes respective concentrations of the initial sediment.

3.2.2. Early phase

In the first 4 weeks following the label addition, we observed a redistribution from the porewater- and $NaHCO_3$-P_i pools into the NaOH-P_i and CDB-P_o pools. In the SPL treatment, the NaOH-P_i concentration increased significantly by 82% to 437 ± 30.1 mg kg^{-1}, when compared to the initial values 1 day after label application (**Figure C-6 d**). Moreover, the CDB-P_o concentrations increased significantly by 280% to 76.3 ± 18.7 mg kg^{-1} (**Figure C-7 d**). The $\delta^{18}O_{Pi}$ values of the $NaHCO_3$-P_i pool decreased as compared to the initial phase, reaching +125 ‰ (**Figure C-8 a**). The difference between the calculated theoretical equilibrium $\delta^{18}O_{Pi\text{-}equ}$ and the measured $\delta^{18}O_{Pi}$ values ($\Delta^{18}O_{Pi}$) in the $NaHCO_3$-P_i pool was about 120 ‰ above the theoretical equilibrium value ($\delta^{18}O_{Pi\text{-}equ}$: +23 ‰, **Figure C-8 d**). In the NaOH-P_i pool, the $\delta^{18}O_{Pi}$ values decreased slightly after 4 weeks from +26 to +22 ‰ (**Figure C-8 g**) and were close to equilibrium ($\Delta^{18}O_{Pi}$ = -0.8 ‰, **Figure C-8 j**). In addition, after 4 weeks, the observed values in the NaOH-P_i pool were 55 ‰ lower than the expected values (+77 ‰) calculated based on a mass balance approach (**Table C-S4**). Observed $\delta^{18}O_{Pi}$ values in the NaOH pool at 5°C (+34 ‰) were also consistently lower than the expected ones (+64 ‰, **Table C-S4**). No changes and therefore label effects were visible in the $\delta^{18}O_{Pi}$ values of the other P pools after 4 weeks (e.g., HCl pool, **Figure C-S5**).

In the LPL treatment the P_i concentrations in the porewater-P pool decreased significantly by 6%, to 7.00 ± 0.9 mg l^{-1} (**Figure C-5 b**) 4 weeks after labeling. In the same period, the NaOH-P_i concentrations increased significantly by 123% to 536 ± 77.1 mg kg^{-1} (**Figure C-6 e**). Considering P_o, there was a significant increase in the CDB-P_o pool visible. Here, concentrations rose by 110% to concentrations of 41.8 ± 9.1 mg kg^{-1} (**Figure C-7 e**).

In the L treatment the porewater-P_i concentrations also decreased significantly by 87% to 2.80 ± 1.0 mg l^{-1} (**Figure C-5 c**) after 4 weeks. Moreover, the $NaHCO_3$-P_i concentrations decreased significantly by 70%, corresponding to a value of 164 ± 25.5 mg kg^{-1} (**Figure C-6 c**). In the same period, the NaOH-P_i concentrations increased significantly by 100%, reaching maximum concentrations of 480 ± 65.5 mg kg^{-}

^{1} (**Figure C-6 f**). Also, CDB-P_o concentrations increased significantly by 205% to 60.8 ± 12.0 mg kg^{-1} (**Figure C-7 f**).

Temperature effects were visible for the P_{mic} concentrations in the SPL treatment after 4 weeks, with significantly lower ($p < 0.05$) concentrations at 20°C (9.12 ± 12.9 mg kg^{-1}) as compared to the 5°C treatment (108 ± 33.0 mg kg^{-1}).

After 4 weeks, the hydrological regimes already resulted in pronounced differences for several variables among the three treatments. Considering the relative proportion of TP, the $NaHCO_3$-P_i pool was significantly lower ($p < 0.001$) for the L treatment (12% of TP) as compared to SPL and LPL treatments (27% for each, **Figure C-S7 a**). The CDB-P_o pool was lowest in the LPL treatment (3%) and differed significantly from the SPL treatment (6%, **Figure C-S7 e**). There were no significant differences in the percental distribution of the other P pools. Biological variables like P_{mic} concentrations were significantly lower ($p < 0.05$) for the SPL (9 mg kg^{-1}) than the LPL treatment (89 mg kg^{-1}, **Figure C-S7 h**). The TA values of the SPL and LPL treatments (215 and 350 mg HCO_3^- l^{-1}, respectively) were significantly lower ($p < 0.05$) than in the L treatment (847 mg HCO_3^- l^{-1}, **Figure C-S7 j**).

3.2.3. Intermediate phase

Between 4and 16 weeks, in the SPL treatment only the CDB-P_o concentrations changed significantly ($p < 0.05$) and decreased by 75% to 19 ± 8.0 mg kg^{-1} (**Figure C-7 d**).

In the LPL treatment, porewater-P_i decreased significantly ($p < 0.01$) by 34% to 4.5 ± 0.3 mg l^{-1} **(Figure C-5 b)** between 4 and 8 weeks**.** The NaOH-P_i concentrations also decreased significantly to 274 ± 33.9 mg kg^{-1} (**Figure C-6 e**). In the same period, the NaOH-P_o concentrations increased significantly ($p < 0.05$) by 116%, reaching 188 ± 40.9 mg kg^{-1}. Moreover, the CDB-P_o concentrations increased significantly ($p < 0.05$) by 222% to 145 ± 13 mg kg^{-1} **(Figure C-7 e**). The H_2SO_4-TP concentrations increased slightly but constantly from the early to the intermediate phase, reaching a maximum of 213 ± 16.5 mg kg^{-1}. After 8 weeks, the observed $\delta^{18}O_{Pi}$ values of the $NaHCO_3$-P_i pool decreased to +74 ‰ (**Figure C-8 b**), with $\Delta^{18}O_{Pi}$ significantly differing from zero (**Figure C-8 e**). In the same period, the $\delta^{18}O_{Pi}$ values of the NaOH-P_i pool increased to +44 ‰ (**Figure C-8 h**). The differences between observed $\delta^{18}O_{Pi}$ and calculated $\delta^{18}O_{Pi\text{-}equ}$ values increased to +20 ‰ (see $\Delta^{18}O_{Pi}$ in **Figure C-8 k**). After 8 weeks, the $\delta^{18}O_{Pi}$ values for NaOH- P_i were 6 ‰ higher than the expected values based on the mass balance calculation (+38 ‰, **Table C-S4**). Moreover, $\delta^{18}O_{Pi}$ values of the HCl pool decreased slightly by 7 ‰ (from 32 ‰ to +25 ‰) compared to the initial phase (**Figure C-S5 b**).

In the L treatment, only significant changes in P pools were visible for $NaHCO_3$-P_i, which increased significantly by 27% to 503 ± 59.2 mg kg^{-1} between 4 and 8 weeks **(Figure C-6 c**). There were noticeable but not significant increases in the NaOH-P_o, CDB-P_o (**Figure C-7 c, f**) and H_2SO_4-TP **(Figure C-6 o**) pools, which reached maximum concentrations after 8 weeks. The $\delta^{18}O_{Pi}$ values of $NaHCO_3$-P_i decreased slightly by 20 ‰ (**Figure C-8 c**), reaching a $\Delta^{18}O_{Pi}$ of +122 ‰ (**Figure B - 8 f**). In contrast, the $\delta^{18}O_{Pi}$ values of the NaOH-P_i pool increased by 48 ‰, reaching +74 ‰ (**Figure B - 8 i**), with a $\Delta^{18}O_{Pi}$ of +24 ‰ above the calculated equilibrium (**Figure C-8 l**). The $\delta^{18}O_{Pi}$ values for NaOH-P_i were close to the expected ones (+72 ‰) based on the mass balance calculation (difference +2 ‰), **Table C-S4**). Further note that $\delta^{18}O_{Pi}$ values of the HCl pool showed slightly higher values than 1 day after labeling (6 ‰, **Figure C-S5 c**).

Significant temperature effects in P pools were visible in the $NaHCO_3$-P_i and NaOH-P_i concentrations in the SPL treatment after 16 weeks (**Figure C-6 a, d**). In the $NaHCO_3$-P_i pool, the concentrations at 20°C were 24% lower than at 5°C ($p < 0.05$), while the NaOH-P_i concentrations were 10% higher at 20°C ($p < 0.05$). In the LPL treatment, $\delta^{18}O_{Pi}$ values of the $NaHCO_3$ pool at 5°C were significantly higher (92 ‰, $p < 0.05$) than those at 20°C (**Figure C-8 b**). Also, in the L treatment the HCl-TP concentrations after 8 weeks were 39% higher at 20°C as compared to the 5°C treatment ($p < 0.05$), (**Figure C-6 l**).

At the end of the intermediate phase (after 16 weeks in SPL and 8 weeks in LPL and L), the hydrological regimes resulted in pronounced differences of the P pools among the three treatments. Here, the relative proportions of the P pools (with the exception of NaOH-P_o) differed significantly among all three treatments. The $NaHCO_3$-P_i pool in the SPL treatment was with a proportion of 19% of TP significantly ($p<0.01$) lower as in the LPL (28%) and L (37%) treatments (**Figure C-S8 a)**. The proportions of NaOH-P_i as well as CDB-P_i were significantly lower in the LPL (19% and 7%) and L (20% and 6%) treatments as compared to the SPL treatment (27% and 12%, **Figure C-S8 b, c**). For CDB-P_o, the proportion in the SPL treatment was with 2% significantly ($p<0.001$) lower as for the L (6%) and the LPL treatments (9%, **Figure C-S8 e**). For HCl-TP, the LPL (8%) and L (7%) treatments were significantly lower as the SPL treatment (12%, **Figure C-S8 f**). Regarding H_2SO_4-TP, the L treatment (14%) was significantly lower than the SPL (24%) and LPL (26%) treatments (**Figure C-S8 g**). For the biological variables P_{mic} and APA, no significant differences among the various hydrological regimes were found at this phase (**Figure C-S8 h, i**).

3.2.4. Late phase

Between 16 to 24 weeks, several P pools showed minor concentration changes in the SPL treatment, although most were not significant (see **Figures C-6 a, d, m and C-7 d**). What clearly changed were the isotopic values of the P pools. After 24 weeks, the observed $\delta^{18}O_{Pi}$ values of the $NaHCO_3$-P_i pool decreased further by 86 ‰ to +39 ‰ (**Figure C-8 a**) as compared to 4 weeks after labeling. At the end of the incubation, $\delta^{18}O_{Pi}$ values of the $NaHCO_3$-P_i pool were 103 ‰ lower than directly after labeling. Generally, the $\delta^{18}O_{Pi}$ values of the $NaHCO_3$-P_i were still slightly above the respective theoretical equilibrium values (see $\Delta^{18}O_{Pi}$ of +17 ‰, **Figure C-8 d**). In the NaOH-P_i pool, the $\delta^{18}O_{Pi}$ values decreased by 25 ‰ to +47 ‰ (**Figure C-8 g**). Note that respective $\Delta^{18}O_{Pi}$ values differed significantly from zero (**Figure C-8 j**). Moreover, $\delta^{18}O_{Pi}$ values of the HCl-extractable P reached after 24 weeks +22 ‰, being close to the $\delta^{18}O_{Pi\text{-}equ}$ value (**Figure C-S5 d**).

In the LPL treatment, several P pools showed variations in respective P concentrations between 8 and 24 weeks. For example, the $NaHCO_3$-P_i concentrations remained constant with a slight peak after 16 weeks **(Figure C-6 b***)*. The NaOH-P_i concentrations showed the same trend as $NaHCO_3$-P_i with an increase after 16 weeks before concentrations reached the same values again (**Figure C-6 e**). Compared to the last time step of the intermediate phase, the CDB-P_o concentrations decreased significantly ($p < 0.01$) after 16 weeks by 74% (from 136 ± 13 to 36 ± 4 mg kg^{-1}, **Figure C-7 e**). In addition, H_2SO_4-TP also decreased significantly ($p < 0.01$) by 23% (from 216 ± 16 to 167 ±12 mg kg^{-1}, **Figure C-6 n**). Furthermore, dissolved P_i concentrations in porewater stabilized at low levels of below 2.0 ± 0.1 mg l^{-1} (**Figure C-5 a**). After 24 weeks, $\delta^{18}O_{Pi}$ values of the $NaHCO_3$ pool remained similar compared to the previous time step (**Figure C-8 b**), with $\Delta^{18}O_{Pi}$ still differing significantly from zero (**Figure C-8 e**). In the NaOH-P_i pool, the $\delta^{18}O_{Pi}$ values decreased only slightly by 15 ‰ (+ 29 ‰) and

differed significantly from zero (**Figure C-8 k**). Furthermore, observed $\delta^{18}O_{Pi}$ values of the HCl pool increased by 6 ‰ after 24 weeks (+30 ‰, **Figure C-S5 f**).

In the L treatment, only slight concentration changes occurred in the P pools between 8 and 24 weeks. Here, NaOH-P_i decreased slightly by 13% (from 409 ± 57 to 357 ± 73 mg kg^{-1}). The HCl-TP concentrations showed significant changes with an increase of 28% to 147 ± 15.5 mg kg^{-1} ($p < 0.05$) after 16 weeks of incubation **(Figure C-6 l**). The CDB-P_o concentrations decreased significantly ($p < 0.05$) after 24 weeks by 86% (from 110 ± 18 to 15 ± 2 mg kg^{-1}), (Figure 7 f). Also, H_2SO_4-TP decreased slightly by 13% (from 226 ± 21 to 196 ± 18 mg kg^{-1}), (Figure 6 o). After 24 weeks, the $\delta^{18}O_{Pi}$ values in the $NaHCO_3$-P_i pool decreased by 52 ‰ to +71 ‰ (**Figure C-8 c**), but were still well-above the theoretical equilibrium value (see $\Delta^{18}O_{Pi}$ of +47 ‰, **Figure C-8 f**). In the NaOH-P_i pool, the $\delta^{18}O_{Pi}$ values decreased by 40 ‰ to +34 ‰ (**Figure C-8 g**)**,** thereby remaining slightly above the $\delta^{18}O_{Pi\text{-}equ}$ value ($\Delta^{18}O_{Pi}$ of +14 ‰, **Figure C-8 j**).

Regarding the two temperature treatments, the only systematic differences in P_i und P_o pools were visible in the surface-adsorbed P_i pools ($NaHCO_3$- and NaOH-P_i) after 16 weeks for all treatments. At 5 °C, the $NaHCO_3$-P_i concentration was 33 to 43% ($p < 0.05$) and the NaOH-P_i concentration 35 to 40% ($p < 0.05$) lower as compared to the 20°C treatment. At the end of the experiment, only the CDB-P_o concentration in the L treatment was at 5°C 127% significantly higher ($p < 0.05$) as compared to the 20°C treatment (**Figure C-7 f**).

At the end of the incubation after 24 weeks, differences in P pools among the three treatments were surprisingly lower as compared to the previous intermediate phase. Here, the percental proportions of P_i related to the total P only differed for the $NaHCO_3$-P_i pool, which was in the SPL treatment with 27% significantly lower as the LPL and L treatments (29 and 35%, respectively, **Figure C-S9 a**). Regarding the P_o pools, the NaOH-P_o proportion was in the L treatment with 11% significantly lower ($p < 0.05$) as compared to the SPL and LPL treatments (15% each, see **Figure C-S9 d**). Also, the proportion of CDB-P_o was significantly lower in the L treatment (0.5%) than in the SPL and LPL treatments (2 and 4%, respectively, **Figure C-S9 e**). Notably, the $\Delta^{18}O_{Pi}$ values of the respective P_i pools differed significantly among the three treatments. Lowest $\Delta^{18}O_{Pi}$ values occurred in the $NaHCO_3$-P_i pool for the SPL treatment, whereas the picture was reversed for the NaOH-P_i and HCl- P_i pools (**Figure C-S9 h, i, j**).

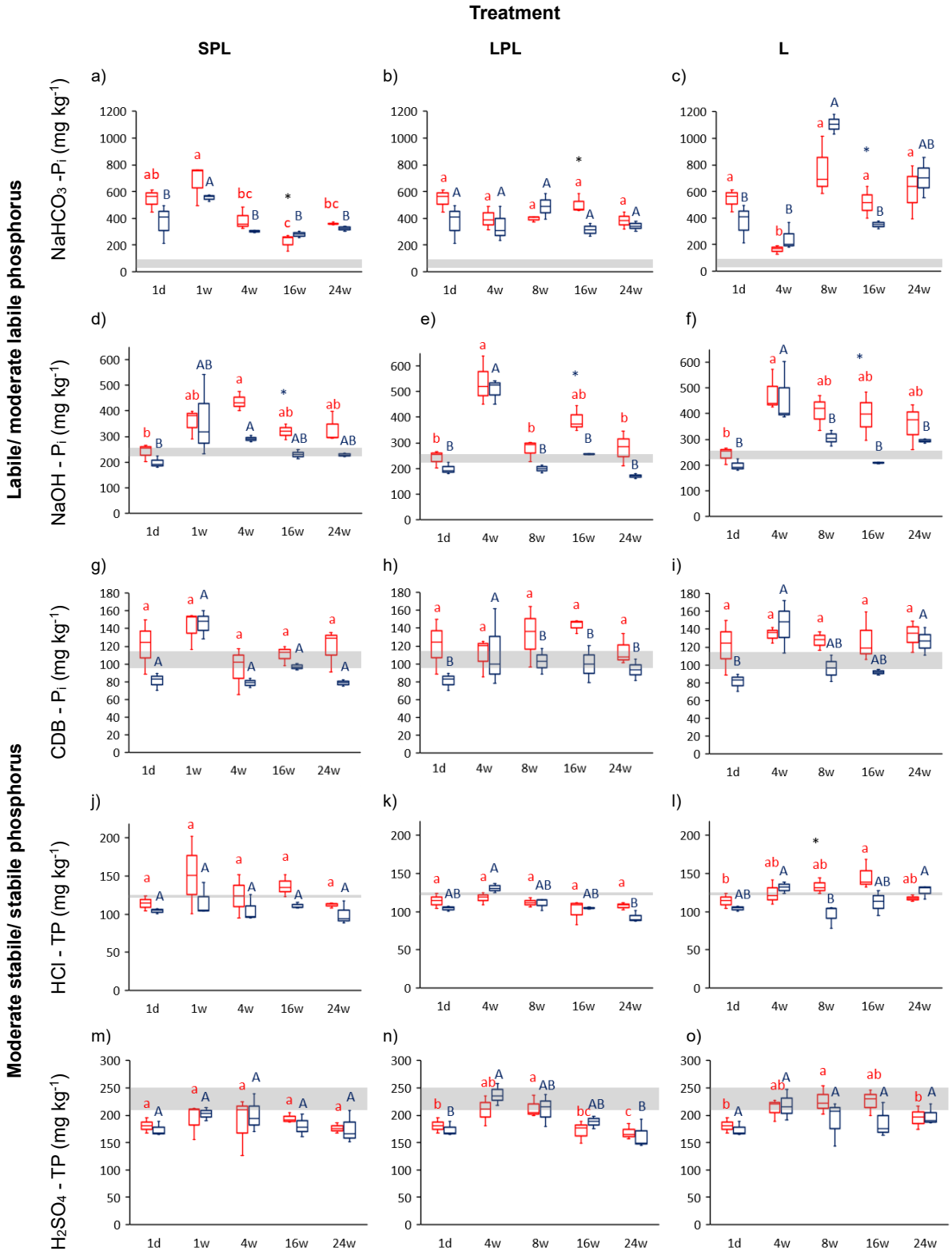

Figure C-6: Temporal variation in inorganic phosphorus (P_i) and total phosphorus (TP) concentrations in P pools in the short-pulsed logged (SPL), long-pulsed logged (LPL) and permanently waterlogged (L) treatments. (a, b, c) $NaHCO_3$ - P_i (mg kg^{-1}) concentrations, (d, e, f) NaOH - P_i (mg kg^{-1}) concentrations, (g, h, i) CDB - P_i (mg kg^{-1}) concentrations, (j, k, l) HCl - TP (mg kg^{-1}) concentrations and (m, n, o) H_2SO_4 - TP (mg kg^{-1}) concentrations from beginning (1 day after labeling) until the end of the incubation (after 24 weeks). Red boxplots represent 20°C temperature treatments, blue boxplots represent 5°C treatments. Small letters show significant differences between groups of 20°C, capital letters show differences between groups of 5°C. Asterisks illustrate significant differences between 20°C and 5°C at the respective point in time (* $p < 0.05$, ** $p < 0.01$, *** $p < 0.001$). Shaded grey area symbolizes respective concentrations of the initial sediment.

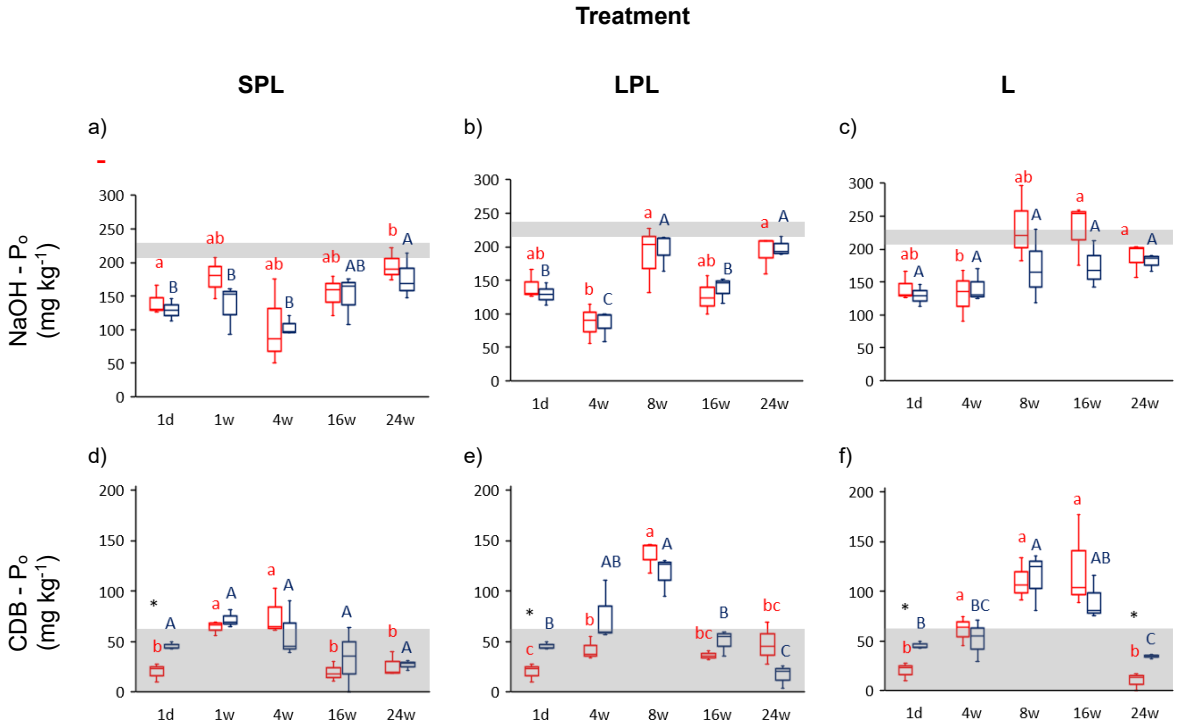

Figure C-7: Temporal variation in organic phosphorus (P_o) concentrations in the NaOH- and CDB-P pools in the short-pulsed logged (SPL), long-pulsed logged (LPL) and permanently waterlogged (L) treatments. (a, b, c) NaOH - P_o (mg kg^{-1}) concentrations, (d, e, f) CDB - P_o (mg kg^{-1}) concentrations from beginning (1 day after labeling) until the end of the incubation (after 24 weeks). Red boxplots represent 20°C temperature treatments, blue boxplots represent 5°C treatments. Small letters show significant differences between groups of 20°C, capital letters show differences between groups of 5°C. Asterisks illustrate significant differences between 20°C and 5°C at the respective point in time (* $p < 0.05$, ** $p < 0.01$, *** $p < 0.001$). Shaded grey area symbolizes respective concentrations of the initial sediment.

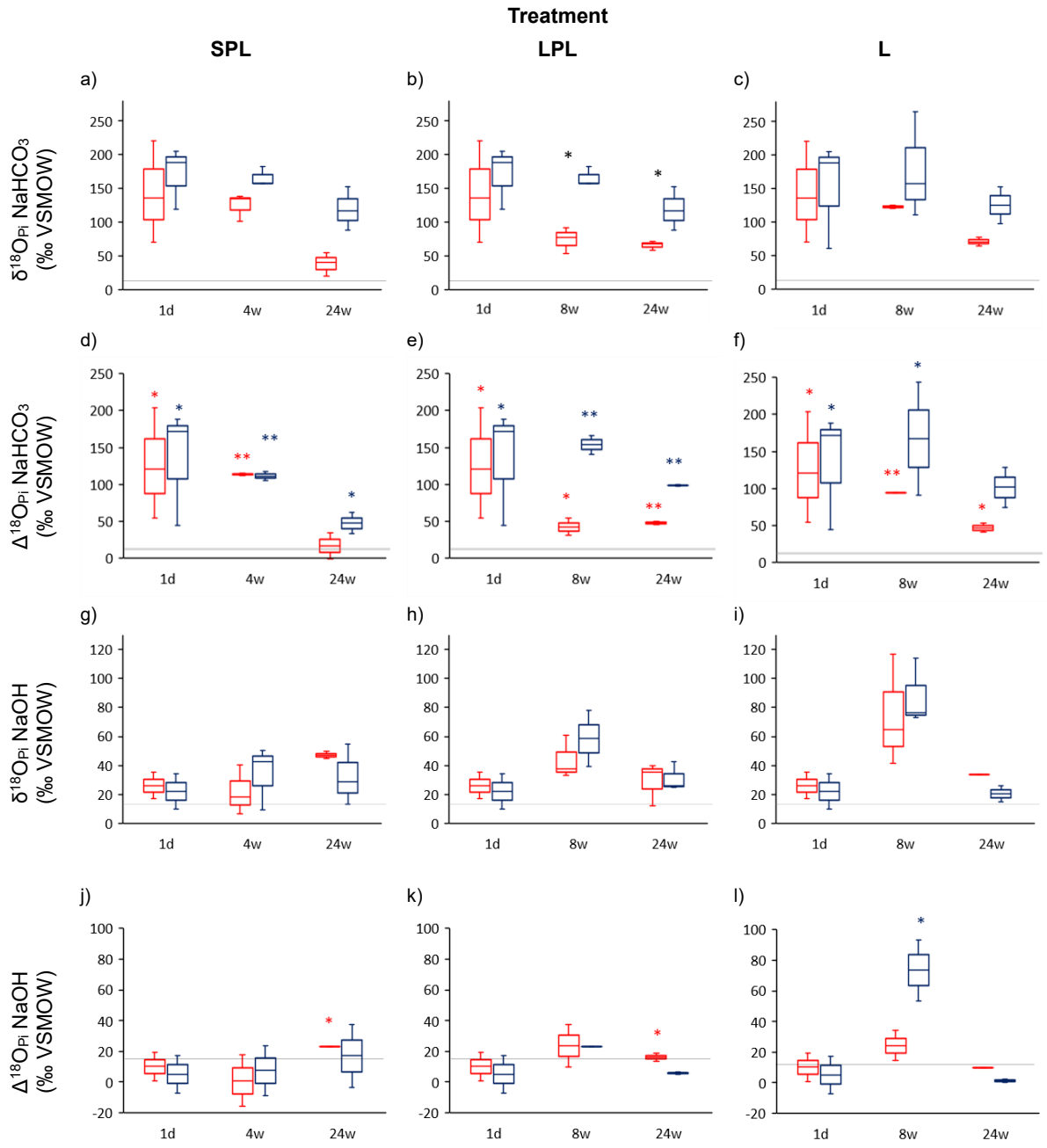

Figure C-8: Temporal variation in $\delta^{18}O$-P_i values in P_i pools in the short-pulsed logged (SPL), long-pulsed logged (LPL) and permanently waterlogged (L) treatments. Observed $\delta^{18}O$ values ($\delta^{18}O_{Pi}$, ‰ VSMOW) of (a, b, c) $NaHCO_3$ P_i-pool and (g, h, i) NaOH P_i-pool from beginning (1 day after labeling) till the end of the incubation (after 24 weeks). Difference between observed $\delta^{18}O_{Pi}$ and $\delta^{18}O_{Pi\text{-}equ}$ values ($\Delta^{18}O_{Pi}$, ‰ VSMOW) of the (d, e, f) $NaHCO_3$ P_i-pool and (j, k, l) NaOH P_i-pool from beginning (1 day after labeling) until the end of the incubation (after 24 weeks). Red boxplots represent 20°C temperature treatments, blue boxplots represent 5°C treatments. Black asterisks illustrate significant differences between 20°C and 5°C (a, b, c), red and blue asterisks illustrate significant differences from zero (d, e, f and j, k, l) at the respective point in time (* $p < 0.05$, ** $p < 0.01$, *** $p < 0.001$). Shaded grey area symbolizes respective values of the initial sediment.

4. Discussion

4.1. General temporal changes

The following overview focusses on the three incubation treatments that were carried out at 20°C. Over the 24-week duration of the experiment, the geochemistry of the system underwent pronounced changes. The E_h of the two pulsed-logged treatments clearly differed from the permanently waterlogged treatment due to the frequent drying and rewetting cycles. In the SPL and LPL treatments, the E_h first rapidly decreased towards strongly reducing conditions, which, however, gradually increased again and fluctuated between slightly and moderately reducing. Similar redox dynamics have been observed by Włodarczyk et al. (2007) during an incubation of arable soils over 2 months. In the L treatment, the E_h rapidly declined and stabilized at strongly reducing conditions, as also reported by Ajmone-Marsan et al. (2006) for soils incubated over 120 days under continuous water logging. Thus, the hydrological regime treatments resulted in distinct redox conditions as desired, which subsequently impacted a suite of other variables.

Both, pH_{H2O} and $pH_{sediment}$, increased in all treatments, ultimately reaching alkaline conditions. We attribute this increase in pH to the growth and metabolic activity of microorganisms, which consumed dissolved CO_2 under saturated conditions, causing a decrease in $H_2CO_{3\ (aq)}$ and therefore H^+ concentrations (Lu et al., 2016). The impact of metabolic activity was further reflected by a decrease in TA and E_h. Such a link of pH, alkalinity and E_h to the microbial mineralization of organic matter in soils and sediments has been previously highlighted, for example by Bünemann (2015) and Husson (2013). The only exception was the L treatment, with an steep increase in TA after 4 weeks. Here, microbial activity under permanently anoxic conditions likely lead to the production and enrichment of bases such as ammonium or hydroxide ions (Yan et al., 1996), subsequently increasing alkalinity and pH.

4.2. Behavior of P pools

4.2.1. Initial labeling

After the first 24 hours of introducing ^{18}O-enriched PO_4 solution, the label was predominantly transferred from porewater to the $NaHCO_3$-P_i pool, thereby tripling its relative proportion (**Figure C-S4**), resulting in a pronounced isotopic labeling (average $\delta^{18}O_{Pi}$-$NaHCO_3$: 143 ‰). This rapid transfer of the P_i label into the $NaHCO_3$-P_i pool aligns with prior soil incubation studies (Barrow, 1984; Joshi et al., 2016). Given the initially circum-neutral pH in porewater and sediment, P_i was predominantly present in its negatively charged species, $H_2PO_4^-$ and HPO_4^{2-}, facilitating its adsorption onto positively charged mineral surfaces and soil organic matter (Barrow et al., 2020). We also observed a pronounced enrichment of dissolved P_i in the porewater after 24 hours (23.2 mg l^{-1}, accounting for 2% of the total P, **Figure C-S4**), thereby marking porewater as a significant additional P pool. After 24 hours, the other P pools were not visibly affected neither in terms of concentrations nor O isotope ratios of phosphate. Our observations are in line with our first hypothesis (H1) and agree with Joshi et al. (2016), who reported that applied P_i readily partitioned into porewater and the $NaHCO_3$-P_i pool.

4.2.2. Early phase

In the first 4 weeks following labeling, porewater and $NaHCO_3$-P_i were subsequently transferred into the NaOH-P_i pool which aligns with observations made by Joshi et al. (2016) and Guo (2000). The transfer of P_i was closely linked to a significant increase in pH, which mobilized weakly bound $NaHCO_3$-P_i, (e.g., by changes of mineral surface charges and sorption competition with OH^-), while enhancing strong adsorption to metal oxides and hydroxides (Barrow et al., 2020; De Gerónimo and Aparicio, 2022; Gustafsson et al., 2012; Pérez et al., 2014; Zhou et al., 2005).

Despite a decline in the E_h towards moderately and mildly reducing conditions in the SPL and LPL treatments, this did not result in a release of NaOH-P_i through reductive dissolution of Fe(III)-oxides (Aldous et al., 2005; Dupas et al., 2015b). Reductive dissolution of Fe(III)-oxides was neither reflected in the NaOH-P_i pool, nor in the concentrations of dissolved Fe and Mn in porewater (**FigureC-S6**). Thus, the impact of the E_h on the repartition of P_i was less relevant as compared to the increase in the pH during the initial 4 weeks, corroborating findings by Zhou et al. (2005).

Furthermore, the isotope data revealed the importance of intracellular P cycling, as evident from the SPL treatment. Here, a significant concentration increase in the NaOH-P_i pool occurred after 4 weeks, which was, however, not fully supported by the isotope data. Despite a pronounced transfer of P_i from the initially highly labelled $NaHCO_3$-P_i pool, $\delta^{18}O_{Pi}$ values of the receiving NaOH-P_i pool were surprisingly lower (~50 ‰) than expected based on the concentration change and initial isotopic value. We attribute this loss of the isotopic label and shift in direction of the theoretical equilibrium value **(Figure C-8**) to microbial uptake and intracellular cycling associated with an exchange of ^{18}O from the initial P_i label with ^{16}O originating from ambient water molecules. In line, $\delta^{18}O_{H2O}$ showed a significant increase towards heavier isotopic values in all treatments over time (up to +7 ‰). As this was also the case in the 5°C temperature treatment, we consider the influence of evaporation on the $\delta^{18}O_{H2O}$ values as less relevant as compared to the influence of the isotopic label. We further ruled out the possibility that the isotopic composition of our laboratory water changed by frequent monitoring of the respective $\delta^{18}O_{H2O}$ values over the entire experiment as indicated by an average value of -3.7 with a very low standard deviation of ± 0.2 ‰ (n = 81). Thus, the isotopically heavier ^{18}O atoms were released to the porewater in form of $H_2{}^{18}O$ from the applied $^{18}O_{Pi}$ label through intracellular enzymatic cycling. Thereafter, P_i was subsequently (re)released from the microorganisms and transferred into the NaOH-P_i pool. The (re)release of P_i from microorganisms is corroborated by P_{mic} concentrations, which were significantly lower (50 to 80 mg kg^{-1}) than in the other two treatments (**Figure C-S7 h**). We attribute the decline in P_{mic} concentrations to the two drying phases in the SPL treatment, which exposed the microorganisms to stress through desiccation (Luo et al., 2022).

Moreover, APA values indicated that the extracellular cycling of P could have persisted (under all hydrological regimes, **Figure C-S7 i**), regenerating P_i from P_o. This process may have also influenced isotopic values through a kinetic disequilibrium fractionation, leading to a preferential incorporation of lighter ^{16}O isotopes into P_i preceding the transfer into the NaOH-P_i pool (Davies et al., 2014; Gross and Angert, 2015; Liang and Blake, 2006; von Sperber et al., 2014). Taken together with the stress-induced die-off of microorganisms, this suggests that short cycles of drying and rewetting harmed microorganisms, while the enzyme activity remained even after the microorganisms have declined (Schimel et al., 2018). Thus, biological P cycling results in an exchange of O-isotopes between P_i and

ambient-water , which has been previously described for biologically active oxic topsoil and aquatic sediments (Amelung et al., 2015; Bauke et al., 2022; Davies et al., 2014; Gross and Angert, 2015; Helfenstein et al., 2018; Joshi et al., 2016; Siegenthaler et al., 2020; Tamburini et al., 2012), but not for semi-aquatic sediments exposed to frequent drying and rewetting.

Compared to the two drying and rewetting treatments, the L treatment was characterized by a significantly lower relative proportion of $NaHCO_3$-P_i (**Figure C-S7 a**), indicating a pronounced remobilization of labile P_i under the permanently waterlogged conditions. This agrees with Zhang et al. 2021, who reported that waterlogged conditions may cause sufficient anoxic conditions for P mobilization, while plant and microbial activities are reduced, but not entirely suppressed. Notably, a slight but significant increase in the CDB-P_o pool concentration was visible in all treatments, suggesting a transformation of P_i into P_o and the build-up of organic molecules related to reducible metal oxides. This process became even more pronounced in the following weeks as discussed below.

Thus, our second hypothesis (H2) was partially confirmed, as labile P_i was transferred into the moderately labile NaOH-P_i pool. Furthermore, microbial overprinting was visible in the $\delta^{18}O_{Pi}$ values prior to the transfer of P_i into the NaOH-P_i pool. The higher P_{mic} concentrations in the LPL and L treatments suggest more favorable living conditions for microorganism, whereas other microbially induced effects were similar among all three treatments.

4.2.3. Intermediate phase

Changes in P pools further advanced between 4 to 16 weeks (SPL) and 4 to 8 weeks (LPL and L), as indicated by a continued increase in CDB-P_o, which rose along with NaOH-P_o and H_2SO_4-TP. These increases were at the expense of dissolved P_i in porewater and the moderately labile NaOH-P_i pool, in which concentrations decreased. We interpret these changes as a microbially mediated conversion of P_i into P_o, which is distributed in form of surface-adsorbed and recalcitrant organic molecules across the three P pools (Ivanoff et al., 1998). The biological transformation of added P_i to P_o has recently been revealed for a P-limited forest soil (Siegenthaler et al., 2024) by stable-O-isotope and ^{31}P-NMR analyses. Considering the pronounced proportion of CDB-P_o and concentrations of CDB-extractable Fe (see SPL after 4 weeks and LPL and L after 8 weeks, **Figure C-S6**), Fe(III)-oxides must have been involved as well in our experiment. We therefore assume that Fe(III)-oxides served as a primary host for the biofilms produced by the microorganisms (Bi et al., 2014; Jarvie et al., 2002; Wu et al., 2018). Generally, Fe(III)-reducing bacteria may colonize surfaces of Fe(III)-minerals where P_i is surface-adsorbed (Roden, 2003) and form biofilms in association with other microorganisms (Lu et al., 2016). Biofilms comprise living microorganisms and residues of dead cells as well as extracellular polymeric substances, where a variety of P_o molecules such as phospholipids, nucleic acids, phosphoproteins and phosphate esters occur (Liu et al., 2021; Shi and Xu, 2019). In our experiment, the Fe(III)-minerals underwent reductive dissolution in the CDB step and we assume that the attached biofilm including incorporated P_o was liberated into the extraction solution. A build-up of CDB-P_o in soils and drainage ditch sediments in particular, has been largely overlooked so far, resulting in a considerable underestimation of this dynamic P pool.

In the L treatment, microorganisms were at first able to adjust to the permanently logged conditions and continued to mineralize organic matter by changing their metabolic pathways to Mn(IV)- and Fe(III)-reduction as reflected by increasing concentrations of dissolved Mn, Fe and TA in the porewater.

However, after 4 weeks, dissolved Fe and Mn concentrations decreased again, which was accompanied by a significant decline in P_{mic}, indicating in concert a pronounced inhibition of the microbial activity. Here, the prolonged water stress supposedly caused a decline in microbial activity and possibly even partial cell death (Luo et al., 2022; Romaní et al., 2013), primarily caused by a limited O_2 diffusion and potentially by the release of toxic heavy metals (Yan et al., 2015). A similar behavior was reported by Zhang et al. (2021) for the incubation of agricultural soil. A dieback and subsequent lysis of microbial cells releasing formerly intracellular enzymes was further reflected by trends in APA, which significantly increased over the course of the experiment, aligning with observations made by Chen et al. (2023). This was also reflected in decreasing TA concentrations, which reflected the onset of a reduced microbial metabolic activity. However, this dieback was not (yet) reflected in the P pools or other measured variables, but became later evident in the late phase.

For the two drying and rewetting treatments, living conditions for microorganisms were also unfavorable as indicated by the declining P_{mic} concentrations. Furthermore, the labile P_i pools showed differences with regard to the two temperatures, especially for LPL (here, $NaHCO_3$- and NaOH-P_i concentrations at 20°C being significantly higher as in the 5°C treatment). Increasing NaOH- and CDB-P_i concentrations pools at 20°C have been previously reported by Huang et al. (2011), where an increasing temperature favored the transformation of weakly bound P_i into Al- and Fe-bound P_i, whereas cooler temperatures hampered such a change.

In the NaOH-P_i pool, $\delta^{18}O_{Pi}$ values for both, L and LPL, significantly increased, indicating a labelling of this pool despite the concentration losses. According to mass balance calculations (based on net concentration increase as compared to the initial phase and the label observed in the $NaHCO_3$-P_i pool), the NaOH-P_i pool showed $\delta^{18}O_{Pi}$ values for both treatments that were nearly identical to the observed isotopic values after 8 weeks (difference 3 to 5 ‰). We therefore conclude that no de-labeling has occurred through intracellular enzymatic cycling, possibly due to the presumed reduction in microbial metabolic activities (i.e. intracellular enzymatic turnover).

This observation agreed well with $\delta^{18}O_{Pi}$ values of the previously labeled $NaHCO_3$-P_i pool in case of the L treatment. In the LPL treatment, however, the $\delta^{18}O_{Pi}$ values in the $NaHCO_3$-P_i pool (20°C) were halved after 8 weeks, indicating a shift in direction of the theoretical equilibrium values and therefore intracellular P cycling (Joshi et al., 2016). This could be related to a faster exchange of P_i in the $NaHCO_3$-P_i pool and intensive microbial turnover as compared to the more stable NaOH-P_i pool, which must have occurred before the microbial metabolic activities were largely reduced.

After 4 to 16 (SPL) and 8 to 16 weeks (LPL, L), P_{mic} concentrations decreased to zero, indicating cell death caused by osmotic stress resulting from the repeated drying and rewetting cycles and permanently waterlogged conditions, respectively (Milligan and Häggblom, 1999). In contrast to the decline in P_{mic}, the enzyme activity (APA) remained either stable or even increased towards the end, particularly in the waterlogged treatment **(Figure C-3**). This observation suggested that enzymes were stabilized in the sediments by organic matter through the formation of enzyme-humus complexes (Zhang et al., 2020), allowing them to remain active even after cell death and subsequent release by lysis (Zhang et al., 2023). Thus, extracellular P cycling was possible during the incubation experiment.

Regarding the relative proportions of the P pools, the CDB-P_o pool was significantly lower in the SPL and L treatments as in the LPL treatment, which we attribute to a slower microbially mediated conversion of P_i into P_o, resulting from highly unfavorable living conditions for microorganisms (Luo et al., 2022). In

agreement with our third hypothesis, we observed a gradual build-up and subsequent decline of P_o across all treatments. However, this was unexpectedly related to the CDB-P_o pool. The transfer of P_i into the CDB-P_o pool represents an underestimated interim immobilization mechanism, which is, however, particularly susceptible to drying and rewetting, as well as to lower temperatures, which both hamper biologically mediated P transformation processes. This was accompanied by a significant decrease in the $\delta^{18}O_{Pi}$ values of $NaHCO_3$-P_i in the LPL treatment at 20°C as compared to the respective 5°C temperature treatment. Furthermore, in the L treatment the $\delta^{18}O_{Pi}$ values of $NaHCO_3$-P_i were close to the initial values 1 day after labeling at 20°C as well as at 5°C, which suggests less microbial turnover under waterlogged conditions after several weeks.

4.2.4. Late phase

In the late phase (between 16 to 24 weeks for SPL and 8 to 24 weeks for LPL and L), CDB-P_o concentrations showed notable decreases alongside H_2SO_4-TP, while $NaHCO_3$- and NaOH-P_i increased in all treatments. We attribute these changes to a combination of i) microbial cell death interrupting the generation of P_o and ii) the subsequent decay and mineralization of organic molecules containing P_o, leading to a re-release as P_i and its subsequent surface adsorption.

This assumption was supported by trends in P_{mic} and APA, which stabilized at lower levels as compared to the intermediate phase. Nevertheless, $\delta^{18}O_{Pi}$ values in the $NaHCO_3$-P_i and NaOH-P_i pools continued to decline, suggesting that microbial turnover has largely removed the initial ^{18}O label from the surface-adsorbed P_i pools despite unfavorable living conditions (see intermediate phase). The APA clearly showed that extracellular enzymes remained active, which have the potential to influence the $\delta^{18}O_{Pi}$ values in P_i (Stout et al., 2014; Tamburini et al., 2012). Also, the removal of the ^{18}O label was less pronounced in the 5°C treatment. This is a strong indication that the microbial turnover was reduced at lower temperatures, which agrees with previous observations in controlled laboratory experiments (von Sperber et al., 2015; Wallenstein et al., 2009). Although other variables, such as P_{mic} and APA, implied that the microorganisms were largely suffering from the applied treatments, it is not possible to definitively determine whether intracellular or extracellular enzymes were primarily responsible for the observed label removal as both can be directed in the same direction.

The assumed enhanced adsorption of P_i was further supported by increasing concentrations in both, $NaHCO_3$- and NaOH-P_i. This increase in surface-adsorbed P_i also corresponded to the observed increase in pH and concomitant decline in dissolved P_i concentrations in porewater. An increasing adsorption of P_i with rising pH to alkaline levels has been reported by Barrow et al. (2020) and De Geronimo et al. (2022). To the best of our knowledge, such a dynamic in the P_o pool linked to Fe(III)-oxides has not been described in literature so far, probably it occurs in a relatively late and also short time window, which can be easily missed in laboratory incubation experiments.

After 24 weeks, induced changes were most pronounced in the L treatment, suggesting living conditions here were least unfavorable for microorganisms. Here, the proportion of the $NaHCO_3$-P_i pool (**Figure C-S9 a**) was highest, whereas the proportion of the CDB-P_o pool (**Figure C-S9 e**) was lowest as compared to the SPL and LPL treatments. This indicates that the microbially mediated transformation of P_i into P_o was heavily disturbed under waterlogged conditions through the prolonged anoxic conditions (Ylivainio at al., 2018). The influence of strongly reducing redox conditions may have further fostered a transfer of

Fe(III)-oxide associated P_i into the labile ($NaHCO_3$-) P_i pool. This agrees with other laboratory experiments (Ajmone-Marsan et al. 2006, Shober et al. 2009) and has also been observed *in-situ* in drainage ditch sediments over time (Emelko et al., 2016). Such a transfer of P_i into the weakly, surface-adsorbed pool may have implications regarding the mobility of P_i and subsequent eutrophication of aquatic ecosystems.

In contrast, microorganism in the SPL treatment seem to be more resilient against the exposure to short drying and rewetting cycles, which became not only visible in the P pool composition, but also in the $\delta^{18}O_{Pi}$ values of the $NaHCO_3$ pool. the removal of the label was lowest after 4 weeks, whereas it was most pronounced after 24 weeks as compared to the other two treatments (LPL and L). Hence, if microbial communities are exposed to frequent drying and rewetting, each subsequent cycle event results in a less harsh perturbation, due to an increased resilience towards drying and rewetting. adapted to different moisture conditions, as demonstrated by De Nijs et al. (2019) in a drying–rewetting experiment. Such a diversity enables the microbial community to remain active even in frequently changing environments (Meisner et al., 2016).

In agreement with our fourth hypothesis (H4), we observed microbial dieback, but, however, no concomitant release of P_i into the dissolved P pool. Instead, P_i was adsorbed and transferred into the surface-adsorbed pools ($NaHCO_3$- and NaOH-P_i). We also observed no concentration increase in the stable P pools. The HCl-P_i pool only increased after 16 weeks in the L treatment, later it was comparable to the initial situation. This lack of long-term P_i incorporation into the Ca-P_i pool could be linked to the general absence of $CaCO_3$ in the drainage ditch sediments, consequently rendering non-calcareous sediments especially unsuitable for the long-term fixation of P_i. However, the $\delta^{18}O_{Pi}$ values differed significantly. An increase in the LPL treatment indicated that incorporation in the Ca-P_i pool in sediments with little to no $CaCO_3$ is only possible under certain hydrological conditions. However, it may also be due to the included CDB extraction step, that we found no evidence for the precipitation of Ca-P minerals, which contradicts previous observations (e.g., Joshi et al., (2016)). Without the CDB step, Fe(III)-associated P_i will be extracted in the HCl step, therefore causing an overestimation of the Ca-Pi pool. Thus, the CDB-extraction step is highly important in redox active systems and should not be omitted.

4. Conclusions and environmental implications

At a first, only few P pools of the drainage ditch sediments showed significant concentration differences between the initial labeling and after the 24 weeks incubation. However, our experimental approach revealed pronounced dynamics in P pools over time. Shortly after the label application, we observed a significant transfer of $^{18}O_{Pi}$ into the $NaHCO_3$-P_i pool and, to a lesser extent, into the porewater. In the following 4 weeks (early phase), significant shifts in the distribution of the $^{18}O_{Pi}$ label across various P pools occurred, with pronounced decreases in porewater-P_i and $NaHCO_3$-P_i concentrations and a substantial increase in NaOH-P_i and a slight but significant increase in CDB-P_o. These shifts underlined different processes; first, the transformation from weakly to strongly bound P_i, which was primarily influenced by pH changes and resulting de- and re-adsorption of P_i. In addition, the ^{18}O labeling approach highlighted the critical role of microbial cycling in altering the isotopic composition of P_i before its incorporation into the NaOH-P_i pool. Furthermore, P_i was transformed into P_o as reflected by the

increasing CDB-P_o pool. Over the course of the following weeks (intermediate phase), we observed a microbially mediated transformation of strongly bound P_i into P_o, which was likely associated with the formation of biofilms by anoxic microorganisms on mineral surfaces, particularly Fe(III)-oxides. This change in P pools was accompanied by a significant decline in P_{mic} due to stress from the applied treatments, which potentially reduced the microbial metabolic activity. However, extracellular APA persisted as indicated by ongoing alterations in the isotopic values of weakly bound P_i, highlighting the complex interactions of biological processes and environmental conditions. The late phase was characterized by notable decreases in CDB-P_o and H_2SO_4-TP concentrations alongside increases in $NaHCO_3$- and NaOH-P_i concentrations across all treatments. We attribute this shift towards surface-adsorbed P_i to microbial death and the decay and mineralization of P_o molecules. Despite substantial microbial stress, evidenced by low P_{mic} and TA levels, ongoing enzymatic activities contributed to P cycling as indicated by $\delta^{18}O_{Pi}$ values, offering insights into microbial dynamics and stress responses in changing environmental conditions.

Future studies should recognize the crucial dynamics within P pools that can only be observed through temporally resolved monitoring. In our study, the CDB-P_o pool played an unexpected role in the mid-term storage of P. Thus, P_o dynamics should be generally not underestimated, especially in biological active environments characterized by a high variability in the hydrological regime such as small and nutrient-rich streams in agricultural catchments. Our results further indicate that in the long-term, P_i retention dynamics in drainage ditch sediments are mainly governed by surface adsorption and not the formation of stable P_i pools, at least for non-calcareous sediments. To conclude, our findings highlight the role of small streams and drainage ditches as a crucial interim storage for P, which is situated between arable land and larger watercourses. This connection should be considered in management strategies aiming to reduce P discharge from agricultural catchments, especially in the context of a changing climate.

Acknowledgements

The authors would like to thank the German Research Foundation (DFG) for funding (NE-1852/4-1, Project number: 412678780). We are further grateful for further financial support through the Equal Opportunities Commission of the University of Tübingen. We also thank our laboratory staff (Sabine Flaiz, Rita Mögenburg) and students and student helpers (Diana Fiedler, Carolin Rieber, Louis Hausner, Pauline Stiller, Silvana Oldenburg, Niklas Wendenburg, Hannah Lemke, Lukas Schwella, Aline Ott-Fuchs, Pauline Röhner), as well as our colleagues from the AG Geoecology (Simon Hauenstein, Arnim Kessler, Wen Shao, Camilo Maliqueo-Murga) for support of our project.

Author contributions

Christiane Nagel: Conceptualization, Visualization, Methodology, Formal analysis, Writing – original draft, Writing – review & editing. **Yvonne Oelmann:** Resources, Methodology, Writing – review &

editing, Supervision. **Harald Neidhardt:** Conceptualization, Methodology, Writing – review & editing, Project administration, Supervision, Funding acquisition.

5. Refrences

Ajmone-Marsan, F., Côté, D., & Simard, R. R. (2006). Phosphorus transformations under reduction in long-term manured soils. Plant and soil, 282, 239-250. https://doi.org/10.1007/s11104-005-5929-6.

Aldous, A., McCormick, P., Ferguson, C., Graham, S., & Craft, C. (2005). Hydrologic regime controls soil phosphorus fluxes in restoration and undisturbed wetlands. Restoration ecology, 13(2), 341-347. https://doi.org/10.1111/j.1526-100X.2005.00043.x.

Amelung, W., Antar, P., Kleeberg, I., Oelmann, Y., Lücke, A., Alt, F., ... & Barej, J. A. M. (2015). The δ18O signatures of HCl-extractable soil phosphates: methodological challenges and evidence of the cycling of biological P in arable soil. European Journal of Soil Science, 66(6), 965-972. https://doi.org/10.1111/ejss.12288.

Bai, J., Ye, X., Jia, J., Zhang, G., Zhao, Q., Cui, B., & Liu, X. (2017). Phosphorus sorption-desorption and effects of temperature, pH and salinity on phosphorus sorption in marsh soils from coastal wetlands with different flooding conditions. Chemosphere, 188, 677-688. https://doi.org/10.1016/j.chemosphere.2017.08.117.

Barczok, M., Smith, C., Di Domenico, N., Kinsman-Costello, L., Singer, D., & Herndon, E. (2023). Influence of contrasting redox conditions on iron (oxyhydr) oxide transformation and associated phosphate sorption. Biogeochemistry, 166(2), 87-107. https://doi.org/10.1007/s10533-023-01094-z.

Barrow, N. J. (1984). Modelling the effects of pH on phosphate sorption by soils. Journal of Soil Science, 35(2), 283-297. https://doi.org/10.1111/j.1365-2389.1984.tb00283.x.

Barrow, N. J., Debnath, A., & Sen, A. (2020). Measurement of the effects of pH on phosphate availability. Plant and Soil, 454, 217-224. https://doi.org/10.1007/s11104-020-04647-5.

Bauke, S. L., Wang, Y., Saia, S. M., Popp, C., Tamburini, F., Paetzold, S., ... & von Sperber, C. (2022). Phosphate oxygen isotope ratios in vegetated riparian buffer strip soils. Vadose Zone Journal, 21(3), e20193. https://doi.org/10.1002/vzj2.20193.

Bennett, E. M., Carpenter, S. R., & Caraco, N. F. (2001). Human impact on erodable phosphorus and eutrophication: a global perspective: increasing accumulation of phosphorus in soil threatens rivers, lakes, and coastal oceans with eutrophication. BioScience, 51(3), 227-234. https://doi.org/10.1641/0006-3568(2001)051.

Bi, Z., Liu, Y., Rutoh, W. C., & Huang, Y. (2024). Influence of operation sequences on phosphorus recovery by polyphosphate-accumulating organisms biofilm: Performance, kinetics and metabolic response. Journal of Water Process Engineering, 61, 105356. https://doi.org/10.1016/j.jwpe.2024.105356.

Blake, R. E., Alt, J. C., & Martini, A. M. (2001). Oxygen isotope ratios of PO4: an inorganic indicator of enzymatic activity and P metabolism and a new biomarker in the search for life. Proceedings of the National Academy of Sciences, 98(5), 2148-2153. https://doi.org/10.1073/pnas.051515898.

Blake, R. E., O'Neil, J. R., & Surkov, A. V. (2005). Biogeochemical cycling of phosphorus: insights from oxygen isotope effects of phosphoenzymes. American Journal of Science, 305(6-8), 596-620. https://doi.org/10.2475/ajs.305.6-8.596.

Bünemann, E. K. (2015). Assessment of gross and net mineralization rates of soil organic phosphorus–A review. Soil Biology and Biochemistry, 89, 82-98. https://doi.org/10.1016/j.soilbio.2015.06.026.

Carpenter, S. R. (2005). Eutrophication of aquatic ecosystems: bistability and soil phosphorus. Proceedings of the National Academy of Sciences, 102(29), 10002-10005. https://doi.org/10.1073/pnas.0503959102.

Chang, S. J., & Blake, R. E. (2015). Precise calibration of equilibrium oxygen isotope fractionations between dissolved phosphate and water from 3 to 37 C. Geochimica et Cosmochimica Acta, 150, 314-329. https://doi.org/10.1016/j.gca.2014.10.030.

Chen, J., Xu, H., Seven, J., Zilla, T., Dippold, M. A., & Kuzyakov, Y. (2023). Microbial phosphorus recycling in soil by intra-and extracellular mechanisms. ISME Communications, 3(1), 135. https://doi.org/10.1038/s43705-023-00340-7.

Chen, X., Yan, X., Wang, M., Cai, Y., Weng, X., Su, D., ... & Zhang, F. (2022). Long-term excessive phosphorus fertilization alters soil phosphorus fractions in the acidic soil of pomelo orchards. Soil and Tillage Research, 215, 105214. https://doi.org/10.1016/j.still.2021.105214.

Cross, A. F., & Schlesinger, W. H. (1995). A literature review and evaluation of the. Hedley fractionation: Applications to the biogeochemical cycle of soil phosphorus in natural ecosystems. Geoderma, 64(3-4), 197-214. https://doi.org/10.1016/0016-7061(94)00023-4.

Davies, C. L., Surridge, B. W., & Gooddy, D. C. (2014). Phosphate oxygen isotopes within aquatic ecosystems: global data synthesis and future research priorities. Science of the Total Environment, 496, 563-575. https://doi.org/10.1016/j.scitotenv.2014.07.057.

De Gerónimo, E., & Aparicio, V. C. (2022). Changes in soil pH and addition of inorganic phosphate affect glyphosate adsorption in agricultural soil. European Journal of Soil Science, 73(1), e13188. https://doi.org/10.1111/ejss.13188.

de Nijs, E. A., Hicks, L. C., Leizeaga, A., Tietema, A., & Rousk, J. (2019). Soil microbial moisture dependences and responses to drying–rewetting: the legacy of 18 years drought. Global Change Biology, 25(3), 1005-1015. https://doi.org/10.1111/gcb.14508.

Dieter, D., Herzog, C., & Hupfer, M. (2015). Effects of drying on phosphorus uptake in re-flooded lake sediments. Environmental Science and Pollution Research, 22, 17065-17081. https://doi.org/10.1007/s11356-015-4904-x.

DIN ISO 10390 (2005): Bodenbeschaffenheit—Bestimmung des pH Wertes. ISO 10390.

DIN ISO 11465 (1996-12). Bodenbeschaffenheit-Bestimmung der Trockensubstanz und des Wassergehalts auf Grundlage der Masse-Gravimetrisches Verfahren (ISO 11465: 1993).

DIN EN ISO 20130:2021-02: Bodenbeschaffenheit - Messung von Enzymaktivitätsmustern in Bodenproben mit kolorimetrischen Substraten in Mikrotiterplatten (ISO 20130:2018); Deutsche Fassung EN ISO 20130:2020.

Dupas, R., Delmas, M., Dorioz, J. M., Garnier, J., Moatar, F., & Gascuel-Odoux, C. (2015). Assessing the impact of agricultural pressures on N and P loads and eutrophication risk. Ecological Indicators, 48, 396-407. https://doi.org/10.1016/j.ecolind.2014.08.007.

Dupas, R., Gruau, G., Gu, S., Humbert, G., Jaffrézic, A., & Gascuel-Odoux, C. (2015). Groundwater control of biogeochemical processes causing phosphorus release from riparian wetlands. Water research, 84, 307-314. https://doi.org/10.1016/j.watres.2015.07.048.

Edwards, A. C., & Withers, P. J. A. (2007). Linking phosphorus sources to impacts in different types of water body. Soil Use and Management, 23, 133-143. https://doi.org/10.1111/j.1475-2743.2007.00110.x.

Efobo O. (2023). Transport of Suspended Sediments and Phosphorus in an Agricultural Watershed: A Case Study of the Money Creek Watershed, Central Illinois (Master's thesis, Illinois State University). https://doi.org/10.30707/ETD2023.20231004061828269197.999980.

Emelko, M. B., Stone, M., Silins, U., Allin, D., Collins, A. L., Williams, C. H., ... & Bladon, K. D. (2016). Sediment-phosphorus dynamics can shift aquatic ecology and cause downstream legacy effects after wildfire in large river systems. Global Change Biology, 22(3), 1168-1184. https://doi.org/10.1111/gcb.13073.

Eriksson, A. K., Hesterberg, D., Klysubun, W., & Gustafsson, J. P. (2016). Phosphorus dynamics in Swedish agricultural soils as influenced by fertilization and mineralogical properties: Insights gained from batch experiments and XANES spectroscopy. Science of the Total Environment, 566, 1410-1419. https://doi.org/10.1016/j.scitotenv.2016.05.225.

Frossard, E., Condron, L. M., Oberson, A., Sinaj, S., & Fardeau, J. C. (2000). Processes governing phosphorus availability in temperate soils. Journal of environmental quality, 29(1), 15-23. https://doi.org/10.2134/jeq2000.00472425002900010003x.

Gross, A., & Angert, A. (2015). What processes control the oxygen isotopes of soil bio-available phosphate. Geochimica et Cosmochimica Acta, 159, 100-111. https://doi.org/10.1016/j.gca.2015.03.023.

Guo, F., Yost, R. S., Hue, N. V., Evensen, C. I., & Silva, J. A. (2000). Changes in phosphorus fractions in soils under intensive plant growth. Soil Science Society of America Journal, 64(5), 1681-1689. https://doi.org/10.2136/sssaj2000.6451681x.

Gustafsson, J. P., Mwamila, L. B., & Kergoat, K. (2012). The pH dependence of phosphate sorption and desorption in Swedish agricultural soils. Geoderma, 189, 304-311. https://doi.org/10.1016/j.geoderma.2012.05.014.

Hamilton, S. K. (2012). Biogeochemical time lags may delay responses of streams to ecological restoration. Freshwater Biology, 57, 43-57. https://doi.org/10.1111/j.1365-2427.2011.02685.x.

Haygarth, P. M., Condron, L. M., Heathwaite, A. L., Turner, B. L., & Harris, G. P. (2005). The phosphorus transfer continuum: linking source to impact with an interdisciplinary and multi-scaled approach. Science of the total environment, 344(1-3), 5-14. https://doi.org/10.1016/j.scitotenv.2005.02.001.

Haygarth, P. M., Jarvie, H. P., Powers, S. M., Sharpley, A. N., Elser, J. J., Shen, J., ... & Liu, X. (2014). Sustainable phosphorus management and the need for a long-term perspective: The legacy hypothesis. https://doi: 10.1021/es502852s.

Hedley, M. J., Stewart, J. W. B., & Chauhan, B. (1982). Changes in inorganic and organic soil phosphorus fractions induced by cultivation practices and by laboratory incubations. Soil Science Society of America Journal, 46(5), 970-976. https://doi.org/10.2136/sssaj1982.03615995004600050017x.

Helfenstein, J., Tamburini, F., von Sperber, C., Massey, M. S., Pistocchi, C., Chadwick, O. A., ... & Frossard, E. (2018). Combining spectroscopic and isotopic techniques gives a dynamic view of phosphorus cycling in soil. Nature communications, 9(1), 3226. https://doi.org/10.1038/s41467-018-05731-2.

Huang, L., Fu, L., Jin, C., Gielen, G., Lin, X., Wang, H., & Zhang, Y. (2011). Effect of temperature on phosphorus sorption to sediments from shallow eutrophic lakes. Ecological Engineering, 37(10), 1515-1522. https://doi:10.1016/j.ecoleng.2011.05.006.

Huang, L. M., Jia, X. X., Zhang, G. L., & Shao, M. A. (2017). Soil organic phosphorus transformation during ecosystem development: A review. Plant and Soil, 417 17-42. https://doi.org/10.1007/s11104-017-3240-y.

Husson, O. (2013). Redox potential (Eh) and pH as drivers of soil/plant/microorganism systems: a transdisciplinary overview pointing to integrative opportunities for agronomy. Plant and soil, 362, 389-417. https://doi.org/10.1007/s11104-012-1429-7.

Ivanoff, D. B., Reddy, K. R., & Robinson, S. (1998). Chemical fractionation of organic phosphorus in selected histosols1. Soil Science, 163(1), 36-45. https://doi.org/10.1097/00010694-199801000-00006.

Jaisi, D. P., & Blake, R. E. (2010). Tracing sources and cycling of phosphorus in Peru Margin sediments using oxygen isotopes in authigenic and detrital phosphates. Geochimica et Cosmochimica Acta, 74(11), 3199-3212. https://doi.org/10.1016/j.gca.2010.02.030.

Jaisi, D. P., Kukkadapu, R. K., Stout, L. M., Varga, T., & Blake, R. E. (2011). Biotic and abiotic pathways of phosphorus cycling in minerals and sediments: Insights from oxygen isotope ratios in phosphate. Environmental science & technology, 45(15), 6254-6261. https://dx.doi.org/10.1021/es200456e.

Jarvie, H. P., Neal, C., Warwick, A., White, J., Neal, M., Wickham, H. D., ... & Andrews, M. C. (2002). Phosphorus uptake into algal biofilms in a lowland chalk river. Science of the Total Environment, 282, 353-373. https://doi.org/10.1016/S0048-9697(01)00924-X.

Jeppesen, E., Kronvang, B., Meerhoff, M., Søndergaard, M., Hansen, K. M., Andersen, H. E., ... & Olesen, J. E. (2009). Climate change effects on runoff, catchment phosphorus loading and lake ecological state, and potential adaptations. Journal of environmental quality, 38(5), 1930-1941. https://doi.org/10.2134/jeq2008.0113.

Joshi, S. R., Kukkadapu, R. K., Burdige, D. J., Bowden, M. E., Sparks, D. L., & Jaisi, D. P. (2015). Organic matter remineralization predominates phosphorus cycling in the mid-bay sediments in the Chesapeake Bay. Environmental science & technology, 49(10), 5887-5896. https://doi.org/10.1021/es5059617.

Joshi, S. R., Li, X., & Jaisi, D. P. (2016). Transformation of phosphorus pools in an agricultural soil: An application of oxygen-18 labeling in phosphate. Soil Science Society of America Journal, 80(1), 69-78. https://doi.org/10.2136/sssaj2015.06.0219.

Kleinman, P., Sharpley, A., Buda, A., McDowell, R., & Allen, A. (2011). Soil controls of phosphorus in runoff: Management barriers and opportunities. Canadian Journal of Soil Science, 91(3), 329-338. https://doi.org/10.4141/cjss09106.

Kouno, K., Tuchiya, Y., & Ando, T. (1995). Measurement of soil microbial biomass phosphorus by an anion exchange membrane method. Soil Biology and Biochemistry, 27(10), 1353-1357. https://doi.org/10.1016/0038-0717(95)00057-L.

Lannergård EE, Agstam-Norlin O, Huser BJ, Sandström S, Rakovic J, Futter MN. (2020). New insights into legacy phosphorus from fractionation of stream bed sediment. Journal of Geophysical Research: Biogeosciences 125(9). https://doi.org/10.1029/2020JG005763.

Leibundgut, C., & Eisele, M. (2005). Weiterentwicklung des Bewertungsverfahrens „Hydrologische Güte “als Expertensystem zum operationellen Einsatz im Flussgebietsmanagement. Abschlußbericht–Programm Lebensgrundlage Umwelt und ihre Sicherung, FKZ BWC.

Li, X., Huang, L., Fang, H., Chen, M., Cui, Z., Sun, Z., & Reible, D. (2021). Phosphorus adsorption by sediment considering mineral composition and environmental factors. Environmental Science and Pollution Research, 28, 17495-17505. https://doi.org/10.1007/s11356-020-12206-9.

Liang, Y., & Blake, R. E. (2006). Oxygen isotope signature of Pi regeneration from organic compounds by phosphomonoesterases and photooxidation. Geochimica et Cosmochimica Acta, 70(15), 3957-3969. https://doi.org/10.1016/j.gca.2006.04.036.

Liu, J., Lu, H., Wu, L., Kerr, P. G., & Wu, Y. (2021). Interactions between periphytic biofilms and dissolved organic matter at soil-water interface and the consequent effects on soil phosphorus

fraction changes. Science of the Total Environment, 801, 149708. https://doi.org/10.1016/j.scitotenv.2021.149708.

Longinelli, A., & Nuti, S. (1973). Revised phosphate-water isotopic temperature scale. Earth and Planetary Science Letters, 19(3), 373-376. https://doi.org/10.1016/0012-821X(73)90088-5.

Lu, H., Wan, J., Li, J., Shao, H., & Wu, Y. (2016). Periphytic biofilm: A buffer for phosphorus precipitation and release between sediments and water. Chemosphere, 144, 2058-2064. https://doi.org/10.1016/j.chemosphere.2015.10.129.

LUBW. (2015). Abschätzung der erforderlichen Reduzierung von Nährstoffeinträgen in die Fließgewässer Baden-Württembergs. Place published: LUBW Landesanstalt für Umwelt, Messungen und Naturschutz Baden-Württemberg, Karlsruhe.

Lucas, E., Kennedy, B., Roswall, T., Burgis, C., & Toor, G. S. (2023). Climate change effects on phosphorus loss from agricultural land to water: a review. Current Pollution Reports, 9(4), 623-645. https://doi.org/10.1007/s40726-023-00282-7.

Luo, X., Yang, Y., Xie, S., Wang, W., Li, N., Wen, C., ... & Chen, L. (2022). Drying and rewetting induce changes in biofilm characteristics and the subsequent release of metal ions. Journal of Hazardous Materials, 433, 128832. https://doi.org/10.1016/j.jhazmat.2022.128832.

Mattingly, G. E. G., Chater, M., & Johnston, A. E. (1975). Experiments made on Stackyard Field, Woburn, 1876-1974. III. Effects of NPK Fertilisers and Farmyard Manure on Soil Carbon, Nitrogen and Organic Phosphorus. Rothamsted Experimental Station Report, 1974(2), 61-77. https://doi.org/10.23637/ERADOC-1-33160.

McDowell, R., & Sharpley, A. (2002). Availability of residual phosphorus in high phosphorus soils. Communications in soil science and plant analysis, 33(7-8), 1235-1246. https://doi.org/10.1081/CSS-120003884.

McDowell, R. W., & Haygarth, P. M. (2024). Reducing phosphorus losses from agricultural land to surface water. Current Opinion in Biotechnology, 89, 103181. https://doi.org/10.1016/j.copbio.2024.103181.

Meisner, A., Jacquoid, S., Snoek, L. B., van der Putten, W. H., Schmidt, I. K., Larsen, K. S., ... & Rousk, J. (2016). Soil microbial responses to drought and rewetting. In 3rd Thünen Symposium on Soil Metagenomics; From gene predictions to systems ecology: plus Workshop on Bioinformatic Tools.

Melby, E. S., Soldat, D. J., & Barak, P. (2011). Synthesis and detection of oxygen-18 labeled phosphate. Plos one, 6(4), e18420. https://doi.org/10.1371/journal.pone.0018420

Milligan, P. W., & Häggblom, M. M. (1999). Biodegradation and biotransformation of dicamba under different reducing conditions. Environmental science & technology, 33(8), 1224-1229. https://doi.org/10.1021/es981117e.

Nagul, E. A., McKelvie, I. D., Worsfold, P., & Kolev, S. D. (2015). The molybdenum blue reaction for the determination of orthophosphate revisited: Opening the black box. Analytica chimica acta, 890, 60-82. https://doi.org/10.1016/j.aca.2015.07.030.

Negassa, W., & Leinweber, P. (2009). How does the Hedley sequential phosphorus fractionation reflect impacts of land use and management on soil phosphorus: A review. Journal of Plant Nutrition and Soil Science, 172(3), 305-325. https://doi.org/10.1002/jpln.200800223.

Neidhardt, H., Achten, F., Kern, S., Schwientek, M., & Oelmann, Y. (2019). Phosphorus pool composition in soils and sediments of transitional ecotones under the influence of agriculture. Journal of environmental quality, 48(5), 1325-1335. https://doi.org/10.2134/jeq2019.01.0012.

Neidhardt, H., Rudischer, S., Eiche, E., Schneider, M., Stopelli, E., Duyen, V. T., ... & Berg, M. (2021). Phosphate immobilisation dynamics and interaction with arsenic sorption at redox transition zones in floodplain aquifers: Insights from the Red River Delta, Vietnam. Journal of Hazardous Materials, 411, 125128. https://doi.org/10.1016/j.jhazmat.2021.125128.

Perez, C., Antelo, J., Fiol, S., & Arce, F. (2014). Modeling oxyanion adsorption on ferralic soil, part 1: parameter validation with phosphate ion. Environmental toxicology and chemistry, 33(10), 2208-2216. https://doi.org/10.1002/etc.2612.

Pionke, H. B., Gburek, W. J., & Sharpley, A. N. (2000). Critical source area controls on water quality in an agricultural watershed located in the Chesapeake Basin. Ecological engineering, 14(4), 325-335. https://doi.org/10.1016/S0925-8574(99)00059-2.

Reddy, K. R., Kadlec, R. H., Flaig, E., & Gale, P. M. (1999). Phosphorus retention in streams and wetlands: a review. Critical reviews in environmental science and technology, 29(1), 83-146. https://doi.org/10.1080/10643389991259182.

Roden, E. E. (2003). Fe (III) oxide reactivity toward biological versus chemical reduction. Environmental Science & Technology, 37(7), 1319-1324. https://doi.org/10.1021/es026038o.

Romaní, A. M., Amalfitano, S., Artigas, J., Fazi, S., Sabater, S., Timoner, X., ... & Zoppini, A. (2013). Microbial biofilm structure and organic matter use in mediterranean streams. Hydrobiologia, 719, 43-58. https://doi.org/10.1007/s10750-012-1302-y.

Rubæk, G. H., Kristensen, K., Olesen, S. E., Østergaard, H. S., & Heckrath, G. (2013). Phosphorus accumulation and spatial distribution in agricultural soils in Denmark. Geoderma, 209, 241-250. https://doi.org/10.1016/j.geoderma.2013.06.022.

Ruttenberg, K. C. (1992). Development of a sequential extraction method for different forms of phosphorus in marine sediments. Limnology and oceanography, 37(7), 1460-1482. https://doi.org/10.4319/lo.1992.37.7.1460.

Sandström, S., Futter, M. N., O'Connell, D. W., Lannergård, E. E., Rakovic, J., Kyllmar, K., ... & Djodjic, F. (2021). Variability in fluvial suspended and streambed sediment phosphorus fractions among small agricultural streams (Vol. 50, No. 3, pp. 612-626). https://doi.org/10.1002/jeq2.20210.

Schimel, J. P. (2018). Life in dry soils: effects of drought on soil microbial communities and processes. Annual review of ecology, evolution, and systematics, 49(1), 409-432.) https://doi.org/10.1146/annurev-ecolsys-110617-062614.

Schlesinger, W. H., Bruijnzeel, L. A., Bush, M. B., Klein, E. M., Mace, K. A., Raikes, J. A., & Whittaker, R. J. (1998). The biogeochemistry of phosphorus after the first century of soil development on Rakata Island, Krakatau, Indonesia. Biogeochemistry, 40, 37-55. https://doi.org/10.1023/A:1005838929706.

Schoumans, O. F. (2014). Description of the phosphorus sorption and desorption processes in coarse calcareous sandy soils. Soil science, 179(5), 221-229. https://doi.org/10.1097/SS.0000000000000065.

Schwientek, M., Osenbrück, K., & Fleischer, M. (2013). Investigating hydrological drivers of nitrate export dynamics in two agricultural catchments in Germany using high-frequency data series. Environmental earth sciences, 69, 381-393. https://doi.org/10.1007/s12665-013-2322-2.

Sharpley, A., Jarvie, H. P., Buda, A., May, L., Spears, B., & Kleinman, P. (2013). Phosphorus legacy: overcoming the effects of past management practices to mitigate future water quality impairment. Journal of environmental quality, 42(5), 1308-1326. https://doi.org/10.2134/jeq2013.03.0098.

Sharpley, A. N., Chapra, S. C., Wedepohl, R., Sims, J. T., Daniel, T. C., & Reddy, K. R. (1994). Managing agricultural phosphorus for protection of surface waters: Issues and options. Journal of environmental quality, 23(3), 437-451. https://doi.org/10.2134/jeq1994.00472425002300030006x.

Shi, S., & Xu, G. (2019). Identification of phosphorus fractions of biofilm sludge and phosphorus release, transformation and modeling in biofilm sludge treatment related to pH. Chemical Engineering Journal, 369, 694-704. https://doi.org/10.1016/j.cej.2019.03.120.

Shober, A. L., & Sims, J. T. (2009). Evaluating phosphorus release from biosolids and manure-amended soils under anoxic conditions. Journal of environmental quality, 38(1), 309-318. https://doi.org/10.2134/jeq2007.0660.

Shore, M., Murphy, S., Mellander, P. E., Shortle, G., Melland, A. R., Crockford, L., ... & Jordan, P. (2017). Influence of stormflow and baseflow phosphorus pressures on stream ecology in agricultural catchments. Science of the Total Environment, 590, 469-483. https://doi.org/10.1016/j.scitotenv.2017.02.100.

Shore, M., Jordan, P., Mellander, P. E., Kelly-Quinn, M., Daly, K., Sims, J. T., ... & Melland, A. R. (2016). Characterisation of agricultural drainage ditch sediments along the phosphorus transfer continuum in two contrasting headwater catchments. Journal of Soils and Sediments, 16, 1643-1654. https://doi.org/10.1007/s11368-015-1330-0.

Siegenthaler, M. B., McLaren, T. I., Frossard, E., & Tamburini, F. (2024). Dual isotopic (33P and 18O) tracing and solution 31P NMR spectroscopy to reveal organic phosphorus synthesis in organic soil horizons. Soil Biology and Biochemistry, 197, 109519. https://doi.org/10.1016/j.soilbio.2024.109519.

Siegenthaler, M. B., Tamburini, F., Frossard, E., Chadwick, O., Vitousek, P., Pistocchi, C., ... & Helfenstein, J. (2020). A dual isotopic (32P and 18O) incubation study to disentangle mechanisms controlling phosphorus cycling in soils from a climatic gradient (Kohala, Hawaii). Soil Biology and Biochemistry, 149, 107920. https://doi.org/10.1016/j.soilbio.2020.107920.

Slomp, C. P., Malschaert, J. F. P., & Van Raaphorst, W. (1998). The role of adsorption in sediment-water exchange of phosphate in North Sea continental margin sediments. Limnology and Oceanography, 43(5), 832-846.). https://doi.org/10.4319/lo.1998.43.5.0832.

Stout, L. M., Joshi, S. R., Kana, T. M., & Jaisi, D. P. (2014). Microbial activities and phosphorus cycling: An application of oxygen isotope ratios in phosphate. Geochimica et Cosmochimica Acta, 138, 101-116. https://doi.org/10.1016/j.gca.2014.04.020.

Sugiyama, S., & Hama, T. (2013). Effects of water temperature on phosphate adsorption onto sediments in an agricultural drainage canal in a paddy-field district. Ecological engineering, 61, 94-99. https://doi.org/10.1016/j.ecoleng.2013.09.053.

Tabatabai, M. A., & Bremner, J. M. (1969). Use of p-nitrophenyl phosphate for assay of soil phosphatase activity. *Soil biology and biochemistry*, *1*(4), 301-307.

Tamburini, F., Pfahler, V., Bünemann, E. K., Guelland, K., Bernasconi, S. M., & Frossard, E. (2012). Oxygen isotopes unravel the role of microorganisms in phosphate cycling in soils. Environmental Science & Technology, 46(11), 5956-5962. https://doi.org/10.1021/es300311h.

Tamburini, F., Pistocchi, C., Helfenstein, J., & Frossard, E. (2018). A method to analyse the isotopic composition of oxygen associated with organic phosphorus in soil and plant material. European Journal of Soil Science, 69(5), 816-826. https://doi.org/10.1111/ejss.12693.

Tiessen, H. (1993). Characterization of Available P by Sequential Fractionation. CRC Press, Soil Sampling and Method of Analysis, pp. 75–87.

Turner, B. L., & Haygarth, P. M. (2001). Phosphorus solubilization in rewetted soils. Nature, 411(6835), 258-258. https://doi.org/10.1038/35077146.

Van Ee, N. (2021). Transport and Fate of Phosphorus in the Nearshore Zone of Lake Michigan (Master's thesis, The University of Wisconsin-Milwaukee). https://doi.org/10.13140/RG.2.2.27989.64489.

von Sperber, C., Kries, H., Tamburini, F., Bernasconi, S. M., & Frossard, E. (2014). The effect of phosphomonoesterases on the oxygen isotope composition of phosphate. Geochimica et Cosmochimica Acta, 125, 519-527. https://doi.org/10.1016/j.gca.2013.10.010.

von Sperber, C., Tamburini, F., Brunner, B., Bernasconi, S. M., & Frossard, E. (2015). The oxygen isotope composition of phosphate released from phytic acid by the activity of wheat and

Aspergillus niger phytase. Biogeosciences, 12(13), 4175-4184. https://doi.org/10.5194/bg-12-4175-2015.

Wallenstein, M. D., McMahon, S. K., & Schimel, J. P. (2009). Seasonal variation in enzyme activities and temperature sensitivities in Arctic tundra soils. Global Change Biology, 15(7), 1631-1639. https://doi.org/10.1111/j.1365-2486.2008.01819.x.

Włodarczyk, T., Szarlip, P., Brzezińska, M., & Kotowska, U. (2007). Redox potential, nitrate content and pH in flooded Eutric Cambisol during nitrate reduction. Res Agr Eng, 53(1), 20-28. https://doi.org/10.17221/2132-RAE.

Wu, Y., Liu, J., & Rene, E. R. (2018). Periphytic biofilms: a promising nutrient utilization regulator in wetlands. Bioresource technology, 248, 44-48. https://doi.org/10.1016/j.biortech.2017.07.081.

Yan, F., Schubert, S., & Mengel, K. (1996). Soil pH increase due to biological decarboxylation of organic anions. Soil Biology and Biochemistry, 28(4-5), 617-624. https://doi.org/10.1016/0038-0717(95)00180-8.

Yan, N., Marschner, P., Cao, W., Zuo, C., & Qin, W. (2015). Influence of salinity and water content on soil microorganisms. International soil and water conservation Research, 3(4), 316-323. https://doi.org/10.1016/j.iswcr.2015.11.003.

Ylivainio, K., Jauhiainen, L., Uusitalo, R., & Turtola, E. (2018). Waterlogging severely retards P use efficiency of spring barley (Hordeum vulgare). Journal of Agronomy and Crop Science, 204(1), 74-85. https://doi.org/10.1111/jac.12241.

Yuan, H., Wang, H., Dong, A., Zhou, Y., Huang, R., Yin, H., ... & Cai, Y. (2022). Tracing the sources of phosphorus in lake at watershed scale using phosphate oxygen isotope (δ18OP). Chemosphere, 305, 135382. https://doi.org/10.1016/j.chemosphere.2022.135382.

Zhang, D., Wu, J., Yang, F., Chen, Q., Feng, J., Li, Q., ... & Cheng, X. (2020). Linkages between soil organic carbon fractions and carbon-hydrolyzing enzyme activities across riparian zones in the Three Gorges of China. Scientific Reports, 10(1), 8433. https://doi.org/10.1038/s41598-020-65200-z.

Zhang, H., Zhang, S. S., Zhang, W., Ma, W. C., Pan, Y., Chen, L., ... & Li, J. R. (2023). Clarification of the phosphorus release mechanism for recovering phosphorus from biofilm sludge in alternating aerobic/anaerobic biofilm system. Science of The Total Environment, 904, 166811. https://doi.org/10.1016/j.scitotenv.2023.166811.

Zhang, S., Yang, X., Hsu, L. C., Liu, Y. T., Wang, S. L., White, J. R., ... & Rinklebe, J. (2021). Soil acidification enhances the mobilization of phosphorus under anoxic conditions in an agricultural soil: Investigating the potential for loss of phosphorus to water and the associated environmental risk. Science of the Total Environment, 793, 148531). https://doi.org/10.1016/j.scitotenv.2021.148531.

Zhou, A., Tang, H., & Wang, D. (2005). Phosphorus adsorption on natural sediments: Modeling and effects of pH and sediment composition. Water research, 39(7), 1245-1254. https://doi.org/10.1016/j.watres.2005.01.026.

Zhu, J., Li, M., & Whelan, M. (2018). Phosphorus activators contribute to legacy phosphorus availability in agricultural soils: A review. Science of the Total Environment, 612, 522-537. https://doi.org/10.1016/j.scitotenv.2017.08.095.

Zhijing, C. A. O., Zhang, X., & Nanshan, A. I. (2011). Effect of sediment on concentration of dissolved phosphorus in the Three Gorges Reservoir. International Journal of Sediment Research, 26(1), 87-95). https://doi.org/10.1016/S1001-6279(11)60078-4.

Supporting information Section C

Section C-S1: Details of chemical analysis

$^{18}O_{Pi}$ Label synthesis

First, 2.0 ml of ^{18}O-enriched water (>98%, Rotem Industries Ltd.) were weighted into a 1 l two-neck round flask which is placed on a 2.5 l beaker (21 x 16 cm) filled with ice water. Next, 5 g of powdered PCl_5 (>95%; Merck) were poured slowly into the flask containing ^{18}O-enriched water. The powder was dissolved in the ^{18}O-enriched water and then fumigated in a water bath at 80°C for 90 min to remove HCl that has formed in the solution. Because the reaction is very exothermic, it was performed inside a fume hood. The reaction path is:

$$PCl_5 + 4H_2O \rightarrow H_3PO_4 + 5HCl$$

After cooling down to room temperature, 20 ml of 0.5M NaOH were added to neutralize the solution to pH 7. The product was diluted with 10 ml of ultrapure water to generate an initial $^{18}O_{Pi}$ stock solution with a $\delta^{18}O_{Pi}$ value of about +3.5 Mio. ‰ VSMOW (calculated after Melby et al. 2011). The obtained PO_4-P concentration was determined by a photometer (UV-VIS, Analytik Jena Specord 200 plus), before the solution was highly diluted with a KH_2PO_4 solution (0.5 g l^{-1} PO_4-P and a $\delta^{18}O$ value of 13.51 ‰, Fisher Chemical, p.a. ≥99%). The obtained label solution had a concentration of 485 mg PO_4-P l^{-1} and a $\delta^{18}O$ value of +354 ‰ VSMOW. Respective $^{18}O_{PO4}$ values were measured by an isotopic ratio mass spectrometer (IRMS, Elementar Analysensysteme GmbH, Langenselbold, Germany).

Stable oxygen isotope analysis

For the isotopic analyses, dissolved P_i in the respective extraction solutions ($NaHCO_3$, NaOH, CDB and HCl) was purified following the protocol of Tamburini et al. (2018) and Joshi et al. (2015), which consisted basically of the following four steps.

Step 1 - Ammonium phospho-molybdate (APM) precipitation and dissolution: The sequential extraction solutions were transferred to 200-ml Erlenmeyer flasks. First, 25 ml of 4.2M NH_4NO_3 was added and the flasks placed in a warm bath set at 50°C. Next, 40 ml of ammonium molybdate solution (prepared by dissolving 53.3 g of $(NH_4)6Mo_7O_{24} * 4H_2O$ (Grüssing, p.a. ≥ 99) in 480 ml of Milli-Q water) was added to each flask. Finally, 1 ml of concentrated H_2SO_4 (67%) was added to acidify the samples. A yellow APM precipitate occurs after shaking for 16h at 50°C. The APM precipitates were filtered through a 0.2-µm filter (Merck) and rinsed with 0.6M NH_4NO_3. Afterwards, the filters were placed in 100-ml Erlenmeyer flasks and the APM crystals were dissolved in a minimal amount (30–50 ml) of citric acid-NH_4OH solution (10 g citric acid (Sigma-Aldrich, p-a 99.5-100.5) mixed with 140 ml concentrated NH_4OH (Merck, p.a. ≥ 25%) and 300 ml Milli-Q water). The filters were removed and the solution stirred on a magnetic stirrer for 16h at 24°C.

Step 2 - Magnesium ammonium phosphate (MAP, struvite) precipitation and dissolution: After stirring 25 ml of magnesia solution (50 g $MgCl_2 * 6H_2O$ (Merck, p.pa.) and 100 g NH_4Cl dissolved in 500 ml Milli-Q water) were added to induce MAP precipitation. White MAP crystals formed after 12 to 16 hours were filtered through 0.2 µm cellulose nitrate filters (Isopore, Merck) and rinsed with a 1:20 NH_4OH solution. The MAP crystals obtained were then dissolved with 20ml 0.5M HNO_3.

Step 3 - Cation removal: The solution obtained was now mixed with 6 ml of BioRad resin slurry AG50 X8 cation resin (H+ form, 100–200 mesh). The cation exchange resin was previously conditioned with 1M HNO_3 overnight and then thoroughly washed with Milli-Q water until the pH of the solution reached neutrality. Solution and resin

slurry were filtered through 0.2-µm polycarbonate filter (Isopore, Merck) and washed twice with Milli-Q water. The solution was kept in a centrifuge tube until the precipitation of silver phosphate.

Step 4 - Silver phosphate precipitation: About 5 ml of Silver-ammine solution (10.2 g of $AgNO_3$ (Grüssing, p.a. ≥ 99.5%), 9.6 g of NH_4NO_3 (Sigma-Aldrich, p.a.), 18.5 ml of concentrated NH_4OH and 81.5 ml of Milli-Q water) was added to the collected solution. Centrifuge tubes were placed in an oven at 50°C for few days, and for keeping the volume of the solution constant, Milli-Q water was added repeatedly as required. After 1 to 3 days yellow Ag_3PO_4 crystals formed. If no crystals were formed, the pH of the solution was checked and adjusted to 7.0 if necessary. Ag_3PO_4 crystals were finally filtered with a 0.2 µm polycarbonate filter, washed 2 to 3 times with Milli-Q water and dried overnight in an oven at 50°C for drying and stored inside a desiccator to prevent re-moistening. The crystals were removed from the dried filters carefully by scratching with a steel spatula prior to the IRMS analysis.

Microbial phosphorus concentration

Microbial P (P_{mic},) concentrations were determined from fresh samples after the method of Kouno et al. (1995), modified by Bünemann et al. (2015. Fresh sample material with a weight of 2.0 g (dry weight equivalent) was transferred into 60 ml polyethylene bottles and mixed therein with 30 ml of Milli-Q water and one anion exchange membrane (AEM, VWR international), which was activated by shaking 16 hours with 0.5M $NaHCO_3$. Each sample was prepared in triplicates, with one replicate without further treatment, one with addition of 1 ml of hexanol (Merck, p.a.) and one sample with a spike of 1 ml of PO_4 -P standard solution (PO_4 -P concentration of 20 µg ml^{-1}). Samples were shaken by a horizontal shaker (16 hours, 125 rpm). Then the membranes were taken out, transferred into 50 ml PE–bottles with 30 ml of 0.2M HNO_3 and shaken on a horizontal shaker (2 hours, 125 mot). Here, adsorbed P_i was transferred from the membranes into the nitric acid solution and concentrations of P_i were measured immediately by UV-VIS (Analytik Jena Specord 200 plus, Germany).

Section C-S2: Treatment effects

Redox: Over the course of the experiment, the redox potential strongly reacted to the three hydrological treatments applied. The E_h first rapidly decreased towards strongly reducing conditions, which, however, gradually increased again and fluctuated between slightly and moderately reducing (Figure S3). Due to the frequent changes between dry and wet, oxygen was regularly entering into the system, preventing the development of strongly reducing redox conditions. Note that samples were always collected at the end of a wet cycle, and we therefore cannot infer if other treatment effects have occurred during the dry cycles as only E_h and temperature have been monitored.

Temperature: Generally, porewater variables (e.g., dissolved P_i concentration, pH, alkalinity) reacted more sensitive to the temperature treatment as solid phase variables. Dissolved P_i concentrations declined faster at 20°C as compared to 5°C, which is likely related to an enhanced microbial uptake and cycling as well as a pronounced temperature impact on the adsorption behavior of P_i (Bai et al., 2017). A reduced microbial activity at 5°C was further reflected by significantly lower pH in porewater of both, SPL and LPL treatments across most time points, as well as reduced E_h fluctuations. Also, the LPL treatment showed a consistently lower alkalinity at 5° as compared to 20°, which in sum underlines the impact of temperature on biogeochemical variables. Temperature differences between variables of the L treatment were generally much lower, which was likely caused by the generally reduced biological activities arising from the permanent water saturation.

Section C-S3: ^{31}P NMR analysis

^{31}P NMR anlysis of samples of DDS (triplicates DCS 1-3) of $NaHCO_3$ and NaOH fractions 24 hours (1 day) after labeling.

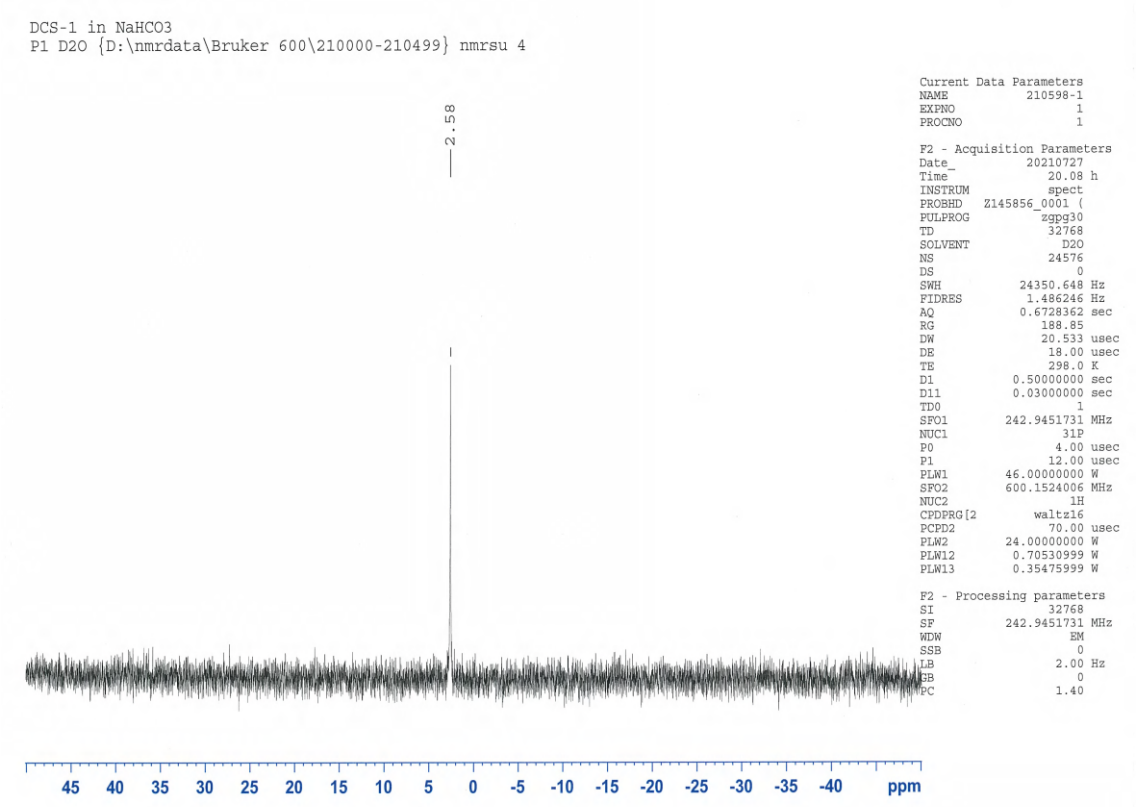

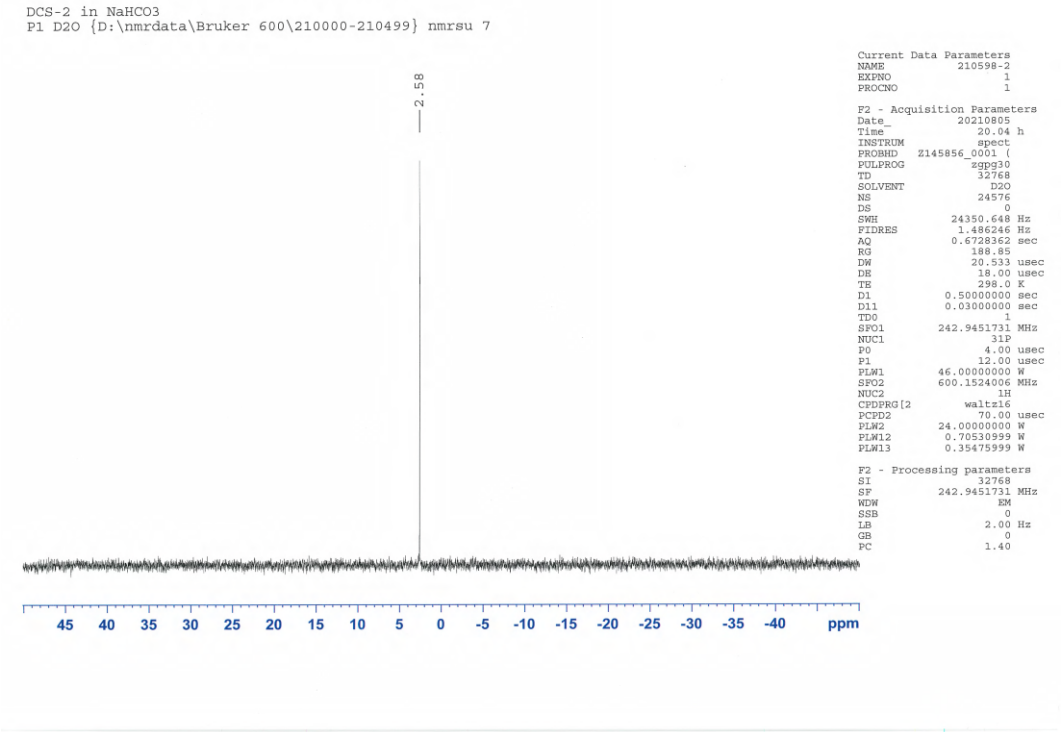

DCS-3 in NaHCO3
P1 D2O {D:\nmrdata\Bruker 600\210000-210499} nmrsu 10

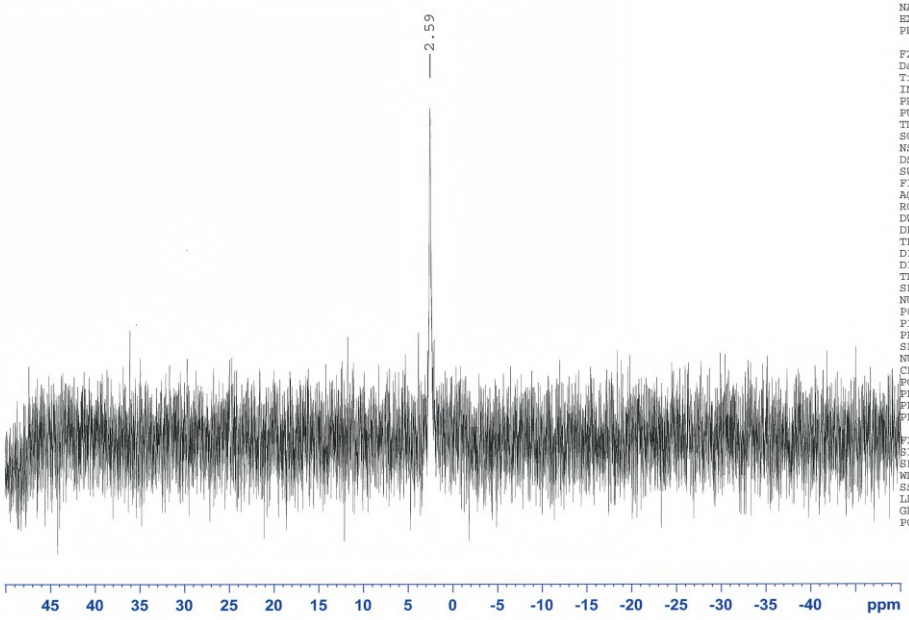


```
Current Data Parameters
NAME                 210598-3
EXPNO                       1
PROCNO                      1

F2 - Acquisition Parameters
Date_               20210806
Time                    4.33 h
INSTRUM                 spect
PROBHD   Z145856_0001 (
PULPROG             zgpg30
TD                       32768
SOLVENT                   D2O
NS                       24576
DS                           0
SWH                 24350.648 Hz
FIDRES               1.486246 Hz
AQ                   0.6728362 sec
RG                      188.85
DW                      20.533 usec
DE                      18.00 usec
TE                      298.0 K
D1                  0.50000000 sec
D11                 0.03000000 sec
TD0                          1
SFO1               242.9451731 MHz
NUC1                        31P
P0                       4.00 usec
P1                      12.00 usec
PLW1               46.00000000 W
SFO2               600.1524006 MHz
NUC2                         1H
CPDPRG[2                waltz16
PCPD2                   70.00 usec
PLW2               24.00000000 W
PLW12               0.70530999 W
PLW13               0.35475999 W

F2 - Processing parameters
SI                       32768
SF                 242.9451731 MHz
WDW                         EM
SSB                          0
LB                       2.00 Hz
GB                           0
PC                       1.40
```

DCS-1 in NaOH
P1 D2O {D:\nmrdata\Bruker 600\210000-210499} nmrsu 3

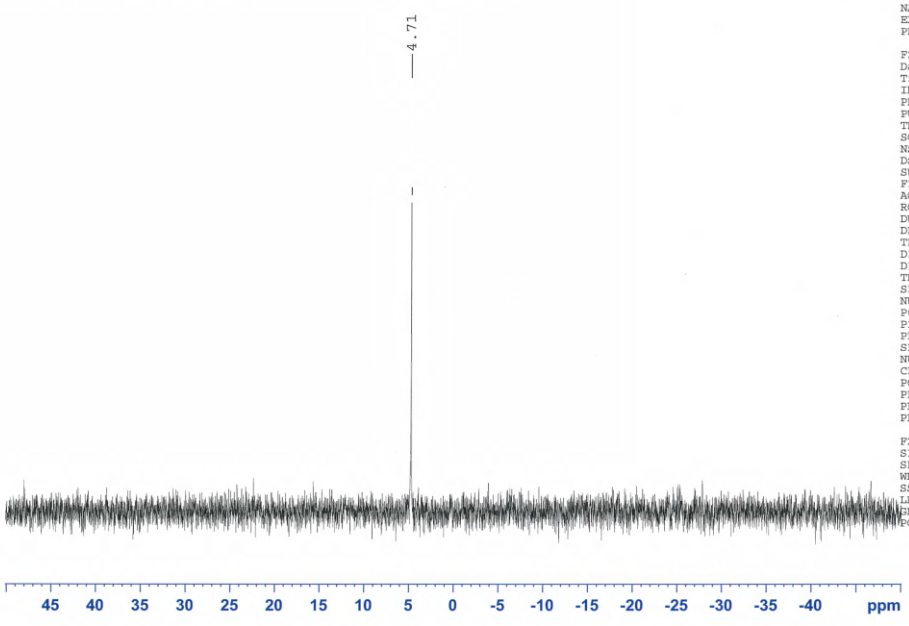


```
Current Data Parameters
NAME                 210598-4
EXPNO                       1
PROCNO                      1

F2 - Acquisition Parameters
Date_               20210716
Time                    3.17 h
INSTRUM                 spect
PROBHD   Z145856_0001 (
PULPROG             zgpg30
TD                       32768
SOLVENT                   D2O
NS                       24576
DS                           0
SWH                 24350.648 Hz
FIDRES               1.486246 Hz
AQ                   0.6728362 sec
RG                      188.85
DW                      20.533 usec
DE                      18.00 usec
TE                      298.0 K
D1                  0.50000000 sec
D11                 0.03000000 sec
TD0                          1
SFO1               242.9451731 MHz
NUC1                        31P
P0                       4.00 usec
P1                      12.00 usec
PLW1               46.00000000 W
SFO2               600.1524006 MHz
NUC2                         1H
CPDPRG[2                waltz16
PCPD2                   70.00 usec
PLW2               24.00000000 W
PLW12               0.70530999 W
PLW13               0.35475999 W

F2 - Processing parameters
SI                       32768
SF                 242.9451731 MHz
WDW                         EM
SSB                          0
LB                       2.00 Hz
GB                           0
PC                       1.40
```

DCS-2 in NaOH
P1 D2O {D:\nmrdata\Bruker 600\210000-210499} nmrsu 16

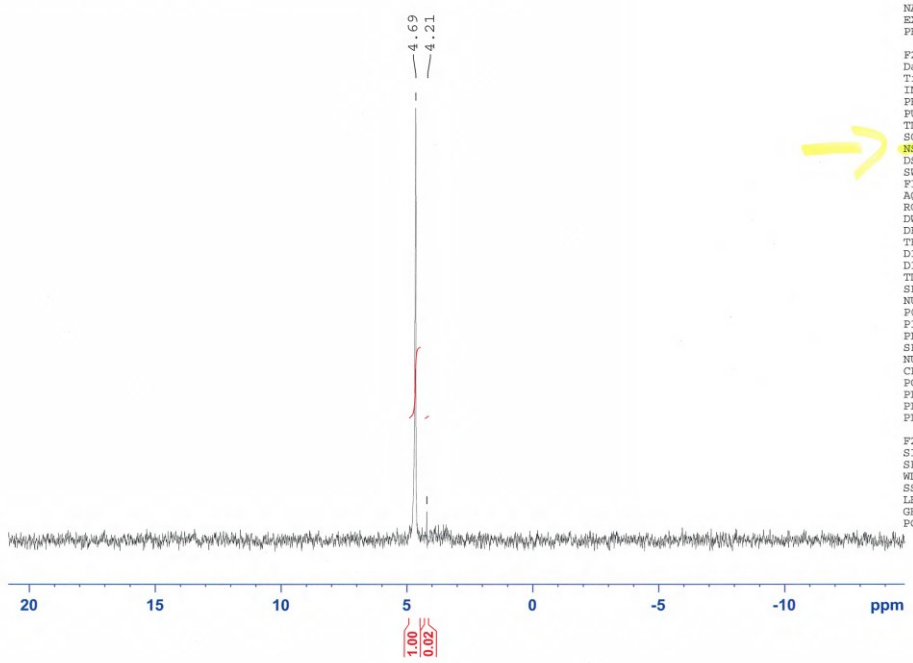


```
Current Data Parameters
NAME                 210598-5
EXPNO                       2
PROCNO                      1

F2 - Acquisition Parameters
Date_               20210809
Time                    8.53 h
INSTRUM                 spect
PROBHD    Z145856_0001 (
PULPROG                 zgpg30
TD                      32768
SOLVENT                   D2O
NS                        98304
DS                          0
SWH                24350.648 Hz
FIDRES              1.486246 Hz
AQ                  0.6728362 sec
RG                     188.85
DW                     20.533 usec
DE                     18.00 usec
TE                     298.0 K
D1                 0.50000000 sec
D11                0.03000000 sec
TD0                         1
SFO1               242.9451731 MHz
NUC1                       31P
P0                      4.00 usec
P1                     12.00 usec
PLW1               46.00000000 W
SFO2               600.1524006 MHz
NUC2                       1H
CPDPRG[2               waltz16
PCPD2                  70.00 usec
PLW2               24.00000000 W
PLW12               0.70530999 W
PLW13               0.35475999 W

F2 - Processing parameters
SI                      32768
SF                 242.9451731 MHz
WDW                        EM
SSB                         0
LB                      2.00 Hz
GB                          0
PC                      1.40
```

DCS-2 in NaOH
P1 D2O {D:\nmrdata\Bruker 600\210000-210499} nmrsu 6

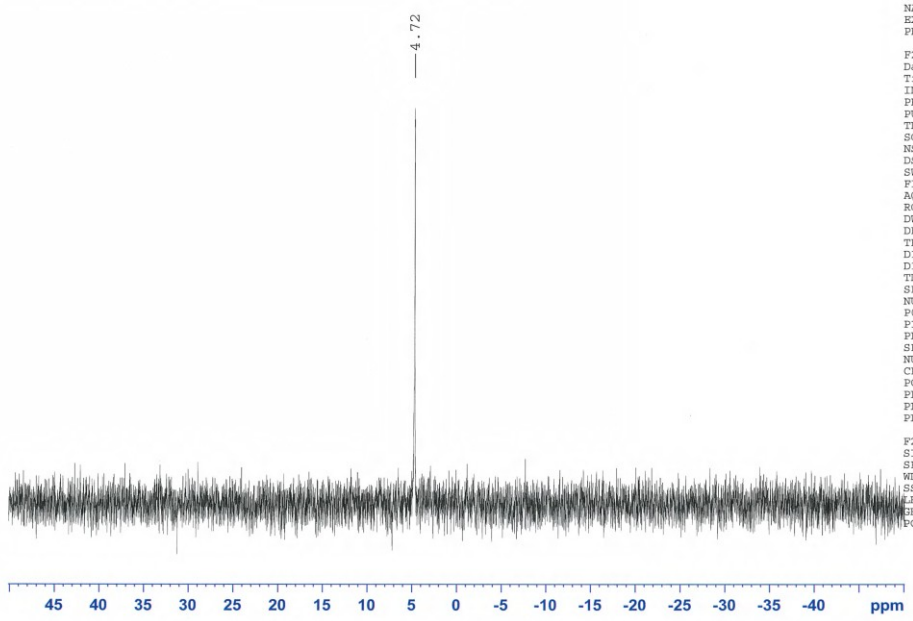


```
Current Data Parameters
NAME                 210598-5
EXPNO                       1
PROCNO                      1

F2 - Acquisition Parameters
Date_               20210717
Time                   21.07 h
INSTRUM                 spect
PROBHD    Z145856_0001 (
PULPROG                 zgpg30
TD                      32768
SOLVENT                   D2O
NS                        24576
DS                          0
SWH                24350.648 Hz
FIDRES              1.486246 Hz
AQ                  0.6728362 sec
RG                     188.85
DW                     20.533 usec
DE                     18.00 usec
TE                     298.0 K
D1                 0.50000000 sec
D11                0.03000000 sec
TD0                         1
SFO1               242.9451731 MHz
NUC1                       31P
P0                      4.00 usec
P1                     12.00 usec
PLW1               46.00000000 W
SFO2               600.1524006 MHz
NUC2                       1H
CPDPRG[2               waltz16
PCPD2                  70.00 usec
PLW2               24.00000000 W
PLW12               0.70530999 W
PLW13               0.35475999 W

F2 - Processing parameters
SI                      32768
SF                 242.9451731 MHz
WDW                        EM
SSB                         0
LB                      2.00 Hz
GB                          0
PC                      1.40
```

DCS-3 in NaOH
P1 D2O {D:\nmrdata\Bruker 600\210000-210499} nmrsu 3

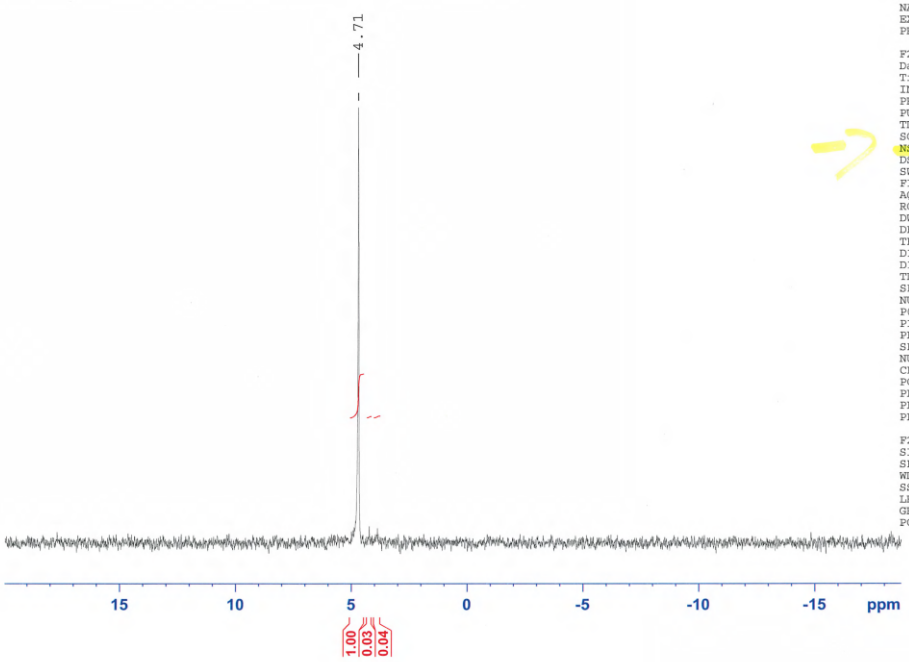


```
Current Data Parameters
NAME                 210598-6
EXPNO                       2
PROCNO                      1

F2 - Acquisition Parameters
Date_               20210807
Time                   23.04 h
INSTRUM                spect
PROBHD    Z145856_0001 (
PULPROG                zgpg30
TD                      32768
SOLVENT                  D2O
NS                     98304
DS                          0
SWH                24350.648 Hz
FIDRES              1.486246 Hz
AQ                  0.6728362 sec
RG                     188.85
DW                     20.533 usec
DE                     18.00 usec
TE                     298.0 K
D1                 0.50000000 sec
D11                0.03000000 sec
TD0                         1
SFO1               242.9451731 MHz
NUC1                       31P
P0                      4.00 usec
P1                     12.00 usec
PLW1               46.00000000 W
SFO2               600.1524006 MHz
NUC2                       1H
CPDPRG[2               waltz16
PCPD2                  70.00 usec
PLW2               24.00000000 W
PLW12               0.70530999 W
PLW13               0.35475999 W

F2 - Processing parameters
SI                      32768
SF                 242.9451731 MHz
WDW                        EM
SSB                         0
LB                      2.00 Hz
GB                          0
PC                      1.40
```

DCS-3 in NaOH
P1 D2O {D:\nmrdata\Bruker 600\210000-210499} nmrsu 3

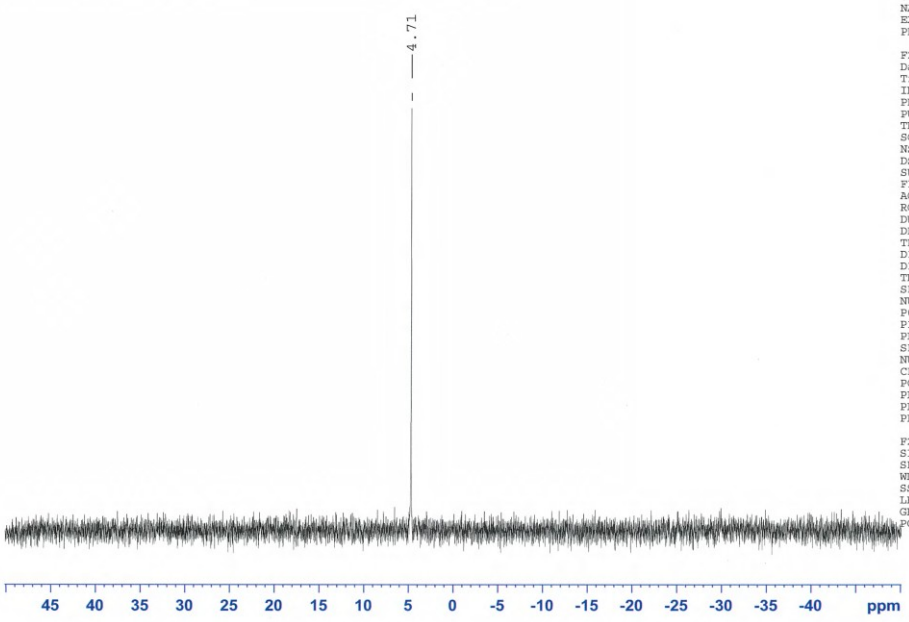


```
Current Data Parameters
NAME                 210598-6
EXPNO                       1
PROCNO                      1

F2 - Acquisition Parameters
Date_               20210727
Time                    9.10 h
INSTRUM                spect
PROBHD    Z145856_0001 (
PULPROG                zgpg30
TD                      32768
SOLVENT                  D2O
NS                     24576
DS                          0
SWH                24350.648 Hz
FIDRES              1.486246 Hz
AQ                  0.6728362 sec
RG                     188.85
DW                     20.533 usec
DE                     18.00 usec
TE                     298.0 K
D1                 0.50000000 sec
D11                0.03000000 sec
TD0                         1
SFO1               242.9451731 MHz
NUC1                       31P
P0                      4.00 usec
P1                     12.00 usec
PLW1               46.00000000 W
SFO2               600.1524006 MHz
NUC2                       1H
CPDPRG[2               waltz16
PCPD2                  70.00 usec
PLW2               24.00000000 W
PLW12               0.70530999 W
PLW13               0.35475999 W

F2 - Processing parameters
SI                      32768
SF                 242.9451731 MHz
WDW                        EM
SSB                         0
LB                      2.00 Hz
GB                          0
PC                      1.40
```

Table C-S1: Overview of the sampling site in the Ammer catchment where the drainage ditch sediments were collected from three adjacent spots.

Study site	Samples	Coordinates (WGS84-UTM)	Topography	Geology	Soil type in the area*	Land use
Arable land	Drainage ditch	E 500969.172 N 5373752.969	Elevation: 345 m N.N. Slope: 6.5 %	Keuper (kmGr: Gipskeuper)	Fluvisols Luvisols Anthrosols	Agriculture

*H. Neidhardt 2019 (Phosphorus Pool Composition in Soils and Sediments of Transitional Ecotones under the Influence of Agriculture), according to LGRB 82017)

Table C-S2: Quality controls (QC, p.a, Roth GmbH) and their respective recovery rates (% of certified value including ± as standard deviation) of the major and trace elements determined in the ICP-OES runs. Quality controls covering different concentrations (0.2 to 50 mg l^{-1}) were prepared in 0.2M HNO_3.

Al 396.153 axial		**As 188.979 axial**		**Ca 317.933 radial**		**Cu 327.393 axial**		**Fe 238.204 axial**	
QC	**Recovery**	**QC**	**Recovery**	**QC**	**Recovery**	**QC**	**Recovery**	**QC**	**Recovery**
0.20	0.20	0.02	0.02	0.20	0.20	0.10	0.10	0.20	0.19
2.00	2.04	0.05	0.05	5.00	5.20	0.20	0.20	1.00	1.01
2.00	1.99	0.10	0.13	2.00	2.04	0.50	0.50	2.50	2.51
5.00	5.13	0.20	0.20	12.0	12.8	1.00	1.00	2.00	1.94
20.0	19.7	2.00	1.99	20.0	20.1	10.0	9.68	20.0	18.2
50.0	48.6	5.00	4.92	50.0	49.4	25.0	24.5	50.0	42.1
Recovery Rate [%]	**100 ± 1.63%**		**104 ± 4.13%**		**103 ± 3.41%**		**100 ± 1.74%**		**99.2 ± 5.84%**
K 766.490 radial		**Mg 285.213 radial**		**Mn 257.610 radial**		**Na 589.592 radial**		**Ni 231.604 axial**	
QC	**Recovery**	**QC**	**Recovery**	**QC**	**Recovery**	**QC**	**Recovery**	**QC**	**Recovery**
0.20	0.22	0.20	0.20	0.10	0.10	0.20	0.19	0.10	0.10
1.00	1.05	2.00	2.03	0.01	0.10	1.00	1.09	0.50	0.41
2.00	1.99	5.00	5.19	0.25	0.25	2.00	2.01	1.00	1.02
2.50	2.61	12.0	12.8	1.00	1.02	2.50	2.57	1.00	1.01
20.0	19.9	20.0	19.8	10.0	10.0	20.0	20.0	10.0	9.41
50.0	49.8	50.0	46.7	25.0	24.9	50.0	49.8	25.0	22.7
Recovery Rate [%]	**104 ± 2.83%**		**103 ± 3.23%**		**100 ± 2.28%**		**105 ± 4.67%**		**101 ± 4.75%**
P 213.617 axial		**Ti 334.940 axial**		**Zn 206.200 axial**					
QC	**Recovery**	**QC**	**Recovery**	**QC**	**Recovery**				
0.20	0.20	0.01	0.10	0.10	0.10				
0.50	0.41	0.10	0.11	0.50	0.54				
1.00	1.03	0.20	0.26	1.00	1.01				
2.00	2.03	1.00	1.00	1.50	1.33				
20.0	19.9	10.0	9.61	10.0	9.31				
50.0	49.2	25.0	23.2	20.0	22.0				
Recovery Rate [%]	**103 ± 3.02%**		**104 ± 4.12%**		**105 ± 7.22%**				

Table C-S3: Results for international certified reference standards (‰ VSMOW) determined in the IRMS runs, standard deviation and official refence values provided by the manufacturer (Reston Stable Isotope Laboratory, USGS 80/ 81 and IAEA Benzoic Acid 601). We also included an internal house standard, KH_2PO_4 (Fisher Chemical, p.a. ≥99%), to check for reproducibility of the IRMS analyses.

International standard	Number of samples (n)	$\delta^{18}O$ mean (‰ VSMOW)	Standard deviation (‰ VSMOW)	Nominal value	Difference to certified value (‰ VSMOW)
USGS81	13	36.3	0.72	35.4	+0.85
USGS80	20	13.5	0.35	13.1	+0.35
Benzoic Acid 601	12	23.0	0.88	23.1	-0.11
KH_2PO_4	15	13.7	0.85	n.a.	n.a.

Table C-S4: Expected and observed $\delta^{18}O_{Pi}$ values for the NaOH-P_i pool calculated by mass balance. Expected $\delta^{18}O_{Pi}$ and observed mean $\delta^{18}O_{Pi}$ values (‰ VSMOW) of measured replicates (a,b,c) at certain time points of the incubation (4 and 8 weeks, respectively) as well differences between both (‰ VSMOW) for the SPL (short-pulsed logged, only replicate a and c), LPL (long-pulsed logged) and L (permanently water-logged) treatments. Expected $\delta^{18}O_{Pi}$ values for the NaOH-P_i pool at a respective time step were calculated considering the $\delta^{18}O$ values of the receiving P_i pool at time point t_i prior and after label transfer, the label value of the source P_i pool as well as the P_i concentration change in the receiving P_i pool at the time point t_i (see main text, material and methods).

Treatment/ Replicate	Time point	Temperature (°C)	Expected $\delta^{18}O_{Pi}$ NaOH (‰ VSMOW)	Observed $\delta^{18}O_{Pi}$ NaOH (‰ VSMOW)	Difference (‰ VSMOW)
SPL-a	4w	20°C	112	40	72
SPL-c	4w	20°C	74	19	56
LPL-a	8w	20°C	45	61	-16
LPL-b	8w	20°C	23	33	-11
LPL-c	8w	20°C	47	37	10
L-a	8w	20°C	98	42	57
L-b	8w	20°C	38	65	-27
L-c	8w	20°C	79	117	-37

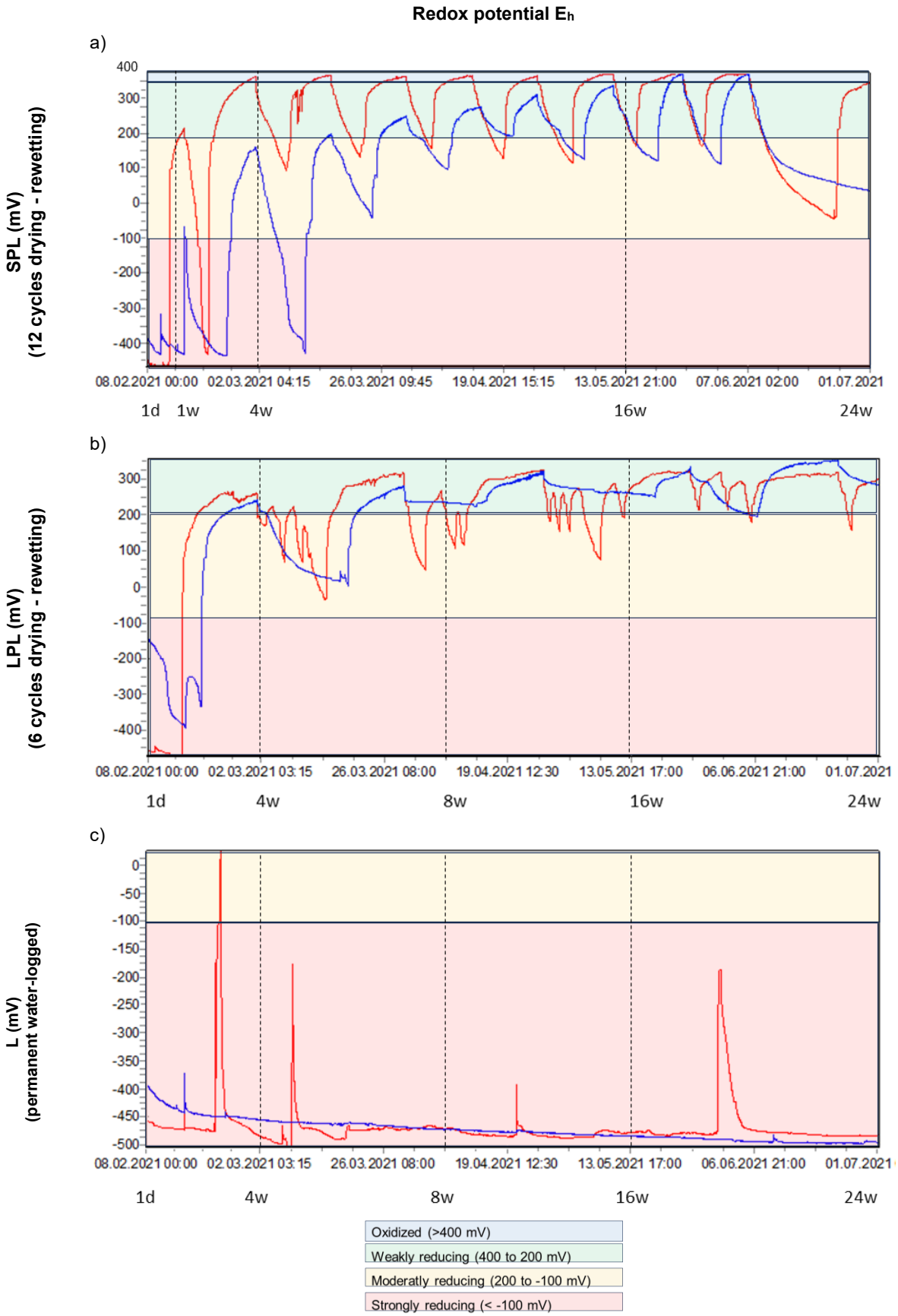

Figure C-S1: Temporal variation in redox potential (E_h) during the experiment. E_h (mV) of (a) the short-pulsed logged (SPL), (b) long-pulsed logged (LPL) and (c) permanently water-logged (L) treatments over 24 weeks of incubation. Red line representing 20°C temperature treatments, blue line indicating 5°C treatments. Black dashed lines show time steps of sampling.

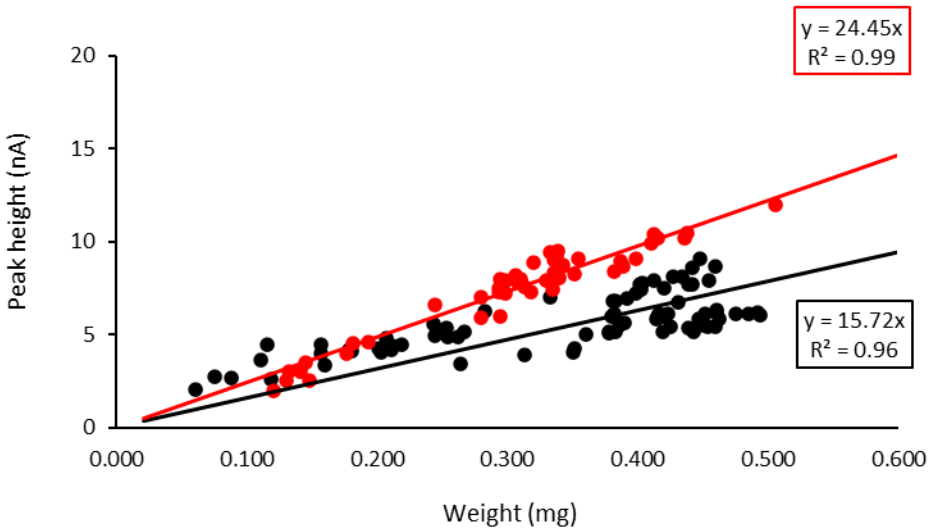

Figure C-S2: Quality control determined in the IRMS runs: Regression of CO peak areas (nA) on analyte weight (mg) of Ag_3PO_4 standards USGS-80 and USGS-81 (red dots, n = 39) and Ag_3PO_4 obtained from the sample extractions solutions (black dots, n = 108, comprising 46 samples from the $NaHCO_3$-pool, 41 from the NaOH-pool and 28 from the HCl-pool) as a measure of the O yield.

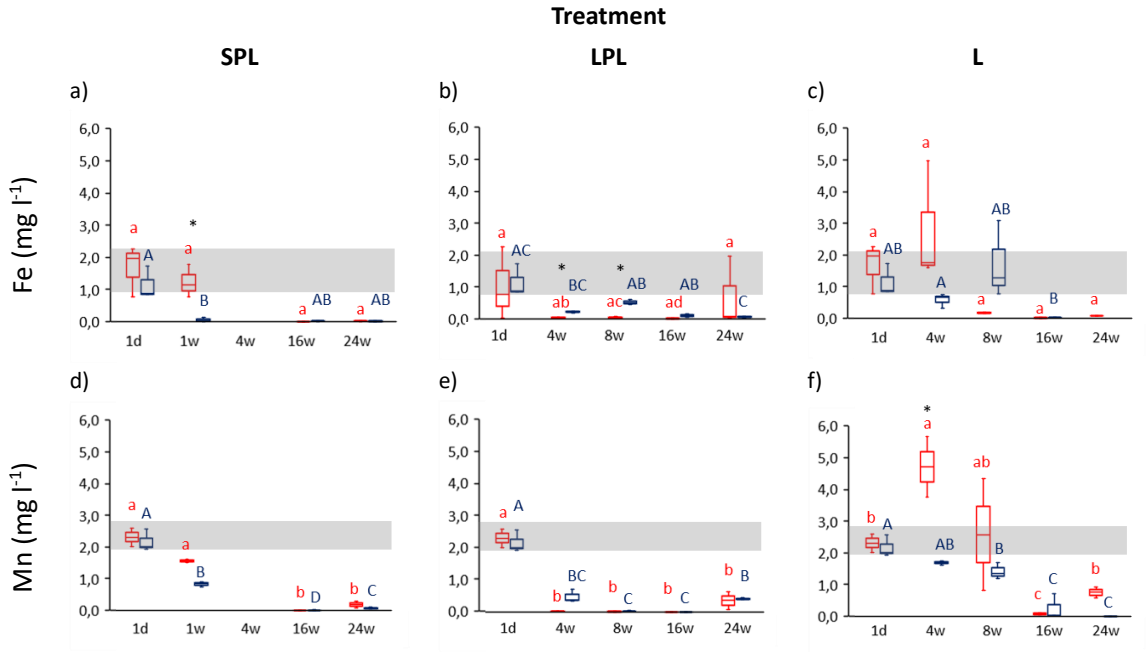

Figure C-S3: Temporal variation in dissolved iron (Fe) and manganese (Mn) concentrations in porewater (mg l^{-1}) in the short-pulsed logged (SPL), long-pulsed logged (LPL) and permanently water-logged (L) treatments. (a, b, c) Fe concentrations (mg l^{-1}) and (d, e, f), Mn concentrations (mg l^{-1}) from beginning (1 day after labeling) until the end of the incubation (24 weeks). Red boxplots represent 20°C temperature treatments, blue boxplots represent 5°C treatments. Small letters show significant differences between samples of the 20°C treatments, capital letters show differences between samples of 5°C treatments at the respevtive time. Asterisks indicate significant differences between 20°C and 5°C treatments at the respective point in time (* $p < 0.05$, ** $p < 0.01$, *** $p < 0.001$). Shaded grey area symbolizes respective concentrations of the initial sediment prior label application.

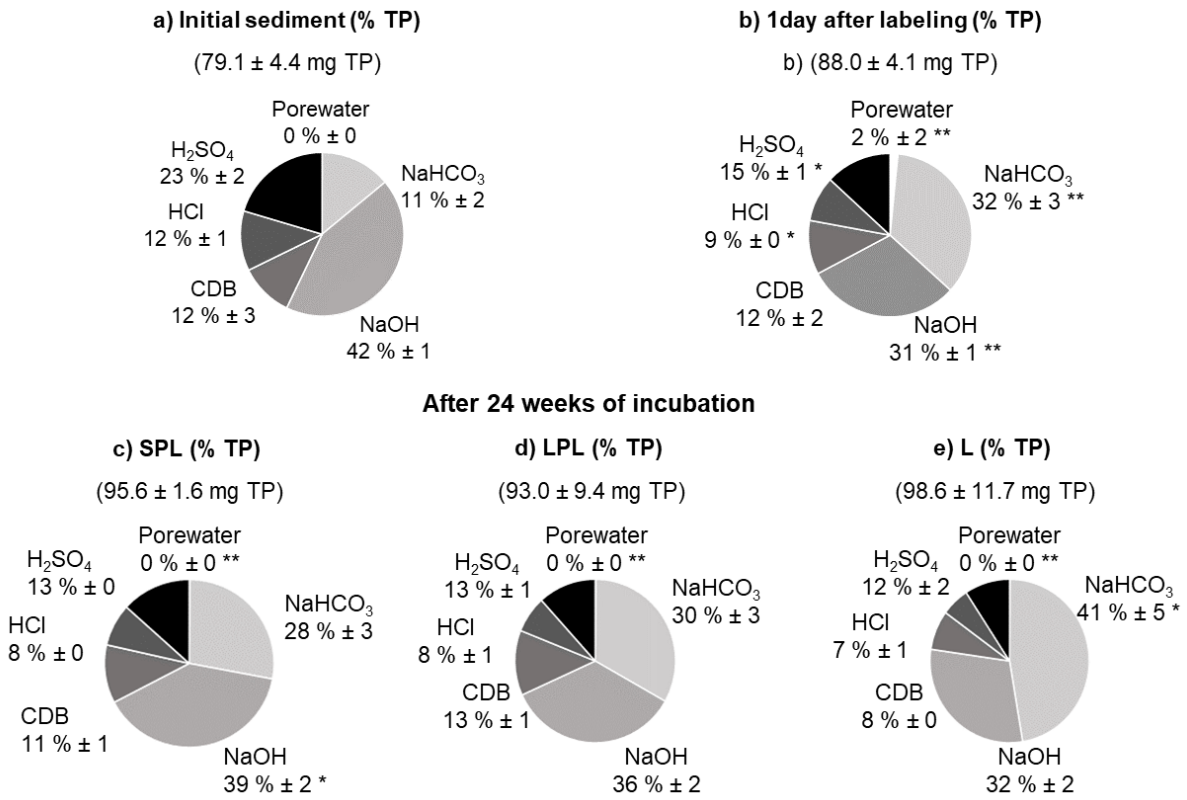

Figure C-S4: Relative distribution of total phosphorus (TP) in the different P pools of the 20°C temperature treatments. Absolute amount of TP calculated based on the respective concentration for each pool and the volume of porewater and dry-weight of sediment, respectively, within the experimental pots. (a) at the beginning (initial sample), (b) after one day (24 hours after labeling) and (c, d, e) at the end of the incubation (after 24 weeks) in the short-pulsed logged (SPL), long-pulsed logged (LPL) and permanently water-logged (L) treatments. Numbers in brackets representing mean contents of total phosphorus (mg TP) per pots (triplicates). Asterisks indicating significant differences between (b) initial sample and one day after labeling, (c, d, e) one day after labeling and after 24 weeks of incubation (* $p < 0.05$, ** $p < 0.01$, *** $p < 0.001$).

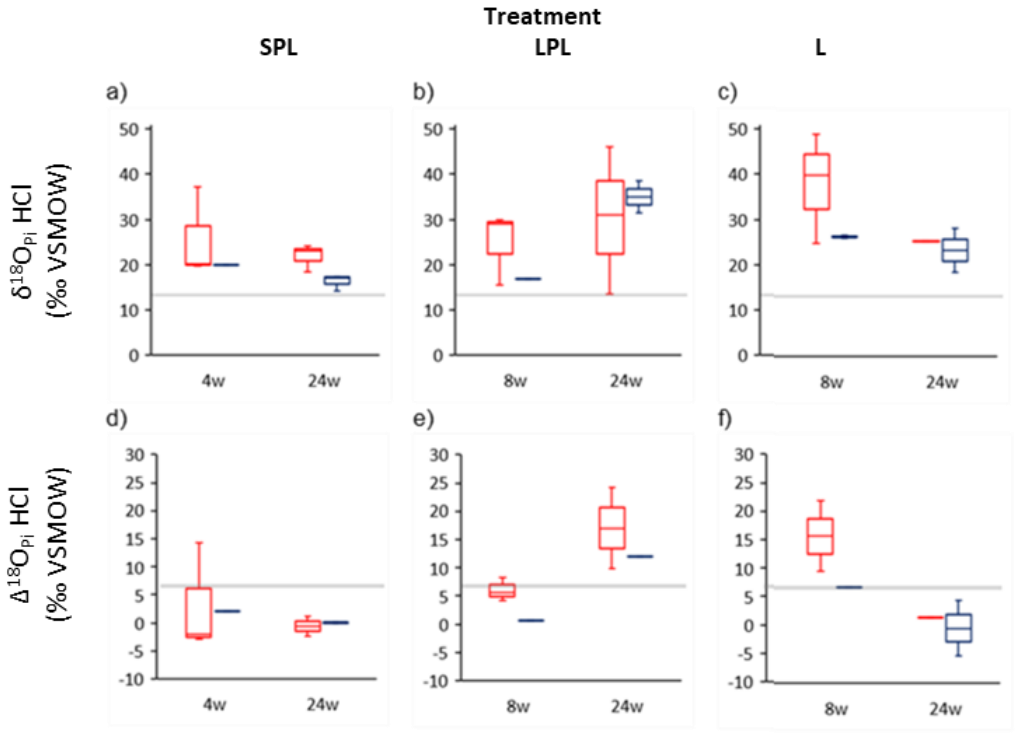

Figure C-S5: Temporal variation in $\delta^{18}O_{Pi}$ values of the HCl-P pool in the short-pulsed logged (SPL), long-pulsed logged (LPL) and permanently water-logged (L) treatments. Observed $\delta^{18}O$ values ($\delta^{18}O_{Pi}$, ‰ VSMOW) of (a, b, c) HCl-P_i pool at 4/ 8 weeks after labeling until the end of the incubation (after 24 weeks). Differences between observed $\delta^{18}O_{Pi}$ and $\delta^{18}O_{Pi\text{-}equ}$ values ($\Delta^{18}O_{Pi}$, ‰ VSMOW) of the HCl-P pool (d, e, f). Red boxplots represent 20°C temperature treatments, blue boxplots represent 5°C treatments. Shaded grey area symbolizes

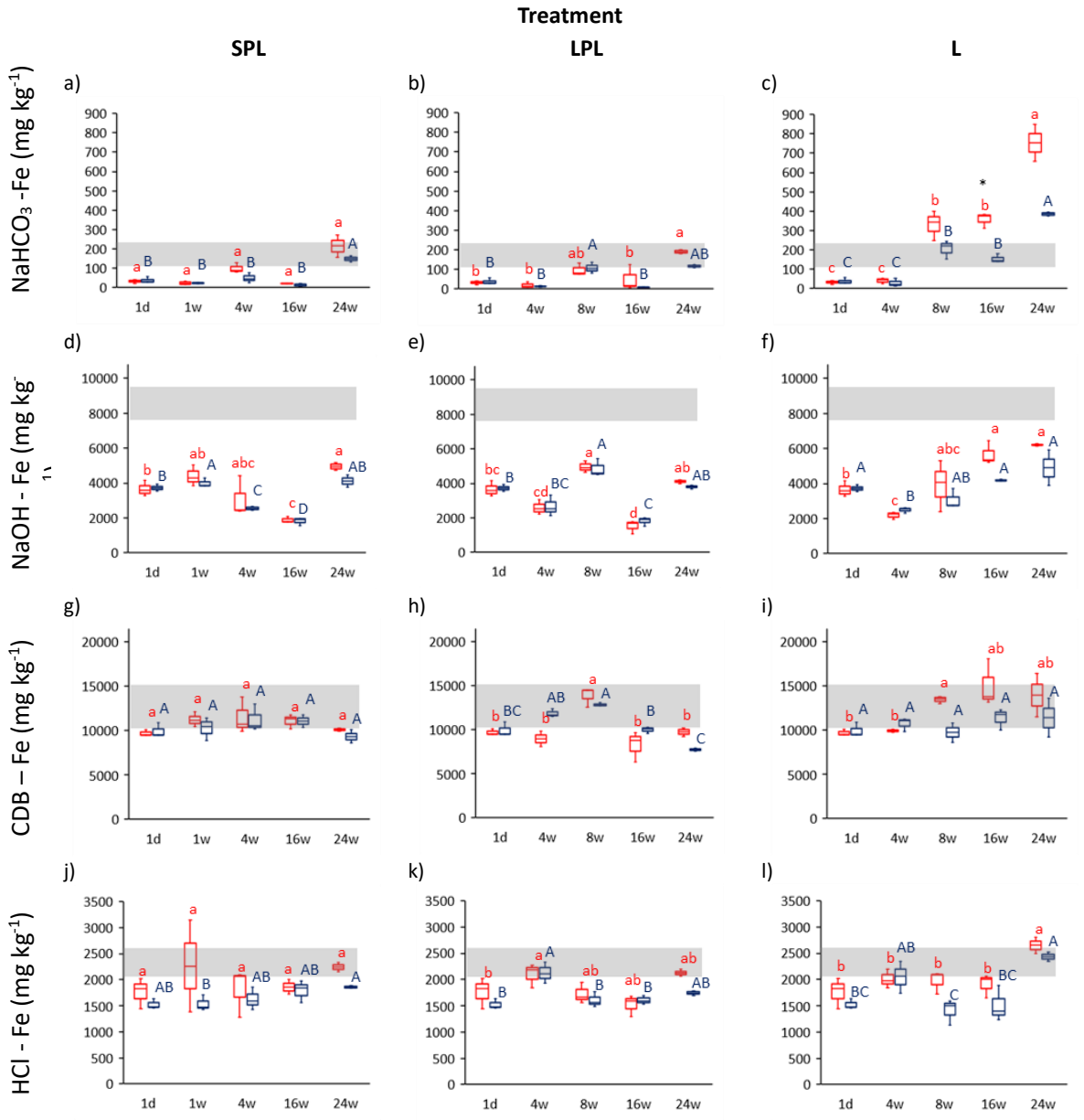

Figure C-S6: Temporal variation in Fe concentrations (mg kg^{-1}) in various extraction solutions in the short-pulsed logged (SPL), long-pulsed logged (LPL) and permanently water-logged (L) treatments from beginning (1 day after labeling) until the end of the incubation (after 24 weeks). a, b, c) $NaHCO_3$ - Fe concentrations, (d, e, f) NaOH - Fe concentrations, (g, h, i) CDB - Fe concentrations, (j, k, l) HCl - Fe concentrations. Red boxplots represent 20°C temperature treatments, blue boxplots represent 5°C treatments. Small letters showing significant differences between samples of 20°C, capital letters differences between samples of 5°C at the respective time. Asterisks illustrating significant differences between 20°C and 5°C at the respective point in time (* $p < 0.05$, ** $p < 0.01$, *** $p < 0.001$). Shaded grey area symbolizes respective concentrations of the initial sediment prior label application.

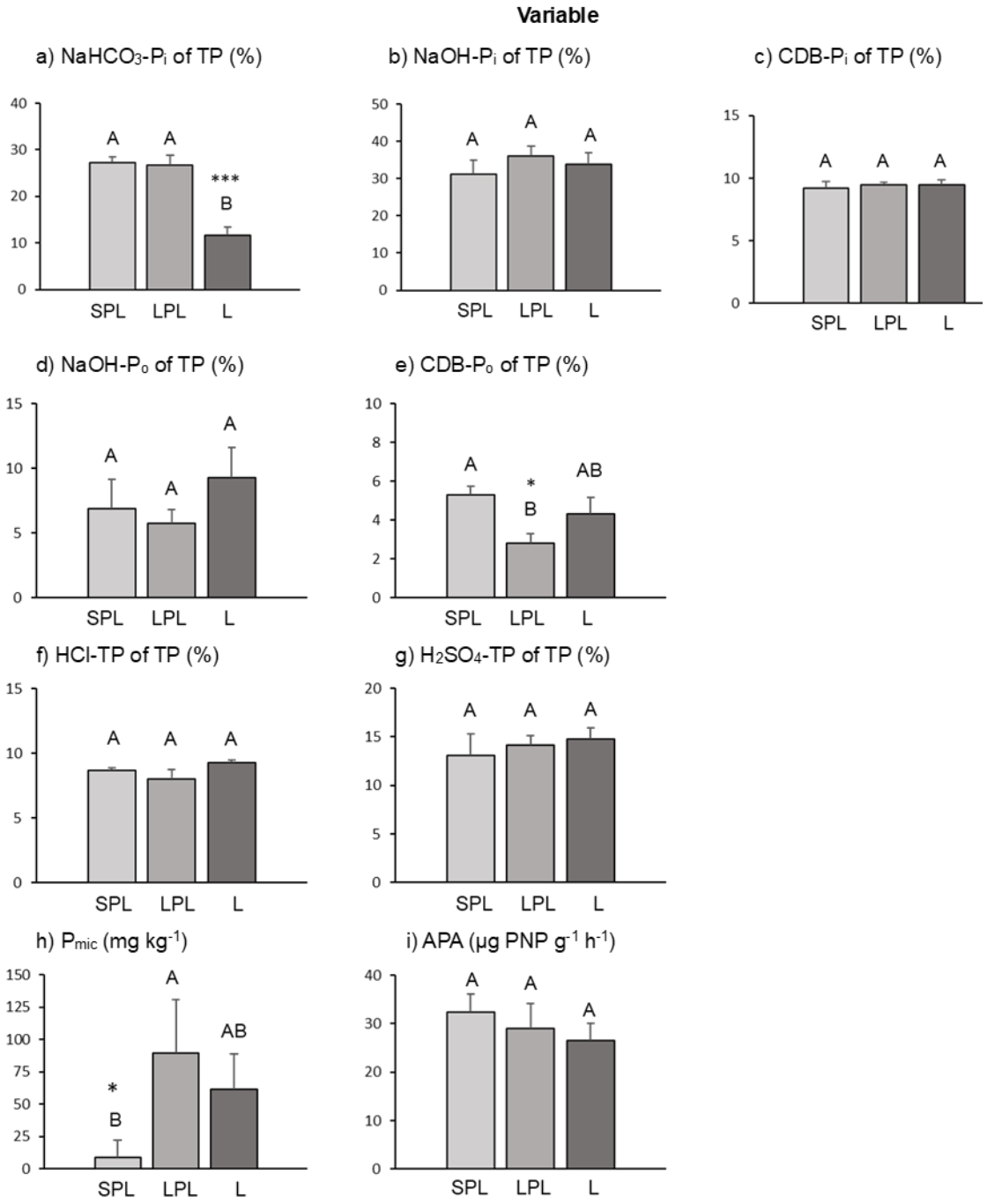

Figure C-S7: Variation in P pools, P_{mic} and APA in the short-pulsed logged (SPL), long-pulsed logged (LPL) and permanently water-logged (L) treatments at the end of the early phase (4 weeks). (a) Relative proportion of $NaHCO_3$-P_i of TP (%), (b) relative proportion of NaOH-P_i of TP (%), (c) relative proportion of CDB-P_i of TP (%), (d) relative proportion of NaOH-P_o of TP (%), (e) relative proportion of CDB-P_o of TP (%), (f) relative proportion of HCl-TP of TP (%), (g) relative proportion of H_2SO_4-TP of TP (%), (h) P_{mic} (mg kg^{-1}) , (i) acid mono-phosphatase (APA; µg PNP g^{-1} h^{-1}). Letters representing differences among the treatments SPL, LPL and L (ANOVA), asterisks indicating level of significance (* $p < 0.05$; ** $p < 0.01$; *** $p < 0.001$).

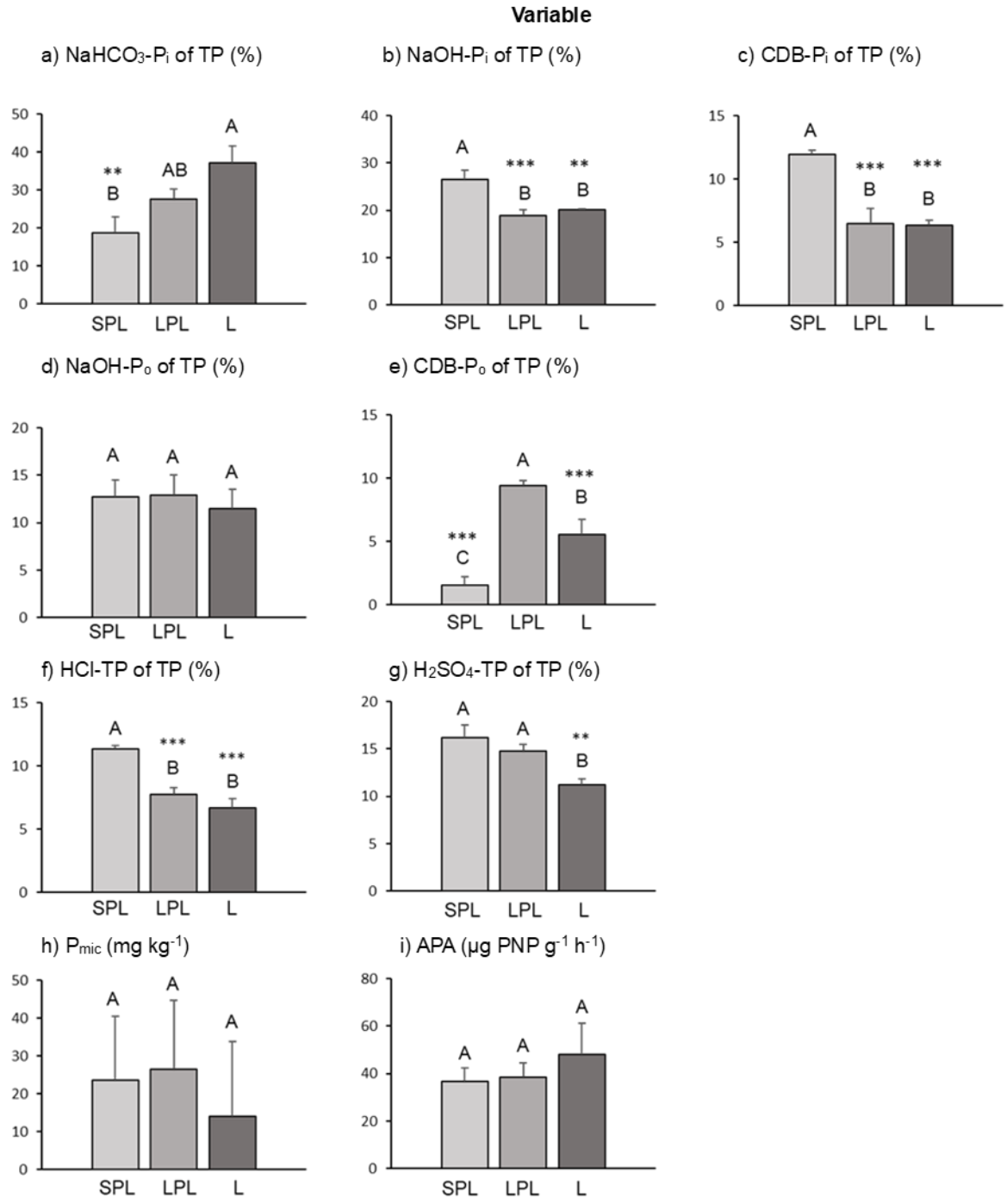

Figure C-S8: Variation in P pools, P_{mic} and APA in the short-pulsed logged (SPL), long-pulsed logged (LPL) and permanently water-logged (L) treatments at the end of the intermediate phase (SPL: 16 weeks; LPL and L: 8 weeks). (a) relative proportion of $NaHCO_3$-P_i of TP (%), (b) relative proportion of NaOH-P_i of TP (%), (c) relative proportion of CDB-P_i of TP (%), (d) relative proportion of NaOH-P_o of TP (%), (e) relative proportion of CDB-P_o of TP (%), (f) relative proportion of HCl-TP of TP (%), (g) relative proportion of H_2SO_4-TP of TP (%), (h) P_{mic} (mg kg^{-1}) , (i) acid mono-phosphatase (APA; µg PNP g^{-1} h^{-1}). Letters representing differences among the treatments SPL, LPL and L (ANOVA), asterisks indicating level of significance (* $p < 0.05$; ** $p < 0.01$; *** $p < 0.001$).

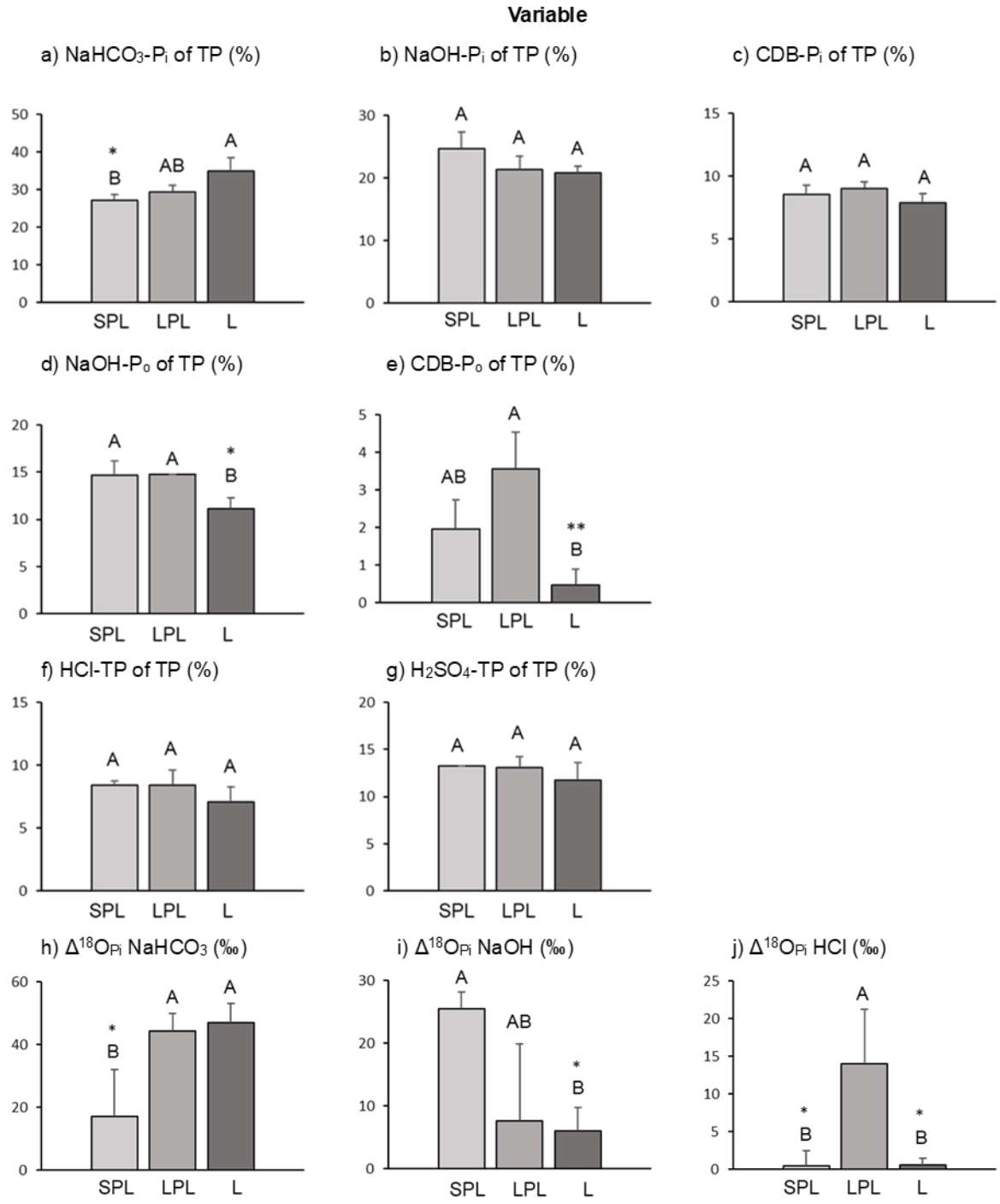

Figure C-S9: Variation in P pools and $\Delta^{18}O_{Pi}$ (differences between calculated $\delta^{18}O_{Pi\text{-}equ}$ and observed $\delta^{18}O_{Pi}$ in a respective P_i pool) in the short-pulsed logged (SPL), long-pulsed logged (LPL) and permanently water-logged (L) treatments at the end of the intermediate phase (24 weeks). (a) relative proportion of $NaHCO_3$-P_i of TP (%), (b) relative proportion of NaOH-P_i of TP (%), (c) relative proportion of CDB-P_i of TP (%), (d) relative proportion of NaOH-P_o of TP (%), (e) relative proportion of CDB-P_o of TP (%), (f) relative proportion of HCl-TP of TP (%), (g) relative proportion of H_2SO_4-TP of TP (%), (h) $\Delta^{18}O_{Pi}$ $NaHCO_3$ (‰), (i) $\Delta^{18}O_{Pi}$ NaOH (‰), (j) $\Delta^{18}O_{Pi}$ HCl (‰). Letters representing differences among the treatments SPL, LPL and L (ANOVA), asterisks indicating level of significance (* $p < 0.05$; ** $p < 0.01$; *** $p < 0.001$).

References

Bowman, R. A., & Cole, C. V. (1978). Transformations of organic phosphorus substrates in soils as evaluated by NaHCO3 extraction. Soil science, 125(1), 49-54. https://doi.org/10.1097/00010694-197801000-00008.

Bünemann, E. K. (2015). Assessment of gross and net mineralization rates of soil organic phosphorus–A review. Soil Biology and Biochemistry, 89, 82-98. https://doi.org/10.1016/j.soilbio.2015.06.026.

Joshi, S. R., Kukkadapu, R. K., Burdige, D. J., Bowden, M. E., Sparks, D. L., & Jaisi, D. P. (2015). Organic matter remineralization predominates phosphorus cycling in the mid-bay sediments in the Chesapeake Bay. Environmental science & technology, 49(10), 5887-5896. https://doi.org/10.1021/es5059617.

Kouno, K., Tuchiya, Y., & Ando, T. (1995). Measurement of soil microbial biomass phosphorus by an anion exchange membrane method. Soil Biology and Biochemistry, 27(10), 1353-1357. https://doi.org/10.1016/0038-0717(95)00057-L.

Melby, E. S., Soldat, D. J., & Barak, P. (2011). Synthesis and detection of oxygen-18 labeled phosphate. Plos one, 6(4), e18420. https://doi.org/10.1371/journal.pone.0018420

Neidhardt, H., Achten, F., Kern, S., Schwientek, M., & Oelmann, Y. (2019). Phosphorus pool composition in soils and sediments of transitional ecotones under the influence of agriculture. Journal of environmental quality, 48(5), 1325-1335. https://doi.org/10.2134/jeq2019.01.0012.

Tamburini, F., Pistocchi, C., Helfenstein, J., & Frossard, E. (2018). A method to analyse the isotopic composition of oxygen associated with organic phosphorus in soil and plant material. European Journal of Soil Science, 69(5), 816-826. https://doi.org/10.1111/ejss.12693.

List of publication

a) Accepted publication

Nagel, C., Neidhardt, H., & Oelmann, Y. (2025). Dynamics of phosphorus pools in drainage ditch sediments within an agricultural catchment. Applied Geochemistry, 106633. https://doi.org/10.1016/j.apgeochem.2025.106633.

Nagel, C., Neidhardt, H., Oelmann, Y. (2025). Data from: Dynamics of phosphorus pools in drainage ditch sediments within an agricultural catchment [Dataset]. Dryad. https://doi.org/10.5061/dryad.2z34tmpxm.

b) Manuscript in progress

Christiane Nagel, Yvonne Oelmann, Harald Neidhardt (2025): Insight into P pool transformations under dynamic redox conditions in soils of vegetated buffer strips. Journal of Soil Science and Plant Nutrients.

c) Co-authorship, presentations, poster

Li, Y., Neidhardt, H., Guo, H., Nagel, C., Shao, W., Yu, C., ... & Oelmann, Y. (2024). Microbial cycling contributes to the release of dissolved inorganic phosphate into the groundwater of floodplain aquifers. *Communications Earth & Environment*, *5*(1), 494.

Li, Y., Yu, C., Zhao, B., Chen, D., Ye, H., Nagel, C., ... & Guo, H. (2022). Spatial variation in dissolved phosphorus and interactions with arsenic in response to changing redox conditions in floodplain aquifers of the Hetao Basin, Inner Mongolia. *Water Research*, *209*, 117930.

Oelmann, Y., Nagel, C., Brauckmann, H. J., Broll, G., & Schreiber, K. F. (2015). Maßnahmen zur Offenhaltung von Grünlandstandorten: Effekte auf die P-Fraktionen im Boden vierzig Jahre nach Versuchseinrichtung.

C. Nagel, Wen Shao, Niklas Wendenburg, Y. Oelmann, H. Neidhardt (2020). Dynamics in Phosphorus Pools in Soils and Sediments along the Land-Freshwater Continuum of Agricultural Catchments. Vortrag (Campos).

C. Nagel, J. Walter, H. Neidhardt, Y. Oelmann (2019). Shifts in plant-available nutrients along a hydrological gradient in a short-term experiment. Poster (DFG).